

**HUMAN SMALL HEAT SHOCK PROTEINS  
HSP22 AND ALPHA-CRYSTALLIN:  
STRUCTURAL AND FUNCTIONAL ASPECTS**

**THESIS**

Submitted for the degree of  
**DOCTOR OF PHILOSOPHY**

To

**JAWAHARLAL NEHRU UNIVERSITY**

New Delhi

**DEVENDRA SINGH**

**CENTRE FOR CELLULAR AND MOLECULAR BIOLOGY**

**HYDERABAD 500007**

**2008**

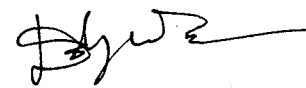
## CERTIFICATE

The research work embodied in this thesis has been carried out at the Centre for Cellular and Molecular Biology, Hyderabad, India. This work is original and has not been submitted in part or full for any other degree or diploma of any other university.

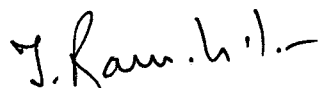


Dr. Ch. Mohan Rao

Supervisor



Devendra Singh



Dr. T. Ramakrishna Murti

Co-supervisor

## ACKNOWLEDGEMENT

*"All of life is a journey; which paths we take, what we look back on, and what we look forward to is up to us. We determine our destination, what kind of road we will take to get there, and how happy we are when we finally get there"*

*This thesis dissertation marks the end of a long and eventful journey for which there are many people that I would like to acknowledge for their support along the way. My utmost gratitude goes to my thesis advisors, Dr. Mohan Rao for allowing me to join his team, for his expertise, kindness, and most of all for his unwavering encouragement and support in various ways, and Dr. T. Ramakrishna Murti, fondly called as Ramki, who shared with me a lot of his expertise and research insight. His truly scientific intuition has made him a constant oasis of ideas and passions in science, which exceptionally inspired and enriched my growth as a student and a researcher. I am indebted to them more than they know. I would also like to express my gratitude to Dr B. Raman, who was closely associated with my work, his valuable advice in discussions often served to give me a sense of direction during my PhD studies.*

*I would also like to thank Dr. Lalji Singh for giving me an opportunity to work in a institute like CCMB, and the Council for the scientific and industrial research fellowship, which has supported me during my five years of research.*

*I would like to express my appreciation for Dr. V. Srinivas for all his interest in teaching me valuable hints on stock markets and mutual funds. I am grateful for the highly responsive support from Dr. K. Sridhar Rao.*

*During this work I have collaborated with many colleagues for whom I have great regard, and I wish to extend my warmest thanks to all those who have helped me with my work. In particular, I am thankful to Amit, Saloni, Waseem, Tirumal, Faiz, Bhairab, Abhay, Aftab, Abhishek, Prabhu, Saad and Abdullah. Ramki, Abhishek and Prabhu have provided detailed review, constructive criticism and excellent advice during the preparation of this thesis.*

*Thanks to members of Dr. Madhu's and Dr. Yogendra's lab especially Dr. Vijaya gopal, Dr. Vijaya Lakshmi, Jenny, Satya, Rajni, Zahid, Arvind Poornima, Virendra, and Rajeev for being the ultimate lab-neighbors, and providing a great work environment. My discussions with Jobby and Shoeb have been very fruitful. Wild wild west wing first floor rocks.*

I would like to express my sincere thanks to Dr. Tushar, His overly enthusiasm and integral view on research and his mission for providing 'only high-quality work and not less', has made a deep impression on me. My many thanks to Nasir, Brajesh and Nitin for all the good times in their lab.

Anuradha's help in official work is also highly acknowledged. I lost count how many times I troubled her to check the title of my thesis. I would also like to thank Hanumanthu ji, Sayeed ji, Venu ji and late Ehsaan ji for their invaluable help during the course of my PhD. The entire staff of instrumentation especially Asha has been very helpful and efficient in maintaining the facilities. Care taken by Ramesh in the canteen and Raju in hostel is deeply acknowledged. Joshi ji from finechem has been very helpful.

I would like to express my deep gratitude to Usha for her constant encouragement, steadfast support and without whom I would have struggled to find the inspiration and motivation needed to complete this thesis.

The episode of acknowledgement would not be complete without the mention of my friends Gudia, Sandeep and Rajdeep for always being there when I needed their help and company. My batchmates here in CCMB, Bony, Chandru, Sahu and Yamuna have been very helpful.

I would like to thank the little hurricane in my life, Shruti, who turned it upside down, for her boundless support, constant encouragement and care.

I cannot end without thanking my family I am grateful for my two brothers for rendering me the sense and the value of brotherhood. I am glad to be one of them. Above all I would like to acknowledge the tremendous sacrifices that my mom and dad made to ensure that I had an excellent education. For this and much more, I am forever in their debt.

I feel a deep sense of gratitude for my late father who formed part of my vision and taught me the good things that really matter in life. The happy memory of my father still provides a persistent inspiration for my journey in this life. His unflinching courage and conviction will always inspire me. **It is to him that I dedicate this work.**

DEVENDRA SINGH



# CONTENTS

<b>SYNOPSIS.....</b>	<b>i</b>
<b>PUBLICATIONS.....</b>	<b>vi</b>
<b>CHAPTER 1: INTRODUCTION</b>	
1.1 Proteins - The Fulcrum of Life.....	1
1.2 Protein folding in normal and stress conditions and need for chaperones.....	1
1.3 Multiple chaperone families.....	2
1.4 Small heat shock proteins (sHsps) family.....	3
1.4.1 Human sHsps.....	5
1.4.2 Small Hsp structure-function relationship.....	7
1.4.2.1 Oligomeric assemblies of human sHsps.....	7
1.4.2.2 Structural organization of sHsps.....	8
1.4.2.3 sHsps structure: Insights from the available sHsps crystal structures.....	11
1.4.2.4 Chaperone-like activity of sHsps.....	14
1.5 Protein misfolding diseases.....	17
1.6 Defective chaperones: Chaperonopathies.....	18
1.7 Genetic chaperonopathies.....	19
1.7.1 Mutation in mammalian sHsps and related chaperonopathies.....	20
1.7.1.1 sHsps and ischemia / reperfusion injury.....	20
1.7.1.1.1 $\alpha$ B-crystallin in cardiomyopathy / myopathy.....	22
1.7.1.1.2 $\alpha$ A- and $\alpha$ B-crystallin in hereditary cataracts.....	25
1.7.1.1.3 sHsps and neurological diseases.....	31
1.7.1.3.1 Hsp22 and Hsp27 in inherited peripheral neuropathies.....	31
1.8 Scope of the present study.....	35
<b>CHAPTER 2: A CATARACT-CAUSING MUTATION IN CLASS II sHSP, <math>\alpha</math>-CRYSTALLIN</b>	
2.1 INTRODUCTION.....	37
2.2 EXPERIMENTAL PROCEDURES.....	39
2.2.1 Materials.....	39

2.2.2	Creating the mutant of $\alpha$ A-crystallin.....	40
2.2.3	Expression and purification of the wild type and G98R mutant protein.....	41
2.2.4	Circular dichroism studies.....	41
2.2.5	Steady-state fluorescence studies.....	42
2.2.6	Time-resolved fluorescence studies.....	42
2.2.7	FPLC gel permeation chromatography.....	43
2.2.8	Dynamic light scattering studies.....	43
2.2.9	Proteolysis of the wild type and the mutant $\alpha$ A-crystallin by proteinase K.....	43
2.2.10	Thermal aggregation of wild type and G98R mutant protein.....	44
2.2.11	Chaperone assay.....	44
2.3	RESULTS AND DISCUSSION.....	45
2.3.1	Structural insights from the crystal structure of <i>M. jannaschii</i> Hsp16.5 and <i>T. aestivum</i> Hsp16.9.....	45
2.3.2	Cloning, expression and purification of mutant G98R $\alpha$ A-crystallin.....	47
2.3.3	Study of conformational change in mutant $\alpha$ A-crystallin.....	49
2.3.3.1	Secondary structural propensities.....	49
2.3.3.2	Secondary and tertiary structure analyses using circular dichroism.....	50
2.3.3.3	Steady-state fluorescence studies to analyze structure and surface hydrophobicity.....	51
2.3.3.4	Quaternary structural studies.....	53
2.3.4	Studies on the stability of the wild type and G98R $\alpha$ A-crystallin.....	54
2.3.4.1	Thermal stability.....	55
2.3.4.2	Urea-induced denaturation studies of $\alpha$ A- and G98R $\alpha$ A-crystallin.....	56
2.3.4.2.1	Equilibrium urea-unfolding studies.....	56
2.3.4.2.2	Intermediate states in the urea-induced unfolding of the wild type and the mutant $\alpha$ A-crystallin.....	60
2.3.4.2.3	Structural differences and intermediate states in the urea-induced unfolding of the $\alpha$ A- and G98R $\alpha$ A-crystallin probed by limited proteolysis.....	63
2.3.5	Chaperone-like activity of the wild type and G98R $\alpha$ A-crystallin.....	65
2.4	CONCLUSION.....	68

## CHAPTER 3: MIXED OLIGOMER FORMATION: CATARACTOGENESIS

3.1 INTRODUCTION.....	70
3.2 EXPERIMENTAL PROCEDURES.....	70
3.2.1 Materials.....	70
3.2.2 Fluorescent labeling of $\alpha$ A-crystallin and its mutant for subunit exchange studies using fluorescence resonance energy transfer (FRET).....	71
3.2.3 Preparation of mixed oligomers from homo-oligomers of wild type $\alpha$ A-crystallin and G98R $\alpha$ A-crystallin.....	71
3.2.4 Circular dichroism studies.....	72
3.2.5 Fluorescence studies.....	72
3.2.6 Dynamic light scattering studies.....	72
3.2.7 Thermal stability.....	72
3.2.8 Proteolysis of the different $\alpha$ A-crystallins by proteinase K.....	73
3.2.9 Chaperone assay.....	73
3.2.10 Cloning and co-expression of $\alpha$ A-crystallin and G98R $\alpha$ A-crystallin in pETDuet-1 vector.....	73
3.3 RESULTS AND DISCUSSION.....	74
3.3.1 Effect of G98R mutation on the subunit exchange of $\alpha$ A-crystallin.....	74
3.3.2 Study of conformational change in the mixed-oligomers of the wild type and mutant $\alpha$ A-crystallin.....	76
3.3.2.1 Secondary and tertiary structure analyses using circular dichroism.....	77
3.3.2.2 Characterization of the tertiary structure and surface hydrophobicity of mixed oligomers using fluorescence.....	78
3.3.2.3 Characterization of the quaternary structure of mixed oligomers.....	79
3.3.3 Comparative stability of $\alpha$ A-, G98R $\alpha$ A-crystallin and mixed oligomers.....	79
3.3.3.1 Thermal stability.....	80
3.3.3.2 Stability towards urea-induced unfolding.....	81
3.3.3.3 Structural stability probed by limited proteolysis.....	81
3.3.4 Chaperone-like activity of mixed oligomers.....	84
3.3.5 Co-expression of the $\alpha$ A- and G98R $\alpha$ A-crystallin in <i>E.coli</i> .....	86
3.4 CONCLUSION.....	87

## CHAPTER 4: METAL IONS: PRESENILE CATARACTOGENESIS

4.1 INTRODUCTION.....	89
4.2 EXPERIMENTAL PROCEDURES.....	92
4.2.1 Materials.....	92
4.2.2 Purification of $\alpha$ A-crystallins and exchange of buffer.....	92
4.2.3 Metal-binding studies.....	92
4.2.4 Fluorescence spectroscopic analysis.....	93
4.2.5 Isothermal titration calorimetry.....	93
4.2.6 Effect of $\alpha$ A- and G98R $\alpha$ A-crystallin on the ascorbate-mediated Cu <sup>2+</sup> -catalyzed generation of ROS.....	93
4.2.7 Estimation of ascorbate consumption.....	94
4.2.8 Metal ions-induced self-aggregation of $\alpha$ -crystallins and its reversibility.....	95
4.2.9 Chaperone assay.....	95
4.2.10 Circular dichroism.....	95
4.2.11 Dynamic light scattering.....	96
4.2.12 Effect of Cu <sup>2+</sup> on the thermal stability of $\alpha$ A- and G98R $\alpha$ A-crystallin.....	96
4.3 RESULTS AND DISCUSSION.....	96
4.3.1 Binding of Cu <sup>2+</sup> to $\alpha$ A- and G98R $\alpha$ A-crystallin.....	96
4.3.1.1 Studies using fluorescence spectroscopy.....	96
4.3.1.2 Studies using isothermal titration calorimetry.....	97
4.3.2 Redox-silencing of Cu <sup>2+</sup> by $\alpha$ A- and G98R $\alpha$ A-crystallin.....	99
4.3.2.1 Inhibition of ROS generation by $\alpha$ A-crystallins using fluorescein probe...	100
4.3.2.2 Studies on inhibition of OH <sup>•</sup> generation by $\alpha$ A- and G98R $\alpha$ A-crystallin using another fluorescent probe, 3-CCA.....	101
4.3.2.3 $\alpha$ A- & G98R $\alpha$ A-crystallin prevents Cu <sup>2+</sup> -induced oxidation of ascorbate..	102
4.3.3 Cu <sup>2+</sup> -induced self-aggregation of $\alpha$ A- and G98R $\alpha$ A-crystallin and their mixed oligomer.....	103
4.3.3.1 G98R $\alpha$ A-crystallin exhibits increased propensity to Cu <sup>2+</sup> -induced self-aggregation .....	104
4.3.3.2 Effect of mixed-oligomer formation on the self-aggregation .....	105
4.3.3.3 Reversibility of the Cu <sup>2+</sup> -binding and induced aggregation of $\alpha$ A-, G98R $\alpha$ A-crystallin and their mixed oligomers.....	106
4.3.4 Cu <sup>2+</sup> -induced conformational changes in $\alpha$ A- and G98R $\alpha$ A-crystallin.....	107

4.3.4.1 Cu <sup>2+</sup> -induced secondary and tertiary structural changes.....	107
4.3.4.2 Cu <sup>2+</sup> -induced quaternary structural changes.....	108
4.3.5 Effect of Cu <sup>2+</sup> -binding on thermostability of $\alpha$ A- and G98R $\alpha$ A-crystallin.....	109
4.3.6 Effect of Cu <sup>2+</sup> on the chaperone-like activity of wild type $\alpha$ A-crystallin and the mutant G98R $\alpha$ A-crystallin.....	110
4.3.7 Effect of Zn <sup>2+</sup> , Cd <sup>2+</sup> and Ca <sup>2+</sup> on self-aggregation and chaperone-like activity of $\alpha$ A- and G98R $\alpha$ A-crystallin.....	112
4.4 CONCLUSIONS.....	114
<b>CHAPTER 5: A DISEASE-CAUSING MUTATION IN CLASS I sHSP, HSP22</b>	
5.1 INTRODUCTION.....	116
5.2 EXPERIMENTAL PROCEDURES.....	121
5.2.1 Materials.....	121
5.2.2 Creating the K141N and K141E mutants of Hsp22.....	121
5.2.3 Expression and purification of the wild type, K141N and K141E Hsp22.....	122
5.2.4 Circular dichroism spectroscopy.....	123
5.2.5 Fluorescence studies.....	123
5.2.6 FPLC gel permeation chromatography.....	123
5.2.7 Glycerol density gradient centrifugation .....	124
5.2.8 Isolation and purification of native zeta-crystallin from guinea pig lens.....	124
5.2.9 Assay for chaperone-like activity.....	124
5.3 RESULTS AND DISCUSSION.....	125
5.3.1 Cloning, expression and purification of mutant Hsp22.....	125
5.3.2 Study of conformational change in K141NHsp22 and K141EHsp22.....	127
5.3.2.1 Secondary and tertiary structure analyses using circular dichroism.....	127
5.3.2.2 Fluorescence studies to analyze structure and surface hydrophobicity...	128
5.3.2.3 Quaternary structural studies.....	130
5.3.3 Changes in chaperone activity of Hsp22 upon K141N/E mutation.....	133
5.4 CONCLUSIONS.....	135
<b>CHAPTER 6: CONCLUDING REMARKS.....</b>	<b>138</b>
<b>BIBLIOGRAPHY.....</b>	<b>141</b>

---

## SYNOPSIS

How proteins fold to their native conformation remains a major quest in biology. Despite the fact that the amino acid sequence of a protein has the information for native fold, many proteins *in vivo* need the assistance of molecular chaperones for folding and maturation. One such specialized group of molecular chaperones is heat shock proteins (Hsps), which get selectively upregulated under diverse physiological stresses. In addition to conferring stress-tolerance by preventing the aggregation of misfolded proteins formed as a result of stress, they play a crucial role in the folding of nascent polypeptides and protein quality control under normal physiological conditions. Protein misfolding and aggregation eventually lead to disruption of cellular processes, cytotoxicity and cell death. Mutations or other modifications in Hsps can render them dysfunctional, leading to disease.

**Chapter 1** discusses (i) the protein folding problem and the need for Hsps in protein folding under normal and stress conditions, (ii) multiple chaperone families with a focus on human small heat shock proteins (sHsps), their structural organization and function and (iii) pathology caused due to various point mutations in sHsps. Hsps, apart from their well known chaperoning role, participate in different cellular functions such as apoptosis, differentiation, vesicular trafficking and cell motility. Hsps are categorized into different classes based on their monomer molecular weights as Hsp100, Hsp90, Hsp70, Hsp60 and sHsps.

The sHsps have monomeric molecular mass in the range of 12-43 kDa and form a distinct subgroup of the Hsp family having a characteristic highly conserved ~90 amino acids-long sequence, 'α-crystallin domain'. This domain is flanked by an N-terminal domain and a C-terminal extension, which show significant sequence and size variation among different sHsps. The α-crystallin domain adopts an immunoglobulin-like fold - a compact β-sheet sandwich made of two anti-parallel β-sheets. *In vivo* and *in vitro*, sHsps form large homo- or hetero-oligomeric complexes, which are dynamic in nature due to frequent exchange of subunits. sHsps exhibit chaperone activity in preventing the aggregation of denatured proteins by binding to the exposed hydrophobic surfaces. They work in an ATP-independent manner and refold the bound substrates either independently or in concert with other Hsps. Large oligomeric structure, exposed hydrophobic surfaces and rapid subunit exchange are believed to be important for the chaperone activity of sHsps.

---

---

Genome exploration based on sequence homology has led to the identification of ten human sHsps, which are further subcategorized depending on their expression pattern, stress-inducibility and the nature of oligomeric complexes they form *in vivo* into two classes. HspB1, HspB5, HspB6 and HspB8 are classified into class I as they show expression in wide variety of tissues. Class II members, HspB2, HspB3, HspB4, HspB7, HspB9 and HspB10, show restricted expression in specific tissues. Hsp22 (HspB8), a class I member, is stress-inducible chaperone and is widely expressed in several tissues such as the brain, spinal cord, lung, kidney, liver, stomach, skeletal and cardiac muscle. On the other hand,  $\alpha$ A-crystallin (HspB4), a class II member, does not show stress-inducibility and its expression is almost restricted to ocular tissues with trace amounts present in spleen, thymus, liver and kidney.  $\alpha$ A-crystallin exhibits  $\beta$ -sheet structure and forms high molecular weight polydisperse oligomers whereas Hsp22 is unique in having predominantly random coiled secondary structure and a monomeric quaternary structure *in vitro*. Thus,  $\alpha$ A-crystallin and Hsp22 clearly represent the diversity of the sHsp family.

A large number of missense mutations have been identified in sHsps including  $\alpha$ B-crystallin, Hsp27,  $\alpha$ A-crystallin and Hsp22. Although these mutations span the entire sequence of different sHsps, nearly 80% of those present in the  $\alpha$ -crystallin domain are present in the  $\beta$ 5- $\beta$ 7 region. The importance of this region is further highlighted by the fact that five mutations have been reported in this region in Hsp27 which cause motor neuropathy. Mutations in  $\alpha$ A-crystallin have been associated with cataracts whereas mutations in Hsp22 resulted in neuropathy. Of all the cataract-causing mutations in  $\alpha$ -crystallins, G98R mutation in  $\beta$ 5 strand of  $\alpha$ A-crystallin is unique as it causes presenile cataract. Further, in all the missense mutations in  $\alpha$ A-crystallin, arginine is replaced by other amino acids, whereas in this mutation glycine is replaced by arginine. K141N/E mutations in  $\beta$ 7 strand of Hsp22 are involved in CMT2 or dHMN disorders. This residue is highly conserved and mutation at the homologous residues in Hsp27,  $\alpha$ A- and  $\alpha$ B-crystallin have been associated with pathology. The present study was initiated with a broad objective of elucidating the consequences of these mutations on the structure and function of human  $\alpha$ A-crystallin and Hsp22, and to understand the molecular basis of the pathologies caused by these mutations.

**Chapter 2** describes our investigations on the effect of G98R mutation on the structure, stability and function of  $\alpha$ A-crystallin. We created the G98R mutation in  $\alpha$ A-

---

---

crystallin by site-directed mutagenesis. Interestingly, the mutant protein was found to partition exclusively into inclusion bodies unlike wild type  $\alpha$ A-crystallin and other reported point mutants of  $\alpha$ -crystallins. Lowering the temperature and/or inducer concentration did not result in better yield of soluble protein suggesting that G98R $\alpha$ A-crystallin is inherently aggregation-prone. The mutant protein, refolded from inclusion bodies, showed significant changes in the secondary and tertiary structure as seen by far- and near-UV circular dichroism (CD) as well as tryptophan fluorescence. Gel-filtration chromatography and dynamic light scattering (DLS) studies showed that G98R $\alpha$ A-crystallin forms large oligomers. The mutant protein when preincubated at 37°C for 3.5 h formed much larger oligomers. Thermal stability of the mutant  $\alpha$ A-crystallin, in terms of self-aggregation, is compromised significantly. G98R $\alpha$ A-crystallin protein is more susceptible to heat-induced aggregation compared to the wild type protein. Urea-induced unfolding studies showed that the tryptophan in the mutant protein is completely solvent-exposed at lower concentration of urea compared to the wild type protein. Limited proteinase K digestion of the wild type and mutant  $\alpha$ A-crystallin shows that (i) the mutant protein is more susceptible to proteolysis and (ii) its digestion pattern is distinctly different, indicating that the folded structure of the mutant protein is less compact. Interestingly, the mutant protein exhibits aggregation during initial stages of proteolysis. This result assumes significance in the physiological context of eye lens and cataract as activation of proteases with age has been observed.

**Chapter 2** further explores the effect of mutation on functional properties of  $\alpha$ A-crystallin. Despite showing increased bis-ANS binding compared to wild type  $\alpha$ A-crystallin, the mutant protein exhibits complete loss of chaperone activity with insulin as substrate. Although the mutant protein has the target protein binding ability, its complex with the insulin B-chain is aggregation-prone. However, it shows increased protection with another substrate, citrate synthase, thereby exhibiting a substrate-dependent loss of activity.

The folding defects as well as drastic differences in the structure and stability of the mutant protein would be expected to result in congenital cataract. One possibility for the observed presenile phenotype could be that the wild type  $\alpha$ A-crystallin (from another allele) or  $\alpha$ B-crystallin could influence the property of the mutant protein as sHsps exchange their subunits. **Chapter 3** describes our investigations on the properties of the mixed oligomers formed between  $\alpha$ A- and G98R $\alpha$ A-crystallin in relation to those of their homo-oligomers. Fluorescence resonance energy transfer (FRET) studies demonstrate the exchange of

---



---

subunits between the wild type and mutant protein. Mixed oligomers, thus formed, exhibit properties dominated by those of the mutant protein in structural aspects, oligomeric size, chaperone-like activity and urea-induced unfolding. However, mixed oligomer formation leads to a decreased propensity to aggregate (as a function of temperature or upon proteolysis) as compared to the homo-oligomers of the mutant protein. The co-expression of the G98R $\alpha$ A-crystallin along with the wild type protein results in prevention of inclusion body formation of the mutant protein – both the mutant and the wild type protein are expressed predominantly in the soluble form, probably due to the mixed oligomer formation.

Since the wild type protein rescues the mutant subunits from aggregation and insolubilization, it can be a balancing factor, which prevents congenital cataract. However, an important question arises – once congenital cataract is prevented, what ensues that leads to the onset of presenile cataract? It is possible that the effectiveness of the balancing factor is susceptible to age-related modifications or other environmental factors triggering their aggregation. **Chapter 4** describes our investigations on the effect of one such environmental risk factor, metal ions, on the properties of the mutant protein and its mixed oligomers. Being a component of oxidative stress,  $\text{Cu}^{2+}$  represents a risk in terms of both structural destabilization and functional failure. Using isothermal titration calorimetry (ITC) and fluorescence spectroscopy, we have shown that both the wild type and mutant proteins bind  $\text{Cu}^{2+}$  selectively with picomolar affinity, exhibit redox-silencing and inhibit ROS generation. However, binding of  $\text{Cu}^{2+}$  promotes the self-aggregation of mutant protein and its mixed oligomers.  $\text{Cu}^{2+}$  has an adverse effect on the chaperone-like activity of G98R $\alpha$ A-crystallin, while it increases the chaperone-like activity of wild type  $\alpha$ A-crystallin. Other heavy metal ions such as  $\text{Cd}^{2+}$  and  $\text{Zn}^{2+}$ , which are also known to accumulate in the lens with age, have a similar effect on the self-aggregation propensities and chaperone-like activity of G98R $\alpha$ A-crystallin and its mixed oligomers. Thus, our study suggests how environmental factors can augment the effects of G98R mutation and influence the manifestation of presenile phenotype.

**Chapter 5** describes the results of the studies performed to elucidate the role of K141N/E mutations in Hsp22, a class I sHsp, in neuromuscular disorders. The desired mutation was generated and proteins were overexpressed in an *E. coli* host system. Unlike G98R $\alpha$ A-crystallin, both K141NHsp22 and K141EHsp22 are expressed in the soluble fraction. Proteins were purified to homogeneity in order to study their structural and

---

functional changes compared to the wild type Hsp22. Far-UV CD indicates a randomly coiled structure for both K141NHsp22 and K141EHsp22 similar to Hsp22. However, they exhibit increased secondary structural unfolding compared to the wild type. Near-UV CD and intrinsic fluorescence also showed structural changes. K141NHsp22, which is involved in both CMT and dHMN, has a more pronounced effect on the structural destabilization compared to K141EHsp22. Quaternary structure analysis by glycerol density gradient centrifugation and gel filtration chromatography show that both the mutants, like wild type Hsp22, exist as a monomer *in vitro*. Attempts were made to understand the effect of mutation on the chaperone-like activity of Hsp22 using citrate synthase and zeta-crystallin as target proteins. Interestingly, K141NHsp22 showed enhanced chaperone-like activity with a few model substrates, whereas K141EHsp22 showed substrate-dependent changes in chaperone-like activity. Taken together fluorescence, circular dichroism, gel filtration studies and chaperone assays clearly demonstrate that K141N/E mutations in Hsp22 cause subtle conformational changes but alter the chaperone activity of Hsp22.

**Chapter 6** concludes the thesis by briefly pointing out findings of our study with two mutations in the  $\beta$ 5- $\beta$ 7 region of class I (Hsp22) and class II ( $\alpha$ A-crystallin) small heat shock proteins.

---

## PUBLICATIONS

**Singh D**, Raman B, Ramakrishna T, Rao CM. The cataract-causing mutation G98R in human  $\alpha$ A-crystallin leads to folding defects and loss of chaperone activity. *Mol Vis* (2006) 12:1372-1379.

**Singh D**, Raman B, Ramakrishna T, Rao CM. Mixed oligomer formation between human  $\alpha$ A-crystallin and its cataract-causing G98R mutant: Structural, stability and functional differences. *J Mol Biol* (2007) 373:1293-1304.

Ahmad F, \* **Singh D**, \* Taiyab A, Ramakrishna T, Raman B, Rao CM. Selective  $\text{Cu}^{2+}$  binding, redox silencing and cytoprotective effects of the small heat shock proteins,  $\alpha$ A- and  $\alpha$ B-crystallin. *J Mol Biol* (2008) 382:812-824.

\*Contributed equally

# INTRODUCTION

1

## 1.1 Proteins - The Fulcrum of Life:

Proteins (from the Greek *proteios*, meaning "primary") are the primary agents that carry out all biological functions. The fact that proteins are a diverse and abundant class of biomolecules, reflects the central role of proteins in virtually all aspects of cell structure and function: there are structural, catalytic, transport, storage, regulatory and immune system proteins. Like the Greek sea god Proteus, who could assume different forms, proteins bring versatility by folding to different conformations. Folding proteins to their specific conformation and maintaining them is critical for cell survival. Molecular chaperones and heat shock proteins (Hsps) assist proteins in proper folding, assembly, localization and also degradation. It is becoming increasingly evident that numerous diseases having different symptoms and aetiologies may have in common, a perturbation of protein conformation due to mutations, post-translational modifications or environmental factors.

## 1.2 Protein folding in normal and stress conditions and need for chaperones:

Protein folding is a very rapid multistep process of conformational fluctuation yielding transition states of lower free energy and finally, stable and functional three-dimensional structure (Ellis and Hartl, 1999). Protein folding *in vivo* is very complex due to the 'crowded' cellular environment resulting from enormously high concentration (300-400 mg/ml) of cytosolic macromolecules including proteins and nucleic acids (Goodsell, 1991; Minton, 1997). Such crowding can favor non-productive folding and lead to non-specific association of macromolecules (Ellis and Hartl, 1999). Further, due to the vectorial nature of translation (from N- to the C-terminus), complete folding domains do not emerge from the ribosomal exit site at once. These premature newly synthesized (nascent) polypeptides expose significant amount of their hydrophobic residues, which can lead to their non-specific aggregation resulting in loss of functional protein or cytotoxicity. Thus, folding not only allows the production of functional structure but also prevents inappropriate interactions between proteins.

Although the primary structure or the amino acid sequence of a polypeptide chain contains the information that determines the native three-dimensional structure of the functional protein (Anfinsen, 1973), many proteins do not fold spontaneously *in vivo* and their folding requires the assistance of a pre-existing machinery of a specialized group of proteins called 'molecular chaperones' (Ellis, 1987; Craig, 1993; Bukau *et al.*, 2000; Hartl and Hayer-Hartl, 2002; Deuerling and Bukau, 2004). Chaperones are defined as "a family of

---

cellular proteins which mediate the correct folding of other polypeptides, and in some cases their assembly into oligomeric structure, but which are not components of the final functional structures" (Ellis, 1987). Molecular chaperones transiently bind to the exposed hydrophobic regions of nascent polypeptide chain, prevent off-pathway folding reactions that lead to their deleterious aggregation and facilitate the correct folding of non-native proteins through regulated binding and release *in vivo*. Chaperoning occurs both co-translationally and post-translationally (Bukau *et al.*, 2000). Even under optimal conditions, besides spontaneous unfolding of proteins due to their conformational flexibility, the rapid biogenesis of proteins in a growing cell puts a high pressure on the protein folding machinery.

Further, various stress conditions cause modifications of the intracellular milieu and pose a serious threat to the integrity of the fully functional and properly folded proteins. Stress conditions, such as a sudden increase in temperature, not only interfere with normal protein synthesis machinery but also cause unfolding or partial denaturation of many folded proteins. Protein quality control under such unfavorable conditions becomes very crucial for cell viability. In order to combat stress, cells generally up-regulate the expression of stress proteins including chaperones, which are either not expressed or are weakly expressed under non-stress conditions. Chaperones assist the damaged molecule to regain its functional conformation and direct damaged or abnormal polypeptides that have little chance for proper folding to the proteolytic machinery (Höhfeld *et al.*, 2001). Despite all the folding and degradation efforts, some misfolded proteins, considered dead-end products, end up in inclusion bodies in the cell. Certain chaperones of both prokaryotes and eukaryotes (ClpB and DnaK in *E.coli*; Hsp104, Hsp70 and Hsp40 in yeast) have been shown to help in the disaggregation and resolubilization of these aggregated proteins *in vivo*, directing them back to proper folding (Glover and Lindquist, 1998; Mogk *et al.*, 1999; Motohashi *et al.*, 1999).

### **1.3 Multiple chaperone families:**

The observation that nucleoplasmin supports histone assembly into nucleosome led to the concept of molecular chaperones (Laskey *et al.*, 1978; Ellis, 1987). Molecular chaperones assist the *de novo* folding of proteins. They prevent aggregation, help misfolded proteins to fold and facilitate the degradation of the proteins that cannot be helped. In addition, chaperones participate in diverse cellular functions such as signal transduction, apoptosis, vesicle formation and cellular transport (Muchowski and Wacker, 2005).

Molecular chaperones comprise several families of related proteins many of which show increased expression during heat shock [hence named as Heat shock proteins (Hsps)] and other proteotoxic stresses. Although Hsps do not have a common structural or mechanistic property; they are classified on the basis of their molecular masses into five major families. Table 1.1 summarizes the structure and function of multiple chaperone families with corresponding prokaryotic and eukaryotic members, as well as their co-chaperones. Several diversities between different members and families are probably responsible for differences in their substrate specificity, substrate handling and processing.




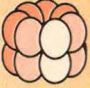

Recently, based on the Human Genome Organisation (HUGO) Gene Nomenclature Committee guidelines, a new nomenclature of the human HSP families, HSPH (HSP100), HSPC (HSP90), HSPA (HSP70), DNAJ (HSP40), and HSPB (small HSP) as well as for the human chaperonin families, HSPD/E (HSP60/HSP10) and CCT (TRiC) has been proposed (Vos *et al.*, 2008). Among all the chaperone families, the relatively less studied small heat shock proteins (sHsps) family is unique, as the members of this family exhibit chaperone activity independent of adenosine triphosphate (ATP). As a consequence, sHsps cannot promote the refolding of misfolded proteins into the native state by themselves and transfer them to the ATP-dependent Hsp60 or Hsp70 chaperones for refolding (Ehrnsperger *et al.*, 1997; Veinger *et al.*, 1998). Interestingly, there have been a few reports of ATP-binding to  $\alpha$ -crystallins and subsequent enhancement of substrate refolding yield (Muchowski and Clark, 1998; Biswas and Das, 2004; Ghosh *et al.*, 2006). However, the role of ATP in the regulation of chaperone activity of sHsps is still debatable.

#### **1.4 Small heat shock proteins (sHsps) family:**

sHsps are a widespread and diverse class of molecular chaperones with monomeric molecular masses of the members ranging from 12-43 kDa, a majority of them being between 14 and 27 kDa (Wistow, 1985). They are ubiquitously expressed throughout all kingdoms from archaea to humans except in some pathogenic bacteria such as *Mycoplasma genitalium* and *Helicobacter pylori* (Narberhaus, 2002). sHsps share some characteristic features such as presence of a highly conserved ~90 residue long ' $\alpha$ -crystallin domain' in their C-terminal domain (a qualifying feature for including new members into the sHsp family), formation of large oligomeric structures (~9 to 40 subunits), induction by stress conditions, and chaperone activity in preventing substrate aggregation through their exposed hydrophobic patches (Raman and Rao, 1994; Haslbeck *et al.*, 2005). While most of

the bound proteins are refolded with the assistance of ATP-dependent chaperones, in a few instances, sHsps have been shown to refold target proteins to their native states (Goenka *et al.*, 2001; Nath *et al.*, 2002; Kumar *et al.*, 2005). The number of sHsps has expanded from bacteria, archaea and single-celled eukaryotes (1-2 sHsps) to higher multicellular eukaryotes (4-19 sHsps), possibly due to their developmental and cell-specific function. To date, ten human sHsps have been identified. In contrast to plant sHsps, human

**Table 1.1:** Multiple chaperone families: Structure and functions (Mogk *et al.*, 2002)

Chaperone Family	Examples	Need for ATP	Co-chaperone	Function
<b>Hsp100</b> (6-7mer) 	ClpB (Prok) ClpA (Prok)	+		Disaggregation along with Hsp70 Protein unfolding for proteolysis by ClpP protease
	Hsp104 (Euk)			Thermotolerance Disaggregation with Hsp70
<b>Hsp90</b> (dimer) 	HtpG (Prok)	+	Hop, p23, CDC37	Tolerance to extreme heat shock
	Hsp90 (Euk)			Stress-tolerance Maintaining folding and stability of steroid hormone receptors, protein kinases etc.
<b>Hsp70</b> (monomer) 	DnaK (Prok)	+	DnaJ, GrpE  Hsp40, Hop, Bag1, Chip, HspBP1, Hip	<i>de novo</i> protein folding Prevention of protein aggregation Solubilization of protein aggregates Regulation of heat shock response
	Hsp70, Hsc70 (Euk)			<i>de novo</i> protein folding Prevention of protein aggregation Solubilization of protein aggregates Regulation of heat shock response Stabilizing transcription factors and kinases along with Hsp90
<b>Hsp60</b> (14/ 16mer) 	GroEL (Prok)	+	GroES  Hsp10, Prefoldin	<i>de novo</i> protein folding Prevention of protein aggregation
	Hsp60, CCT/ TRiC (Euk)			Mitochondrial protein folding <i>de novo</i> folding of actin and tubulin
<b>sHsps</b> (8-24mer) 	IbpA, IbpB (Prok)	?		Prevention of protein aggregation Binding to inclusion bodies
	HspB1-10 (Euk)			Prevention of protein aggregation Stabilization of cytoskeleton Possibly various cellular functions

Prok- Prokaryotic member; Euk- Eukaryotic member; ?- some members can bind ATP



---

(mammalian) sHsps do not localize to many cellular compartments and are restricted to the cytosol and the nucleus.

#### 1.4.1 Human sHsps:

A recent classification scheme, in accordance with the guidelines of HUGO nomenclature committee, named human sHsps as HspB1-HspB10 (Kappé *et al.*, 2003). Considering that orthologs of the ten human sHsps are present in mouse and rat, it is possible that these orthologs will also be present in all mammalian species. Table 1.2 lists the ten human sHsps and their tissue distribution. Overall, different human sHsps exhibit 20-55% sequence homology with each other.

Taylor and Benjamin (2005) further subcategorized mammalian sHsps into two classes based on their tissue expression, stress inducibility and *in vivo* oligomerization characteristics. Hsp27 (HspB1),  $\alpha$ B-crystallin (HspB5), Hsp20 (HspB6) and Hsp22 (HspB8) are classified into class I and show expression in a wide variety of tissues such as skeletal and cardiac muscle, liver, lung, kidney, retina, skin, placenta, uterus, breast, cervix, platelets and brain tissues. Myotonic dystrophy protein kinase binding protein (HspB2), HspL27 (HspB3),  $\alpha$ A-crystallin (HspB4), Cardio vascular Hsp (HspB7), HspB9 and Outer denser fiber protein 1 (HspB10) are categorized into class II and their expression is primarily restricted to ocular (Ile) or myogenic (IIm) or testicular (IIt) tissues. Class I members are predominantly heat-inducible and therefore, play a major role in cell survival under stress conditions. Class II members with tissue-restricted pattern of expression are likely to play a role in development, differentiation and other specialized tissue-specific functions.

Interestingly, all myogenic tissues show very high levels of expression of different sHsps. It is speculated that continuous exposure of muscle cells to oxidative insults and other physiological stresses warrants the recruitment of such high levels of different sHsps, which in turn confer stress tolerance (Sugiyama *et al.*, 2000). In addition to their well characterized chaperone activity in preventing the aggregation of unfolding proteins (Haslbeck and Buchner, 2002), sHsps are involved in a variety of cellular processes such as cytoskeletal rearrangements (Quinlan, 2002) and apoptosis (Arrigo *et al.*, 2002).

**Table 1.2:** Human sHsps: Nomenclature, characteristics and relative abundance

sHsps	Alternative Name	Inducibility	Mass (kDa)	Length (aa)	Chromosomal Location	Introns	Tissue Distribution	Class
HspB1	Hsp27	+	22.8	205	7p12.3	2 (Phase 1 & 2)	Ubiquitous	Class I
HspB2	MKBP	-	20.2	182	11q22-q23	1 (Phase 1)	Cardiac and skeletal muscle	Class II <sub>m</sub>
HspB3	HspL27	-	17.0	150	5q11.2	Intronless	Cardiac and skeletal muscle	Class II <sub>m</sub>
HspB4	$\alpha$ A-crystallin	-	19.9	173	21q22.3	2 (Phase 0)	Eye lens, spleen, thymus	Class II <sub>e</sub>
HspB5	$\alpha$ B-crystallin	+	20.2	175	11q22.3-q23.1	2 (Phase 0)	Ubiquitous	Class I
HspB6	Hsp20	-	16.8	157	19q13.13	2 (Phase 0)	Ubiquitous	Class I
HspB7	cvHsp	-	18.6	170	1p36.23-p34.3	2 (Phase 0 & 1)	Cardiac and skeletal muscle	Class II <sub>m</sub>
HspB8	Hsp22, H11 kinase	+	21.6	196	12q24.23	2 (Phase 1 & 2)	Ubiquitous	Class I
HspB9	None	-	17.5	159	17q21.2	Intronless	Testis	Class II <sub>t</sub>
HspB10	ODF1	-	30	262	8q22	1 (Phase 2)	Testis	Class II <sub>t</sub>

In HspB1 and HspB8 genes, two introns are present at the same position. HspB4, HspB5 and HspB6 genes have two phase 0 introns at identical positions. Phase 1, 2 and 0 introns interrupt codons after the first, second and third codon positions. Note that apart from head-to-head located HspB2 and HspB5 genes on chromosome 11, remaining all eight sHsp genes are dispersed on eight different chromosomes. aa – amino acids; kDa – kilodaltons

## 1.4.2 Small Hsp structure-function relationship:

### 1.4.2.1 Oligomeric assemblies of human sHsps:

Tendency to assemble into large, oligomeric complexes is one of the most notable features of the members of sHsps family (MacRae, 2000; Ganea, 2001; Narberhaus, 2002). However, the size of oligomeric assemblies formed by most mammalian sHsps is variable. For example, recombinant  $\alpha$ B-crystallin shows an oligomer size ranging from 400-800 kDa *in vitro*, whereas recombinant Hsp20 forms only dimers or tetramers. Multimeric quaternary structure is considered a structural prerequisite of sHsps for their chaperone function (Kato *et al.*, 1994; van de Klundert *et al.*, 1998). However, studies from our laboratory provided results contradicting this hypothesis - monomeric Hsp22 exhibits chaperone activity (Chowdary *et al.*, 2004), whereas highly oligomeric mutants of  $\alpha$ -crystallins (R116CaA-crystallin and R120GaB-crystallin) completely lack chaperone activity (Kumar *et al.*, 1999). This signifies that the correlation between oligomeric status and chaperone activity is different for individual sHsps.

Since many sHsps, with an inherent tendency to assemble into higher-oligomeric structures, occur in the same cell, they can form hetero-oligomeric complexes or mixed oligomers. Indeed, many studies describe such mixed sHsps complexes, for example complexes containing  $\alpha$ B-crystallin/Hsp20 (Pipkin *et al.*, 2003), Hsp27/Hsp20 (Bukach *et al.*, 2004), Hsp27/ $\alpha$ B-crystallin (Fu and Liang, 2003) etc. The formation of hetero-oligomeric assemblies by mammalian sHsps has been extensively studied both *in vivo* and *in vitro* using yeast two-hybrid or other fluorescence-based assays. Using these techniques, Hsp22 was shown to form high molecular mass complexes in the heart in association with Hsp27, Hsp20, cvHsp, MKBP and  $\alpha$ B-crystallin (Sun *et al.*, 2004; Fontaine *et al.*, 2005). Hsp27 exchanges its subunits with  $\alpha$ A- and  $\alpha$ B-crystallin (Bova *et al.*, 2000). In the muscle, presence of two distinct types of oligomeric complexes of sHsps was shown: one type of complex consists of Hsp27,  $\alpha$ B-crystallin and Hsp20, while MKBP and HspB3 form another type of complex (Sugiyama *et al.*, 2000). It appears that the hetero-oligomerization is not merely an interaction between structurally related sHsps - it can offer an opportunity to take advantage of different properties of various sHsps; it could be a means of tailoring their properties according to specialized requirements. Native  $\alpha$ -crystallin isolated from the eye lens, which is composed of closely related  $\alpha$ A- and  $\alpha$ B-crystallin subunits in a 3:1 ratio, is more thermostable and compact than either of the homo-oligomers (Sun and Liang, 1998;

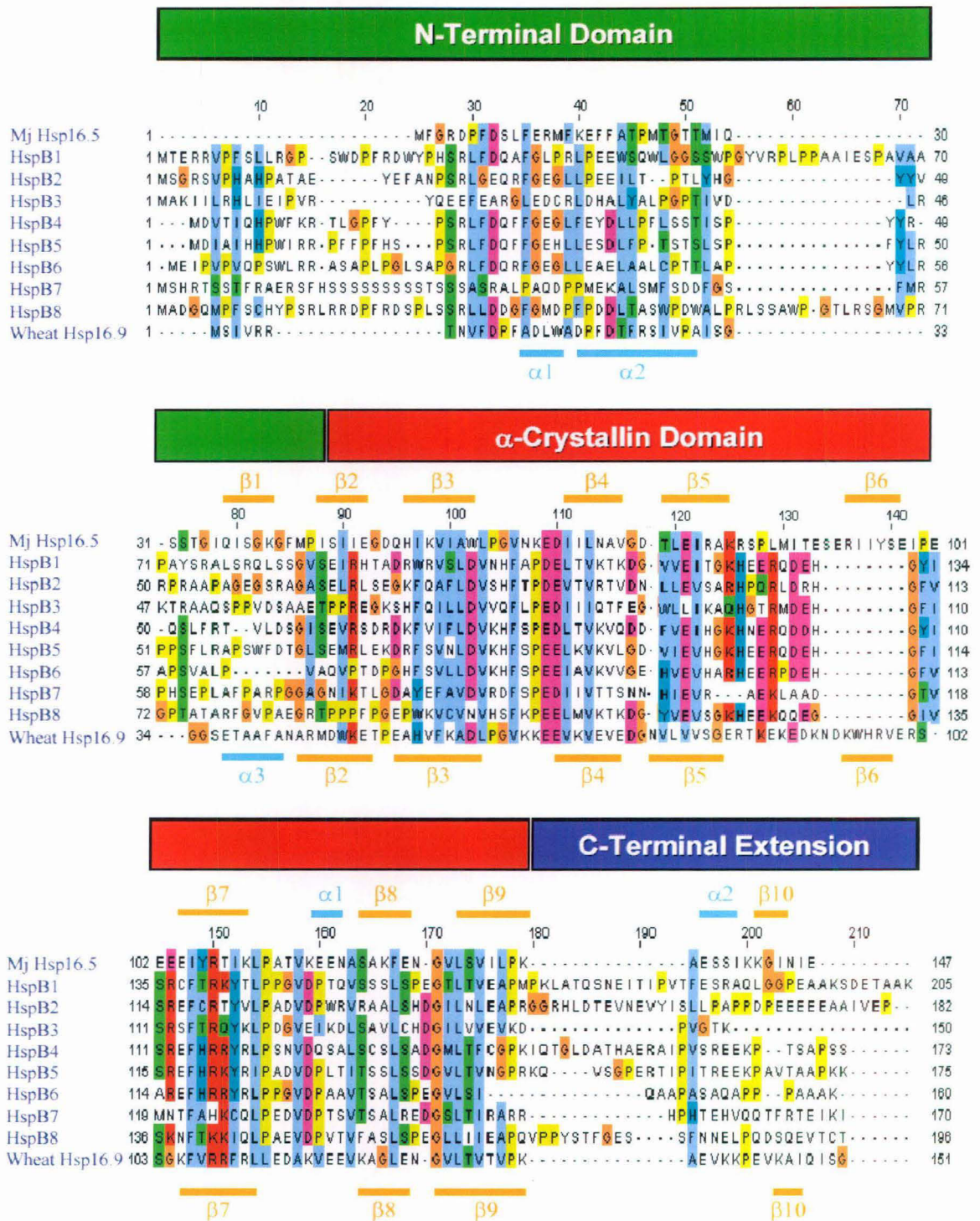
Datta and Rao, 1999). Apart from the structural and stability changes, altered subunit composition can provide broader functional specificity to these sHsp complexes.

Unlike *Methanococcus jannaschii* Hsp16.5, which forms monodisperse spherical oligomers of 24 subunits, various members of the mammalian sHsp family such as  $\alpha$ B-crystallin and Hsp27 show a high degree of heterogeneity in the quaternary structure (Haley *et al.*, 2000). Increase in temperature induces structural transitions in sHsp complexes (Raman and Rao, 1997; Datta and Rao, 1999). Temperature (stress)-induced transition in  $\alpha$ A-crystallin is clearly reflected in the observation that  $\alpha$ A-crystallin is a poor chaperone and has less exposed hydrophobic surface than  $\alpha$ B-crystallin at 25°C, compared to at 37°C (Sun *et al.*, 1997; Datta and Rao, 1999). Subunit exchange is affected profoundly by temperature and is more rapid at higher temperature in  $\alpha$ A-crystallin (Bova *et al.*, 1997). Besides temperature, oligomerization of many sHsps can be influenced by various modifications including phosphorylation. Phosphorylation in response to various stimuli is often associated with reduction in oligomeric size of sHsps complexes (Kato *et al.*, 1994; Ahmad *et al.*, 2008a). Thus, plasticity of the oligomeric complexes should be functionally important for recognizing and binding diverse substrate proteins under different physiological conditions.

#### 1.4.2.2 Structural organization of sHsps:

Despite their sequence diversity sHsps have a conserved structural organization; an N-terminal domain followed by the  $\alpha$ -crystallin domain and a C-terminal extension. Most sHsps are thought to have either a two- (Wistow, 1985; Merck *et al.*, 1992; Carver and Lindner, 1998) or three-domain structure (Augusteyn, 1998). The sequence alignment of the eight closely related human sHsps (HspB1-B8) along with *M. jannaschii* Hsp16.5 and *T. aestivum* Hsp16.9, whose crystal structures are known, is shown in Figure 1.1. Recognizable sequence conservation can be seen only in the 80-100 amino acid long,  $\alpha$ -crystallin domain. The  $\alpha$ -crystallin domain is engaged in extensive inter-subunit contacts as revealed by yeast two-hybrid studies (Boelens *et al.*, 1998; Liu and Welsh, 1999); further, residues 57-157 of human  $\alpha$ B-crystallin comprising of essentially the  $\alpha$ -crystallin domain form a dimer (Feil *et al.*, 2001). Site directed spin labeling and electron paramagnetic resonance (EPR) studies indicate that subunit interactions in this domain resulted in formation of dimers or tetramers in mammalian sHsps, which may represent the basic unit for building oligomeric structures (Berengian *et al.*, 1999). Two regions, F-X-R-polar-aromatic-X-L-P and polar-G-V-L-polar-aliphatic-P-basic within this core in the human sHsps,





**Figure 1.1: Sequence alignment of human sHsps HspB1-B8.** Sequence alignment of human sHsps, *M. jannaschii* Hsp 16.5 and *T. aestivum* (wheat) Hsp 16.9 was done using web-based software ClustalW (<http://www.ebi.ac.uk/Tools/clustalw2/index.html>). Secondary structural elements,  $\beta$ -strand (orange) and  $\alpha$ -helix (cyan), detected in crystal structure of *M. jannaschii* Hsp 16.5 and *T. aestivum* Hsp 16.9 are also shown on the top and the bottom of the alignment adjacent to their corresponding sequences. Positions of different domains of sHsps are shown.

corresponding to  $\beta$ 7- and  $\beta$ 9-strands of Hsp16.5 and Hsp16.9, are highly conserved.

The N-terminal domain and the C-terminal extension, flanking the  $\alpha$ -crystallin domain, are highly variable in both sequence and length. The N-terminal region varies from just 24 residues in *C. elegans* Hsp12.2 (Candido, 2002) to 247 residues in *S. cerevisiae* Hsp42p (Wotton *et al.*, 1996). Similarly, C-terminal extension is virtually absent (only one or two residues) in a family of four *C. elegans* sHsps and it is as long as 49 residues in *Artemia* P26 and *Drosophila* Hsp27 (de Jong *et al.*, 1998). N-terminal domain is hydrophobic and provides important interaction sites for sHsps oligomerization, whereas C-terminal extension is polar in nature. Studies from our laboratory showed that swapping the N-terminal domains or C-terminal extensions between  $\alpha$ A- and  $\alpha$ B-crystallin affected oligomeric size, hydrophobicity and chaperone-like activity of the chimeras, suggesting that variability in length and sequence of these regions provides variety in structural organization and chaperone function (Kumar and Rao, 2000; Pasta *et al.*, 2002). In a similar study using chimeric proteins of Hsp12.2 and  $\alpha$ B-crystallin, N-terminal domain and C-terminal extension was shown to be required for the formation of oligomers and modulation of chaperone activity respectively (Kokke *et al.*, 2001).

The N-terminal domain is required for higher order structure formation. The N-terminal region was found to be an important determinant of aggregate size of  $\alpha$ A-crystallin (Yang *et al.*, 2005). Truncation of the first 63 residues, but not the first 19 residues of N-terminal domain of  $\alpha$ A-crystallin, results in drastic reduction of size to dimer and tetramers (Merck *et al.*, 1992; Bova *et al.*, 2000). Being hydrophobic, the N-terminal domain is believed to be sequestered in the interior of the complex. Interestingly, the N-termini of certain sHsps can be remarkably insensitive to sequence extensions. For example, addition of 42 kDa maltose-binding protein (MBP) to the N-terminal of  $\alpha$ B-crystallin did not disrupt its oligomeric assembly and chaperone activity (Muchowski *et al.*, 1997).

Poorly conserved C-terminal extensions do not participate directly in oligomerization. Due to the high distribution of charged residues, they are believed to play a role as solubilizer for relatively hydrophobic sHsps as well as their complexes with substrates. Deletion of last 17 residues from the C-terminal extension of human  $\alpha$ A-crystallin results in its precipitation (Andley *et al.*, 1996). However, a study from our laboratory showed that in addition to their solubilizer function, C terminal extensions of  $\alpha$ A- and  $\alpha$ B-crystallin play a crucial role in long range interactions affecting their structure and chaperone function (Pasta *et al.*, 2002). Proton nuclear magnetic resonance ( $^1$ H-NMR) and deuterium exchange

experiments on  $\alpha$ -crystallin and Hsp25 suggest that the C-terminal extensions are flexible and solvent-exposed (Carver and Lindner, 1998). Immobilization by introducing a hydrophobic residue, tryptophan, in the C-terminal extension of bovine  $\alpha$ A-crystallin reduced its stability and chaperone-like activity (Smulders *et al.*, 1996).

A few small pockets of conserved sequence are seen in mammalian sHsps such as SRLFDQXFG in the N-terminal domain and the IXI/V motif in the C-terminal extension. Our laboratory has shown that the SRLFDQXFG region in  $\alpha$ A- and  $\alpha$ B-crystallin is important in their higher order oligomerization (Pasta *et al.*, 2003). Crystal structures of bacterial Hsp16.5 and wheat Hsp16.9 show that IXI/V motif makes inter-subunit contacts (Kim *et al.*, 1998; van Montfort *et al.*, 2001). Hsp22, which lacks this motif, is predominantly monomeric *in vitro* (Chowdary *et al.*, 2004). Similarly, Hsp20 lacks the C-terminal extension and primarily forms dimers (van de Klundert *et al.*, 1998). Another study from our laboratory demonstrated that this motif in  $\alpha$ -crystallins has a propensity to form inter-subunit interactions and mutations of I or V residues affect the oligomeric size and chaperone function (Pasta *et al.*, 2004). Using protein pin array technique, Ghosh and Clark (2005) have identified a N-terminal helix motif,  $\alpha$ -crystallin core domain and the IXI/V motif as sites of inter-subunit interactions in  $\alpha$ B-crystallin.

#### 1.4.2.3 sHsps structure: Insights from the available sHsps crystal structures:

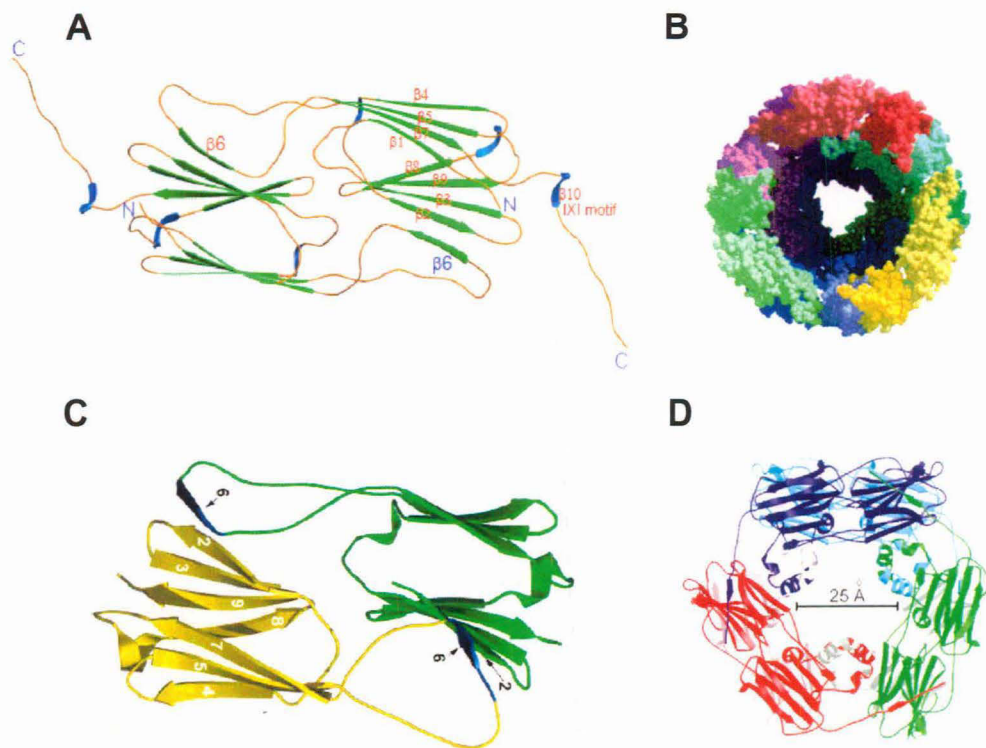
The globular complexes formed by sHsps are often polydisperse and dynamic, readily exchanging subunits. Crystallization is, therefore, a problem and crystal structures of only two sHsps that form regular oligomers, a prokaryotic sHsp from *Methanococcus jannaschii*, *Mj*Hsp16.5, and a eukaryotic sHsp from wheat, *Ta*Hsp16.9, are available (Kim *et al.*, 1998; van Montfort *et al.*, 2001). The *Mj*Hsp16.5 structure at 2.9 Å resolution shows a hollow spherical complex of 24 subunits with an outer diameter of ~120 Å, an inner diameter of ~65 Å. The *Ta*Hsp16.9 structure solved to 2.7 Å resolution is a barrel-shaped dodecameric structure assembled from two hexameric discs of 55 Å height and ~95 Å diameter.

The  $\alpha$ -crystallin domain of each monomer consists of a  $\beta$ -sheet sandwich of two anti-parallel  $\beta$ -sheets similar to the immunoglobulin-like fold (Figure 1.2 A and C). A 21- (*Ta*Hsp16.9) or 19-amino acid (*Mj*Hsp16.5) loop between  $\beta$ 5 and  $\beta$ 7 strands, containing the  $\beta$ 6 strand, extends out from the  $\beta$ -sandwich and forms a dimer through a strand-exchange mechanism. The C-terminal extension is primarily extended and contains the short  $\beta$ 10



strand. The N-terminal region of *MjHsp16.5* is unordered except for an additional  $\beta 1$ -strand that packs alongside  $\beta 7$ , allowing hydrophobic residues of  $\beta 1$  to contribute to the  $\alpha$ -crystallin domain hydrophobic core and dimer stabilization. In contrast, the same region in *TaHsp16.9* forms a short  $\alpha$ -helix (Figure 1.1 and 1.2 D). The remaining N-terminal sequence of *TaHsp16.9* has two more  $\alpha$ -helices connected by random coil. *MjHsp16.5* and *TaHsp16.9* appear to form a hollow complex, which suggests that the unstructured N-terminal domain is most likely located inside the complex (Figure 1.2 B and D). Interestingly, 49% of the solvent-accessible surfaces in the interior of the sphere are composed of non-polar residues, in contrast to 22% on the outside surface. This implies that the inside surface of the sphere is much more hydrophobic than the outside surface (van Montfort *et al.*, 2001).

Although sequence conservation between *MjHsp16.5* and *TaHsp16.9* is low (~23%), their  $\alpha$ -crystallin domains and their use of dimers as higher-assembly building blocks are similar. The orientations of the C-terminal extensions are different in both sHsps possibly due to a hinge-like region between  $\beta 9$  and  $\beta 10$ -strands. In both the crystal structures, the



**Figure 1.2: X-ray structure of *MjHsp16.5* and *TaHsp16.9*.** Arrangement of  $\beta$ -strands in the two subunits of a dimer of *MjHsp16.5* (A) and *TaHsp16.9* (C) is shown. The  $\alpha$ -crystallin domain adopts a  $\beta$ -sandwich immunoglobulin-like fold. Overall assembly of *MjHsp16.5* (B) and *TaHsp16.9* (D) are also shown (Kim *et al.*, 1998; van Montfort *et al.*, 2001).



---

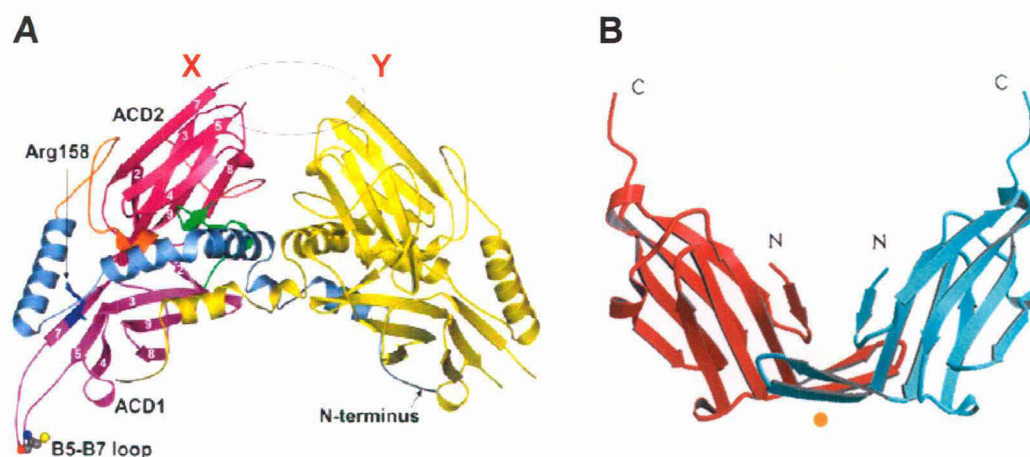
conserved IXI/V motif corresponding to the  $\beta$ 10-strand, stabilizes the oligomer by locking into a hydrophobic groove in the  $\alpha$ -crystallin domain of another monomer. The  $\beta$ 7-strand, which has one of the two highly conserved regions in the  $\alpha$ -crystallin domain is seen to interact with its N-terminal arm and with the dimerization loop of another monomer in the assembly. Both crystal structures show these regions to be primarily involved in maintaining the structural integrity of the  $\alpha$ -crystallin domain.

Recently, in addition to these non-metazoan sHsps, the crystal structure of a parasitic flatworm sHsp, Tsp36 from *Taenia saginata*, was solved to 2.5 Å resolution (Stamler *et al.*, 2005). Tsp36 has two  $\alpha$ -crystallin domains (ACD1 and ACD2), possesses good chaperone activity and exists as a dimer or a tetramer in reducing or oxidising conditions respectively (Kappe *et al.*, 2004). Both ACDs form  $\beta$ -sandwich structures with a seven-strand arrangement similar to that of previously solved sHsps (Figure 1.3 A). However, the two ACD domains of monomers orient such that the comparatively shorter  $\beta$ 5- $\beta$ 7 loops point away from each other and are not involved in dimer formation through strand exchange. Unlike *TaHsp16.9* and *MjHsp16.5*, the N-terminal region of Tsp36 is clearly visible in the crystal structure and crosses over the dimeric interface to mediate the dimeric assembly. The  $\beta$ 5- $\beta$ 7 loop of ACD1 contains a cysteine residue, and therefore, is a site for tetramer formation by disulphide bonding.

A novel dimeric interface for the mammalian sHsps based on X-ray solution scattering data of the isolated  $\alpha$ -crystallin domain of  $\alpha$ B-crystallin was also proposed (Feil *et al.*, 2001). In their model, the loop region forms a strand-turn-strand motif, and interaction of two monomers creates a four-stranded, anti-parallel, inter-subunit composite  $\beta$ -sheet (Figure 1.3 B). The two  $\alpha$ -crystallin domain  $\beta$ -sandwiches are oriented in a V shape and the dimer exhibits an increased surface area as well as potentially flexible dimer interface compared to the *MjHsp16.5* or *TaHsp16.9* dimers.

Possibility of more than one orientation of either  $\alpha$ -crystallin domain or C-terminal extensions may be responsible for polydispersity among the sHsps family. It can also account for yielding mixed sHsps of variable sizes and compositions. Despite the low sequence identity, a  $\beta$ -sandwich-like organization was demonstrated in the  $\alpha$ -crystallin domains of  $\alpha$ A-crystallin and Hsp27 by site directed spin labeling (Berengian *et al.*, 1999; Koteiche and McHaourab, 1999) indicating that the immunoglobulin-like fold is highly conserved across sHsps. As shown in crystal structure, two categories of interactions contributed to quaternary structure *viz.* inter-subunit interactions leading to dimer formation

---



**Figure 1.3: X-ray structure of dimeric Tsp36 and  $\alpha$ -crystallin domain.** (A) Molecule X forms a dimer with molecule Y (yellow) of Tsp36. In molecule X, the single cysteine in the  $\beta$ 5- $\beta$ 7 loop is indicated in ball-and-stick format, the conserved arginine (Arg158) in stick format. The black oval indicates interface between ACD2 domains with missing density. Note the orientation of  $\beta$ 5- $\beta$ 7 loop and dimeric interface formed by the N-terminal helices (Stamler *et al.*, 2005). (B) V-shaped model of dimer, formed by isolated  $\alpha$ -crystallin domain of  $\alpha$ B-crystallin, obtained by rigid body refinement (Feil *et al.*, 2001).

and dimer-dimer interaction resulting in formation of large oligomeric assemblies. Thus, dimer is believed to be the building block even in mammalian sHsps. The dimerization loop connecting the  $\beta$ 5- $\beta$ 7 strands, however, is much shorter, and appears to lack the  $\beta$ 6-strand in metazoan sHsps (Figure 1.1) suggesting that dimeric interactions are different in mammalian sHsps and they may not assemble into dimers via strand exchange. Moreover, it is seen that structural features used for higher-order assembly such as hinges, N-terminal arms and dimerization loops correlate to regions of high sequence variation in sHsps that may account for differences in their size, geometry and polydispersity of sHsps complexes.

#### 1.4.2.4 Chaperone-like activity of sHsps:

As mentioned earlier, sHsps exhibit chaperone activity both *in vivo* and *in vitro*. *In vivo* chaperone activity of sHsps in protecting vital cellular proteins, enzymes and prevention of amyloid fibril formation of proteins leading to neurodegenerative diseases is well documented (Muchowski and Walker, 2005). Pioneering *in vitro* studies by Horwitz (1992) showed that  $\alpha$ -crystallin binds denatured proteins and prevents their irreversible aggregation, thereby demonstrating its molecular chaperone activity. Bovine  $\alpha$ -crystallin, murine Hsp25 and human Hsp27 were the first sHsps reported to have chaperone activity (Horwitz, 1992; Jakob *et al.*, 1993).

sHsps bind specifically to the molten globule states of substrate proteins, either on the unfolding or the refolding pathway (Rajaraman *et al.*, 1996; Raman *et al.*, 1997; Rawat and Rao, 1998; Rajaraman *et al.*, 2001) through their exposed hydrophobic patches by making hydrophobic interactions (Das *et al.*, 1996; Lee *et al.*, 1997). A study from our laboratory showed that exposed hydrophobicity is an important structural feature of sHsps and chaperone activity is related to surface hydrophobicity (Raman and Rao, 1994; Raman *et al.*, 1995a). This is well corroborated by binding studies of hydrophobic probes, ANS and bis-ANS, to sHsps (Das and Surewicz, 1995; Raman and Rao, 1997; Sharma *et al.*, 1998).

Several putative substrate-binding sites have been mapped to the N-terminal and  $\alpha$ -crystallin domain in many sHsps based on bis-ANS binding (Smulders and de Jong, 1997; Sharma *et al.*, 1998) and deuterium exchange studies (Smith *et al.*, 1996). These proposed substrate-binding sites are mostly hydrophobic but contain some intervening charged residues suggesting that efficient binding of substrate is mediated by hydrophobic residues, while charged amino acids might serve to optimally space the residues (Lee *et al.*, 1997).

Since the substrate-chaperone complexes are stable, non-native substrates are neither transferred between different sHsp complexes nor spontaneously released (Lee *et al.*, 1997; Ehrnsperger *et al.*, 1997). In the case of eye lens,  $\alpha$ -crystallin is thought to bind the aggregation-prone denatured proteins irreversibly to maintain the transparency (Horwitz, 2000). However, in the case of cells having normal protein turnover, it is detrimental to harbor a chaperone system that binds non-native proteins irreversibly and does not allow their refolding and release. *In vitro* experiments have shown that the target proteins can be released in the active form with the assistance of other chaperone systems such as Hsp70/Hsp40 and Hsp104 in the presence of ATP (Lee *et al.*, 1997; Ehrnsperger *et al.*, 1997; Wang and Spector, 2000). However, in a few instances, sHsps have also been shown to assist the refolding of some target enzymes to the active state, with the change in conditions such as temperature or ATP. For example  $\alpha$ A- or  $\alpha$ B-crystallin make reversible, transient interactions with early unfolding intermediates of citrate synthase, which can be reactivated by its substrate, oxaloacetate, whereas the binding with late unfolding intermediates is irreversible (Rajaraman *et al.*, 2001). Jakob *et al.* (1993) showed that Hsp27 promoted the functional refolding of citrate synthase and  $\alpha$ -glucosidase, similar to GroEL and Hsp90.

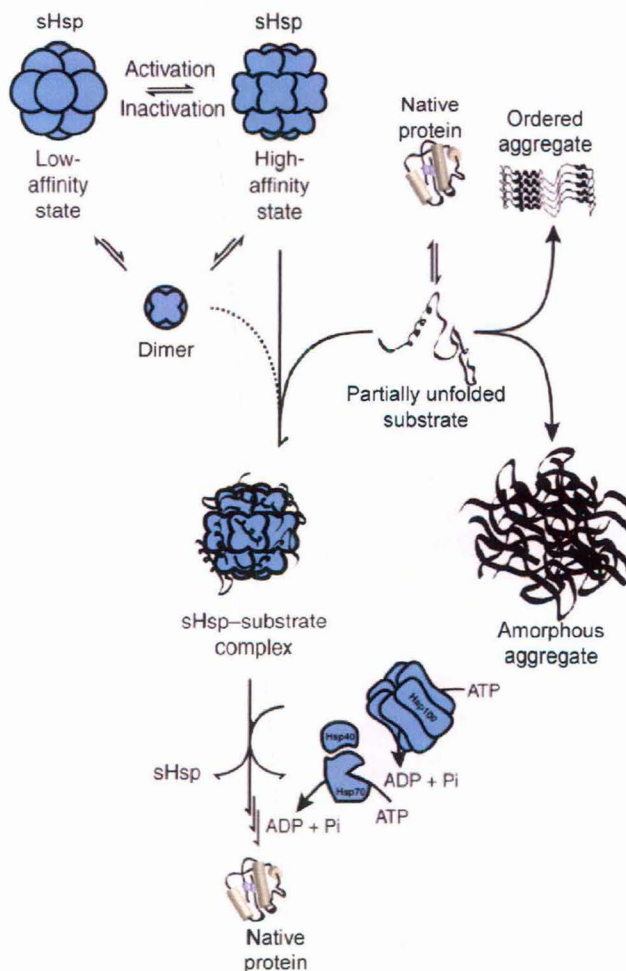
For sHsps, the mechanism involving shifting between active and inactive states is not fully understood. A few sHsps are not constitutively active and show significant

enhancement of chaperone activity at elevated temperatures. Temperature-dependent structural changes and enhanced chaperone activity has also been reported in other Hsps like GroEL and Hsp70 (Hansen and Gafni, 1993). A study from our laboratory has shown that  $\alpha$ -crystallin protects  $\gamma$ -crystallin against UV-induced photoaggregation only at temperatures above 30°C. Based on pyrene solubilization, gel-filtration chromatography studies and chaperone activity studies at different temperatures, it was hypothesized that a structural transition above 30°C (another above 50°C) increases the protective ability by enhancing or reorganizing surface hydrophobicity (Raman and Rao, 1994). Subsequent studies from our laboratory (Raman *et al.*, 1995a), as well as those of Smith *et al.* (1996) showed that  $\alpha$ -crystallin exhibits significantly enhanced hydrophobic patches above 30°C explaining the mechanism of temperature dependence of  $\alpha$ -crystallin chaperone activity. This transition is associated with a minor perturbation of  $\alpha$ -crystallin tertiary structure above 30°C. A second transition in chaperone activity of  $\alpha$ -crystallin towards aggregation of  $\beta$ L-crystallin upon refolding from its denatured state is observed at around 55°C with a concomitant structural transition to a multimeric molten globule-like state (Raman and Rao, 1997). Dudich *et al.* (1995) showed that mammalian Hsp27 also undergoes similar structural transitions around 36°C and 60°C. Increased chaperone activity and hydrophobicity at elevated temperatures was also demonstrated for Hsp22 (Chowdary *et al.*, 2004).

As mentioned earlier, sHsp complexes are dynamic in nature exchanging subunits constantly and this oligomer dynamics is affected by change in temperature or phosphorylation. The dynamics of sHsp complexes expose the hydrophobic substrate-binding sites during dissociation, which are otherwise buried. Dissociation of Hsp27 oligomer is required for recognition of the substrate (Shashidharamurthy *et al.*, 2005). However, yeast Hsp26 dissociates into dimeric species (active form) with increase in temperature and exhibits chaperone activity (Haslbeck *et al.*, 1999). Mild structural perturbation by small molecules such as urea (Raman and Rao, 1994), GdmCl (Das and Liang, 1997) or arginine hydrochloride (Srinivas *et al.*, 2003) also leads to a similar enhancement of chaperone activity *in vitro*. Based on above discussed observations, current model for sHsp chaperone activity is shown in Figure 1.4.

In summary, cells employ a regulatable arsenal of chaperones to prevent unproductive folding reactions and to increase the yield of properly folded native proteins. Of all chaperone families, sHsps are not essential 'folding' factors, but they contribute substantially to the folding capacity of the cells especially under stress conditions. They

contribute immensely to protein quality control and complete the chaperone network of the cell. Misfolding and aggregation, however, occur frequently both *in vitro* and *in vivo* due to several reasons. Though protein aggregation *in vitro* causes major economical and technical problem in biotechnology and pharmaceuticals industries, protein aggregation *in vivo* can be lethal in patients who suffer from a variety of diseases involving protein aggregation.



**Figure 1.4: Model for chaperone function of sHsps.**

Native protein gets partially unfolded spontaneously or under stress conditions. These aggregation-prone intermediates can either form amorphous aggregates or amyloid like ordered aggregates. Interaction of these partially unfolded intermediates with sHsps involves activation of sHsps to a high affinity state. Mechanism of this conversion can be rearrangement within the oligomer or dissociation of the oligomeric structure. Active sHsps form stable complex with substrate, preventing its aggregation. Release of active substrates from this complex requires cooperation from ATP-dependent chaperone families. (Figure modified from Haslbeck *et al.*, 2005).

### 1.5 Protein misfolding diseases:

Imbalance of proteins either through too little of a particular protein being present, or too much of a protein, or a protein being rendered dysfunctional, or produced at the wrong place or the wrong time, can result in 'proteinopathies'. Improper folding is one way in which protein imbalance can arise – the misfolded protein may be non-functional or sub-optimally functional, or it may be degraded by the cellular machinery, or it may lead to dysfunctional



interactions with other proteins. Stress can also contribute to proteinopathies by tilting the balance towards irreversible denaturation beyond the refolding power of the cellular chaperone system. There are a number of debilitating human diseases, which appear to involve improper folding of a particular protein and are collectively called as 'protein misfolding diseases'.

Many protein misfolding diseases are characterized by absence of a key protein, as it has been recognized dysfunctional and eliminated by the cell's own machinery. These include cystic fibrosis (misfolded CFTR), Marfan syndrome (misfolded fibrillin), Fabry disease (misfolded  $\alpha$ -galactosidase), Gaucher's disease (misfolded  $\beta$ -glucocerebrosidase), retinitis pigmentosa 3 (misfolded rhodopsin) and some cancers (misfolded von Hippel-Lindau protein or p53). Some misfolded proteins that overwhelm the chaperone and proteosomal machinery, aggregate either in the form of fibrils or amorphous aggregates. Thus, many protein misfolding diseases are characterized by deposition of protein in insoluble aggregates. Such protein aggregation diseases include Alzheimer's (deposits of amyloid- $\beta$  and tau), Parkinson's (deposits of  $\alpha$ -synuclein), spongiform encephalopathies (deposits of prion), Type II diabetes (deposits of amylin), hereditary transthyretin amyloidosis (deposits of transthyretin) and cataract (deposits of  $\gamma$ -crystallins). However, it is not clear whether the consequent pathology is due to the non-functioning of the protein involved or toxicity of the aggregates.

### **1.6 Defective chaperones: Chaperonopathies:**

In all of these instances of proteinopathies, the cause of the problems was defects in the protein themselves rather than deficiencies in the mechanism that assist them to fold. Together with protein degradation machineries, chaperones form the core of the cellular protein quality control mechanism. Mutation in or modifications of chaperones can result in failure of protein folding and refolding or other antistress mechanisms in which they participate, and therefore, have pathologic consequences. These pathologic conditions constitute 'chaperonopathies', a subset of proteinopathies (Macario and Conway de Macario, 2005). Chaperonopathies are further classified as genetic (due to mutations) or acquired (due to aging or aberrant post-translational modification). Acquired chaperonopathies progress with aging and usually become clinically evident late in life. Retinopathy due to age-related decrease in the expression of  $\alpha$ A-crystallin and its post-translational modification in the retina (Kapphahn *et al.*, 2003), is an example of acquired

---

chaperonopathy. Genetic or acquired defects can affect one or more of the various segments or specialized domains of a chaperone.

### 1.7 Genetic chaperonopathies:

Many disorders characterized by the abnormalities in nervous, muscular or other tissues have been identified that are associated with mutations in genes encoding chaperones, or molecules with chaperones-like domains (Slavotinek and Biesecker, 2001; Macario *et al.*, 2005). Genetic chaperonopathies arising from mutations in different groups of chaperones are listed in Table 1.3. However, the list of genetic chaperonopathies will probably continue to lengthen with further research.

**Table 1.3:** Genetic Chaperonopathies

Chaperone involved	Disease or Syndrome
Chaperone cofactors	
Cofactor C (tubulin folding)	X-linked retinitis pigmentosa
Cofactor E (microtubule biogenesis)	Sanjad-Sakati and Kenny-Caffey syndromes,
Chaperonins of group I	
mitochondrial Hsp60	Hereditary spastic paraplegia
Chaperonins of group II, CCT subunits	
$\alpha$ Subunit (MKKS)	McKusick-Kaufman and Bardet-Biedl syndromes
Peptidyl-prolyl cis-trans isomerase (PPIase)	
FK506-binding protein (FKBP)	Leber congenital amaurosis (severe retinopathy)
Putative candidates	
Mitochondrial protein-specific chaperones	Disorders of the respiratory chain in mitochondria
Proteins with DnaJ and Hsp90 markers (Sacsin)	Autosomal recessive spastic ataxia of Charlevoix-Saguenay
sHsp	
Hsp27	Williams syndrome, Amyotrophic Lateral Sclerosis, Charcot-Marie-Tooth disease, distal hereditary motor neuropathy
$\alpha$ A-crystallin	Cataracts, microcomea
$\alpha$ B-crystallin	Myopathy, cataracts
Hsp22	Charcot-Marie-Tooth disease, distal hereditary motor neuropathy

### 1.7.1 Mutation in mammalian sHsps and related chaperonopathies:

sHsps prevent pathologic protein aggregation by binding to aggregation-prone proteins and keeping them in a folding-competent state. Changes in localization and quantities of sHsps *in vivo* in response to development and other stress conditions are well documented. Furthermore, sHsps interact with each other forming homo- or hetero-oligomeric complexes as well as with a variety of cellular components and thus, they can contribute to the pathology when structurally perturbed. To date, mutations have been reported in four mammalian sHsps namely, Hsp27 (HspB1),  $\alpha$ A-crystallin (HspB4),  $\alpha$ B-crystallin (HspB5) and Hsp22 (HspB8), which are associated with pathological conditions in humans (Table 1.4). The fact that mutations in sHsps are associated with similar, but not identical diseases, support the idea of distinct role for these proteins. Despite the ever increasing list of mutations, many sHsp gene mutations still await discovery, and the wealth of information will present valuable opportunities to decipher the molecular pathways that underlie these diseases.

#### 1.7.1.1 sHsps and ischemia / reperfusion injury:

Except  $\alpha$ A-crystallin, HspB9 and HspB10, the other seven members of the sHsp family show constitutive high expression in muscles, where they constitute 3% or more of total protein. High expression level would allow them to exert an immediate protective effect in response to stress or other injury.  $\alpha$ B-crystallin, a ubiquitously occurring sHsp, is the most abundant sHsp in skeletal and cardiac muscles (Iwaki *et al.*, 1990; Kappé *et al.*, 2003; Golenhofen *et al.*, 2004) and plays a major role in differentiation and protection of myocytes. Another sHsp, MKBP binds and activates the myotonic dystrophy protein kinase (DMPK), an enzyme whose absence results in myotonic dystrophy (Suzuki *et al.*, 1998).

Ischemia / reperfusion injury to cells during heart attack includes protein denaturation, oxidoreductive stress, mitochondrial deterioration, cytoskeleton disruption and membrane lipid peroxidation. Overexpression of sHsps in transgenic animals or cardiomyocytes protects cardiac cells from death upon such injury (Martin *et al.*, 1997; Ray *et al.*, 2001; Hollander *et al.*, 2004). Hearts of  $\alpha$ B-crystallin and HspB2 double knock-out mice develop normally and show normal contractility under non-stress conditions. However, upon exposure to ischemia and reperfusion, they exhibit reduced contractility and less glutathione accompanied by greater necrosis / apoptosis (Morrison *et al.*, 2004). Phosphorylated Hsp20 arrests  $\beta$ -agonist-induced apoptosis experienced by heart failure

---



Table 1.4: Identified missense mutations in human sHsps and associated diseases

sHsp	Mutation	Affected sHsp Region	Diagnosis	References
Hsp27 / HspB1	P182S	C-terminal extension	dHMN	Kijima <i>et al.</i> , 2005
	P182L	C-terminal extension	dHMN	Evgrafov <i>et al.</i> , 2004
	T151I	$\alpha$ -Crystallin domain	dHMN	Evgrafov <i>et al.</i> , 2004
	K141Q	$\alpha$ -Crystallin domain	dHMN	Ikeda <i>et al.</i> , 2008
	R140G*	$\alpha$ -Crystallin domain	dHMN	Houlden <i>et al.</i> , 2008
	R136W	$\alpha$ -Crystallin domain	CMT2	Evgrafov <i>et al.</i> , 2004
	S135F	$\alpha$ -Crystallin domain	dHMN, CMT2	Evgrafov <i>et al.</i> , 2004; Chung <i>et al.</i> , 2008
	R127W	$\alpha$ -Crystallin domain	dHMN, CMT2	Evgrafov <i>et al.</i> , 2004; Tang <i>et al.</i> , 2005a
	L99M	$\alpha$ -Crystallin domain	dHMN	Houlden <i>et al.</i> , 2008
	G84R	N-terminal domain	dHMN	James <i>et al.</i> , 2008; Houlden <i>et al.</i> , 2008
P39L	N-terminal domain	dHMN	Houlden <i>et al.</i> , 2008	
$\alpha$ A-crystallin / HspB4	R116C*	$\alpha$ -Crystallin domain	ADCC, some with Microcornea and Iris coloboma	Litt <i>et al.</i> , 1998; Vanita <i>et al.</i> , 2006; Beby <i>et al.</i> , 2007
	R116H*	$\alpha$ -Crystallin domain	ADCC	Richter <i>et al.</i> , 2008; Hansen <i>et al.</i> , 2007; Gu <i>et al.</i> , 2008
	G98R	$\alpha$ -Crystallin domain	ADPC	Santhiya <i>et al.</i> , 2006
	R54C	N-terminal domain	ARCC ADCC	Khan <i>et al.</i> , 2007; Devi <i>et al.</i> , 2008
	R49C	N-terminal domain	ADCC	Mackay <i>et al.</i> , 2003
	R21W	N-terminal domain	ADCC	Hansen <i>et al.</i> , 2007; Devi <i>et al.</i> , 2008
	R21L	N-terminal domain	ADCC	Graw <i>et al.</i> , 2006
	R12C	N-terminal domain	ADCC	Hansen <i>et al.</i> , 2007; Devi <i>et al.</i> , 2008
	W9X	N-terminal domain	ARCC	Pras <i>et al.</i> , 2000
$\alpha$ B-crystallin / HspB5	A171T	C-terminal extension	ADCC	Devi <i>et al.</i> , 2008
	R157H	C-terminal extension	DCM	Inagaki <i>et al.</i> , 2006
	G154S	C-terminal extension	DCM	Pilotto <i>et al.</i> , 2006
	464delCT	C-terminal extension	MM	Selcen and Engel, 2003
	Q151X	C-terminal extension	MM	Selcen and Engel, 2003
	450delA	C-terminal extension	ADCC	Berry <i>et al.</i> , 2001
	D140N	$\alpha$ -Crystallin domain	ADCC	Liu <i>et al.</i> , 2006a
	R120G*	$\alpha$ -Crystallin domain	DRM / CM + ADCC	Fardeau <i>et al.</i> , 1978; Vicart <i>et al.</i> , 1998
	P20S	N-terminal domain	ADCC	Liu <i>et al.</i> , 2006b
Hsp22 / HspB8	K141E*	$\alpha$ -Crystallin domain	dHMN	Irobi <i>et al.</i> , 2004
	K141N*	$\alpha$ -Crystallin domain	dHMN, CMT2	Irobi <i>et al.</i> , 2004; Zhang <i>et al.</i> , 2005; Tang <i>et al.</i> , 2005b

\*Mutations in homologous positions.

TH-16521

dHMN, distal hereditary motor neuropathy; CMT2, Charcot-Marie-Tooth disease type 2; ADCC, autosomal dominant congenital cataract; ADPC, autosomal dominant presenile cataract; ARCC, autosomal recessive congenital cataract; DCM, dilated cardiomyopathy; MM, myofibrillar

612-01575 D4929 HU



patients (Fan *et al.*, 2004).  $\alpha$ B-crystallin, but not Hsp27, preserves microtubules during ischemia (Bluhm *et al.*, 1998). Five mammalian sHsps ( $\alpha$ B-crystallin, HspB2, Hsp27, Hsp20 and cvHsp) translocate from cardiac cell cytosol to myofibrils during ischemia, with varying localization to Z-lines, I-bands and intercalated discs where they bind tightly to microfibrils and possibly stabilize sarcomeres (Barbato *et al.*, 1996; Golenhofen *et al.*, 1998; Yoshida *et al.*, 1999). Another sHsp, Hsp22, is also expressed predominantly in heart and skeletal muscles, and mediates cardiac cell growth and hypertrophy (Depre *et al.*, 2002). In patients with prolonged ischemia, its expression is further increased along with that of other genes promoting cell survival (Depre *et al.*, 2004).

Ischemic preconditioning protects subsequent ischemia. Hyperthermia induces  $\alpha$ B-crystallin in renal tissues of rats and protects against damage caused by subsequent renal ischemia / reperfusion (Kelly *et al.*, 2001). Similarly, overexpression of Hsp22 in hearts of transgenic mice provides protection against myocardial ischemia by preemptive preconditioning through activation of survival kinases (Depre *et al.*, 2006). Though more than one sHsp is known to play a protective role in heart and other muscles, point mutations are discovered only in  $\alpha$ B-crystallin that lead to the degeneration of distinct tissues, including cardiac and skeletal muscles (Table 1.4).

#### **1.7.1.1.1 $\alpha$ B-crystallin in cardiomyopathy / myopathy:**

$\alpha$ -Crystallin has been suggested to modulate the equilibrium between soluble and insoluble type III intermediate filaments (IFs) in the cell (Nicholl and Quinlan, 1994). There is a specific interaction between  $\alpha$ B-crystallin and desmin, a type III IF at the Z-bands in skeletal myofibrils and cardiomyocytes (Bennardini *et al.*, 1992).  $\alpha$ B-crystallin plays a role in the remodeling of the cytoskeleton that occurs during development and cell differentiation (Wang and Spector, 1996) as well as after heat shock (Singh *et al.*, 2007a). In lens fiber cells exposed to thermal stress,  $\alpha$ B-crystallin was shown to associate with lens-specific IFs phakinin and filensin (Muchowski *et al.*, 1999a). In many of the neurological diseases,  $\alpha$ B-crystallin is found to be associated with IFs in cytoplasmic inclusion bodies (Head *et al.*, 1993). However, interactions between IFs and sHsps can be disrupted by disease-causing mutations in either IFs or sHsps, leading to respective pathological aggregates (Goldfarb *et al.*, 2004).

A missense mutation, R120G, in  $\alpha$ B-crystallin has been shown to co-segregate with a particular subtype of myofibrillar myopathy [desmin-related myopathy (DRM) or  $\alpha$ B-

---

crystallinopathy] with associated cardiac involvement and cataract formation in a French family (Vicart *et al.*, 1998). DRM is an adult-onset neuromuscular disease characterized by abnormal accumulation of desmin within muscle fibres. In this family, a subsarcolemmal and intermyofibrillar accumulation of dense granulofilamentous material with various degenerative changes was observed in electron microscopy. This is the first sHsp missense mutation shown to cause inherited human muscle disease.

R120G $\alpha$ B-crystallin exhibits alterations in its secondary, tertiary, and quaternary structural features as well as decreased *in vitro* chaperone-like activity (Perng *et al.*, 1999a; Kumar *et al.*, 1999; Bova *et al.*, 1999; Simon *et al.*, 2007a). <sup>1</sup>H-NMR spectroscopy showed that R120G $\alpha$ B-crystallin promoted unfolding of reduced  $\alpha$ -lactalbumin and unlike wild type  $\alpha$ B-crystallin does not stabilize the molten globule state of reduced  $\alpha$ -lactalbumin (Treweek *et al.*, 2005). R120G $\alpha$ B-crystallin is inherently unstable in solution (Treweek *et al.*, 2005; Simon *et al.*, 2007a) and exhibits increased instability toward heat-induced denaturation (Perng *et al.*, 1999a). In the muscle, the loss of a specific chaperone function of  $\alpha$ B-crystallin at the level of the IFs resulting in the aggregation of desmin has been suggested as being the cause of the R120G $\alpha$ B-crystallin-mediated disease (Perng *et al.*, 1999a).

R120G $\alpha$ B-crystallin directly promotes the aggregation of the desmin filament network and that desmin networks are differently affected, depending on the cellular backgrounds (Perng *et al.*, 2004). R120G $\alpha$ B-crystallin aggregates in a time-dependent manner in various cell lines resulting in amorphous perinuclear aggregates formed by microtubule-dependent accumulation of small aggregates that initially develop at the cell periphery in the cytoplasm (Chávez Zobel *et al.*, 2003; Simon *et al.*, 2007a). However, in HeLa cells, R120G localized to inclusion bodies, lacking desmin and the formation is microtubule-independent (Ito *et al.*, 2003). Nuclear speckles are thought to participate in RNA transcription and splicing and R120G mutant inhibits speckle formation in several transfected cell lines (van den IJssel *et al.*, 2003), which can be a reason for the observed phenotype. Gain of toxic function by the aggregated R120G $\alpha$ B-crystallin is also a possible cause of the disease, particularly because stress activates the transcription of the  $\alpha$ B-crystallin gene (Chávez Zobel *et al.*, 2003).

Cardiomyopathy was induced in transgenic mice with modest expression of R120G $\alpha$ B-crystallin in cardiomyocytes, whereas more severe phenotype and 100% mortality by early adulthood occurred in high expressing lines (Wang *et al.*, 2001). In these transgenic mice, the desmin network, myofibril arrangement, mitochondrial-sarcomere architecture,

mitochondrial function, and the ubiquitin/proteasome system were significantly impaired (Maloyan *et al.*, 2005; Chen *et al.*, 2005). Recently, Rajasekaran *et al.* (2007) proposed 'reductive stress' as a causative mechanism in R120G-induced cardiomyopathy. They found increase in reduced GSH concentrations and the ratio of GSH/GSSG in transgenic mice, which is due to the augmented expression and enzymatic activities of glucose-6-phosphate dehydrogenase.

R120G $\alpha$ B-crystallin and its pseudo-phosphorylated mutants are unable to confer resistance to apoptosis during C2C12 myoblast differentiation because of their impaired capacity to inhibit the proteolytic activation of caspase-3 (Kamradt *et al.*, 2002). Moreover, R120G $\alpha$ B-crystallin exhibits attenuated antiapoptotic ability due to its decreased ability to sequester Bax and Bcl-XS in the cytoplasm (Mao *et al.*, 2004). R120G $\alpha$ B-crystallin results in activation of apoptosis and subsequent heart failure in transgenic mice (Maloyan *et al.*, 2005). Taken together, it appears that all the known protective functions of  $\alpha$ B-crystallin are impaired in R120G $\alpha$ B-crystallin.

Hsp20 is involved in cardiac protection (Fan *et al.*, 2004) and R120G $\alpha$ B-crystallin shows a major decrease in interaction with Hsp20 compared to wild type  $\alpha$ B-crystallin (Simon *et al.*, 2007b), which possibly explains cardiac involvement in the disease. R120G $\alpha$ B-crystallin also shows increased interaction with Hsp22 (Simon *et al.*, 2007b) and Hsp22 co-expression leads to solubilization of mutant protein in cells (Chávez Zobel *et al.*, 2003). R120G $\alpha$ B-crystallin forms amyloid oligomers by self-interaction, which is interrupted by co-expression of Hsp22 or Hsp25, with concomitant recovery of the cellular viability (Sanbe *et al.*, 2007). Hsp27 and  $\alpha$ B-crystallin reduced the aggregate formation by R120G $\alpha$ B-crystallin expression in several cell lines (Chávez Zobel *et al.*, 2003; Ito *et al.*, 2003), offering a molecular explanation for the delayed adult-onset of DRM through chaperone action. Moreover, environmental enrichment such as exercise reverses the accumulation of cytotoxic preamyloid oligomers formed by R120G $\alpha$ B-crystallin and prolongs the survival of  $\alpha$ B-crystallin-based desmin-related cardiomyopathy mice (Maloyan *et al.*, 2007).

Two other  $\alpha$ B-crystallin mutations, Q151X that results in a C-terminal truncation of 25 residues and 464delCT that results in a C-terminal substitution from residue 155, are associated with adult-onset progressive myofibrillar myopathy (Selcen and Engel, 2003). Pathological features include myofibrillar degeneration commencing at Z-disk, accumulation of abnormal degraded filamentous material and aberrant accumulation of different proteins

in abnormal fiber regions. The C-terminal region is important for sHsp solubilization, chaperone activity and oligomer formation (Derham and Harding, 1999; Narberhaus, 2002). Simon *et al.*, (2007b) recently established that myopathy-associated  $\alpha$ B-crystallin mutants (R120G, Q151X, 464delCT) show abnormal protein aggregation, subcellular localization and hyper-phosphorylation. Moreover, each myopathy-associated mutant has a specific pattern of abnormal interactions, be it with wild type  $\alpha$ B-crystallin (464delCT), with themselves (R120G, Q151X, 464delCT), with Hsp20 (R120G, Q151X, 464delCT), or with Hsp22 (R120G, Q151X). The Q151X and 464delCT mutation in  $\alpha$ B-crystallin dramatically altered its secondary and tertiary structure. It further led to destabilization of  $\alpha$ B-crystallin increasing its tendency to self-aggregate *in vitro* and *in vivo* (Hayes *et al.*, 2008).

Other mutants (R157H, G154S) caused mild and late-onset dilated cardiomyopathy (DCM) without cataract (Table 1.4). DCM is a disease characterized by cardiac enlargement accompanied by systolic dysfunction and often manifested with congestive heart failure. These mutations are also present in the C-terminal region of  $\alpha$ B-crystallin very close to the IXI/V motif, which possibly affect its structure and function. It was reported that the  $\alpha$ B-crystallin binds titin/connectin, a giant muscle protein expressed in the cardiac and skeletal muscles spanning the entire sarcomere from Z-line to M-line in the I-band region, more specifically at the I26/I27 domain and the cardiac-specific N2B domain (Bullard *et al.*, 2004). Interestingly, R157H $\alpha$ B-crystallin showed decreased binding with the N2B domain but not with the I26/I27 domain and these functional alterations were not associated with the formation of mutant protein aggregates in cells. In contrast, the R120G mutation decreased binding to both N2B and I26/I27 domain and led to the accumulation of protein aggregates (Inagaki *et al.*, 2006). Thus, it is possible that due to cardiac-specific functional alteration in R157H $\alpha$ B-crystallin, the mutation caused cardiac muscle dysfunction but not skeletal muscle myopathy.

#### **1.7.1.2 $\alpha$ A- and $\alpha$ B-crystallin in hereditary cataracts:**

$\alpha$ -,  $\beta$ - and  $\gamma$ -crystallins account for nearly 95% of lens proteins. Crystallins contribute to the transparency and refractive index of the lens by short-range interactions among themselves in a highly concentrated protein matrix (Horwitz, 2000; Andley, 2007). Molecular diversity, generated by multiple homologues in each family, polydisperse structure and hetero-oligomerization, prohibits long-range interactions that can cause pockets of crystallization and thus fluctuations in refractive index (Jaenicke and Slingsby, 2001).

Although crystallins mainly function as structural proteins in lens fibre cells,  $\alpha$ -crystallin (hetero-oligomer of sHsps  $\alpha$ A- and  $\alpha$ B-crystallin) can also function as a molecular chaperone (Horwitz, 1992) and as an anti-apoptotic protein (Kamradt *et al.*, 2002).

Unlike  $\alpha$ B-crystallin knockout mice, which show muscle deformity and die prematurely (Brady *et al.*, 2001),  $\alpha$ A-crystallin knockout mice developed cataract and formed inclusion bodies of  $\alpha$ B-crystallin in lens fibre cells (Brady *et al.*, 1997), highlighting the importance of  $\alpha$ A-crystallin for maintenance of transparency and solubility of  $\alpha$ B-crystallin. Double knockout mice lacking  $\alpha$ A- and  $\alpha$ B-crystallin show cataract with severe fibre cell disintegration (Boyle *et al.*, 2003) due to increased caspase activation (Morozov and Wawrousek, 2006). Studies on lens epithelial cells (LECs) derived from knockout mice have revealed a protective effect of  $\alpha$ A-crystallin against apoptosis *in vivo* (Xi *et al.*, 2003) and of  $\alpha$ B-crystallin on genomic stability of cells in culture (Andley *et al.*, 2001; Bai *et al.*, 2003). In the absence of any protein turnover, crystallins are affected by the host's age, numerous post-translational modifications as well as environmental factors such as cigarette smoking, UV radiation, low antioxidant intake, hyperglycemic or oxidative damage etc. All these factors can result in age-related cataracts due to catastrophic structural changes and protein aggregation, a characteristic linking cataract to other protein misfolding diseases (Groenen *et al.*, 1994; Derham and Harding, 1999).

Cataract is an opacity of the normally clear eye lens, affecting vision. It is the most common cause of blindness worldwide and hereditary non-syndromic childhood cataracts occurs at a frequency of about 1-6 cases per 10000 live births (Francis *et al.*, 2000). Hereditary cataracts show clinically and genetically heterogeneous lens pathology. Clinical descriptions of hereditary cataracts are based on physical location, size and appearance of opacity in different developmental regions of the lens. Cataracts can also be defined by the age at onset: a congenital or infantile cataract presents within the first year of life; a juvenile cataract presents within the first decade of life; a presenile cataract presents before the age of about 45 years, and senile or age-related cataract after that. There are a large number of potential candidate genes for inherited cataract and mutations have been identified in genes encoding membrane proteins (GJA3, GJA8, LIM2 and MIP), transcription factors (FOXE3, MAF, PAX6, PITX3, SIX5 and SOX2), enzymes (GALK1), intermediate filament proteins (BFSP1 and BFSP2) and members of the crystallin family (Graw, 2004; Hejtmancik, 2008). Besides  $\beta$ - and  $\gamma$ -crystallins, a large number of point mutations scattered over an entire region of  $\alpha$ A- and  $\alpha$ B-crystallin are known to cause inherited cataracts (Table 1.4). Most of

these mutations are congenital and inherited by autosomal dominant mechanism, but a few also exhibit autosomal recessive mode of inheritance. There is remarkable heterogeneity in these cataract phenotypes – spatially, temporally and morphologically (Table 1.5).

Several studies have examined the cellular and molecular mechanisms by which these mutations can lead to cataract. It is intriguing that mutations in  $\alpha$ B-crystallin cause isolated cataracts, myopathy, or cataracts along with myopathy (Table 1.4). R120G mutation in  $\alpha$ B-crystallin, which causes both cataract and myopathy, exhibits large oligomeric size and reduced chaperone activity (Perng *et al.*, 1999a; Kumar *et al.*, 1999; Bova *et al.*, 1999; Simon *et al.*, 2007a). R120G $\alpha$ B-crystallin is susceptible to truncation from the C-terminal extension. Probably due to this, R120G mutation results in partial unfolding and increased exposure of hydrophobic regions, reducing its stability and promoting its aggregation (Treweek *et al.*, 2005). The interactions of R120G $\alpha$ B-crystallin with  $\alpha$ A- and  $\alpha$ B-crystallin decreased, but those with  $\beta$ B2- and  $\gamma$ C-crystallin increased slightly (Fu and Liang, 2003). Thus, altered interaction indicates that R120G $\alpha$ B-crystallin maintains lens protein solubility less effectively.

D140N mutation in  $\alpha$ B-crystallin altered the tertiary structure, formed large oligomers, decreased thermal stability and decreased chaperone activity of  $\alpha$ B-crystallin (Liu *et al.*, 2006a). All these changes are similar to those exhibited by R120G $\alpha$ B-crystallin, but the D140N mutation causes only cataract. Since the effect of the mutation is dominant negative and hence dose-dependent, it is possible that higher expression of  $\alpha$ B-crystallin in the lens compared to muscles affects its chaperone activity more severely in the lens.

450delA mutation in  $\alpha$ B-crystallin manifests in congenital posterior polar cataract. It alters the coding sequence of the C-terminal extension from residue 150 onwards, introducing a novel C-terminal peptide that has no homology to the existing C-terminal extension of  $\alpha$ B-crystallin (Berry *et al.*, 2001). 450delA mutant protein shows self-aggregation and can only be refolded *in vitro* in the presence of wild type  $\alpha$ B-crystallin. This mutant/wild type mixture is neither thermostable nor an effective chaperone compared with the wild type protein alone (Hayes *et al.*, 2008).

P20S mutation in  $\alpha$ B-crystallin also manifests in congenital posterior polar cataract. Heteroaggregates of wild type  $\alpha$ A- and P20S $\alpha$ B-crystallin show nearly the same molecular mass as those of wild type  $\alpha$ A- and  $\alpha$ B-crystallin, but the subunit-exchange rate and chaperone activity are decreased markedly (Li *et al.*, 2008). In human LECs, unlike wild type  $\alpha$ B-crystallin, the P20S mutant protein shows abnormal nuclear localization, and unusual



**Table 1.5:** List of point mutations identified in human alpha-crystallins leading to the pathological conditions

Alpha A-crystallin		
Mutation	Disease	Remarks
R116C	Congenital zonular central nuclear opacity or cortical and posterior subcapsular cataract (Litt <i>et al.</i> , 1998). Fan-shaped microcornea-cataract syndrome (Vanita <i>et al.</i> , 2006). Nuclear cataract associated with iris coloboma and microphthalmia (Bebby <i>et al.</i> , 2007).	Change in secondary, tertiary, quaternary structure and decreased chaperone-like activity (Kumar <i>et al.</i> , 1999; Shroff <i>et al.</i> , 2000). Diminished protective ability against stress-induced cell apoptosis (Andley <i>et al.</i> , 2002; Mao <i>et al.</i> , 2004). Increase in substrate binding and loss of chaperone-like activity (Koteiche and Mchaourab, 2006).
R116H	Nuclear with polar and/or equatorial ramification (Hansen <i>et al.</i> , 2007). Clinical diversity of autosomal dominant cataract (anterior polar, fan-shaped, anterior subcapsular, embryonal, cortical), microcornea and corneal opacity. (Richter <i>et al.</i> , 2008). Punctate, nuclear and total cataract with microcornea (Gu <i>et al.</i> , 2008).	Mutant protein exhibits increased hydrophobicity and loss of chaperone-like activity (Gu <i>et al.</i> , 2008).
R49C	Autosomal dominant nuclear cataract (Mackay <i>et al.</i> , 2003).	Abnormal localization to nucleus, failure to protect staurosporine-induced apoptosis (Mackay <i>et al.</i> , 2003). Recombinant protein does not show significant changes in the structure and chaperone-like activity (Pasta SY, Raman B, Ramakrishna T, Rao CM. unpublished results).
R12C	Posterior polar cataract progressing to dense nuclear and lamellar cataract, with involvement of anterior and posterior poles (Hansen <i>et al.</i> , 2007). Congenital nuclear cataract in association with microcornea (Devi <i>et al.</i> , 2008).	Biochemical studies on mutant protein are not yet performed.
R21W	Central and lamellar with varying anterior and posterior polar components (Hansen <i>et al.</i> , 2007). Congenital nuclear cataract in association with microcornea and microphthalmia (Devi <i>et al.</i> , 2008).	Biochemical studies on mutant protein are not yet performed.

Continued ....



Continued ...

<b>R54C</b>	Recessive congenital total cataract with microcornea and punctate lenticular opacities in heterozygous carriers (Khan <i>et al.</i> , 2007). Autosomal dominant congenital nuclear cataract in association with microcornea (Devi <i>et al.</i> , 2008).	Disrupted intracellular structures like actin and mitochondria in lens epithelial and fiber cells (Xia <i>et al.</i> , 2006). Biochemical studies on mutant protein are not yet performed.
<b>R21L</b>	Congenital cataract and macular hypoplasia (Graw <i>et al.</i> , 2006).	Protein not characterized yet. Macular hypoplasia can be due to a concerted interaction with compound heterozygous mutations (R419Q and A481T) in the P gene.
<b>W9X</b>	Autosomal recessive cataract (Pras <i>et al.</i> , 2000).	Aberrantly truncated - only results in 8 amino acids peptide.
<b>G98R</b>	Peripheral ring-like opacity to total cataract with advancing age (Santhiya <i>et al.</i> , 2006).	Biochemical and biophysical studies on the mutant protein are performed and discussed in detail in following chapters.
<b>Alpha B-crystallin</b>		
<b>Mutation</b>	<b>Disease</b>	<b>Remarks</b>
<b>R120G</b>	Desmin-related myopathy and congenital cataract (Vicart <i>et al.</i> , 1998).	Change in secondary, tertiary and quaternary structure and decreased chaperone-like activity (Kumar <i>et al.</i> , 1999; Bova <i>et al.</i> , 1999; Perng <i>et al.</i> , 1999a).
<b>450DeIA</b>	Autosomal dominant congenital posterior polar cataract (Berry <i>et al.</i> , 2001).	Deletion causes a frameshift in codon 150 giving rises to aberrant protein of 184 residues. The mutant protein shows self-aggregation, less thermostability and decreased chaperone-like activity (Hayes <i>et al.</i> , 2008).
<b>D140N</b>	Autosomal dominant congenital lamellar cataract (Liu <i>et al.</i> , 2006a).	Alterations in tertiary, quaternary structure and loss of chaperone-like activity (Liu <i>et al.</i> , 2006a).
<b>A171T</b>	Congenital lamellar cataract (Devi <i>et al.</i> , 2008).	Biochemical studies on mutant protein are not yet performed.
<b>P20S</b>	Autosomal dominant congenital posterior polar cataract (Liu <i>et al.</i> , 2006b).	Reduced subunit exchange and decreased chaperone-like activity of alpha A-crystallin in heteroaggregates. Abnormal nuclear localization and triggers apoptosis of human lens epithelial cells (Li <i>et al.</i> , 2008).

ability to trigger apoptosis (Li *et al.*, 2008). These results suggest that the changes in the structure and function of the  $\alpha$ -crystallin complex and cytotoxicity are vital factors in the pathogenesis of congenital cataract linked to the P20S mutation in the  $\alpha$ B-crystallin.

R116C or R116H mutation in  $\alpha$ A-crystallin causes phenotypically different dominant congenital cataracts (Table 1.5). Equivalent missense mutations in Hsp22 and  $\alpha$ B-crystallin are associated with other human diseases (Table 1.4). Arginine or lysine are found at this residue in almost all sHsps across the phylogeny and are likely to play an important structural role. Site-directed spin-label studies of the amino acid residues between positions 109 and 120 of  $\alpha$ A-crystallin revealed the presence of a  $\beta$ -strand containing the presumably buried residues R112 and R116 forming salt bridges with residues of opposite charges (Berengian *et al.*, 1997). Subsequent studies confirmed the presence of antiparallel  $\beta$ -sheets between residues 84 and 120 (Koteiche *et al.*, 1998). R116C $\alpha$ A-crystallin forms much larger oligomers than the wild type protein (Kumar *et al.*, 1999; Shroff *et al.*, 2000), exhibits an increased membrane association (Cobb and Petrash, 2000) and diminished chaperone activity (Kumar *et al.*, 1999; Shroff *et al.*, 2000; Bera *et al.*, 2002). R116H $\alpha$ A-crystallin exhibits increased lysozyme binding, increase in hydrophobicity and loss of chaperone-like activity (Gu *et al.*, 2008). That loss of positive charge at this position is a key factor for modified structure and function was concluded by substituting R116 of  $\alpha$ A-crystallin with lysine, cysteine, glycine or aspartic acid (Bera *et al.*, 2002). R116C $\alpha$ A-crystallin displays much weaker anti-apoptotic ability compared to  $\alpha$ A-crystallin and results in increased cell death (Andley *et al.*, 2002; Mao *et al.*, 2004). It weakly sequesters Bax and Bcl-XS in the cytosol and cannot prevent their translocation into mitochondria during apoptosis induced by staurosporine, a protein kinase inhibitor (Mao *et al.*, 2004). Transgenic overexpression of R116C $\alpha$ A-crystallin in mouse lens results in lens opacities and sutural defects (Hsu *et al.*, 2006). R116C $\alpha$ A-crystallin binds less to actin relative to  $\alpha$ A-crystallin, which may perturb the normal differentiation processes of lens cells (Brown *et al.*, 2007).

Crystallin-crystallin interactions have also been shown to undergo changes with these mutations. For the R116C $\alpha$ A-crystallin, the interactions with  $\beta$ B2- and  $\gamma$ C-crystallin decreased and those with  $\alpha$ B-crystallin and Hsp27 increased (Fu and Liang, 2003). Although R116C $\alpha$ A-crystallin exhibits a reduced ability to exchange subunits with wild type  $\alpha$ A-crystallin (Cobb and Petrash, 2000), it has a higher affinity for forming heteroaggregates with  $\alpha$ B-crystallin, which have larger size, distinctly different tertiary structure and decreased chaperone activity as compared to heteroaggregates of wild type  $\alpha$ A- and  $\alpha$ B-crystallin (Bera

and Abraham, 2002). Subunit exchange studies by FRET showed that R116C $\alpha$ A-crystallin and R120G $\alpha$ B-crystallin have slightly decreased transfer efficiencies as a result of conformational change (Liang and Liu, 2006). All these results clearly indicate that altered protein-protein interactions due to R116C mutation may contribute to decreased protein solubility and formation of cataract.

In contrast to R116C, R49C $\alpha$ A-crystallin can be detected in the insoluble membrane fraction of the transfected LECs raising a possibility of inappropriate disulphide bridge formation. However, unpublished results from our laboratory indicate no change in structural aspects of the mutant protein. Upon transfection in LECs, wild type  $\alpha$ A-crystallin localizes to cytoplasm but 70-80% of R49C transfectants displayed speckled nuclear localization suggesting a relationship to neurodegenerative disorders characterized by intranuclear glutamine-repeats. The R49C mutant is cytotoxic and less protective against staurosporine-induced apoptosis than its wild type counterpart (Mackay, *et al.*, 2003). Koteiche and Mchaourab (2006) showed that R116C and R49C mutations result in increased binding of  $\alpha$ A-crystallin to destabilized T4 lysozyme mutants and shift the equilibrium towards binding-competent state. This changes the energetic threshold for complex formation with unfolded substrates, leading to saturation of  $\alpha$ A-crystallin binding sites and its subsequent co-aggregation with the substrate. Recently, using a knock-in mouse model, Xi *et al.* (2008) have shown that R49C $\alpha$ A-crystallin heterozygosity led to early nuclear cataracts, whereas homozygous mice showed severe congenital cataracts with small eye phenotype and increase in apoptosis of fiber cells. Both homozygous and heterozygous mice lenses showed an increase in insoluble  $\alpha$ A- and  $\alpha$ B-crystallin with altered R49C $\alpha$ A-crystallin interaction with other lens substrate proteins. Thus, the mutant protein is detrimental to the development of clear lens.

No clinical description of the autosomal recessive cataract morphology associated with W9X nonsense mutation has been published. However, the premature chain termination may mimic the changes observed in  $\alpha$ A-crystallin knockout mouse in homozygous state. Mice carrying R54C mutation showed degenerated fiber cells and severely altered epithelial cells in their lenses. Further, mutant mice are associated with disruptions of essential subcellular structures, such as actin filaments and mitochondria, in embryonic lens fiber cells indicating that this residue is essential for the normal functioning of  $\alpha$ A-crystallin in development (Xia *et al.*, 2006). The G98R mutation in  $\alpha$ A-crystallin causes a presenile cataract and the phenotype is progressive from a peripheral ring-like opacity at the

age of 16 years to total cataract by the age of 24 (Santhiya *et al.*, 2006). Most of the information on this mutation has come from our studies, which are described in the subsequent chapters in this thesis. Not much is known about other mutations in  $\alpha$ -crystallins that have been identified in the last year or so.

The wide variations in morphology of the opacity even for identical mutations suggest interplay of genetic, environmental and local anatomy in the lens. In addition, while the pathophysiology of congenital and hereditary cataracts differs in fundamental ways from that of age-related cataracts, the study of congenital cataracts can provide insights into the mechanisms of lens transparency and to some of the ways in which it can be lost as the lens ages.

### **1.7.1.3 sHsps and neurological diseases:**

Recent studies have shown that sHsps have anti-apoptotic and cyto-protective role (Wagstaff *et al.*, 1999; Bruey *et al.*, 2000; Andley *et al.*, 2002; Kamradt *et al.*, 2002; Benn *et al.*, 2002; Chávez Zobel *et al.*, 2003). At least three sHsps ( $\alpha$ B-crystallin, Hsp27, Hsp22) are abundant in different nerve cells. Increased levels of Hsp27 and  $\alpha$ B-crystallin are found in individuals with neurodegenerative diseases marked by deposition of improperly folded proteins or plaques in nervous system such as Alzheimer's (Shinohara *et al.*, 1993; Dabir *et al.*, 2004), Parkinson's (Renkawek *et al.*, 1999), Alexander's disease (Head *et al.*, 1993; Iwaki *et al.*, 1993) and amyotrophic lateral sclerosis (ALS) (Vleminckx *et al.*, 2002).  $\alpha$ B-crystallin is implicated as a major autoantigen in multiple sclerosis (MS), a chronic autoimmune condition involving brain and spinal cord inflammation (van Noort *et al.*, 1995, van Veen *et al.*, 2003). Hsp22 is also known to be associated with classic senile plaques in Alzheimer's (Benn *et al.*, 2002). Patients having deleted Hsp27 gene along with typical Williams syndrome (WS) deletion region resulted in severe mental retardation than the WS patients with deletions that did not include Hsp27 gene (Stock *et al.*, 2003). Though all these observations provide an indirect link between sHsps and neurological diseases, direct evidence for their role came recently from a host of mutations identified in Hsp22 and Hsp27 leading to hereditary peripheral neuropathies.

#### **1.7.1.3.1 Hsp22 and Hsp27 in inherited peripheral neuropathies:**

Hereditary peripheral neuropathies comprising a wide variety of diseases are among the most common genetic disorders in humans and are primarily, manifestations of

progressive peripheral nerves dysfunction resulting from abnormalities in Schwann cells and their myelin sheaths. The best known peripheral neuropathy is Charcot-Marie-Tooth (CMT) disease (also known as hereditary motor and sensory neuropathies; HMSNs) described by J.M. Charcot, P. Marie and H.H. Tooth. The CMT disorder is the most common genetically heterogeneous group of inherited peripheral neuropathy, with an estimated frequency of 1/2500 individuals (Skre, 1974) exhibiting all forms of Mendelian inheritance (autosomal dominant, X-linked and autosomal recessive). Based on electrophysiological analysis, CMT neuropathies can be divided into two distinct classes - CMT type 1 (CMT1), the demyelinating form, exhibits reduced nerve conduction velocities (NCVs) with intrinsic Schwann cell defect, and CMT type 2 (CMT2), the axonal form, results from neuronal atrophy and exhibits normal NCVs but decreased conduction amplitudes (Harding and Thomas, 1980). Though there is a wide range of variation in clinical presentation and severity in individuals, common clinical hallmarks include progressive weakness of distal limb muscles, sensory loss, decreased or absent tendon reflexes, leg atrophy, steppage gait and other foot deformities.

The exclusively motor variant of CMT without sensory symptoms is designated as spinal CMT or hereditary distal spinal muscular atrophy, and included in distal hereditary motor neuropathy (dHMN). On clinical examination, distal HMN patients are hard to distinguish from CMT2 patients; therefore, electrophysiological examinations are essential to confirm the diagnosis of either distal HMN, where only motor neurons are involved, or CMT2, where motor and sensory neurons are involved. dHMN is further divided into seven subtypes according to the mode of inheritance, age at onset and clinical evolution. Distal HMN type II has onset age of 15-25 years and the presenting symptoms are paresis of the extensor muscles of the big toe and later of extensor muscles of the feet. The disease progresses rapidly to complete paralysis of all distal muscles of the lower extremities.

A number of genes that are defective in patients with the main forms of CMT2 or dHMN such as mitofusion 2 (MFN2), peripheral myelin protein 22 (PMP22), neurofilament light chain (NEFL), dynamin 2 (DNM2), glycyl-tRNA synthetase (GARS), myelin protein zero (MPZ), senataxin (SETX), dynactin (DCTN1) etc. have been identified. Recently, two distinct missense mutations (K141N and K141E) involving the same lysine residue (K141) in the  $\beta$ 7 strand of Hsp22 were reported in four dHMN type II families (Irobi *et al.*, 2004). This positively charged residue is highly conserved across all mammalian sHsps and is essential for the structural and functional integrity of  $\alpha$ A-crystallin (Bera *et al.*, 2002),  $\alpha$ B-crystallin

(Simon *et al.*, 2007a) and Hsp27 (Chávez Zobel *et al.*, 2005). Missense mutations spanning different regions of Hsp27 have also been shown to underlie different form of dHMN or axonal CMT in a number of families (Table 1.4). With the identification of mutations in these genes it also became apparent that mutations in the same gene are associated with clinically separate disease entities, as mutations in Hsp27 (S135F, R127W) and Hsp22 (K141N) have been found both in individuals with CMT2 and distal HMN phenotypes. The underlying pathological mechanism in these disorders is not clear: whether it is misfolding and aggregation of the mutant sHsp, or a defective cytoprotective and chaperone-like activity leading to misfolding and aggregation of other proteins, or a dysfunction in cell death pathways, or a combination of these effects.

Functional studies demonstrate that Hsp22 and Hsp27 are interacting partners (Benndorf *et al.*, 2001; Sun *et al.*, 2004) and the disease-causing mutations in Hsp22 and Hsp27 enhance this interaction (Irobi *et al.*, 2004; Fontaine *et al.*, 2006), suggesting linkage of these two etiologic factors into one common pathway. Neuronal cell lines transfected with mutant forms of Hsp22 or Hsp27 showed reduced viability (Irobi *et al.*, 2004; Evgrafov *et al.*, 2004; Zhai *et al.*, 2007) and their expression promoted the formation of intracellular aggregates (Irobi *et al.*, 2004; Ackerley *et al.*, 2006; Fontaine *et al.*, 2006). Increased interactions involving mutant sHsps may be the molecular basis for their increased tendency to form cytoplasmic protein aggregates. Accumulation of these misfolded proteins can have deleterious effects on neuronal cell function and can ultimately lead to cell death.

It is believed that these sHsp mutations lead to mitochondrial dysfunction or interference in axonal transport (Züchner and Vance, 2006). Hsp27 has been shown to be directly responsible for a stable mitochondrial membrane potential through an increase in reduced form of glutathione (Prévaille *et al.*, 1999). Hsp27 was also shown to be involved in organization of neurofilament network, which is important for maintenance of axonal cytoskeleton and transport (Perng *et al.*, 1999b). The neuropathy-causing mutant Hsp27 affects the neurofilament assembly (Evgrafov *et al.*, 2004; Ackerley *et al.*, 2006; Zhai *et al.*, 2007) and specific aspects of axonal transport (Ackerley *et al.*, 2006).

Most of the disease-causing mutations identified in Hsp22 and Hsp27 are in the  $\alpha$ -crystallin domain (Table 1.4) and can affect the chaperone activity. A cysteine residue, C141, in murine Hsp25 (corresponding to C137 in Hsp27) when substituted showed decreased ability to multimerize and less efficiency in inhibiting staurosporine-induced apoptosis (Diaz-Latoud *et al.*, 2005). C137 as well as the N-terminal region of Hsp27 seems

to be essential for binding to cytochrome C (Bruey *et al.*, 2000). Interestingly, S135F and R136W mutation are located next to this functionally important cysteine and possibly interfere with oligomerization or apoptosis. Since Hsp22 also interacts with other sHsps besides Hsp27 (Sun *et al.*, 2004), mutant Hsp22 may induce apoptosis causing neuronal cell death by disturbing the anti-apoptotic effect of other sHsps.

The P182 residue in the C-terminal extension of Hsp27 is close to the dominant negative mutation of  $\alpha$ B-crystallin that causes myofibrillar myopathy (Selcen and Engel, 2003) and the mutation disrupts the conserved IXI/V motif. This motif is critical for oligomerization of  $\alpha$ A- and  $\alpha$ B-crystallin (Pasta *et al.*, 2004) and chaperone-like activity of many bacterial sHsps (Studer *et al.*, 2002). Co-transfection of wild type Hsp27 with mutant P182LHsp27 results in sequestering of the wild type protein into intracellular aggregates (Ackerley *et al.*, 2006) that could remove a portion of wild type protein from other essential functions within the cell. Similarly, Hsp27 is present in the intracellular aggregates formed by Hsp22 mutants (Irobi *et al.*, 2004). This could be of particular significance in specific cell types such as sensory or motor neurons, where a basal level of expression may be critical.

Neurotoxicity can also be associated with abnormal protein aggregation; thus formation of aggresomes suggests a role for efficient protein folding in pathogenesis. Hsp27 interacts with both wild type and CMT mutant NEFL, triggers reversal of CMT mutant NEFL aggregation and promotes its assembly whereas S135FHsp27 causes NEFL aggregation, indicating that chaperone-like activity and ability of Hsp27 to stabilize the neurofilament network can contribute to its neuroprotective properties (Zhai *et al.*, 2007). This indicates that these missense mutations in the Hsp22 and Hsp27 proteins may have a gain of function effect, which may lead to dysfunction of axonal transport and dysregulation of the cytoskeleton, causing neuronal death.

Up-regulation and phosphorylation of Hsp27, the molecular partner of Hsp22, is necessary for sensory and motor neuron survival following peripheral nerve injury (Benn *et al.*, 2002). Effect of mutation on this kind of transcriptional and post-translational regulation can be another possible mechanism involved in the pathogenesis of CMT2 or dHMN.

The identification of mutations in sHsps associated with human motor and sensory neuropathies indicate their pivotal role in the peripheral nervous system. Hsp27 has been shown to have neuroprotective role both *in vitro* and *in vivo* against variety of stresses (Latchman, 2005). Until now there is no direct evidence that Hsp22 is also neuroprotective. Since Hsp22 acts as a cytoprotective component in non-neuronal cell lines (Chávez Zobel *et*



---

*al.*, 2003), it is plausible that it has the ability to protect neurons from cell death. The specific mechanisms underlying this neuroprotection are still to be defined. A key question in this context is - why are deleterious effects of widely expressed genes limited exclusively to motor and/or sensory neurons? It can be due to highly specialized needs of axonal transport and high requirement of energy due to the length of their axons. It is also possible that mutations in different functional domains affect different functions. It is currently not known how these molecular chaperones act on other proteins involved in motor neuron function.

### 1.8 Scope of the present study:

$\alpha$ A-crystallin, being a member of class II sHsps, shows tissue-restricted expression pattern – abundant in ocular tissues and found in traces in the spleen, thymus and kidney. On the other hand, Hsp22 is the member of class I sHsps, and is widely expressed in the brain, spinal cord, lung, kidney, liver, stomach, skeletal and cardiac muscle. Hsp22 is a unique sHsp, having a monomeric structure *in vitro* and exhibiting chaperone activity. In contrast,  $\alpha$ A-crystallin forms polydisperse oligomers of high molecular weight. Further, Hsp22 is a stress-inducible chaperone, whereas such stress-inducibility is clearly wanting in the case of  $\alpha$ A-crystallin. Though, both the proteins are members of the sHsp family and share a sequence similarity in the ' $\alpha$ -crystallin domain', they clearly represent the diversity of the sHsp family.

Extensive genome research since last decade has identified mutations in sHsps including  $\alpha$ B-crystallin, Hsp27,  $\alpha$ A-crystallin and Hsp22 in many human diseases. Interestingly, although these point mutations are scattered over the entire sequence of different sHsps, of the fourteen mutations present in  $\alpha$ -crystallin domain, eleven mutations are present in the  $\beta$ 5- $\beta$ 7 region. Of the four human sHsps with disease-causing mutations identified so far,  $\alpha$ A-crystallin and Hsp22 have been studied the least.

To date, point mutations identified in  $\alpha$ A-crystallin have been associated only with cataracts - probably due to its almost exclusive expression in the lens. On the other hand, Hsp22 is widely expressed; mutations in Hsp22 resulted in neurological diseases. Of all the cataract-causing mutations in  $\alpha$ -crystallins, G98R mutation in  $\beta$ 5 strand of  $\alpha$ A-crystallin is unique in many aspects. Though the mutation is autosomal dominant, it does not cause congenital cataract. It is the first instance of a novel disease-causing mutation involving a sHsp, found in an Indian family. Finally, so far all the missense mutations in  $\alpha$ A-crystallin associated with cataract show substitution from arginine whereas in this mutation glycine is

replaced by arginine (Table 1.4 and 1.5). There was no information about the molecular basis of this mutation when we started our studies on this mutation.

The conserved K141 residue in Hsp22 corresponds to R116, R120 and R140 residues in  $\beta$ 7 strand of the  $\alpha$ A-crystallin,  $\alpha$ B-crystallin and Hsp27 respectively. This residue in sHsps appears to be a hot spot of mutation as mutation of the corresponding residue in  $\alpha$ A-crystallin (R116C/H) causes congenital cataract, in  $\alpha$ B-crystallin (R120G) causes congenital cataract and desmin related myopathy, and that in Hsp27 (R140G) results in neuropathy (Table 1.4). K141N and K141E mutations are involved in CMT2 or dHMN disorders. Very little information was available on these two mutant proteins related to their aberrant protein interactions in cells. Although, R116C and R120G mutations are best studied among all the known sHsps mutations, the biochemical and biophysical consequences of K141N/E mutations are not known as they had not been purified and characterized.

Since the chaperone function of sHsps strongly depends on its structure, it is important to investigate the effect of mutations on structural change(s) and in turn on chaperone function. Several intriguing questions regarding point mutations in these sHsps are unanswered. (i) What is the effect of these mutations on structure of the proteins and more importantly on their chaperone-like activity? (ii) When all autosomal dominant mutations in  $\alpha$ A-crystallin give rise to congenital cataract, why does G98R mutation results in presenile cataract phenotype? (iii) In heterozygous condition,  $\alpha$ A-crystallin can form mixed complexes with mutant protein. What is the role of such complexes in modulating their structure, chaperone function as well as stability? (iv) Does the G98R mutation make  $\alpha$ A-crystallin sensitive to environmental insults, which in turn are responsible for progression of cataract with advancing age? (v) What are the differences in characteristics of K141E and K141N mutant proteins of Hsp22 and how does one cause only dHMN and the other both CMT2 and dHMN? The present work aims to gain better understanding into the structure-function relationship of human  $\alpha$ A-crystallin and Hsp22.

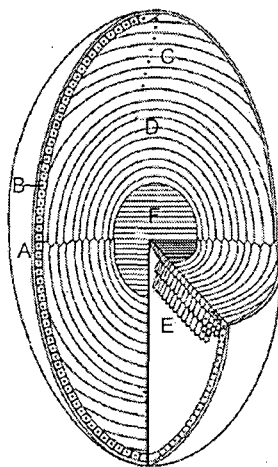
Elucidating the role of these mutations in  $\alpha$ A-crystallin and Hsp22 would thus be helpful in understanding the molecular basis of the pathology. Such an understanding can help in designing strategies to cope with protein-aggregation related problems in biotechnology and development of rechaperoning therapies or other drugs.

A  
CATARACT-CAUSING  
MUTATION IN  
CLASS II sHSP,  
 $\alpha$ A-CRYSTALLIN

2

## 2.1 INTRODUCTION:

Eye lens, a highly specialized tissue, maintains its transparency and necessary refractive index owing to its very high protein concentration [as high as 450 mg/ml in its core (Fagerholm *et al.*, 1981)], by appropriate architecture of lens fiber cells and precise homeostasis of the lens proteins - mainly  $\alpha$ -,  $\beta$ - and  $\gamma$ -crystallins. The eye lens continues to grow throughout one's life as elongated organelle-free lens fibre cells, which are terminally differentiated from a single layer of polarized epithelial cells underlying the anterior surface of the lens, are continuously laid layer upon layer (Figure 2.1). Proteins cannot diffuse between differentiated fibre cells in the center of the lens and recently synthesized cortical region (Harding, 1997). In the virtual absence of any protein turnover in mature lens fibre cells, crystallins exist for the lifespan of an individual undergoing various metabolic and environmental insults. Since lens proteins also undergo various post-translational modifications with age (Hanson *et al.*, 2000), many of which lead to their unfolding and denaturation making them aggregation-prone, a mechanism must exist to maintain these proteins in their native form.  $\alpha$ -Crystallin, constituting nearly 40% of total soluble protein of the mammalian eye lens, acts as a molecular chaperone (Horwitz, 1992; Rao *et al.*, 1993; Jakob *et al.*, 1993) and maintains the transparency of the vertebrate eye lens. It is a large polydisperse oligomer of two  $\sim$ 20 kDa polypeptide chains,  $\alpha$ A- and  $\alpha$ B-crystallin, that share about 57% amino-acid sequence homology (Quax-Jeuken *et al.*, 1985). These are believed to be present in a molar ratio ( $\alpha$ A: $\alpha$ B) of approximately 3:1 in the mammalian lens (Sax and Piatigorsky, 1994). In the absence of any other chaperone system that can refold the proteins in the lens, it is believed that  $\alpha$ -crystallin acts as a one-way irreversible sink that sequesters the partially unfolded proteins preventing the formation of large light scattering



**Figure 2.1: Schematic view of the eye lens showing the main features and regions.** The eye lens is enclosed by lens capsule (A) and the anterior surface of the lens is covered with a single layer of epithelial cells (B). The lens fibre cells are formed from epithelial cells at the lens equator in the cortical region (C) as part of their differentiation pathway. The epithelia elongate until their ends reach the two lens poles and are joined at the lens sutures. One of the striking features of the lens differentiation process at this stage is the removal of membrane-bound organelles (D) including nuclei, as indicated here as black dots. A cross section of the lens reveals the elongated fibre cells with characteristic hexagonal shape (E). The bulk of the lens thus consists of long, ribbon-like fibre cells arranged as concentric layers with the primary fibre cells at the centre of the lens (F). (Perng *et al.*, 2007)

aggregates, thereby preventing cataract (lens opacities). Major target proteins in the lens for  $\alpha$ -crystallin include  $\gamma$ S,  $\gamma$ D, various  $\beta$ -crystallins (Hanson *et al.*, 2000; Boyle and Takemoto, 1994), enzymes like glyceraldehyde-3-phosphate dehydrogenase and enolase (Velasco *et al.*, 1997), cytoskeletal proteins in the lens epithelium and cortical fibre cells (Muchowski *et al.*, 1999) and lens plasma membrane and its associated proteins (Boyle and Takemoto, 1996; Cobb and Petrash, 2002).

Both  $\alpha$ A- and  $\alpha$ B-crystallin share sequence homology with other members of the small heat shock protein (sHsp) family (Ingolia and Craig, 1982) and exhibit chaperone-like activity in preventing the aggregation of other proteins (Horwitz, 1992; Raman and Rao, 1994; Sun *et al.*, 1997; Kumar *et al.*, 1999; Datta and Rao, 1999), in protecting enzyme activity upon heat stress (Hook and Harding, 1997; Hess and FitzGerald, 1998; Marini *et al.*, 2000; Rajaraman *et al.*, 2001) and in helping some enzymes to refold (Rawat and Rao, 1998; Goenka *et al.*, 2001; Nath *et al.*, 2002). Age-related modifications in  $\alpha$ -crystallins lead to formation of large water-insoluble aggregates (Fujii *et al.*, 2007), the mechanism of which is not known.  $\alpha$ -Crystallin from old human lenses (Cherian and Abraham, 1995) and from selenite-induced cataractous lenses of an animal model (Kelley *et al.*, 1993) also exhibit decreased chaperone-like activity.

In humans, the gene coding for  $\alpha$ A-crystallin (173 amino-acid protein) is located on chromosome 21 (Hawkins *et al.*, 1987), whereas the gene coding for  $\alpha$ B-crystallin (175 amino-acid protein) is present on chromosome 11 (Ngo *et al.*, 1989). Using site-directed mutagenesis and *in vitro* assays, several reports have showed that  $\alpha$ -crystallin is generally stable and refractory to changes in its structure and function even upon many amino acid substitutions in its sequence (Berengian *et al.*, 1997; Koteiche *et al.*, 1998; Horwitz *et al.*, 1998; Smulders *et al.*, 1998; Muchowski *et al.*, 1999b; Derham *et al.*, 2001). However, subsequently, several point mutations in  $\alpha$ A- as well as  $\alpha$ B-crystallin have been reported to cause pathological conditions. The mutation of an arginine residue (that is highly conserved in all the sHsps) to cysteine in  $\alpha$ A-crystallin (R116C) and to glycine in  $\alpha$ B-crystallin (R120G) leads to congenital cataract (Litt *et al.*, 1998; Vicart *et al.*, 1998). The R120G mutation in  $\alpha$ B-crystallin also leads to desmin-related myopathy (Vicart *et al.*, 1998). Studies from our laboratory (Kumar *et al.*, 1999) as well as those from other laboratories (Bova *et al.*, 1999; Perng *et al.*, 1999a; Shroff *et al.*, 2000) have shown that mutation of this arginine residue causes altered secondary, tertiary and quaternary structure of  $\alpha$ A- and  $\alpha$ B-crystallin, which results in loss of chaperone-like activity. Subsequently, a few other mutations in  $\alpha$ A- and  $\alpha$ B-

crystallin leading to cataract have also been reported (Table 1.5). A recent study by Santhiya *et al.* (2006) has reported the identification of a mutation (G98R) in  $\alpha$ A-crystallin in three members of an Indian family that leads to onset of cataract at the age of 16 years and loss of vision by the age of 24. The molecular basis for the cataract caused by this mutation was not known. Information on functional and structural aspects of this mutant protein was not available. The objective of the present study was to investigate the effect of this mutation on the structure, stability and function of  $\alpha$ A-crystallin and address the following important questions: Can the mutant protein function as a chaperone *in vivo* and *in vitro* similar to its wild-type counterpart? What are its structural features? How does it cause cataract? Why is the phenotype not congenital but presenile in nature?

We generated the G98R mutation in  $\alpha$ A-crystallin by site-directed mutagenesis, cloned, overexpressed and purified the mutant protein to homogeneity. We studied its secondary and tertiary structure by circular dichroism and fluorescence spectroscopy. We performed gel-filtration chromatography and used dynamic light scattering (DLS) to analyze its quaternary structure. We have also investigated its stability and chaperone-like activity. The results of these studies are discussed in this chapter.

## 2.2 EXPERIMENTAL PROCEDURES:

### 2.2.1 Materials:

pET-21a(+) vector, T7 promoter and terminator primers were obtained from Novagen (Madison, USA). *Xba*I, *Hind*III restriction enzymes and T4-DNA Ligase were acquired from NEB (Madison, USA). Gel filtration chromatographic medium Bio-Gel A-1.5m was purchased from Bio-Rad Laboratories (Hercules, USA). Q-Sepharose, Superose-6 HR 10/30 and a high molecular weight protein calibration kit comprising of thyroglobulin, ferritin, catalase and aldolase were purchased from Amersham Biosciences (Uppsala, Sweden). Proteinase K was obtained from Boehringer-Mannheim (Germany). Urea of ultra pure grade was purchased from United States Biochemicals Inc. (Cleveland, USA). Isopropyl  $\beta$ -D-thiogalactopyranoside (IPTG) and dithiothreitol (DTT) were purchased from Sisco Research Laboratory (Mumbai, India). Phenylmethylsulfonyl fluoride (PMSF) and insulin were from Sigma (St. Louis, USA). 1,1'-bi(4-anilino)naphthalenesulfonic acid (Bis-ANS) was purchased from Molecular Probes (Eugene, USA).





### 2.2.3 Expression and purification of the wild type and G98R mutant protein:

The wild type and the mutant recombinant proteins were overexpressed in *Escherichia coli* BL21(DE3) cells (Stratagene, CA, USA) using 1 mM IPTG. Both bacterial cell pellets were suspended in 50 mM Tris-HCl, pH 7.4, containing 100 mM NaCl and 1 mM EDTA (TNE) buffer. Bacterial cell suspension was incubated for 2 h with lysozyme (0.2 mg/ml) and PMSF (0.2 mM) before sonication and subsequent centrifugation. The wild type protein which partitioned in the soluble fraction was purified essentially as described earlier (Kumar *et al.*, 1999). Briefly, the wild type protein, which partitioned into the soluble fraction of lysate, precipitated at 30-60% ammonium sulfate saturation. The protein pellet was dissolved in TNE buffer and subjected to gel filtration chromatography using a Bio-Gel A-1.5m matrix. The pooled fractions were further purified on a Q-Sepharose ion-exchange column. The mutant protein, which partitioned into inclusion bodies was purified by washing the inclusion bodies with 50 mM Tris-HCl, pH 7.4, and subsequently dissolving them in 50 mM Tris-HCl buffer, pH 7.4, containing 1 mM EDTA and 3 M urea. The solubilized inclusion bodies containing the mutant protein were directly subjected to ion exchange chromatography using a Q-Sepharose column equilibrated with the same buffer. The column was washed with 50 mM Tris-HCl buffer, pH 7.4, containing 1 mM EDTA and 150 mM NaCl without urea so that the protein could refold. The mutant protein was eluted with a step gradient of buffer containing 225 mM NaCl. The purified proteins were dialyzed against the TNE buffer and concentrated by ultra-filtration using the Amicon ultra-filtration stirred cell. The purity of the wild type and mutant proteins was checked by sodium dodecylsulfate (SDS)-polyacrylamide gel electrophoresis. The concentrations of the wild type and mutant protein samples were determined spectrophotometrically using the extinction coefficient ( $\epsilon_{280\text{nm}}$ ) of 0.725 for 1 mg/ml of protein, calculated by a sequence-based method described by Pace *et al.* (1995). The samples were stored at 4°C.

### 2.2.4 Circular dichroism studies:

Near- and far-UV circular dichroism (CD) spectra of the wild type and the mutant  $\alpha$ -crystallin were recorded using a JASCO J-715 spectropolarimeter at 25°C. Spectra were recorded using 1.0 mg/ml of protein in TNE buffer in a 1 cm path length cell for the near-UV region and using 0.5 mg/ml of protein in 0.1 cm path length cell for the far-UV region. Appropriate buffer spectra were subtracted from the sample spectra. All reported spectra are

the average of 4 scans, smoothed and expressed as molar ellipticity,  $[\theta]_{\text{MRM}}$ , in units of  $\text{deg cm}^2 \text{dmol}^{-1}$ .

For urea denaturation studies, far-UV CD spectra of wild type or mutant protein (1.0 mg/ml) incubated with the specified concentrations of urea were recorded in a 0.05 cm path length cuvette in order to increase the signal to noise ratio. Fraction unfolded was calculated on the basis of ellipticity at 220 nm ( $\theta_{220 \text{ nm}}$ ) using the formula  $([\theta]_{\text{N}} - [\theta]) / ([\theta]_{\text{N}} - [\theta]_{\text{U}})$  where  $[\theta]_{\text{N}}$  and  $[\theta]_{\text{U}}$  are the ellipticity at 220 nm of native protein and protein unfolded in 7 M urea respectively;  $[\theta]$  represents the ellipticity of the protein at any given urea concentration.

### 2.2.5 Steady-state fluorescence studies:

All steady-state fluorescence measurements were carried out using a Hitachi F-4500 Fluorescence Spectrophotometer. Intrinsic tryptophan fluorescence spectra of the wild type and mutant  $\alpha$ A-crystallin (0.2 mg/ml in TNE buffer) were recorded by exciting the sample at 295 nm with excitation and emission band passes set at 2.5 nm each.

Surface hydrophobicity was probed using the hydrophobic probe, bis-ANS. A 10  $\mu\text{M}$  methanolic solution of bis-ANS was added to wild type or mutant G98R $\alpha$ A-crystallin (0.2 mg/ml) before incubating the samples at 25°C for 30 min. Fluorescence spectra were recorded from 400 to 600 nm with the excitation wavelength at 390 nm. The excitation and emission band passes were set at 2.5 nm each. All spectra were recorded in corrected spectrum mode.

Similar intrinsic and bis-ANS fluorescence measurements were done for urea denaturation studies by incubating wild type or mutant  $\alpha$ A-crystallin samples (0.1 mg/ml) in buffer containing various concentration of urea.

### 2.2.6 Time-resolved fluorescence studies:

Fluorescence lifetime measurements of all the samples were made using the Model 5000 U-TCSPC Picosecond Lifetime measurement system (Horiba Jobin Yvon, France) in TCSPC (time-correlated single photon counting) mode. A 294 nm wavelength NanoLED pulsed laser with a repetition rate of 1MHz was used for excitation in tryptophan fluorescence intensity decay experiments. Samples of  $\alpha$ A-crystallin or G98R $\alpha$ A-crystallin (0.4 mg/ml) in TNE buffer containing various concentrations of urea were used for all lifetime measurements. In another experiment, samples were incubated with 10  $\mu\text{M}$  bis-ANS in the

presence of specified urea concentrations and then excited with 337 nm wavelength NanoLED pulsed laser with a repetition rate of 1MHz.

The instrument response function (IRF) was obtained at the same wavelength as that of excitation (at 294 nm for tryptophan fluorescence lifetime and 337 nm for bis-ANS fluorescence lifetime) using Ludox suspension. The emission decay (at 337 nm for tryptophan fluorescence lifetime and 500 nm for bis-ANS fluorescence lifetime) data were analyzed using the DAS6 software. Data were fitted using the statistical method of iterative, least-squares reconvolution, assuming three-exponential decay function  $[A+B1.exp(-i/\tau1) + B2.exp(-i/\tau2) + B3.exp(-i/\tau3)]$  where  $\tau1$ ,  $\tau2$  and  $\tau3$  are individual lifetime components with B1, B2 and B3 as their relative amplitudes (pre-exponential factors) respectively. The best fit was assessed based on  $\chi^2$  and distribution of weighted residuals along the zero line. Mean lifetime ( $\tau_m$ ) was calculated using the formula,  $(B1.\tau1 + B2.\tau2 + B3.\tau3) / B1 + B2 + B3$ .

### 2.2.7 FPLC gel permeation chromatography:

The oligomeric size of the wild type and mutant  $\alpha$ A-crystallin was estimated on a Superose-6 HR 10/30 pre-packed FPLC column (dimensions 1 × 30 cm). A 1.5 mg/ml solution of wild type or mutant  $\alpha$ A-crystallin in TNE buffer was filtered with 0.22  $\mu$  syringe filter and 100  $\mu$ l of this sample was applied to the column previously equilibrated with the same buffer. The column was eluted at a flow rate of 0.4 ml/min. High molecular mass standards comprising thyroglobulin (669 kDa), ferritin (440 kDa), catalase (232 kDa) and aldolase (158 kDa) were used for calibration.

### 2.2.8 Dynamic light scattering studies:

The hydrodynamic radii of the wild type and the mutant  $\alpha$ -crystallin were measured using a Photocor Dynamic Light Scattering Instrument from Photocor Instruments Inc. (MD, USA) at 90° angle with 633 nm 25 mW laser. The protein samples (3 mg/ml) were filtered through a 0.22  $\mu$  membrane and measurements made at 25°C. The data were analyzed using Dynals v2.0 software provided with the instrument.

### 2.2.9 Proteolysis of the wild type and the mutant $\alpha$ A-crystallin by proteinase K:

Limited proteolysis was carried out at 37°C by adding proteinase K to wild type or the mutant protein (0.02 mg/ml) in the absence and in the presence of 2, 3, or 4 M urea at a

protein to protease ratio of 200:1 (w/w). Individual samples were incubated for desired periods of time. Proteolysis was inhibited by the addition of PMSF and boiling the sample with SDS-PAGE sample buffer. The samples were analyzed on 15% SDS-PAGE.

### 2.2.10 Thermal aggregation of wild type and G98R mutant protein:

Thermal aggregation of wild type or G98R mutant protein was studied by recording the scattering at 465 nm in a Flurolog-3 Fluorescence Spectrophotometer (Jobin Yvon, USA) from 25°C to 80°C with an increment of 1°C. Protein samples (0.2 mg/ml) in 10 mM phosphate buffer, pH 7.4, containing 100 mM NaCl were incubated at each temperature for 2 min.

### 2.2.11 Chaperone assay:

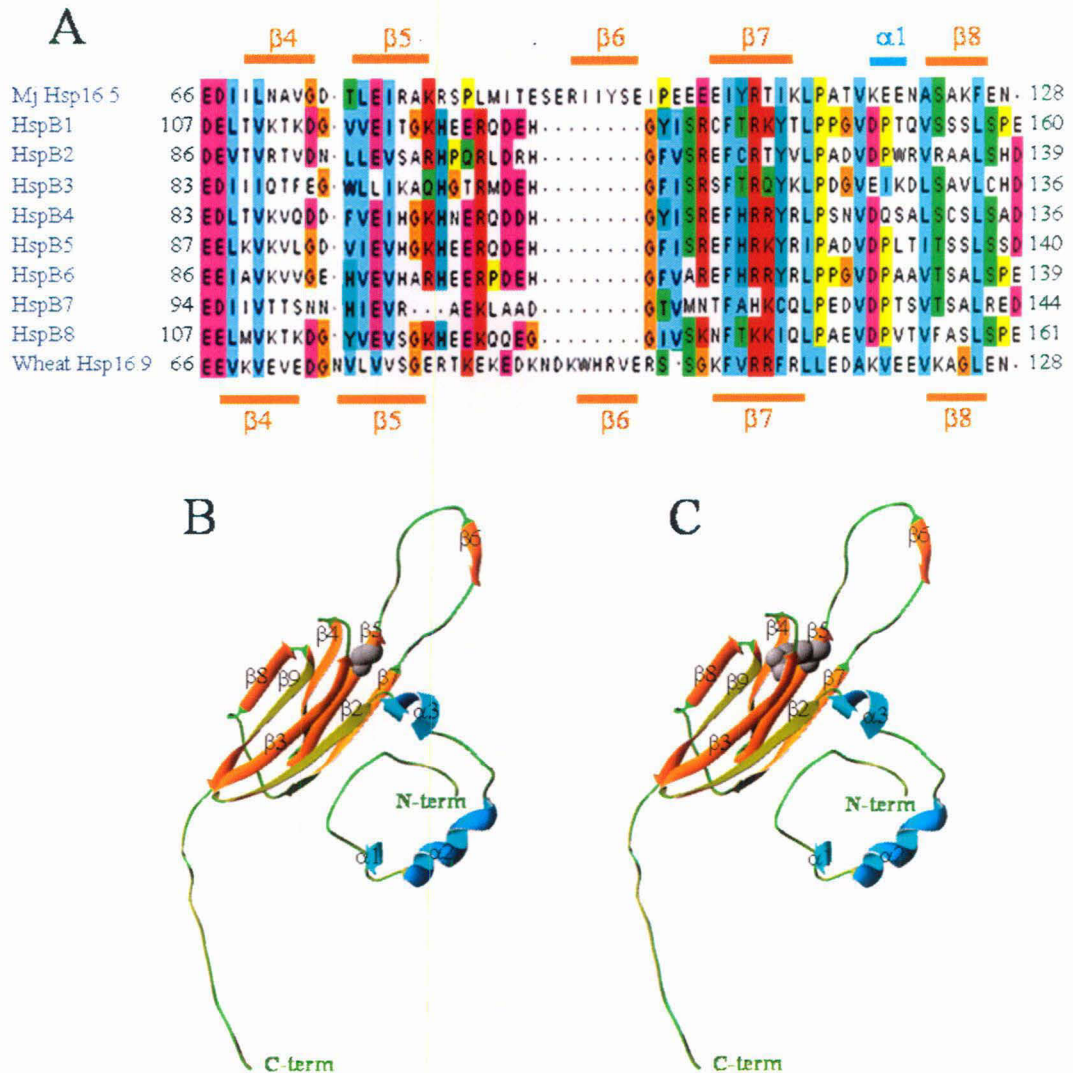
The chaperone-like activity of the wild type or mutant protein was assayed by its ability to prevent the DTT-induced aggregation of insulin or the heat-induced aggregation of citrate synthase (CS) as described earlier (Raman *et al.*, 1995a; Rajaraman *et al.*, 2001). Insulin stock solution was always freshly prepared according to the method described by Ganadu *et al.* (2004), by dissolving 1 mg of insulin (I-5500, Sigma-Aldrich) in 100  $\mu$ l of 10 mM HCl. This solution was immediately diluted 10 times with distilled water, giving a 1 mg/ml stock solution of insulin which was more stable and reproducible. Insulin (0.2 mg/ml) in 10 mM phosphate buffer, pH 7.4, containing 100 mM NaCl was incubated in the absence or the presence of wild type or G98R $\alpha$ A-crystallin at 37°C. Aggregation was initiated by the addition of dithiothreitol (DTT) to a final concentration of 20 mM. In another experiment, CS (25  $\mu$ g/ml) in 40 mM HEPES-NaOH buffer, pH 7.4, was aggregated at 43°C in the absence or the presence of 25  $\mu$ g/ml of  $\alpha$ A- or G98R $\alpha$ A-crystallin. The extent of CS or insulin aggregation on denaturation was measured as a function of time by monitoring the scattering at 465 nm. The measurements were recorded in a Hitachi F-4000 Fluorescence Spectrofluorometer equipped with a temperature-regulated cuvette holder and stirrer, with excitation and emission band passes set at 3 nm. The internal temperature of the cuvette was monitored with a Physitemp Microthermocouple probe.

## 2.3 RESULTS AND DISCUSSION:

### 2.3.1 Structural insights from the crystal structure of *M. jannaschii* Hsp16.5 and *T. aestivum* Hsp16.9:

In the absence of the crystal or NMR structure of any mammalian sHsp, all the structural information is deduced by the comparison with the available crystal structures of *M. jannaschii* Hsp16.5 (Kim *et al.*, 1998) and *T. aestivum* Hsp16.9 (van Montfort *et al.*, 2001). The homology models built for two mammalian sHsps i.e  $\alpha$ B-crystallin (Ghosh and Clark, 2005) and Hsp27 (Thériault *et al.*, 2004) are very similar and the positions of the  $\beta$ -strands correlate well with those of *M. jannaschii* Hsp16.5 and *T. aestivum* Hsp16.9. In human sHsps, the loop connecting  $\beta$ 5 and  $\beta$ 7 strands, which is involved in dimerization of nonmetazoan sHsps, is short and lacks  $\beta$ 6 strand (Figure 2.3 A). The region comprising  $\beta$ 5,  $\beta$ 7 strands and the connecting loop seems to be well conserved and sensitive to mutations. About 80% of the mutations in  $\alpha$ -crystallin domain of sHsps, leading to diseases, in human (R127W, S135F, R136W, R140G and K141Q in Hsp27; K141E and K141N in Hsp22; R120G in  $\alpha$ B-crystallin; R116C, R116H and G98R in  $\alpha$ A-crystallin), have been detected in this region.

Electron spin resonance studies by Koteiche *et al.* (1998), by sequentially replacing every residue with cysteine in the region G60-G108 in  $\alpha$ A-crystallin show that the cataract-causing G98R mutation is present in the same region which forms  $\beta$ 5 strand of the core “ $\alpha$ -crystallin domain” of human  $\alpha$ A-crystallin. This glycine residue is conserved among 28 mammalian species and other vertebrates such as chicken and frog (de Jong *et al.*, 1984). Sequence alignment in Figure 2.3 A, asserts that this residue is also conserved across all mammalian sHsps and in both nonmetazoan species. The fact that this residue is so well conserved suggests its importance in the structural integrity and/or the function of the protein. As shown in Figure 2.3 B and C, the corresponding mutation G83R in the crystal structure of wheat sHsp 16.9 (equivalent to G98R mutation in human  $\alpha$ A-crystallin) leads to the introduction of a charged bulkier group (R) in place of uncharged small and flexible group (G), which in turn can disrupt or significantly alter the “immunoglobulin” fold (Mornon *et al.*, 1998; van Montfort *et al.*, 2001) of the domain, resulting in destabilization of the core structure and functional impairment.



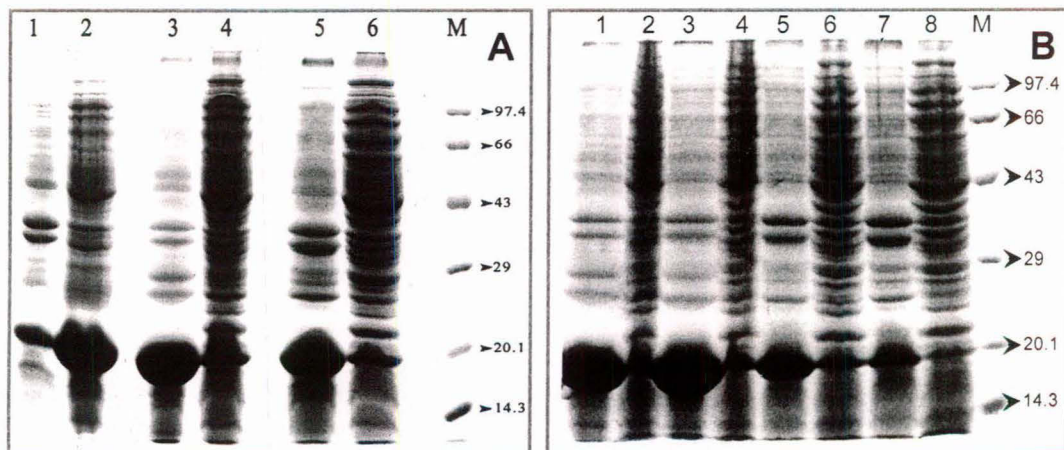
**Figure 2.3: Structural alignment and mutational site of  $\alpha$ A-crystallin.** (A) Sequence alignment of human  $\alpha$ A-crystallin with other human sHsps, *M. jannaschii* Hsp 16.5 and *T. aestivum* (wheat) Hsp 16.9 was done using web-based software ClustalW (<http://www.ebi.ac.uk/Tools/clustalw2/index.html>). A part of the region around  $\beta$ 5 and  $\beta$ 7 strands is shown. Secondary structural elements,  $\beta$ -strand (orange) and  $\alpha$ -helix (cyan), detected in crystal structure of *M. jannaschii* Hsp 16.5 and *T. aestivum* Hsp 16.9 are also shown on the top and the bottom of the alignment adjacent to their corresponding sequences. (B) Ribbon diagram of wheat Hsp 16.9 monomer (Protein Databank Accession code 1GME) showing the G83 (equivalent to mutational site G98) and (C) introduction of bulkier arginine in grey.



### 2.3.2 Cloning, expression and purification of mutant G98R $\alpha$ A-crystallin:

With an objective to study the effect of G98R mutation in human  $\alpha$ A-crystallin, we generated the G98R mutant of  $\alpha$ A-crystallin using the site-directed mutagenesis approach as described in the Experimental Procedures section. The wild type as well as mutant  $\alpha$ A-crystallin were overexpressed in *E.coli* BL21(DE3) cells from a T7 promoter upon induction with 1 mM IPTG for a period of 3 h. Interestingly, unlike wild type  $\alpha$ A-crystallin, the mutant protein forms inclusion bodies and almost exclusively partitions into insoluble fractions (Figure 2.4 A) when expressed in the bacterial cells, suggesting that the mutant protein is defective in folding.

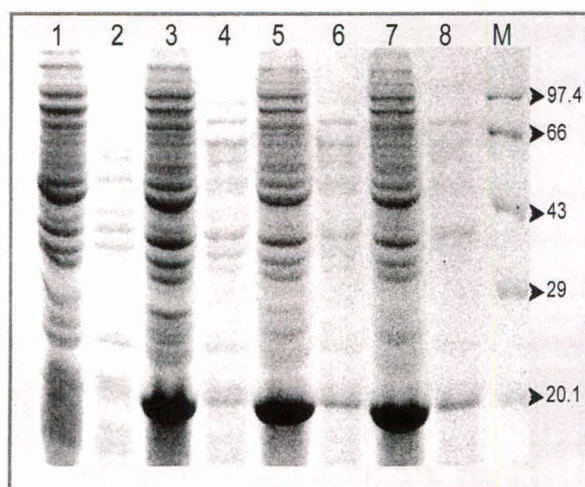
In some cases of heterologous expression, growing the bacterial cells at lower temperatures results in better yield of soluble protein (Schein, 1989; Sorensen and Mortensen, 2005). Decreasing the temperature slows down the rate of protein synthesis giving more time for the correct folding of protein. Therefore, we have lowered the temperature during expression to 30°C to test whether it has any influence on the yield of soluble protein. However, lowering the temperature did not result in appreciable change in the solubility of the expressed mutant protein (Figure 2.4 A).



**Figure 2.4: SDS-PAGE analysis of soluble and insoluble fractions of *E.coli* cells overexpressing G98R $\alpha$ A- and  $\alpha$ A-crystallin.** (A) Lanes 1 & 2: insoluble and soluble fractions respectively of cells grown at 37°C expressing  $\alpha$ A-crystallin. Lanes 3 & 4: insoluble and soluble fractions respectively of cells grown at 37°C expressing G98R $\alpha$ A-crystallin. Lanes 5 & 6: insoluble and soluble fractions respectively of cells grown at 30°C expressing G98R $\alpha$ A-crystallin. (B) Lanes 1, 3, 5 & 7 represent insoluble fraction of cells grown at 37°C expressing G98R $\alpha$ A-crystallin induced by 1, 0.2, 0.15 and 0.1 mM IPTG respectively. Lanes 2, 4, 6 & 8 represent their corresponding soluble fractions. Lane M: medium range molecular-weight protein standards (Bangalore Genei) with molecular masses in kDa shown next to the bands.



Decrease in the inducer concentration leading to decrease in the protein synthesis and decreased aggregation can also help in proper folding and soluble expression of many proteins. Even after lowering the final inducer (IPTG) concentration from 1 mM to 0.2, 0.15, or 0.1 mM, the mutant protein remained in the insoluble fraction (Figure 2.4 B) though the overall expression of the mutant protein decreased as a function of IPTG concentration. Moreover, combination of both the approaches i.e. lowering the IPTG concentration and temperature did not result in increased yield of the soluble protein (data not shown). Upon induction profiling of the mutant  $\alpha$ A-crystallin, we found out that even at 1 h post-induction, it is almost exclusively present in inclusion bodies (Figure 2.5). This suggests that even at lower concentrations, G98R $\alpha$ A-crystallin is more prone to aggregation and partitions into inclusion bodies inside bacterial cells. Taken together, all our expression experiments indicate that the mutant protein is folding-defective and aggregation-prone in the cell. Further, it cannot be rescued by lowering the temperature and/or the inducer concentration. We have also observed that G98R $\alpha$ A-crystallin has aberrant mobility and migrates faster than  $\alpha$ A-crystallin in SDS-PAGE.

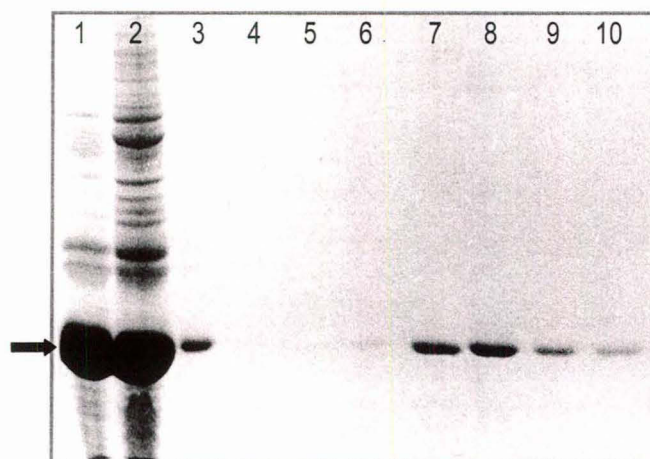


**Figure 2.5: Induction profile of *E. coli* cells overexpressing G98R $\alpha$ A-crystallin.**

Lanes 1, 3, 5 & 7 represent insoluble fraction of cells grown at 37°C expressing G98R $\alpha$ A-crystallin for 0, 1, 2 and 3 h post-induction by 1 mM IPTG respectively. Lanes 2, 4, 6 & 8 represent their corresponding soluble fractions. Lane M: medium range molecular-weight protein standards (Bangalore Genei) with molecular masses in kDa shown next to the bands. Protein loaded in each well was normalized to the OD of the culture at corresponding time. The mutant protein is almost exclusively present in insoluble fraction even at 1 h post induction.

We attempted purification of the mutant protein by dissolving the insoluble mutant protein (washed inclusion bodies) in 3 M urea and subjecting it to on-column refolding using Q-Sepharose ion exchange chromatography (see the experimental procedures section for details). On-column refolding has proved to be an important technique for refolding and purifying proteins from inclusion bodies, especially using ion exchange chromatography (Stempfer *et al.*, 1996; Middelberg, 2002; Liu *et al.*, 2007). The mutant protein bound

strongly to the matrix and after subsequent washing with buffer containing increasing salt concentration, eluted with buffer containing 200-250 mM NaCl (Figure 2.6).



**Figure 2.6: Purification of G98R $\alpha$ A-crystallin from inclusion bodies.** Lane 1 shows solubilised inclusion bodies in 3 M urea. Lane 2 shows washed inclusion bodies before solubilisation. Lane 3 indicates flow through after loading solubilised inclusion bodies on Q-Sepharose column. Lanes 4-10 shows elution using a stepwise gradient of NaCl (0, 100, 150, 200, 225, 250 and 300 mM) in 50 mM Tris-HCl, pH 7.4, containing 1 mM EDTA. Arrow indicates the position of the mutant protein on SDS-PAGE. Maximum amount of pure protein eluted in 225 mM NaCl containing buffer.

The refolded protein thus obtained was found to be homogeneous as determined by SDS-PAGE and remained in solution over prolonged periods of time on storage at 4°C. We also found that when wild type  $\alpha$ A-crystallin was treated with 3 M urea and subjected to refolding, it refolded to its native state regaining its structural and chaperone properties. We, therefore, compared the structural and chaperone properties of the refolded mutant protein with the wild type protein.

### 2.3.3 Study of conformational change in mutant $\alpha$ A-crystallin:

In order to understand if mutant  $\alpha$ A-crystallin adapts a different structure compared to wild type  $\alpha$ A-crystallin, we analyzed its secondary, tertiary and quaternary structure using circular dichroism, fluorescence, gel-filtration and dynamic light scattering techniques.

#### 2.3.3.1 Secondary structural propensities:

Using secondary structural prediction programs, we have analyzed the secondary structural propensities of the region around the G98 residue in  $\alpha$ A-crystallin and the changes upon mutating the glycine to arginine. The full-length sequences were subjected to predictions using web-based software such as Chou-Fasman, Garnier, hydrophobic moment (using software PepTool Lite 1.1), GOR4, SSpro8, nnPredict and Jpred. Some of these algorithms predict a conversion of beta sheet propensities to alpha helix upon changing G to R in the sequence (Figure 2.7).



**$\alpha$ A-crystallin**

**A. acid seq.** IFLDVKHFSPEDLTVKVKQDDFVEI**H**GKHNERQDDHGYISREFHRRYRLPSN

<b>Chou-Fasman</b>	EEEEEEE	-----	EEEE	-----	EEEE	-----	EEEEEE	EEEE	-----
<b>Garnier</b>	EEEE	-----	EEEE	-----	EEEE	-----	HHHHHHHH		-----
<b>Hydro moment</b>	EEEEEEE	-----	EEEE	-----	EEEE	-----	HHHHHHHHHH		-----
<b>GOR4</b>	EE	-----	EE	-----	HHHHH	-----	HHHHH		-----
<b>SSpro8</b>	EEEEEE	GTG	EEEE	-----	EEEEH	-----	TTSEE	HHHHHHE	-----
<b>nnPredict</b>	EEEE	-----	EE	-----	HHHHH	-----	H	HHHH	-----
<b>Jpred</b>	EEEE	-----	EEEE	-----	EEEEEEEE	-----	EEEEEEEEEE		-----

**G98R $\alpha$ A-crystallin**

**A. acid seq.** IFLDVKHFSPEDLTVKVKQDDFVEI**H**RKHNERQDDHGYISREFHRRYRLPSN

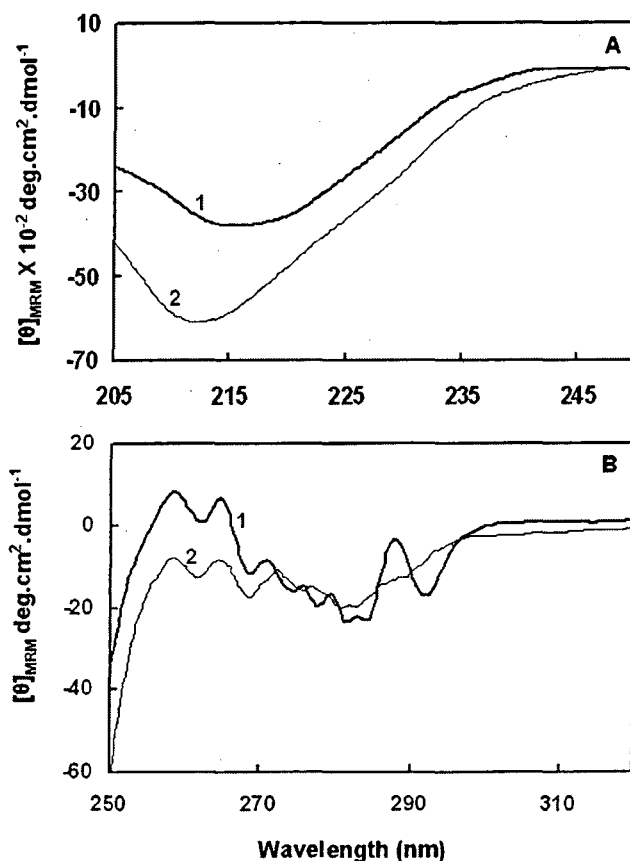
<b>Chou-Fasman</b>	EEEEEEE	-----	EEEE	-----	HHHHHHH	-----	EEEEEE	EEEE	-----
<b>Garnier</b>	EEEE	-----	EEEE	-----	HHHHHHH	HHH	-----	HHHHHHHH	-----
<b>Hydro moment</b>	EEEEEEE	-----	EEEE	-----	HHHHHH	-----	HHHHHHHHHH		-----
<b>GOR4</b>	EE	-----	EE	-----	HHHHHHH	-----	HHHHH		-----
<b>SSpro8</b>	EEEEEE	GTG	EEEE	-----	HHHHHHHHH	H	TTTHE	HHHHHHE	-----
<b>nnPredict</b>	EEEE	-----	EE	-----	HHHHH	-----	H	HHHH	-----
<b>Jpred</b>	EEEE	-----	EEEE	-----	EEEEEEEE	-----	EEEEEEEEEE		-----

**Figure 2.7: Prediction of the secondary structural propensity of the  $\alpha$ A-crystallin and G98R $\alpha$ A-crystallin sequences using different algorithms.** Secondary structural propensities of the sequence from residue 73 to 123 are shown after subjecting the full-length sequences to various programs, listed adjacent to the predictions. Some of the programs predict a change in propensity from strand (E) in the wild type to helical (H) in the mutant in the sequence surrounding the mutated amino acid (shown in red). H, helix; E, extended strand; T, turn; G,  $3_{10}$  helix; S, bend and Dashed line, random coil.

**2.3.3.2 Secondary and tertiary structure analyses using circular dichroism:**

The peptide backbone of the protein absorbs in ultraviolet (UV) region. Dichroism in this region can be used to determine the secondary structural components of a given protein. Far- and near-UV CD spectra reflect the secondary and tertiary structure respectively. As shown in Figure 2.8 A, there is a significant difference in the far-UV CD spectra of mutant  $\alpha$ A-crystallin compared to that of the wild type  $\alpha$ A-crystallin, indicating a change in the secondary structure. The wild type  $\alpha$ A-crystallin exhibits maximum negative ellipticity around 216 nm indicating predominantly  $\beta$ -sheet structure. On the other hand, the mutant protein shows a shift in the maximum negative ellipticity towards lower wavelength (212 nm). The mutant protein also exhibits increased ellipticity. As predicted by various

secondary structural prediction programs, it is possible that the mutation bearing region in the sequence, which has strand propensity in the wild type protein, is perturbed in the mutant protein. Increase in ellipticity and apparent shift of minimum towards 210 nm from 216 nm in the mutant protein indicate possible increase in helical content. Figure 2.8 B compares the near-UV CD spectra of the wild type and mutant  $\alpha$ A-crystallin giving an insight into the environment of aromatic amino acids in the tertiary structure. The transitions between 270 nm and 300 nm are contributed by tryptophan and/or tyrosine residues. Both the proteins exhibit the maxima at 259 nm and 265 nm which are the characteristics of phenylalanine. The chirality of G98R $\alpha$ A-crystallin is considerably reduced compared to that of wild type protein. Although discernible, the fine structure in the 250-270 nm region, due to phenylalanine, shows lower chirality. Signal above 270 nm is almost completely devoid of any structure. This result indicates that the G98R mutation leads to tertiary structural alterations resulting in decreased chirality at the aromatic residues.



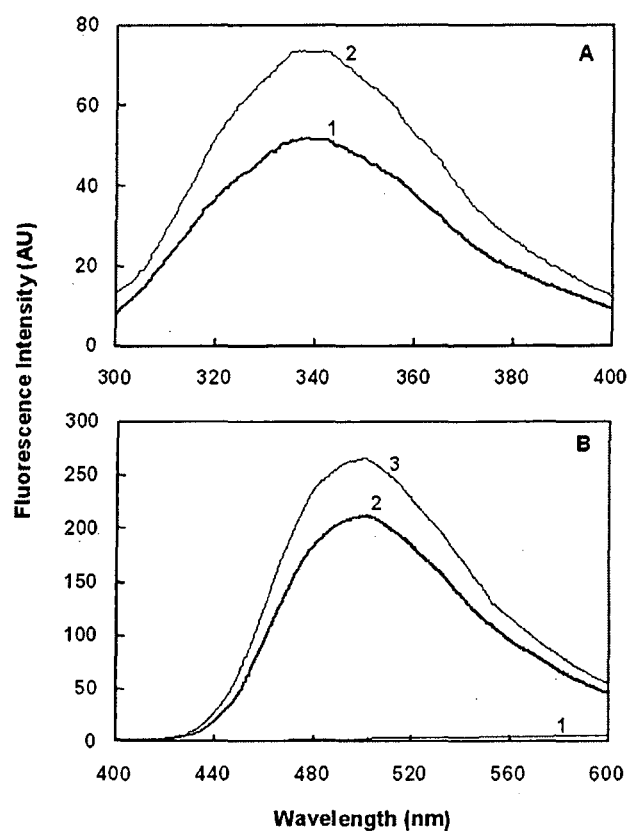
**Figure 2.8: Circular dichroism (CD) spectra of wild type and G98R  $\alpha$ A-crystallin.** (A) Far-UV CD spectra of the wild type (curve 1) and the mutant (curve 2)  $\alpha$ A-crystallin indicating a significant change in the secondary structure of G98R $\alpha$ A-crystallin. (B) Near-UV CD spectra of the wild type (curve 1) and the mutant  $\alpha$ A-crystallin (curve 2) indicating a change in the tertiary structural packing of G98R $\alpha$ A-crystallin upon mutation.  $[\theta]_{MRRM}$ , mean residue mass ellipticity.

### 2.3.3.3 Steady-state fluorescence studies to analyze structure and surface hydrophobicity:

It is well-known that tryptophan fluorescence in a protein is sensitive to its microenvironment and is an index of the extent of exposure of tryptophan side-chains in a

protein to water (Kronman and Holmes, 1971; Burstein *et al.*, 1973). Intrinsic fluorescence data thus reflect gross positioning of tryptophan residues in a protein, which in turn gives information on tertiary and/or quaternary structures of a protein. Figure 2.9 A shows the intrinsic tryptophan fluorescence spectra of  $\alpha$ A-crystallin and the mutant, G98R $\alpha$ -crystallin. The emission maximum (337 nm) is not significantly altered upon mutation. However, the mutant protein exhibits significantly higher fluorescence intensity than that of the wild type protein, indicating a change in the local microenvironment around the sole tryptophan residue of  $\alpha$ A-crystallin. Thus, the mutant  $\alpha$ A-crystallin appears to have adapted a different tertiary and/or quaternary structure from that of the wild type protein. This is highly likely since the replacement of smaller uncharged glycine with bulky positively charged arginine is not isosteric in nature and can affect the packing of individual subunits in homo-oligomers.

Hydrophobic interactions play an important role in the binding of the chaperone to the non-native state of target proteins. We compared the accessible hydrophobic surfaces of the wild type and the mutant protein using the hydrophobic fluorescent probe, bis-ANS. This probe is non-fluorescent in aqueous solutions but after binding to the hydrophobic surface of a protein, its fluorescence intensity increases several fold, accompanied by a blue shift in the emission maximum (Musci *et al.*, 1985). The extent of binding of bis-ANS to any protein is considered to be a



**Figure 2.9: Intrinsic tryptophan fluorescence and bis-ANS binding of the wild type and G98R  $\alpha$ -crystallin.** (A) Intrinsic tryptophan fluorescence spectra of the 0.2 mg/ml in TNE buffer of the wild type (curve 1) and the mutant (curve 2)  $\alpha$ A-crystallin indicating that the mutant protein exhibits enhanced fluorescence intensity. (B) Fluorescence spectra of bis-ANS (10  $\mu$ M) in buffer alone (curve 1) and in the presence of 0.2 mg/ml wild type (curve 2) or G98R  $\alpha$ A-crystallin (curve 3) indicating that the mutant protein exhibits relatively more bis-ANS binding.

measure of the surface hydrophobicity of that protein (Musci *et al.*, 1985; Shi *et al.*, 1994). The fluorescence spectra of bis-ANS bound to both the proteins at room temperature are shown in Figure 2.9 B. A several fold increase in the fluorescence intensity of bis-ANS, accompanied by a blue shift in emission maximum to 500 nm, could be seen when  $\alpha$ A-crystallin was bound to it. G98R $\alpha$ -crystallin also shows a similar increase in the fluorescence and blue shift in the emission maximum. However, the fluorescence intensity was higher in the presence of the mutant protein than in the presence of the wild type protein, suggesting an increase in the accessible hydrophobic surface of the mutant protein. A point mutation of glycine to arginine in  $\alpha$ A-crystallin, by itself, is not expected to increase the hydrophobic surfaces on the protein to such an extent unless there is a conformational change resulting in the exposure of normally buried hydrophobic residues.

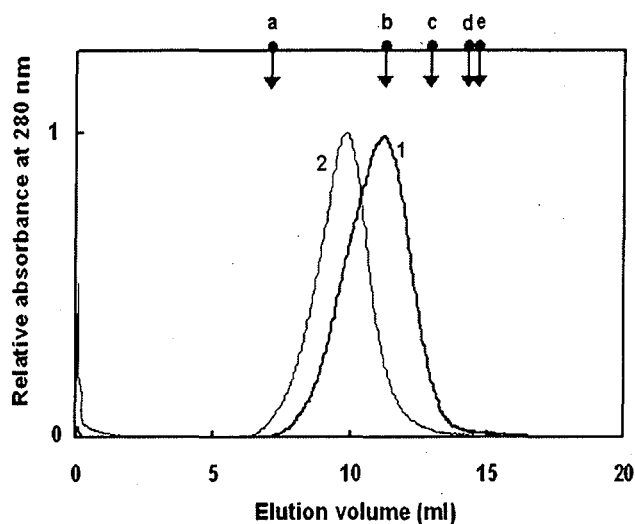
#### 2.3.3.4 Quaternary structural studies:

Most sHsps generally assemble into large oligomeric complexes which appears to be a structural prerequisite for their chaperone-like activity (Leroux *et al.*, 1997; van de Klundert *et al.*, 1998). As mentioned earlier,  $\alpha$ A-crystallin exists as a polydisperse non-covalently linked oligomer with an apparent molecular mass of ~650 kDa in the native state. A delicate balance of columbic and hydrophobic interactions generally determines the size of the soluble aggregate. Siezen *et al.* (1979) reported that successive removal of residues from the highly charged C-terminal extension in  $\alpha$ A-crystallin produced larger aggregates. The G98R mutation results in increased surface hydrophobicity and a gain of 1 unit of positive charge on each subunit compared to its wild type counterpart. Therefore, we investigated the effect of mutation on quaternary structure of  $\alpha$ A-crystallin by gel-filtration chromatography and dynamic light scattering (DLS).

The elution pattern of  $\alpha$ A-crystallin and its mutant is shown in Figure 2.10 along with the positions of the elution volumes of molecular-mass standards. Gel-filtration chromatography shows that the mutant protein elutes prior to the wild type protein indicating that the size of the mutant protein is significantly large compared to that of the wild type  $\alpha$ A-crystallin. The molecular mass of wild type  $\alpha$ A-crystallin, estimated using the elution volumes of the standard proteins, was found to be ~680 kDa, whereas G98R $\alpha$ -crystallin eluted at an elution volume corresponding to a molecular mass of ~1020 kDa. Consistent with the size-exclusion chromatography analysis, the DLS study indicates a large oligomeric status of the mutant protein. Hydrodynamic radius,  $R_h$ , of the wild type  $\alpha$ A-crystallin was



determined to be  $9.14 \pm 0.07$  nm as against  $15.13 \pm 0.19$  nm that of the mutant protein. Thus our quaternary studies show that the G98R mutation in  $\alpha$ A-crystallin results in alteration of oligomerization status with an appreciable increase in the size of oligomers.



**Figure 2.10: Size-exclusion FPLC of  $\alpha$ A- and G98R $\alpha$ A-crystallin on a Superpose 6 HR10/30 FPLC column.** Elution profiles of the wild type (curve 1) and the mutant (curve 2)  $\alpha$ A-crystallin show that the mutant forms relatively larger oligomeric assembly. The elution positions of molecular mass standards are indicated by down arrows. a, blue dextran (2000 kDa); b, thyroglobulin (669 kDa); c, ferritin (440 kDa); d, catalase (232 kDa); e, aldolase (158 kDa).

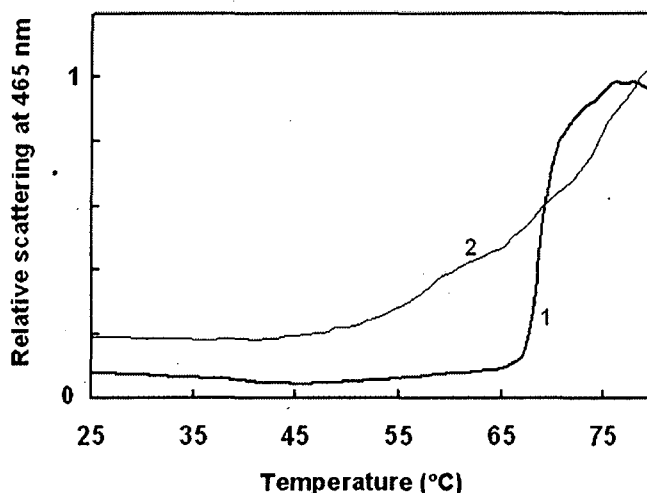
Taken together, far- and near-UV CD spectroscopy, intrinsic fluorescence spectroscopy, bis-ANS binding studies and quaternary structural studies show that side-chain packing of the aromatic residues, mode of folding of secondary structural elements as well as quaternary structure are altered significantly upon mutation of glycine 98 residue to arginine in  $\alpha$ A-crystallin.

#### 2.3.4 Studies on the stability of the wild type and G98R $\alpha$ A-crystallin:

Since the human lens does not have much protein turnover and there is no mechanism to dispose off damaged proteins from lens, the issue of stability of  $\alpha$ -crystallin is very crucial. With age, lens proteins become progressively insoluble resulting in accumulation of high molecular weight protein aggregates leading to lens opacity (Spector, 1984; Ortwerth and Olesen, 1992). A plausible explanation for the mechanism of insolubilization is that proteins present in an unstable or partially unfolded state tend to aggregate when their concentrations are high. Therefore, we studied the stability of both proteins in terms of thermal aggregation and chemical denaturation.

### 2.3.4.1 Thermal stability:

$\alpha$ -Crystallins are normally thermally stable as they do not exhibit significant unfolding even at elevated temperatures. In addition, they can prevent heat-induced aggregation of other proteins (Horwitz, 1992; Raman and Rao, 1997; Datta and Rao, 1999; Reddy *et al.*, 2000). However, they undergo subtle structural perturbations. Earlier circular dichroism, infrared spectroscopy and calorimetric studies on bovine  $\alpha$ -crystallin and recombinant human  $\alpha$ A- or  $\alpha$ B-crystallin have reported a transition between 55°C to 65°C indicating structural alterations (Walsh *et al.*, 1991; Surewicz and Olesen, 1995; Raman and Rao, 1997; Datta and Rao, 1999; Reddy *et al.*, 2000). We compared the thermal stability of the wild type and the mutant  $\alpha$ A-crystallin in terms of its self-aggregation with increasing temperature by monitoring the light scattering (Figure 2.11). The light scattering of the sample of wild type  $\alpha$ A-crystallin remains unchanged up to 65°C beyond which, there is a sharp increase indicating aggregation of the protein. Judging by the sharp transition, the aggregation is cooperative in nature. The mutant protein, at 25°C exhibits high light scattering compared to the wild type protein due to its large oligomeric size. Contrary to the cooperative behavior of the wild type protein, the mutant protein forms light scattering aggregates above 45°C, which are more pronounced beyond 60°C. These results show that the mutant protein is more susceptible to heat-induced aggregation and is sensitive to temperature slightly above the physiological condition. This increased tendency of G98R $\alpha$ A-crystallin to aggregate can probably be attributed to its altered structural stability and its increased hydrophobicity.



**Figure 2.11: Effect of G98R mutation in  $\alpha$ A-crystallin on thermal stability.** Aggregation of the wild type (curve 1) or the mutant (curve 2)  $\alpha$ A-crystallin was monitored by light scattering at 465 nm as a function of temperature. The mutant G98R $\alpha$ A-crystallin aggregates at lower temperature as compared to the wild type.

### 2.3.4.2 Urea-induced denaturation studies of $\alpha$ A- and G98R $\alpha$ A-crystallin:

Apart from the thermal stability studies described above, a number of studies have focused on denaturation of  $\alpha$ -crystallins by various ionic and non-ionic chaotropic agents, detergents, pH etc (van den Oetelaar and Hoenders, 1989; Carver *et al.*, 1993; Das and Liang, 1997; Sun *et al.*, 1999; Saha and Das, 2007). Thermal unfolding at higher temperatures is irreversible (Das and Surewicz, 1995; Das *et al.*, 1997) whereas guanidine hydrochloride (GdnHCl) or urea induced unfolding is reversible in nature (Raman *et al.*, 1995b; Das and Liang, 1997; Saha and Das, 2007).

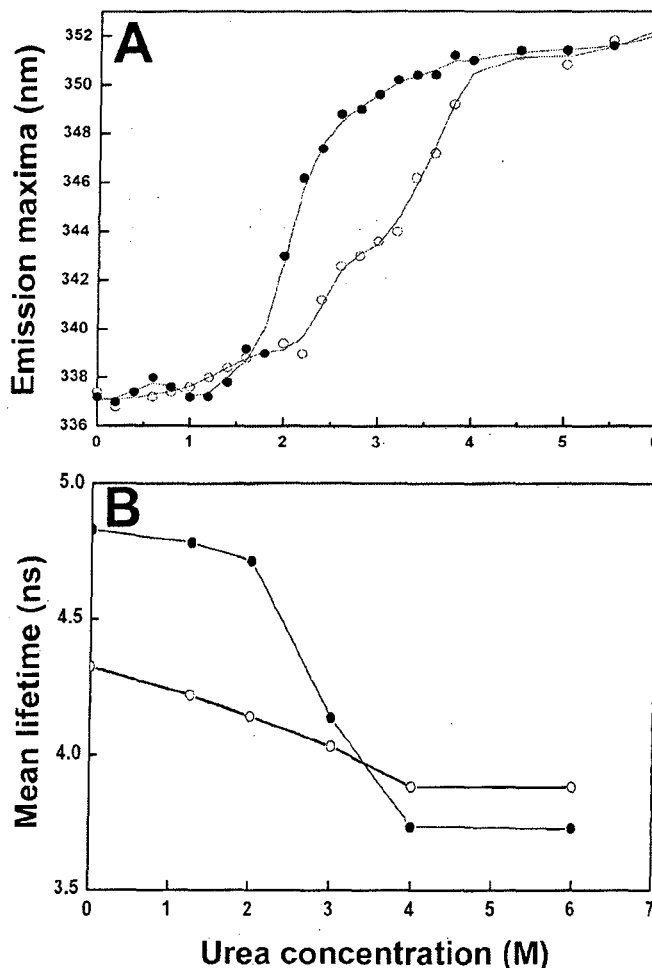
#### 2.3.4.2.1 Equilibrium urea-unfolding studies:

We have investigated urea-induced unfolding of wild type and mutant  $\alpha$ A-crystallin by steady-state and time-resolved tryptophan fluorescence, far-UV CD and bis-ANS binding. Figure 2.12 A shows the wavelength of emission maximum of tryptophan fluorescence of the proteins as a function of urea concentration. In the absence of urea,  $\alpha$ A-crystallin exhibits emission maximum ( $\lambda_{E_{max}}$ ) around 337 nm. The  $\lambda_{E_{max}}$  shifts gradually to about 339 nm in 2 M urea and relatively sharply to about 343 nm by 3 M urea. It further red shifts to 350 nm by 4 M urea indicating almost complete exposure of the tryptophan residue to the solvent. On the other hand, G98R $\alpha$ A-crystallin starts unfolding at a relatively much lower concentration of urea. The tryptophan residue of the mutant protein becomes almost completely solvent-exposed at as low as 2.5 M urea concentration, indicating that the tertiary structure of the mutant protein is more prone to urea-induced destabilization compared to the wild type protein.

We have also probed the urea-induced tertiary structural changes (around the tryptophan residues) using fluorescence lifetime experiments. The emission decay profiles of both  $\alpha$ A- and G98R $\alpha$ A-crystallin can be best fitted with a three exponential decay model with lifetimes of individual components listed in Table 2.1. Though  $\alpha$ A-crystallin has only a single tryptophan residue at position 9 in its sequence, its time-resolved fluorescence exhibits at least three components -  $\tau_1$  (0.735 ns),  $\tau_2$  (3.075 ns) and  $\tau_3$  (6.824 ns) – with  $\tau_2$  and  $\tau_3$  contributing significantly to the fluorescence intensity. Multi-exponential decay from a single tryptophan can arise due to its complex photophysical properties and its exposure to multiple environments in proteins corresponding to different protein conformations (Beechem and Brand, 1985). Thus, this result indicates heterogeneity in the microenvironment of the tryptophan residue of the subunits. The mutant protein also exhibits

three lifetimes,  $\tau_1$  (0.923 ns),  $\tau_2$  (3.375 ns) and  $\tau_3$  (7.095 ns). The differences in the individual lifetimes (Table 2.1) as well as the mean lifetime (Figure 2.12 B) between the wild type and the mutant protein possibly arise from the differences in the microenvironments of the sole tryptophan residue of these proteins. The mean lifetimes of  $\alpha$ A- and G98R $\alpha$ A-crystallin decrease upon urea-induced unfolding (Figure 2.12 B).

In order to further understand the differences between the wild type and the mutant protein in their urea-induced unfolding properties, we have used far-UV CD and bis-ANS binding studies. The fraction unfolded, calculated based on the ellipticity changes at 220 nm from the far-UV CD spectrum at various concentrations of urea, is shown in Figure 2.13 A. It is evident from the figure that the unfolding transition of G98R $\alpha$ A-crystallin occurs at lower concentrations of urea compared to that of the wild type protein, indicating that the secondary structural elements of the mutant protein unfold at lower concentrations of urea than those of the wild type protein.



**Figure 2.12: Urea-induced unfolding of  $\alpha$ A-crystallins.** (A) Unfolding of  $\alpha$ A- (○), G98R $\alpha$ A-crystallin (●) as monitored by change in the emission maximum of the intrinsic tryptophan fluorescence. The protein samples (0.2 mg/ml) in TNE buffer were incubated at 37°C for 6 h in the presence of indicated concentrations of urea. (B) Decrease in mean tryptophan fluorescence lifetime ( $\tau_m$ ) as a function of urea concentration of  $\alpha$ A- (○) or G98R  $\alpha$ A-crystallin (●).  $\tau_m$  was calculated as given in methods using data acquired by magic angle (54.75°) measurements (see Table 2.1).

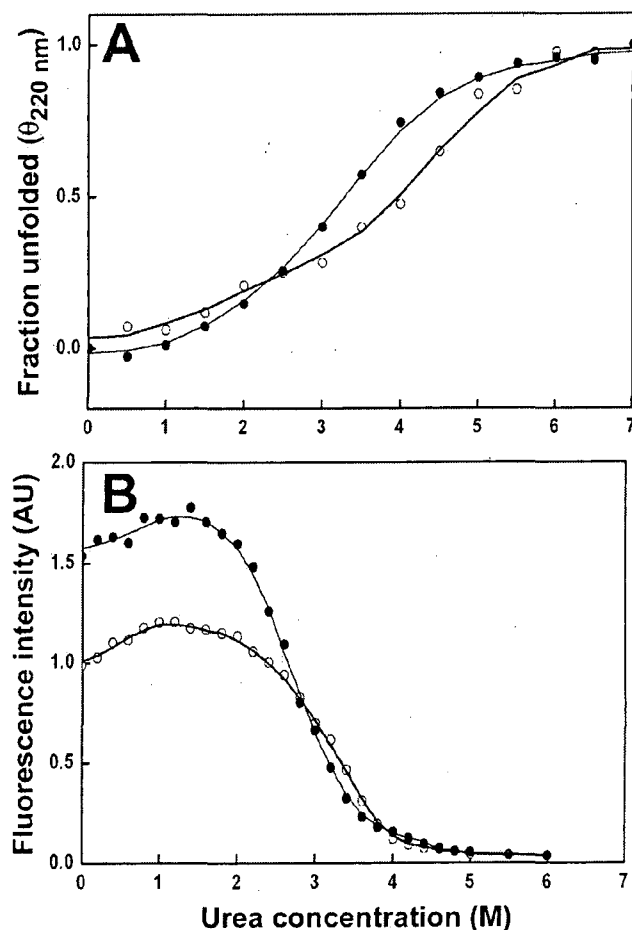
**Table 2.1:** Tryptophan fluorescence lifetime measurements of  $\alpha$ A-crystallin and G98R $\alpha$ A-crystallin

Urea (M)	$\alpha$ A-crystallin								G98R $\alpha$ A-crystallin							
	$\tau_1$ (ns)	$\tau_2$ (ns)	$\tau_3$ (ns)	B1 (%)	B2 (%)	B3 (%)	$\tau_m$ (ns)	$\chi^2$	$\tau_1$ (ns)	$\tau_2$ (ns)	$\tau_3$ (ns)	B1 (%)	B2 (%)	B3 (%)	$\tau_m$ (ns)	$\chi^2$
0	3.075	0.735	6.824	42.89	14.65	42.45	4.32	1.15	3.357	0.923	7.095	43.55	10.34	46.11	4.83	1.18
1.25	2.880	0.693	6.651	40.56	15.16	44.28	4.22	1.24	3.235	0.826	6.896	41.88	9.58	48.53	4.78	1.34
2	2.690	0.601	6.548	39.94	14.56	45.51	4.14	1.25	3.311	0.877	7.019	44.16	10.88	44.96	4.71	1.14
3	2.505	0.562	6.356	39.23	14.05	46.72	4.03	1.14	2.630	0.758	6.069	40.13	10.43	49.44	4.14	1.14
4	2.555	0.650	5.936	39.70	13.46	46.84	3.88	1.20	2.434	0.672	5.419	40.21	10.21	49.58	3.73	1.10
6	2.593	0.714	5.470	38.79	9.95	51.26	3.88	1.22	2.404	0.900	5.280	38.26	10.31	51.43	3.73	1.16

The decay profiles either in buffer alone or in the presence of urea could be best fitted with “three exponential decay” model.  $\tau_1$ ,  $\tau_2$  and  $\tau_3$  represent individual lifetime components, and B1, B2 and B3 represent the respective relative amplitudes (pre-exponential factors). The calculated mean lifetime ( $\tau_m$ ) based on the data is also shown. The goodness of the fit was assessed by the reduced  $\chi^2$  (chi-square) shown in the table as well as by random distribution of residuals. The results were found to be reproducible without significant deviation between the experiments. A representative data set is shown.

In contrast to the intrinsic tryptophan fluorescence, which revealed the changes in the interior of the protein where tryptophan is buried, extrinsic hydrophobic probe (bis-ANS) was used to obtain the tertiary structural information pertaining to the changes in surface of both proteins during unfolding. In the unfolding profile of αA-crystallin, bis-ANS fluorescence increases in the presence of urea and reaches maximum around 1.5 M urea (Figure 2.13 B). Further increase in urea concentration leads to decrease in the bis-ANS fluorescence and the profile attains a plateau by 5 M urea. The mutant protein, even in the absence of urea, exhibits significantly increased bis-ANS fluorescence (Figure 2.13 B). The fluorescence intensity of bis-ANS bound to mutant protein further increases with initial increase in urea concentration as observed in the case of the wild type protein, reaching a maximum around 1.5 M urea. The bis-ANS fluorescence intensity decreases beyond 1.5 M urea concentration and, at 2.8 M, is almost similar to that bound to the wild type protein.

Thus, these studies show that the mutation leads to significant destabilization towards urea-induced unfolding. The difference in conformational stability of αA- and G98RαA-crystallin may contribute to the differential susceptibility to modification-related aggregation and insolubilization. In other words, low conformational stability of G98RαA-



**Figure 2.13: Equilibrium unfolding studies using CD and bis-ANS binding.** (A) Fraction unfolded calculated for denaturation of  $\alpha$ A- (○) or G98R $\alpha$ A-crystallin (●) on the basis of ellipticity at 220 nm ( $\theta_{220}$  nm) obtained from their far-UV CD spectra. (B) Binding of bis-ANS (10  $\mu$ M) to  $\alpha$ A- (○) or G98R $\alpha$ A-crystallin (●) in the presence of specified concentrations of urea was monitored by change in the fluorescence intensity of the probe at 500 nm.



crystallin may imply that *in vivo*, the mutant protein is more susceptible to aggregation than the wild type protein.

### 2.3.4.2.2 Intermediate states in the urea-induced unfolding of the wild type and the mutant $\alpha$ A-crystallin:

A comparison of the results of urea-induced unfolding of  $\alpha$ A-crystallin, monitored by various techniques shown in Figure 2.12 A and 2.13 A, suggests that unfolding profiles lack strong cooperativity indicating multistate transitions. Lack of cooperativity asserts that unfolding did not occur directly from the native state. The  $\lambda_{E_{max}}$  began to increase at low concentration (1.5 M) of urea and leveled off at 4.0 M, in contrast fraction unfolded calculated from CD did not change until urea concentration reached 2 M and it leveled off at 6 M. Thus, the midpoints of transition in secondary and tertiary structural changes did not overlap and confirmed the existence of intermediates.  $\alpha$ -Crystallin has been suggested to have a stable intermediate (van den Oetelaar and Hoenders, 1989; Carver *et al.*, 1993; Raman *et al.*, 1995b). Das and Liang (1997) characterized an intermediate of calf-lens  $\alpha$ -crystallin at 0.8 -1 M GdnHCl with maximum hydrophobicity and chaperone-like activity. A few thermodynamic studies on  $\alpha$ A-crystallin established that the unfolding is a three state transition (Sun *et al.*, 1999; Saha and Das, 2007).

Our results can be interpreted intuitively to reflect that the urea-induced unfolding pathway is populated with at least three intermediate states. Based on these results, we propose the following unfolding pathway:



Where N represents the native state, U the unfolded state and  $I_{w1}$ ,  $I_{w2}$  and  $I_{w3}$  represent the three intermediate states.  $I_{w1}$  represents ensembles of states populated around 1.5 M urea that exhibit perturbed tertiary structure (minor changes in the tryptophan fluorescence, increased bis-ANS fluorescence) with most of its secondary structural elements intact.  $I_{w2}$  represents ensembles of partially unfolded states populated around 2.5-3 M urea that exhibit significant loosening of its tertiary structure (moderately solvent-exposed tryptophan residues and decreased bis-ANS fluorescence) with more than 75% of its secondary structural elements retained.  $I_{w3}$  represents ensembles of partially unfolded states with almost complete loss of tertiary structure (almost completely solvent-exposed tryptophan residue and low bis-ANS fluorescence) but with significant secondary structural elements (~50%) retained. The mutant protein also seems to unfold through three intermediate states.

The intermediate states,  $I_{m1}$  and  $I_{w1}$  exhibit similar spectroscopic properties. The results show that degree of unfolding of  $I_{m2}$  and  $I_{m3}$  could be more than that of the corresponding  $I_{w2}$  and  $I_{w3}$  states. The presence of  $I_{m2}$  in the unfolding profile of G98R $\alpha$ A-crystallin, monitored by the tryptophan emission maximum (Figure 2.12 A), is not as distinct as  $I_{w2}$ , suggesting that the structural differences between  $I_{m2}$  and  $I_{m3}$  are not significantly distinct (in the case of the mutant).

It is interesting to note that  $I_{w2}$  (or  $I_{m2}$ ) and  $I_{w3}$  (or  $I_{m3}$ ) exhibit less bis-ANS fluorescence. It is not clear whether these partially unfolded states, in fact, exhibit less hydrophobic surfaces. However, it is generally observed that partially unfolded states of proteins exhibit more hydrophobic surfaces. It has been reported that urea can dislodge the hydrophobic dye, ANS, from cardiotoxin III leading to decrease in the fluorescence intensity, though the protein does not undergo unfolding in urea (Kumar *et al.*, 1996). In order to understand whether dislodging of bis-ANS by urea could be one of the reasons for the observed decrease in the fluorescence intensity in the cases of  $I_{w2}$  and  $I_{w3}$ , we have performed time-resolved fluorescence of bis-ANS bound to  $\alpha$ A-crystallin in the presence of selected concentrations of urea. The emission decay of bis-ANS bound to native  $\alpha$ A-crystallin could be best fitted to a three exponential decay model (Table 2.2).  $\tau_1$  with sub nanosecond fluorescence component could be due to the unbound dye with very low quantum yield.  $\tau_2$  with a lifetime of approximately 5.5 ns could represent a moderately hydrophobic site, while  $\tau_3$ , with a lifetime of approximately 10 ns, could represent a relatively more hydrophobic site. Based on photo-crosslinking experiments, Sharma *et al.* (1998) have reported two bis-ANS binding sites in  $\alpha$ A-crystallin - one at residues 50-54 towards the end of the N-terminal domain and another at 79-88 located in the  $\alpha$ -crystallin domain. It is possible that the two lifetime components  $\tau_2$  and  $\tau_3$  observed in the present study correspond to the probe bound to these two sites. Table 2.2 lists the measured lifetimes of bis-ANS bound to  $\alpha$ A- and G98R $\alpha$ A-crystallin at different urea concentrations that represent the ensembles of the three intermediate states. The results show that the mean lifetimes of bis-ANS bound to  $I_{w1}$  or  $I_{w2}$  are not significantly different from that of native  $\alpha$ A-crystallin. The lifetime of bis-ANS bound  $I_{w3}$  is less than that of bis-ANS bound to native  $\alpha$ A-crystallin. Similar results are seen in the case of bis-ANS bound to the mutant protein alone and in the presence of different concentrations of urea.

Thus, these results indicate that (i) The microenvironment of the bis-ANS binding sites in the mutant protein is not significantly different from that of the wild type protein and

**Table 2.2:** Fluorescence lifetime measurements of bis-ANS bound to the wild type and G98RαA-crystallin

Urea (M)	$\alpha$ A-crystallin								G98RαA-crystallin							
	$\tau_1$ (ns)	$\tau_2$ (ns)	$\tau_3$ (ns)	B1 (%)	B2 (%)	B3 (%)	$\tau_m$ (ns)	$\chi^2$	$\tau_1$ (ns)	$\tau_2$ (ns)	$\tau_3$ (ns)	B1 (%)	B2 (%)	B3 (%)	$\tau_m$ (ns)	$\chi^2$
0	5.57	10.26	0.08	34.42	63.35	2.22	8.42	0.95	5.46	10.20	0.08	32.55	66.18	1.27	8.53	1.14
1.25	5.40	10.14	0.09	30.55	68.01	1.44	8.55	1.14	5.32	9.97	0.14	32.42	66.36	1.21	8.34	1.05
3	5.74	10.57	0.11	39.38	59.01	1.61	8.50	1.20	5.57	10.48	0.19	39.63	59.18	1.19	8.41	1.07
4	4.99	9.80	0.21	31.14	66.90	1.96	8.12	1.09	4.97	10.47	0.20	37.66	59.51	2.83	8.11	1.08

The decay profiles either in buffer alone or in the presence of urea could be best fitted with “three exponential decay” model.  $\tau_1$ ,  $\tau_2$  and  $\tau_3$  represent individual lifetime components, and B1, B2 and B3 represent the respective relative amplitudes (pre-exponential factors). The calculated mean lifetime ( $\tau_m$ ) based on the data is also shown. The goodness of the fit was assessed by the reduced  $\chi^2$  (chi-square) shown in the table as well as by random distribution of residuals. The results were found to be reproducible without significant deviation between the experiments. A representative data set is shown.

---

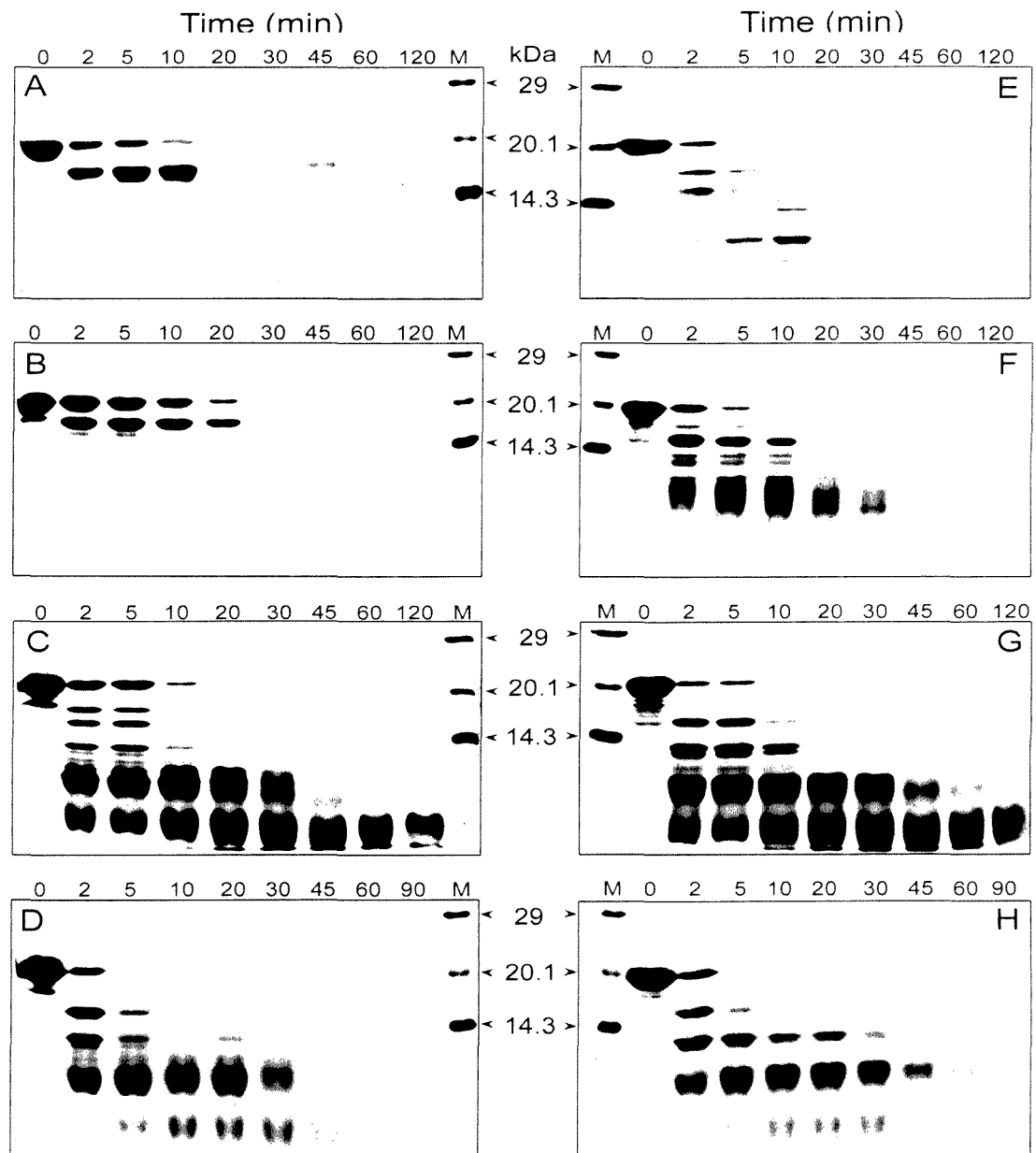
hence the observed increase in the bis-ANS fluorescence in the presence of mutant protein could be due to the increased accessibility of the bis-ANS binding sites to the dye molecule rather than changes in the intrinsic hydrophobicity of the sites. (ii) The bis-ANS binding sites are not significantly altered even at 3 M urea and only slightly perturbed at 4 M urea. Thus, the observed decrease in the bis-ANS fluorescence of the intermediates is not due to the loss of bis-ANS sites due to unfolding but could be due to dislodging of the dye in the presence of high concentrations of urea as observed in the case of cardiotoxin III.

#### **2.3.4.2.3 Structural differences and intermediate states in the urea-induced unfolding of the $\alpha$ A- and G98R $\alpha$ A-crystallin probed by limited proteolysis:**

As folded structure is relatively less susceptible to protease digestion compared to the unfolded or unstructured regions of proteins, studies using limited proteolysis can provide useful information about structural differences of proteins under different conditions and their partially folded/unfolded intermediates (Spolaore *et al.*, 2001; Morrow *et al.*, 2002). We, therefore, probed the structural differences among wild type and mutant G98R $\alpha$ A-crystallin by subjecting them to limited proteinase K digestion (Figure 2.14 A and 2.14 E). The result shows that (i) the mutant protein is more susceptible to proteolysis compared to the wild type protein and (ii) the digestion pattern is distinctly different between the wild type and the mutant protein, indicating structural differences between the two with the folded structure of the mutant protein being less compact.

Proteinase K has been shown to retain its activity up to 4 M urea (Hilz *et al.*, 1975). Therefore, we have compared the protease susceptibility and digestion pattern of the wild type and the mutant protein under different concentrations of urea to get insight into the structural differences, if any, between the unfolding intermediates of these two proteins. At 2 M urea, where  $I_{w1}$  and  $I_{m1}$  are significantly populated, the digestion patterns (Figure 2.14 B and 2.14 F) of the wild type and the mutant proteins do not differ significantly from their respective native states (Figure 2.14 A and 2.14 E).  $I_{w2}$  (the wild type protein at 3 M urea) clearly shows increased susceptibility to proteolysis, indicating decreased structural compactness (Figure 2.14 C). The digestion pattern of  $I_{w2}$  and  $I_{m2}$  also show some differences (Figure 2.14 C and 2.14 G) indicating subtle differences in their structure. However,  $I_{w3}$  and  $I_{m3}$  (at 4 M urea) exhibit similar digestion pattern indicating quite similar structure of these unfolding intermediates (Figure 2.14 D and 2.14 H).

---



**Figure 2.14: Limited Proteinase K digestion of  $\alpha$ A- and G98R  $\alpha$ A-crystallin in presence or absence of urea.** SDS-PAGE showing proteinase K digestion pattern of wild type protein in, absence of urea (A), presence of 2 M urea (B), presence of 3 M urea (C) and presence of 4 M urea (D). The extent of fragmentation was also monitored for G98R mutant protein in absence of urea (E), presence of 2, 3 and 4 M urea respectively (F-H). Numbers above each lane in all gels indicate the time of incubation in minutes with proteinase K before its inactivation. Lane M shows the molecular mass markers with small arrows indicating their corresponding size in kDa.

Our results of equilibrium urea-unfolding studies suggest that there are at least three spectroscopically distinct intermediates in urea-induced unfolding pathway of  $\alpha$ A-crystallin. The denaturation studies showed the lower stability and structural differences in the case of

the mutant protein. It suggests a plausible link between thermodynamic properties and structural perturbations, which can alter protein-protein interactions leading to light scattering aggregate formation. Moreover, higher susceptibility of the mutant protein to protease assumes significance in the physiological context of eye lens as activation of proteases have been implicated in ageing and cataract formation (Biswas *et al.*, 2004).

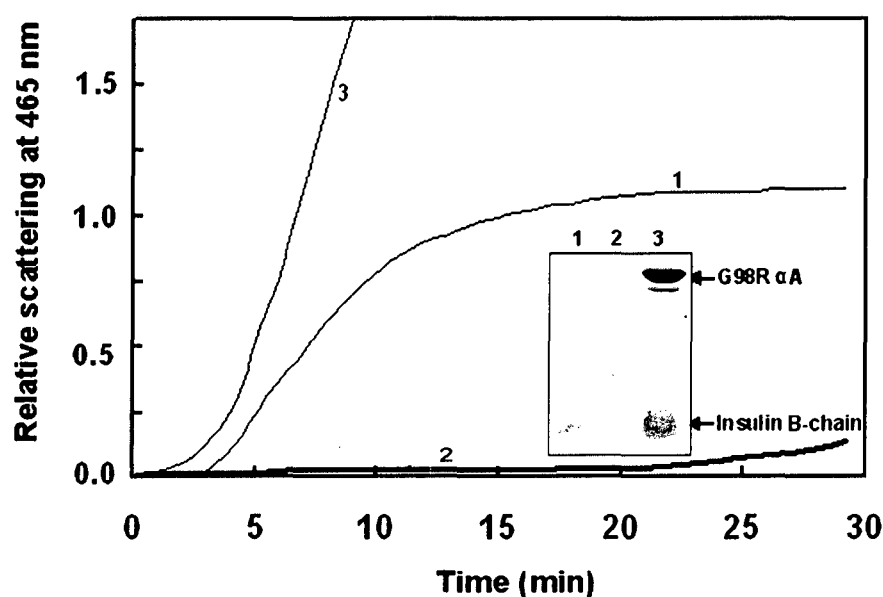
### 2.3.5 Chaperone-like activity of the wild type and G98R $\alpha$ A-crystallin:

The chaperone-like activity of sHsps is usually determined by their capacity to suppress thermally or chemically induced protein aggregation. In order to understand the effect of mutation on the functional role of  $\alpha$ A-crystallin, we compared the chaperone-like activity of the wild type and mutant  $\alpha$ A-crystallin towards DTT-induced aggregation of insulin (Figure 2.15) at 37°C. In the presence of DTT, the disulfide bonds connecting the insulin A- and B-chain break leading to unfolding and aggregation of B-chain, while the A-chain remains soluble (Sanger, 1949). In the absence of chaperone, insulin aggregates on reduction (curve 1) which can be monitored by light scattering. The wild type protein at 1:1 (w/w) ratio prevents the aggregation of insulin almost completely (curve 2). In contrast, the mutant protein at the same ratio was not effective in preventing the aggregation of insulin B chain (curve 3). Rather the addition of G98R $\alpha$ A-crystallin to insulin under reducing conditions enhanced the rate and extent of aggregation as revealed by dramatic increase in the scattering. However, it should be emphasized that DTT and heat (37°C) did not cause aggregation of G98R $\alpha$ A-crystallin when present alone in solution (in the absence of insulin). Thus, this result indicates that the G98R mutation leads to complete loss of chaperone activity of  $\alpha$ A-crystallin with this substrate.

Earlier studies have shown that hydrophobic interaction between accessible hydrophobic surfaces (on chaperone) and newly exposed hydrophobic sites of unfolding substrates is one of the important factors affecting chaperone-like activity of  $\alpha$ -crystallin (Raman and Rao, 1994; Das and Surewicz, 1995; Reddy *et al.*, 2006). Sharma *et al.* (1997, 1998, 2000) have identified target protein binding sites and bis-ANS binding sites in both  $\alpha$ A- and  $\alpha$ B-crystallin and found some overlapping sites (consisting of hydrophobic residues). It is surprising that even though the mutant protein exhibits more surface hydrophobicity compared to the wild type protein (Figure 2.9 B), it lacks chaperone activity. The compromised activity of G98R $\alpha$ A-crystallin could be ascribed to two possible reasons: (1) loss or decreased target protein binding ability and (2) decreased solubility of the target

protein and chaperone complex. Since the mutant protein binds bis-ANS, it is unlikely that the target protein binding ability of the mutant protein is affected. Significantly higher light scattering of the insulin-G98R complex (in comparison to aggregated insulin alone) also suggests an interaction between the mutant and insulin. Therefore, we analyzed the aggregates formed in the presence of wild type and mutant protein by SDS-PAGE. As shown in the inset in Figure 2.15, when the sample containing wild type  $\alpha$ A-crystallin and insulin was centrifuged and a pellet, if any, was subjected to SDS-PAGE, no bands corresponding to insulin B chain or  $\alpha$ A-crystallin could be seen (lane 2). On the other hand, G98R $\alpha$ A-crystallin became a major part of the resulting insoluble pellet (lane 3) indicating that both insulin B chain and the mutant protein co-aggregate.

Insulin aggregates formed at an early stage might act as seed for aggregation-prone mutant  $\alpha$ A-crystallin leading to co-aggregation and precipitation. In order to test this possibility, we have added aggregates of insulin B-chain prepared separately (in buffer alone) to a sample of the mutant protein and monitored the light scattering for 1 h and did

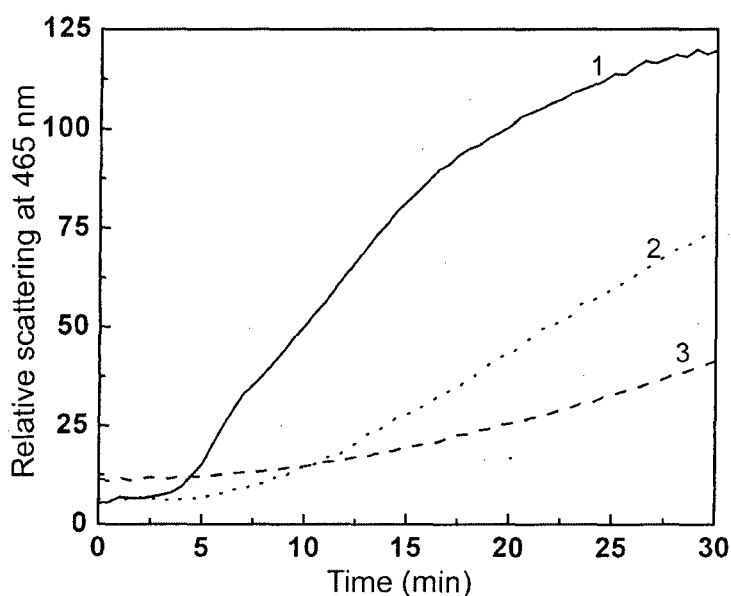


**Figure 2.15: Chaperone-like activity of  $\alpha$ A- and G98R $\alpha$ A-crystallin towards DTT-induced aggregation of insulin.** Aggregation of insulin (0.2 mg/ml), as monitored by light scattering at 465 nm, was initiated by the addition of 20 mM DTT in the absence (curve 1) or in the presence of 0.2 mg/ml wild type (curve 2) or the mutant (curve 3)  $\alpha$ A-crystallin. Inset shows that the mutant protein co-aggregates with the insulin B-chain as analyzed by SDS-PAGE. The pellet obtained after centrifuging (at 10000xg for 20 min) the samples (after DTT-induced aggregation for 30 min) was subjected to electrophoresis on a 17% SDS-PAGE. Samples are insulin alone (lane 1), insulin in the presence of the wild type (lane 2), or the mutant (lane 3)  $\alpha$ A-crystallin.



not find increase in the light scattering. This rules out the possibility of nucleation of aggregation of the mutant  $\alpha$ A-crystallin by the aggregating insulin B-chain. Therefore, it is likely that the complex of the mutant and insulin B-chain is aggregation-prone or insoluble.

We have also examined the differences in chaperone-like activity of the wild type and the mutant protein using thermally-induced aggregation of citrate synthase (CS). Interestingly, G98R $\alpha$ A-crystallin showed higher protection than the wild type protein at a ~1:1 (w/w) ratio of  $\alpha$ A-crystallin to CS (Figure 2.16). Such substrate-dependent chaperone-like activity was also demonstrated for congenital cataract and desmin related myopathy causing R120G mutant of  $\alpha$ B-crystallin (Bova *et al.*, 1999). Recently, Murugesan *et al.* (2007) have corroborated our findings on structural and functional aspects of the G98R $\alpha$ A-crystallin and showed that the mutant protein partially protects EDTA-induced thermal aggregation of alcohol dehydrogenase (ADH) at 43°C and DTT-induced  $\alpha$ -lactalbumin aggregation. All these findings establish some substrate-specificity in chaperone-like activity of G98R $\alpha$ A-crystallin. In  $\alpha$ B-crystallin, 91VLGDVIEVHGK103 encompassing the corresponding mutational site (in bold) in  $\alpha$ A-crystallin was identified as one of the target binding sites in an earlier report (Sharma *et al.*, 1997). However, more than one target binding site have been reported in  $\alpha$ A-crystallin (Sharma *et al.*, 2000), and even if one is affected by mutation other sites can remain functional.



**Figure 2.16: Heat-induced CS aggregation in presence or absence of  $\alpha$ A- and G98R $\alpha$ A-crystallin.** Aggregation of 25  $\mu$ g/ml CS at 43°C was monitored by light scattering at 465 nm in the absence (curve 1) and in the presence of 20  $\mu$ g/ml ( $\approx$  1  $\mu$ M) of either wild type (curve 2) or mutant protein (curve 3).

Recent studies showing enhanced binding of R116C $\alpha$ A-crystallin to membranes despite reduction in its chaperone activity (Cobb and Petrush, 2000) and increased affinity of cataract-causing mutations in  $\alpha$ A-crystallin (R49C and R116C) towards the non-native states of destabilized T4 lysozyme (Koteiche and Mchaourab, 2006), suggest toxic gain of function for these cataract-causing mutants. Mutation-induced enhancement of substrate binding can lead to the saturation of binding sites in  $\alpha$ -crystallin, which acts as a 'sink' to sequester the damaged proteins in lens. It is likely that the ability of the substrate-saturated mutant protein to keep the substrate-chaperone complex in soluble form diminishes resulting in formation of light scattering aggregates leading to loss of optical properties of lens. Jiao *et al.* (2005) showed that insoluble lbpB-substrate complex is formed when lbpB is overloaded with non-native substrates. Our study shows that though the mutant protein has the ability to interact with the target protein, the complex (consisting of both substrate and chaperone) is aggregation-prone or insoluble. Thus, all these mutations result in conformational alterations that affect the solubility of or impart aggregation propensity to the complex rather than decreasing their target protein-binding ability.

Therefore, it should be noted that loss of chaperone-like activity of G98R $\alpha$ A-crystallin with regards to its ability to prevent aggregation of unfolding proteins, propensity of G98R-substrate complex to precipitate coupled with the faulty interactions with other native proteins may result in formation of particulates that scatter light and onset of cataract.

## 2.4 CONCLUSION:

A putative cataract-causing mutation, G98R, in  $\alpha$ A-crystallin has been recently identified in an Indian family, the molecular basis of which is not known. It is interesting to note that except one nonsense mutation (W9X), all other cataract-causing missense mutations discovered in  $\alpha$ A-crystallin (Table 1.5) so far involve arginine substitution. G98R is the only mutation where positively charged arginine replaces the uncharged amino acid unlike other known mutations where arginine is replaced by other non-conservative amino acids. The fact that  $\alpha$ A-crystallin has conserved its charge dispersion throughout evolution (de Jong *et al.*, 1984) and various mutations or truncations of charged residues in  $\alpha$ A-crystallin have resulted in loss of chaperone activity (Takemoto *et al.*, 1993; Smulders *et al.*, 1995; Andley *et al.*, 1996), suggest that charge imbalance may underlie the pathological condition in these charge-interfering mutations. In line with this hypothesis, introduction of charged and bulky arginine seems to be important in manifestation of the cataract

phenotype as the same glycine residue when mutated to cysteine, showed no drastic changes in secondary structure, oligomeric structure and chaperone-like activity towards insulin (Koteiche *et al.*, 1998). Thus, introduction of charge, bulkiness of the arginine residue and its high helical propensity may lead to disruption or alteration of the immunoglobulin fold of the  $\alpha$ -crystallin domain leading to other defects.

Unlike the earlier reported missense mutants of  $\alpha$ A- or  $\alpha$ B-crystallin, almost all the expressed G98R $\alpha$ A-crystallin goes into the inclusion bodies in *E.coli*, suggesting that the mutation leads to folding defects that result in aggregation in cells. It is possible that in the crowded *in vivo* environment of the cell, the mutant protein exhibits folding defects and forms aggregates. The refolded mutant protein shows altered secondary and tertiary structure and forms large oligomers. The mutant protein is more prone to destabilization upon urea and thermal denaturation, indicating structural instability. G98R $\alpha$ A-crystallin has less compact folded structure and is more susceptible to proteolysis. G98R $\alpha$ A-crystallin possesses increased surface hydrophobicity compared to the wild type protein, but fails to protect certain substrates from aggregation and exhibits substrate-dependent chaperone-like activity. Our study also shows that though the mutant protein has the ability to interact with the target protein, it makes the substrate-chaperone complex aggregation-prone or insoluble. It is possible that other damaged or aged proteins bind to the mutant form and the aggregation-prone complex tends to accumulate with time leading to eventual compromise of transparency.

Lack of chaperone-like activity and tendency to aggregate either alone or upon binding to target protein may cause lens turbidity and cataract formation in the affected individuals. Such a molecular defect leading to improper folding would be expected to cause congenital cataract. However, the cataract formation ascribed to G98R mutation is not congenital but presenile in nature - its onset occurs at the age of 16 years. We have investigated the possible reason(s) for the absence of congenital cataract in the next chapter.

**MIXED OLIGOMER  
FORMATION:  
CATARACTOGENESIS**

3

### 3.1 INTRODUCTION:

The point mutation, G98R, in the  $\beta 5$  strand of  $\alpha A$ -crystallin seems to be unique in the onset of cataract formation as other dominant negative mutations reported in  $\alpha A$ -crystallin lead to congenital cataract formation (Table 1.5). Our studies on the mutant protein show that unlike wild type  $\alpha A$ -crystallin and the other reported point mutations in  $\alpha$ -crystallins, it exhibits folding defects that lead to inclusion body formation in *E. coli*. The refolded mutant protein exhibits conformational and quaternary structural differences, decreased stability and loss in chaperone-like activity towards the DTT-induced aggregation of insulin (Singh *et al.*, 2006). Despite such drastic molecular defects, mutation does not result in congenital cataract.

The family described by Santhiya *et al.* (2006) is heterozygous for the mutation i.e. they have one chromosomal copy of normal  $\alpha A$ -crystallin and one copy of the mutant allele. This implies that the eye lens of the patients can have mixed oligomers of wild type  $\alpha A$ -crystallin and the mutant protein. Such mixed oligomers might have a role in the development of cataract.

In order to investigate such mixed oligomers, we formed oligomers containing 1:1 (w/w) ratio of wild type  $\alpha A$ -crystallin and mutant G98R $\alpha A$ -crystallin. Since the folding, structural and chaperone properties of G98R $\alpha A$ -crystallin are drastically different from those of the wild type, this system is useful to study mixed oligomer formation between the mutant and the wild type proteins and the influence of wild type and mutant subunits on each other's properties in mixed oligomers. In the present study, we explored the subunit exchange of G98R mutant protein with wild type  $\alpha A$ -crystallin and its effect on structure, stability and functional aspects of the mixed oligomers.

### 3.2 EXPERIMENTAL PROCEDURES:

#### 3.2.1 Materials:

pETDuet-1 vector was obtained from Novagen (San Diego, USA). *EcoR* V, *Hind* III and *Nde* I restriction enzymes were obtained from NEB (Madison, USA). *Pfu* DNA polymerase was from Promega (Madison, USA). Desalting column (PD10) was from Amersham Pharmacia (Uppsala, Sweden). Fluorescence probes, namely the disodium salt of 4-acetamido-4'-[(iodoacetyl) amino] stilbene-2,2'-disulfonic acid (AIAS), dipotassium salt of lucifer yellow iodoacetamide (LYI) and 1,1'-bi(4-anilino) naphthalenesulfonic acid (Bis-ANS)

were purchased from Molecular Probes (Eugene, USA). Proteinase K was obtained from Boehringer-Mannheim (Germany).

### **3.2.2 Fluorescent labeling of $\alpha$ A-crystallin and its mutant for subunit exchange studies using fluorescence resonance energy transfer (FRET):**

Subunit exchange studies using FRET were performed essentially as described earlier (Bova *et al.*, 1997). The FRET pair of fluorescent probes, AIAS and LYI, was used for covalent labeling of the accessible cysteine residues in  $\alpha$ A-crystallin and the mutant protein. Both proteins, diluted to 1 mg/ml in 20 mM MOPS buffer (pH 7.9) containing 100 mM NaCl, were incubated at 37°C for 18 hours in dark with AIAS or LYI at final probe concentration of 3.2 mM and 8.4 mM respectively. Excess unreacted probes were removed by passing the samples through a desalting column (PD10) equilibrated with 50 mM sodium phosphate buffer, pH 7.5, containing 100 mM NaCl. The fractions containing the labeled proteins were eluted using the same buffer, pooled and their concentrations were determined. Percentage labeling was estimated based on the molar extinction coefficient at 335 nm for AIAS and 435 nm for LYI. In close agreement with previous studies (Bova *et al.*, 1997; Biswas and Das, 2007), percentage labelling revealed that an average of 1 mol of fluorophore was covalently attached to 1 mol of  $\alpha$ A-crystallin subunits.

Subunit exchange experiments were performed by mixing the AIAS- and LYI-labeled proteins at an equal ratio (w/w) in 50 mM sodium phosphate buffer, pH 7.5, containing 100 mM NaCl. This reaction mixture (0.7 mg/ml) was incubated at 37°C from which 10  $\mu$ l aliquots were withdrawn at different time points and diluted to 500  $\mu$ l with the same buffer. Fluorescence spectra were recorded in a corrected spectrum mode from 350-600 nm at room temperature using a Hitachi F-4500 fluorescence spectrophotometer with the excitation monochromator set at 332 nm. The excitation and emission band passes were set at 5 nm each.

### **3.2.3 Preparation of mixed oligomers from homo-oligomers of wild type $\alpha$ A-crystallin and G98R $\alpha$ A-crystallin:**

Mixed oligomers, containing subunits from both the wild type and the mutant proteins, were made essentially as described by Datta and Rao (2000). Homo-oligomers of wild type and mutant  $\alpha$ A-crystallin were mixed at a ratio of 1:1 (w/w) to a final concentration of 2 mg/ml in TNE buffer and incubated at 37°C for 3.5 h to ensure complete exchange of

subunits. Though there is minimal or no exchange on storage at 4°C (Datta and Rao, 2000), mixed oligomers were prepared freshly and used immediately in all studies.

### **3.2.4 Circular dichroism studies:**

To investigate the conformational changes in mixed oligomers, CD measurements were carried out using a JASCO J-715 spectropolarimeter at 25°C in TNE buffer. Near-UV CD spectra were recorded using 1.0 mg/ml of protein in a 1 cm path length cell, whereas 0.5 mg/ml of protein in 0.1 cm path length cell was used for recording far-UV CD spectra. All reported spectra are the average of 4 accumulations.

### **3.2.5 Fluorescence studies:**

Intrinsic tryptophan fluorescence spectra of the proteins (0.2 mg/ml) in TNE buffer either in the absence or in the presence of indicated concentrations of urea were recorded using a Hitachi F-4500 fluorescence spectrophotometer with the excitation wavelength set at 295 nm. To study the surface hydrophobicity, protein samples were incubated with the hydrophobic probe, bis-ANS (10 µM), at room temperature for 20 min. Fluorescence spectra were recorded from 400-600 nm with the excitation wavelength set at 390 nm. All spectra were recorded in corrected spectrum mode with excitation and emission band passes set at 2.5 nm each.

### **3.2.6 Dynamic light scattering studies:**

All the hydrodynamic radius measurements were made at 90° angle with a 25 mW laser of 633 nm at 25°C in a Photocor Dynamic Light Scattering Instrument from Photocor Instruments Inc. (MD, USA). The protein samples (1 mg/ml), before and after incubation at 37°C for 3.5 h, were filtered through a 0.22 µ membrane for measurements. The data were fitted and analyzed using Dynals v2.0 software provided with the instrument.

### **3.2.7 Thermal stability:**

Thermal aggregation of wild type and the mutant protein before and after incubation at 37°C for 3.5 h as well as that of mixed oligomers was studied by measuring the scattering at 465 nm in a Flurolog-3 fluorescence spectrophotometer (Jobin Yvon, USA) from 25°C to 90°C with 1°C increments. All protein samples (0.2 mg/ml) in 10 mM phosphate buffer, pH



7.4, containing 100 mM NaCl were equilibrated for two minutes at each temperature in the thermostatted cuvette holder.

### **3.2.8 Proteolysis of the homo- and hetero-oligomeric $\alpha$ A-crystallins by proteinase K:**

Limited proteolysis experiment was carried out at 37°C by adding proteinase K to different proteins (0.02 mg/ml) at a protein to protease ratio of 200:1 (w/w). Individual samples were incubated for desired periods of time before inhibiting the proteolysis by the addition of PMSF and boiling the sample with SDS-PAGE sample buffer. The samples were analysed on 15% SDS-PAGE.

In another experiment, the protein aggregation of homo- and mixed-oligomers of the wild type and G98R mutant protein (0.2 mg/ml) during proteolysis was monitored by light scattering at 465 nm as a function of time in a Hitachi F-4000 Fluorescence Spectrophotometer. The weight ratio of protein to protease ratio was 200:1.

### **3.2.9 Chaperone assay:**

The chaperone-like activity of the mixed oligomers, wild type and mutant proteins was studied using DTT-induced insulin aggregation, as described in the previous chapter.

### **3.2.10 Cloning and co-expression of $\alpha$ A-crystallin and G98R $\alpha$ A-crystallin in pETDuet-1 vector:**

In order to study co-expression of the wild type and mutant protein, we used pETDuet-1 vector (Novagen) which has two multiple cloning sites (MCS1 and MCS2). The other characteristics of this vector such as nature of promoter, origin of replication, ampicillin resistance are similar to those of pET-21a(+) vector. Thus, we could compare the co-expression of the wild type and mutant protein using the pETDuet-1 vector and their individual expressions using pET-21a(+) vector. Cloning of  $\alpha$ A-crystallin and G98R  $\alpha$ A-crystallin in pETDuet-1 vector was done in two sequential steps. In the first step, pET-21a(+) vector containing recombinant human G98R $\alpha$ A-crystallin gene (cloned in *Nde* I and *Hind* III sites) was digested by *Hind* III and made blunt-ended using *Pfu* DNA polymerase. It was further digested with *Nde* I to release the insert containing the G98R  $\alpha$ A-crystallin gene. This insert was ligated at the *Nde* I and *Eco*R V sites in the MCS2 of the pETDuet-1 expression vector to generate pETDuet1-G98R plasmid. In the second step, insert containing human

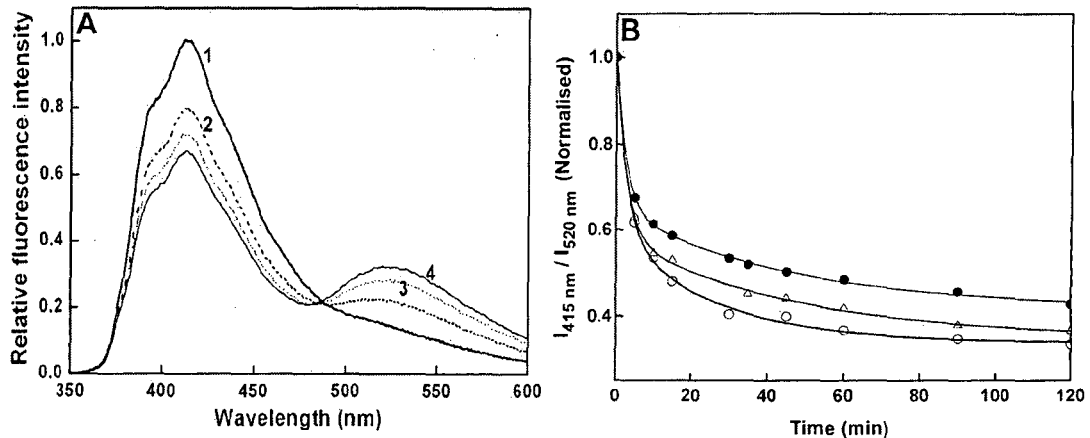
$\alpha$ A-crystallin gene was excised from pET-21a (+) vector (containing recombinant human  $\alpha$ A-crystallin cloned at *Nde* I and *Hind* III sites) by digestion with *Xba* I and *Not* I restriction enzymes. The resulting insert was ligated in the corresponding sites in MCS1 of pETDuet1-G98R plasmid (containing cloned G98R  $\alpha$ A-crystallin in MCS2 from the first step) to generate pETDuet1-G98R $\alpha$ A plasmid. These constructs were verified by insert release using respective restriction enzymes. The pETDuet1-G98R $\alpha$ A plasmid containing both  $\alpha$ A-crystallin and G98R $\alpha$ A-crystallin constructs was transformed in *E. coli* BL21 (DE3) cells. These cells were induced with a final concentration of 1mM IPTG after they reached mid-log phase ( $OD_{600nm}$  of 0.6). The cells were further grown for 3.5 h, pelleted and stored at  $-30^{\circ}C$  until further use. To analyze the effect of co-expression, *E. coli* cells were suspended in 1 ml of TNE buffer, sonicated and centrifuged. The pellet thus obtained was suspended in 1 ml of TNE buffer. 30  $\mu$ l of the soluble and insoluble fractions from each of the samples was boiled with SDS-PAGE loading buffer before loading on a 12 % SDS polyacrylamide gel.

### 3.3 RESULTS AND DISCUSSION:

#### 3.3.1 Effect of G98R mutation on the subunit exchange of $\alpha$ A-crystallin:

Subunit exchange between different oligomers is one of the characteristic features of mammalian sHsps (van den Oetelaar *et al.*, 1990; Bova *et al.*, 1997; Sun and Liang, 1998; Sun *et al.*, 1998; Datta and Rao, 2000; Bova *et al.*, 2000; Bera and Abraham, 2002; Narberhaus, 2002), suggesting that mixed oligomer formation is a common phenomenon in mammalian cells. Homo-oligomers of  $\alpha$ A- and  $\alpha$ B-crystallin are known to exchange subunits among themselves and with each other. It was shown earlier that rearrangement of subunits in  $\alpha$ -crystallin, due to its dynamic quaternary structure could be a mechanism to regulate its chaperone-like activity (Datta and Rao, 2000). Interestingly, the cataract-causing R116C $\alpha$ A-crystallin has four-fold reduced ability to exchange subunits with  $\alpha$ A-crystallin (Cobb and Petrash, 2000), but has a higher affinity for forming mixed oligomers with  $\alpha$ B-crystallin (Bera and Abhram, 2002). The subunit exchange in  $\alpha$ -crystallins has been observed by various methods, including isoelectric focusing (van den Oetelaar *et al.*, 1990; Sun and Liang 1998; Datta and Rao, 2000), fluorescence resonance energy transfer (FRET) (Bova *et al.*, 1997; Sun *et al.*, 1998; Bova *et al.*, 2000; Cobb and Petrash, 2000), and mass spectrometry (Sobott *et al.* 2002; Aquilina *et al.*, 2005).

In order to investigate the effect of G98R mutation in  $\alpha$ A-crystallin on subunit exchange, we monitored subunit exchange by FRET using  $\alpha$ A-crystallin and G98R $\alpha$ A-crystallin, fluorescently labeled at the Cys residues (Figure 3.1). FRET phenomenon require two probes, a donor in the first protein and an acceptor in the second protein. The energy transfer occurs when the two proteins interact and the two probes are sufficiently close to one another as defined by Förster distance (Lakowicz, 1983). As shown in Figure 3.1 A, when the AIAS-labeled  $\alpha$ A-crystallin (donor) and the LYI-labeled  $\alpha$ A-crystallin (acceptor) are mixed, AIAS emission intensity (emission maximum around 415 nm) shows time-dependent decrease with concomitant increase in LYI fluorescence (emission maximum around 520 nm), indicating energy transfer due to the proximity of the two fluorophores resulting from subunit exchange. Figure 3.1 B compares the decrease in the intensity ratio at 415 nm to 520 nm as a function of time in the cases of  $\alpha$ A-crystallin, the mutant and the mixture of the wild type and the mutant protein. It is evident from the figure that like wild type  $\alpha$ A-crystallin, the mutant protein exhibits subunit exchange property. However, the extent and rate of the observed decrease in the  $I_{415\text{nm}}/I_{520\text{nm}}$  in the case of the mutant protein is less compared to that of the wild type protein. After 2 h incubation at 37°C, there was no change in the emission intensity suggesting attainment of equilibrium. Since the mutant



**Figure 3.1: Subunit exchange studies of homo- and mixed-oligomer of  $\alpha$ A-crystallin and G98R $\alpha$ A-crystallin using FRET.** (A) Represents a typical fluorescence spectrum of a mixture of AIAS- and LYI-labeled  $\alpha$ A-crystallin indicating decrease in AIAS (donor) fluorescence with concomitant increase in LYI (acceptor) fluorescence as a function of time. Fluorescence spectrum immediately after mixing (curve 1), after 5 min (curve 2), 30 min (curve 3) and 60 min (curve 4) of incubation at 37 °C shows the subunit exchange leading to FRET. (B) Decrease in the ratio of the fluorescence intensity at 415 nm to 520 nm ( $I_{415\text{ nm}}/I_{520\text{ nm}}$ ) due to exchange of AIAS- and LYI-labeled subunits of either  $\alpha$ A-crystallin (O) or G98R $\alpha$ A-crystallin (●) or both  $\alpha$ A-crystallin and G98R $\alpha$ A-crystallin (Δ).

protein can undergo subunit exchange with wild type  $\alpha$ A-crystallin and with itself, mixed oligomers containing wild type  $\alpha$ A-crystallin and the mutant protein were formed by incubating both proteins together at 1:1 (w/w) ratio at 37°C for 3.5 h (Figure 3.2).



**Figure 3.2: Schematic diagram showing mixed-oligomer formation.** Both  $\alpha$ A-crystallin and G98R $\alpha$ A-crystallin at a concentration of 1 mg/ml each are incubated at 37°C for 3.5 h to form mixed oligomers as they can exchange their subunits.

Subunit exchange of  $\alpha$ -crystallin has been suggested to be related to its chaperone function (Datta and Rao, 2000; Biswas and Das, 2004). As subunit exchange increases with increase in temperature (Bova *et al.*, 1997), chaperone activity is also increased (Raman and Rao, 1994; Das and Surewicz, 1995; Derham and Harding, 1999). Processes that slow down the dynamics of exchange reaction such as substrate binding to  $\alpha$ -crystallin, decrease chaperone activity (Bova *et al.*, 1997; Biswas and Das, 2007). Thus, substantially slow subunit-exchange in the case of the mutant protein might be a reason for its poor chaperone-like activity.

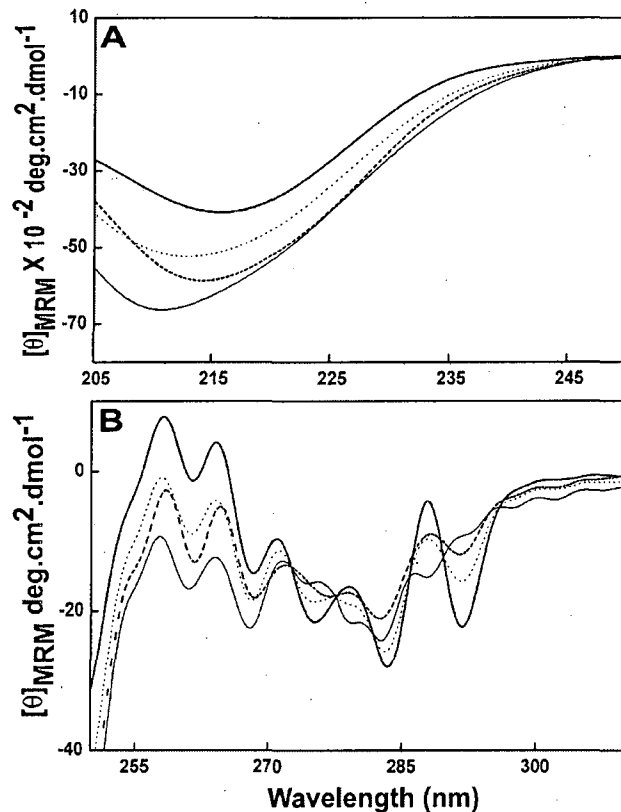
### 3.3.2 Study of conformational change in the mixed-oligomers of the wild type and mutant $\alpha$ A-crystallin:

An earlier study from our laboratory showed that hetero-oligomer formation between the purified bovine  $\alpha$ A- and  $\alpha$ B-crystallin leads to observable changes in the conformation and chaperone-like activity (Datta and Rao, 2000). Systematic investigation on how the mixed oligomers differ from the individual proteins in the structural and functional aspects, is important to understand the role of such mixed oligomers. We have analyzed secondary, tertiary and quaternary structure of mixed oligomers by using the techniques of circular dichroism, fluorescence, gel-filtration and dynamic light scattering.

### 3.3.2.1 Secondary and tertiary structure analyses using circular dichroism:

The far-UV CD spectra of the wild type and mutant  $\alpha$ A-crystallin differ significantly in both the negative ellipticity and the peak position from that of the mixed oligomer (Figure 3.3 A). The wild type protein and the mutant protein exhibit a minimum around 216 nm and 211 nm respectively, while mixed oligomers exhibit a minimum around 214 nm with the negative ellipticity in between that of the wild type and mutant protein. If there are no specific interactions between the subunits in the mixed oligomer, its spectrum should be an algebraic sum of those of homo-oligomers of the wild type and the mutant protein. However, the far-UV CD spectrum of the mixed oligomers does not overlap with the algebraic sum of the spectra of the wild type and the mutant protein (Figure 3.3 A) indicating subunit-packing-induced alterations either in the wild type or in the mutant or both subunits upon mixed oligomer formation.

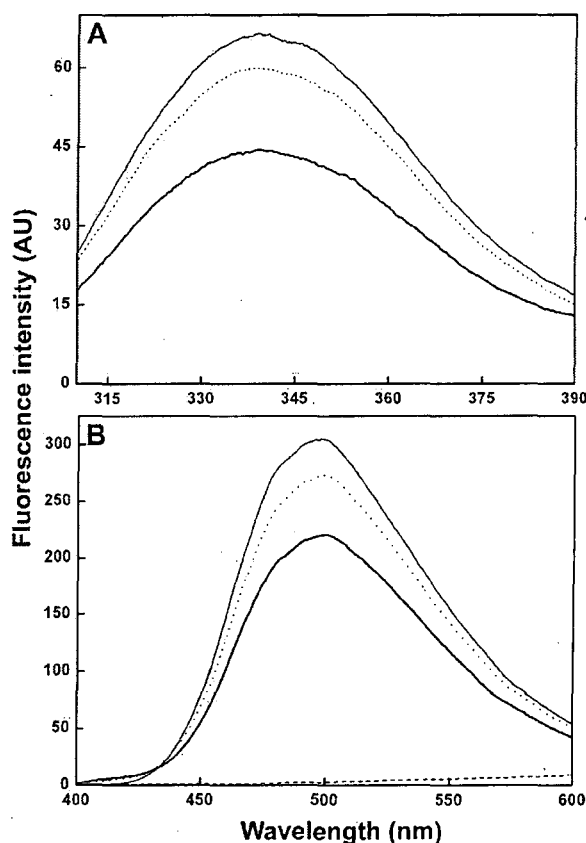
Near-UV CD spectra (Figure 3.3 B) also indicate significant differences in the side chain packing of aromatic residues upon mixed oligomer formation. Near-UV CD spectrum of the mixed oligomers does not overlap with that of the algebraic sum of the spectra of the wild type and the mutant protein (Figure 3.3 B) indicating subtle subunit-packing-induced alterations upon mixed oligomer formation.



**Figure 3.3: Circular dichroism (CD) spectra of the wild type, G98R $\alpha$ A-crystallin and their mixed oligomers.** Far-UV CD spectra (A) and Near-UV CD spectra (B) of different proteins including wild type  $\alpha$ A-crystallin (thick line), G98R $\alpha$ A-crystallin (thin line), mixed-oligomer (dashed line). The algebraic sum of the far- or near-UV CD spectra of wild type  $\alpha$ A-crystallin and mutant  $\alpha$ A-crystallin is also shown (dotted line).  $[\theta]_{MRM}$ , mean residue mass ellipticity.

### 3.3.2.2 Characterization of the tertiary structure and surface hydrophobicity of mixed oligomers using fluorescence:

The differences in the tertiary structure of the homo- and mixed-oligomers are also reflected in the tryptophan fluorescence and bis-ANS binding studies (Figure 3.4). The mixed oligomer exhibits tryptophan fluorescence spectrum with significantly increased intensity compared to the wild type protein (Figure 3.4 A), but less than that of the homo-oligomer of mutant protein, without any observable shift in the  $\lambda_{E_{max}}$  (emission maximum wavelength). Figure 3.4 B shows the relative hydrophobic surfaces in homo- and mixed-oligomers of  $\alpha$ A-crystallin and G98R $\alpha$ A-crystallin probed by bis-ANS. The fluorescence intensities of bis-ANS bound to mixed oligomer is in between that of the wild type and the mutant protein. Interestingly, the near-UV CD spectrum (Figure 3.3 B), intrinsic fluorescence spectrum (Figure 3.4 A) and the fluorescence spectrum of bis-ANS fluorescence bound to the mixed oligomer (Figure 3.4 B) differ subtly from the algebraic sum of the respective spectra of the wild type and mutant protein. Thus, all these results indicate subunit-packing-induced alterations in the mixed oligomers of the wild type and mutant  $\alpha$ A-crystallin.



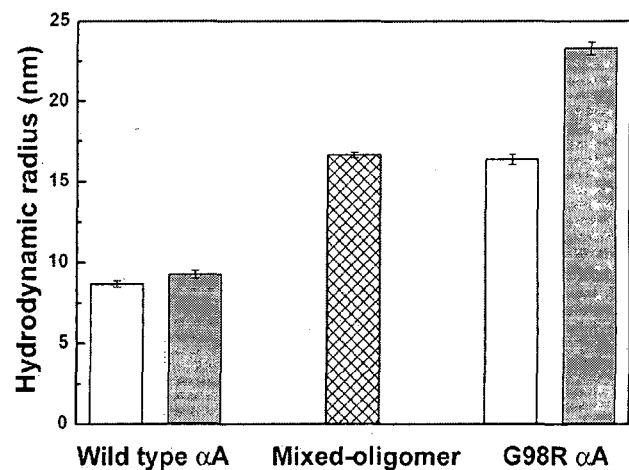
**Figure 3.4: Intrinsic tryptophan fluorescence and bis-ANS binding of the homo- and mixed-oligomers of wild type and G98R $\alpha$ A-crystallin.** (A) Intrinsic tryptophan fluorescence spectra of a 0.2 mg/ml sample of wild type  $\alpha$ A-crystallin (thick line), the mutant  $\alpha$ A-crystallin (thin line) and the mixed-oligomer (dotted line). (B) Fluorescence spectra of bis-ANS (10  $\mu$ M) in buffer alone (dashed line) and in the presence of 0.2 mg/ml wild type  $\alpha$ A-crystallin (thick line), mutant  $\alpha$ A-crystallin (thin line) or the mixed-oligomer (dotted line).



### 3.3.2.3 Characterization of the quaternary structure of mixed oligomers:

We have investigated the quaternary structure of mixed oligomers by dynamic light scattering (Figure 3.5). The average hydrodynamic radii ( $R_h$ ) of the wild type and mutant protein are determined to be 8.8 nm and 16.3 nm, respectively. Upon incubation at 37°C for 3.5 h, the  $R_h$  of the wild type protein is not changed significantly (9.2 nm). On the other hand, the  $R_h$  of the mutant protein is increased significantly to around 23.3 nm. This indicates that the mutant protein has a tendency to form higher oligomers upon incubation at physiologically relevant

temperature (37°C). Interestingly, the mixed oligomers (prepared by incubating at 37°C for a similar time) exhibit  $R_h$  of 16.6 nm, comparable to that of the mutant protein, without incubation at 37°C. These results indicate that (i) the mutant protein is sensitive to physiological temperature and can form large oligomers, which can affect the transparency of lens (ii) the wild type subunits prevent this higher oligomerization of the mutant subunits and (ii) the mixed oligomer size is significantly higher than that of the wild type oligomers.



**Figure 3.5: Changes in quaternary structure of  $\alpha A$ -, G98R $\alpha A$ -crystallin and their mixed oligomers.** DLS shows that the hydrodynamic radius ( $R_h$ ) of the mutant protein is bigger compared to that of wild type  $\alpha A$ -crystallin, whereas it is comparable to that of the mixed oligomer. Filled grey bars represent  $R_h$  values of homo-oligomers of individual proteins incubated at 37°C for 3.5 h; pronounced increase in hydrodynamic radius is observed in the case of G98R  $\alpha A$ -crystallin.

Thus, taken together all our structural studies, in general, suggest that though the wild type protein in mixed oligomers can exert some favorable effects such as inhibiting the increased multimerization of the mutant protein at 37°C, structure of mixed oligomer is likely to reflect relatively more of the mutant character.

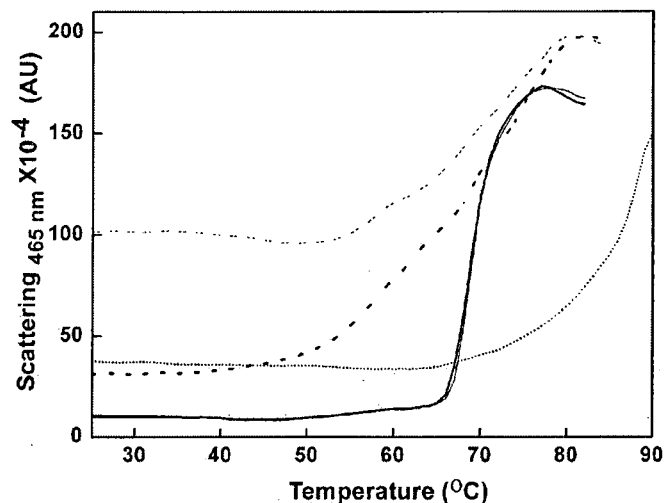
### 3.3.3 Comparative stability of $\alpha A$ -, G98R $\alpha A$ -crystallin and mixed oligomers:

Studies reported in the Chapter 2 clearly demonstrate that the mutant protein is less stable compared to the wild type protein. Mixed oligomers show properties that are non-

additive, indicating possible inter-subunit interaction. Their interactions would be expected to alter the stability of the mixed oligomers. We have investigated the stability by heat, chemical denaturant and proteolytic enzyme.

### 3.3.3.1 Thermal stability:

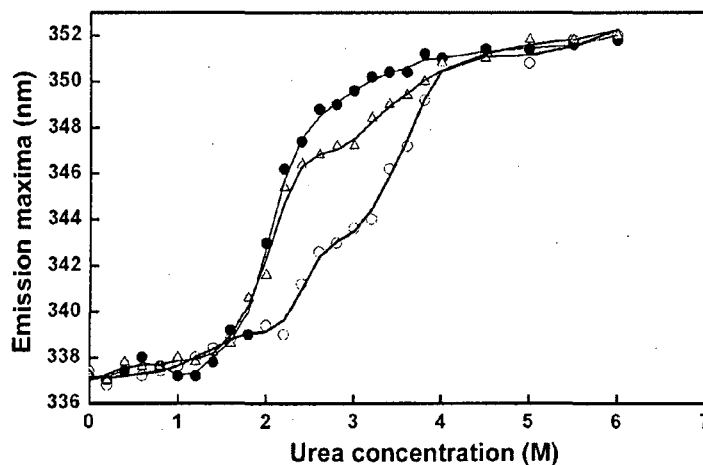
Light scattering as a function of temperature was monitored to investigate the thermal stability of the proteins (Figure 3.6). The light scattering of wild type  $\alpha$ A-crystallin sample is not altered significantly until 66°C, but increases sharply beyond 66°C, indicating that the protein aggregates cooperatively above this temperature. The wild type protein sample pre-incubated at 37°C for 3.5 h also exhibits very similar behavior with a transition around 66°C. On the other hand, the G98R $\alpha$ A-crystallin sample exhibits higher light scattering at 25°C compared to the wild type protein which increases further beyond 45°C in a relatively less cooperative manner. When the mutant protein is pre-incubated at 37°C for 3.5 h, in agreement with the measured large  $R_h$  (Figure 3.5), the sample exhibits even greater light scattering at 25°C, indicating that the sample has formed larger oligomers. Upon heating the sample, a gradual transition is observed above 50°C. The mixed oligomer, obtained by mixing the wild type and mutant proteins at 37°C for 3.5 h, shows light scattering similar to that of the mutant protein at 25°C. However, upon heating, the mixed oligomer shows no change in light scattering till almost 67°C and a gradual increase above this temperature, indicating that the mixed oligomer exhibits more thermal stability than individual subunits of  $\alpha$ A-crystallin and G98R $\alpha$ A-crystallin.



**Figure 3.6: Thermal stability of  $\alpha$ A-, G98R $\alpha$ A-crystallin and their mixed oligomer.** Aggregation of the  $\alpha$ A-crystallin (thick line), the G98R $\alpha$ A-crystallin (thick dashed line) or mixed-oligomer (dotted line) was monitored by light scattering at 465 nm as a function of temperature. Wild type  $\alpha$ A-crystallin, when incubated for 3.5 h at 37°C (thin line), showed no change in the aggregation profile, whereas G98R $\alpha$ A-crystallin (thin dashed line) showed considerable scattering even at 25°C.

### 3.3.3.2 Stability towards urea-induced unfolding:

We have investigated the urea-induced unfolding of wild type  $\alpha$ A-crystallin, G98R $\alpha$ A-crystallin and their mixed oligomers by monitoring changes in intrinsic tryptophan fluorescence in order to understand the effect of mutant  $\alpha$ A-crystallin subunits on the stability of mixed oligomers (Figure 3.7).  $\alpha$ A-crystallin exhibits emission maximum around 337 nm in the absence of urea which gradually shifts to about 339 nm in 2 M urea and relatively sharply to about 343 nm in 3 M urea. It further red shifts to 350 nm in 4 M urea indicating almost complete exposure of the tryptophan residue to the solvent. On the other hand, G98R $\alpha$ A-crystallin starts unfolding at a relatively much lower concentration of urea. The tryptophan residue of the mutant protein becomes almost completely solvent-exposed at as low as 3 M urea concentration as described in Chapter 2. Urea-induced unfolding profile of the mixed oligomers of the wild type and the mutant protein, initially (below 2.5 M urea) assumes the character of the mutant protein alone. Above 2.5 M urea the profile is in between that of the wild type and the mutant protein. This result suggests that packing of the mutant subunits in the mixed oligomer assembly is likely to affect the overall stability.



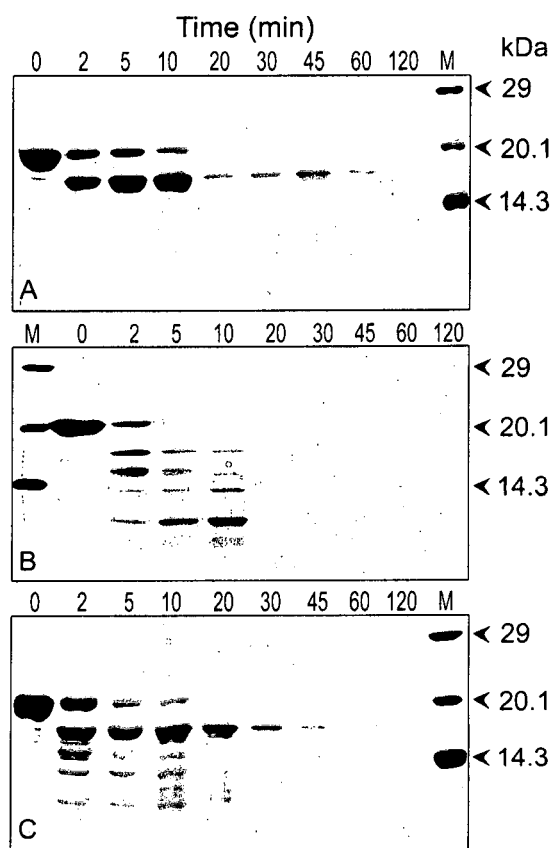
**Figure 3.7: Urea-induced unfolding of  $\alpha$ A-crystallins.** Unfolding of  $\alpha$ A-crystallin ( $\circ$ ), G98R $\alpha$ A-crystallin ( $\bullet$ ) or their mixed oligomer ( $\Delta$ ) as monitored by change in the emission maximum of the intrinsic tryptophan fluorescence. The protein samples (0.2 mg/ml) in TNE buffer were incubated at 37°C for 6 h in the presence of indicated concentrations of urea.

### 3.3.3.3 Structural stability probed by limited proteolysis:

As mentioned earlier studies using limited proteolysis can provide useful information about structural differences and compactness of structure. Figure 3.8 compares the limited

proteolysis of the homo- and mixed- oligomers of  $\alpha$ A- and G98R $\alpha$ A-crystallin. As described in Chapter 2, the mutant protein is more susceptible to proteolysis compared to the wild type protein. Protein band corresponding to the mutant protein disappears within 5 min whereas that corresponding to the wild type disappears in nearly 20 min. Most of the proteolytic fragments observed in the case of homo-oligomers of the wild type and the mutant protein are also represented in the limited proteolysis pattern of the mixed oligomer. However, the relative intensities of the bands seem to show some variation with respect to those in the cases of the individual proteins. The mixed oligomer is completely digested within 20 min comparable to that of the wild type subunit and in contrast to the mutant homo-oligomers. Thus, there is a possibility that wild type subunits help in tight packing of the mixed oligomer making it more compact and structured. However, the mixed oligomers undergo proteolysis with fragments seen in the case of the homo-oligomers of the mutant protein ruling out the possibility that mixed oligomer formation leads to decreased accessibility of the site(s) resulting in decreased susceptibility of the mutant subunits to proteolysis.

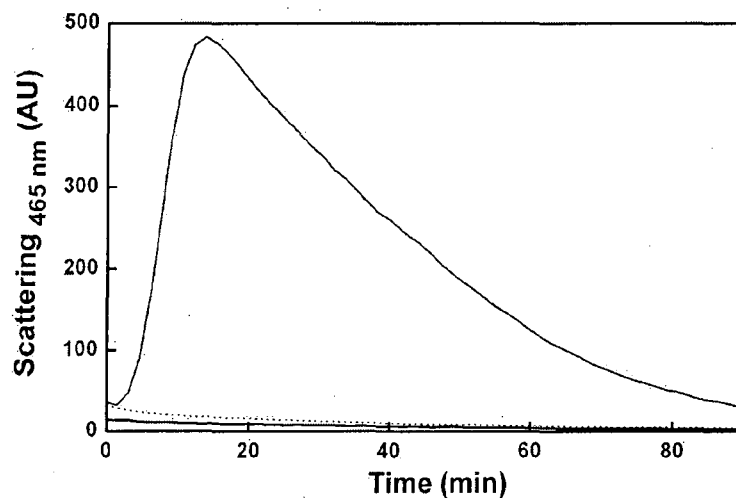
Interestingly, we also found that the mutant protein, but not the wild type protein, exhibits aggregation during initial stages of proteolysis with proteinase K (Figure 3.9). Light scattering increases sharply, reaching a maximum by 14 min followed by a gradual decrease with time. The initial increase in the light scattering indicates that a proteolytic fragment(s) is prone to aggregation. The decrease in the light scattering after initial increase could be



**Figure 3.8: Limited proteolysis studies by proteinase K.** Samples of the wild type (A) or G98R $\alpha$ A-crystallin (B) or their mixed oligomers (C) were treated with proteinase K for the indicated periods of time (in minutes at top of each panel) before analyzing on 15% SDS polyacrylamide gels. M shows marker lane with arrow indicating their corresponding positions and sizes.

either due to flocculation and settling down of the protein, leading to decrease in the population of aggregated species in the light path or due to further proteolysis of the aggregates, as amorphous aggregates are susceptible to proteolysis (Trivedi *et al.*, 1999). We conclude that aggregates undergo further proteolysis resulting in the observed decrease in the light scattering, as we did not observe any flocculate matter or precipitate. However, the wild type protein does not exhibit aggregation during proteolysis. In contrast to the observation with the mutant protein, when we subjected the mixed oligomers (containing mutant protein subunits) to proteolysis, protein aggregation was not seen (Figure 3.9). Since mixed oligomer formation does not lead to the decreased susceptibility of the mutant subunits to proteolysis, it is likely that the aggregation-prone fragments formed transiently are sequestered by the wild type subunits preventing aggregation.

As activation of calpains has been implicated in aging and cataract formation (Biswas *et al.*, 2004), these results assume physiological significance. Susceptibility to proteolysis and transient population of aggregation-prone proteolytic fragments by the mutant protein can be a possible threat to the lens transparency. Though, the wild type subunits (in mixed oligomer) prevent the aggregation of G98R $\alpha$ A-crystallin upon proteolysis probably by binding to the aggregation-prone fragments, this complex can accumulate with time giving way to protein aggregates and consequent opacities.

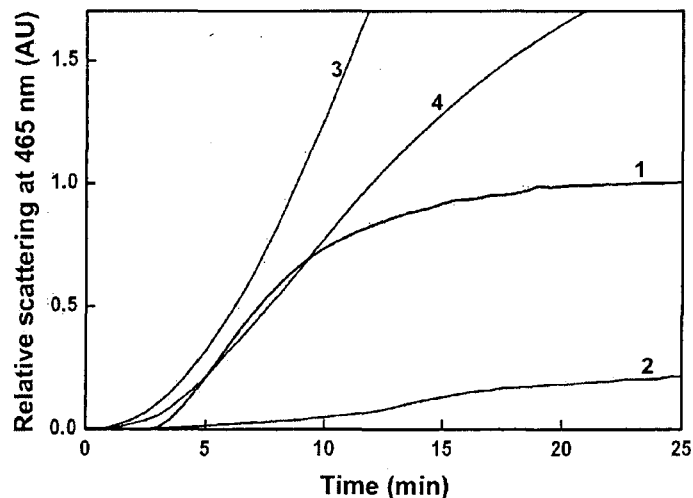


**Figure 3.9: Aggregation of proteolytic fragments during the process of limited proteolysis by proteinase K.** Samples of wild type (thick line) or mutant (thin line) and their mixed oligomers (dotted line) were treated with proteinase K (protein:protease::200:1) and the light scattering was monitored as a function of time.

### 3.3.4 Chaperone-like activity of mixed oligomers:

In order to assess if the formation of mixed oligomers is a result of fortuitous interaction of structurally related  $\alpha$ A- and G98R $\alpha$ A-crystallin or it might be of functional significance in delaying the cataract, we have studied its chaperone-like activity towards DTT-induced aggregation of insulin (Figure 3.10). In the previous chapter it was shown that G98R $\alpha$ A-crystallin does not possess chaperone-like activity towards insulin and it co-aggregates with insulin. The concentration of the mixed oligomer (w/w) used in the assay was equal to that of the target protein (0.2 mg/ml), such that the concentrations of  $\alpha$ A-crystallin and G98R $\alpha$ A-crystallin in the mixed oligomer were 0.1 mg/ml each. The mixed oligomers [at the mixed oligomer to insulin ratio of 1:1 (w/w)], do not prevent the aggregation of insulin, though the rate of co-aggregation is relatively less than that in the presence of mutant  $\alpha$ A-crystallin. Even doubling the concentration of the mixed oligomers (wild type and mutant protein are present at a concentration of 0.2 mg/ml each) did not prevent the aggregation of insulin. Thus, the mixed oligomers also exhibit loss of chaperone-like activity like the homo-oligomers of the mutant protein, despite the fact that the mixed oligomers contain wild type subunits.

In the eye lens, it is believed that  $\alpha$ A-crystallin in mixed complexes with  $\alpha$ B-crystallin serves to maintain lens transparency. It is possible that mutant subunits can interact with

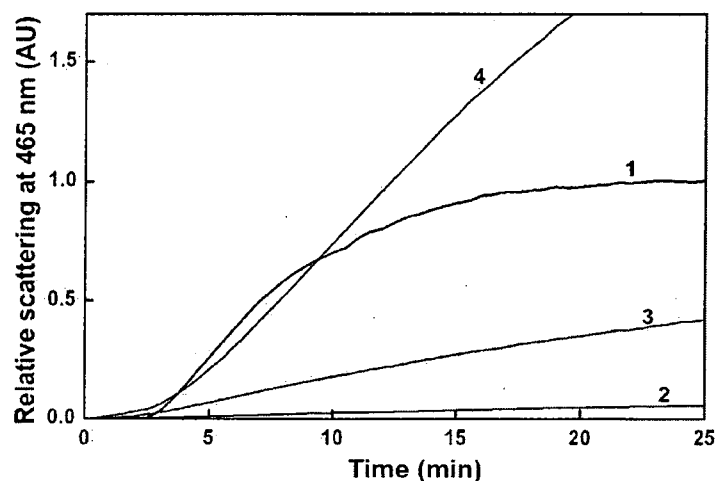


**Figure 3.10: Chaperone-like activity of the mixed oligomer with respect to the individual homo-oligomers towards DTT-induced aggregation of insulin at 37°C.** Aggregation of insulin in the absence (curve 1); or in the presence of wild type (curve 2); or the mutant  $\alpha$ A-crystallin (curve 3) and their mixed oligomer (curve 4). Substrate to chaperone ratio was maintained at 1:1.



$\alpha$ B-crystallin subunits in the lens, although its relative concentration is about one third with respect to  $\alpha$ A-crystallin (Sax and Piatigorsky, 1994). Recombinant  $\alpha$ B-crystallin is shown to be a better chaperone than  $\alpha$ A-crystallin at physiological temperatures (Datta and Rao 1999; Sun *et al.*, 1997). On formation of mixed oligomers, it is also possible that  $\alpha$ B-crystallin prevents the mutant protein from aggregating and in its presence, toxic effects of G98R $\alpha$ A-crystallin are not manifested in early life. Swamy and Abraham (1991) had shown that  $\alpha$ A- and  $\alpha$ B-crystallin can exist in lens as hetero-oligomers of 3:1 to 1:1 ratio depending on the age. Therefore, we have tested whether mixed oligomer formation with  $\alpha$ B-crystallin at these two ratios leads to any change in the chaperone property of the individual wild type and mutant proteins.

As shown in Figure 3.11,  $\alpha$ B-crystallin protects aggregation of insulin almost completely at 1:1 (w/w) substrate to protein ratio. But when complexed with G98R $\alpha$ A-crystallin in 1:1 ratio (0.10 mg/ml G98R $\alpha$ A-crystallin + 0.10 mg/ml  $\alpha$ B-crystallin),  $\alpha$ B-crystallin protects to a lesser extent. However, it improves the chaperone-like activity of the mutant protein. Further increase in the quantity of G98R $\alpha$ A-crystallin in the mixed oligomer (0.15 mg/ml G98R $\alpha$ A-crystallin + 0.05 mg/ml  $\alpha$ B-crystallin) results in decrease in chaperone-like activity of  $\alpha$ B-crystallin (Figure 3.11, curve 4). Similar experiments performed on G98R $\alpha$ A-crystallin using alcohol dehydrogenase (ADH) as substrate



**Figure 3.11: Chaperone-like activity of the mixed oligomer of G98R mutant protein with  $\alpha$ B-crystallin towards DTT-induced aggregation of insulin at 37°C.** Aggregation of insulin in the absence (curve 1); or in the presence of wild type  $\alpha$ B-crystallin (curve 2); or the mixed oligomer of G98R and  $\alpha$ B in 1:1 (w/w) ratio (curve 3); and G98R and  $\alpha$ B in 3:1 (w/w) ratio (curve 4). Substrate to chaperone ratio was maintained at 1:1.

(Murugesan *et al.*, 2007) have confirmed that the extent of aggregation is proportional to the amount of the mutant protein in the mixed oligomers.

Thus, partial improvement in the functional efficiency of the mutant protein on forming complexes with wild type  $\alpha$ A-crystallin or  $\alpha$ B-crystallin can be due to rearrangement of subunits in the mixed oligomer, resulting in possible alteration of relative accessibility of the individual subunits or leading to the generation or exposure of substrate-binding sites. This partially improved activity might result in prevention of congenital cataract phenotype. However, increase in amount of mutant  $\alpha$ A-crystallin obliterated this effect and disrupted the chaperone-like activity of wild type  $\alpha$ -crystallins. It is possible that subsequent insults to lens proteins and age-related modifications can overwhelm the functional chaperone molecules resulting in delayed lenticular opacity.

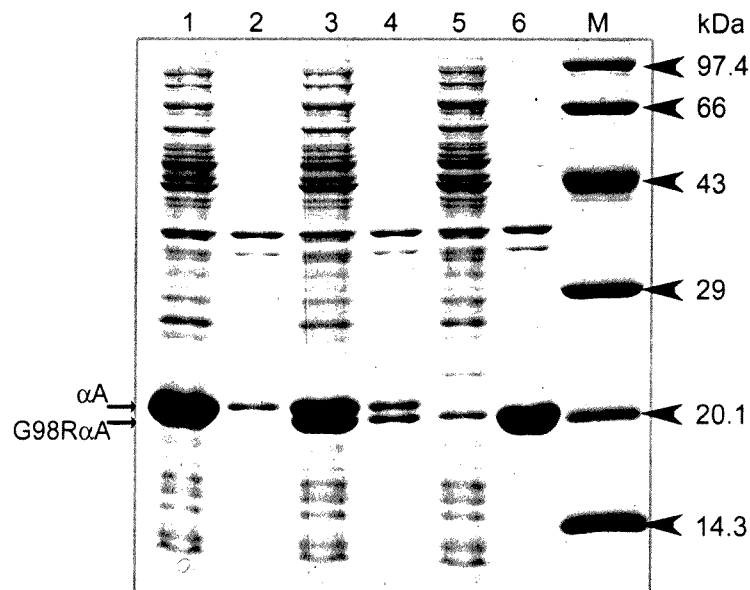
### 3.3.5 Co-expression of the $\alpha$ A- and G98R $\alpha$ A-crystallin in *E.coli*:

Our results show that the mixed oligomers of the wild type and G98R $\alpha$ A-crystallin exhibit properties dominated by those of the mutant protein in structural aspects, chaperone-like activity and urea-induced unfolding. However, mixed oligomer formation leads to a decreased propensity to aggregate as a function of temperature compared to the homo-oligomers of the mutant protein. Considering these *in vitro* results, we set out to test the outcome of co-expression of the wild type and mutant protein *in vivo*. Fortuitously, the wild type and G98R $\alpha$ A-crystallin differ in their mobility on SDS-PAGE, which made it possible to study the effect of co-expression of these proteins.

We have cloned the wild type and mutant cDNA under the same promoter in a pETDuet-1 vector and co-expressed these proteins in *E.coli* (Figure 3.12). As also shown in the previous chapter, when expressed in *E.coli*, the wild type protein is expressed as a soluble protein (Figure 3.12, Lane 1) and the mutant protein forms inclusion bodies partitioning almost exclusively into the insoluble pellet fraction (Figure 3.12, Lane 6). On the other hand, co-expression of the wild type protein along with G98R $\alpha$ A-crystallin results in prevention of inclusion body formation of the mutant protein – both the mutant and the wild type protein expressed predominantly in the soluble form (Figure 3.12, Lane 3), probably due to the mixed oligomer formation.

The co-expression experiment demonstrates that  $\alpha$ A-crystallin can rescue the mutant protein from aggregation and inclusion body formation. This phenomenon may form

the molecular basis for the absence of congenital cataract, though the mutation could severely affect its folding leading to aggregation.



**Figure 3.12: Co-expression of  $\alpha$ A- and G98R $\alpha$ A-crystallin in *E.coli* BL21 (DE3).** Lanes 1 & 2 represent the soluble and insoluble fractions of cells overexpressing wild type  $\alpha$ A-crystallin cloned in pET-21a(+) vector. Lanes 3 & 4 represent the soluble and insoluble fractions of cells co-expressing the wild type  $\alpha$ A-crystallin and G98R $\alpha$ A-crystallin genes cloned in pETDuet-1 vector. Lanes 5 & 6 represent the soluble and insoluble fractions of cells expressing the mutant G98R $\alpha$ A-crystallin cloned in pET-21a(+) vector. Lane M shows the positions of molecular mass markers with arrowheads indicating their corresponding size in kDa. Thin arrows indicate the positions of wild type or mutant  $\alpha$ A-crystallin and depict the difference in mobility of these proteins.

### 3.4 CONCLUSION:

There are increasing evidences showing that point mutations in sHsps lead to pathological conditions, and the mutations are often dominant negative in character. In this context, investigating the structural and functional properties of mixed oligomers formed between the wild type and mutant subunits is important.

Subunit exchange studies using fluorescence resonance energy transfer show that the mutant protein forms mixed oligomers with the wild type protein. The mutant protein is more susceptible to thermal aggregation and upon proteolysis transiently populates fragments that are prone to aggregation, whereas mixed oligomer formation leads to a decreased propensity to aggregate (as a function of temperature or upon proteolysis).

Consistent with these findings *in vitro*, co-expression of the wild type protein with the mutant protein in *E. coli* demonstrates that wild type  $\alpha$ A-crystallin rescues the mutant protein from aggregation and inclusion body formation. Although the mutation could severely affect protein folding leading to aggregation, these observations may underlie the molecular basis for the absence of congenital cataract. We found that subunits of mutant  $\alpha$ A-crystallin significantly reduced the chaperone-like activity of wild type  $\alpha$ A- and  $\alpha$ B-crystallin towards DTT-induced aggregation of insulin. Our study shows that the mixed oligomers of wild type and G98R $\alpha$ A-crystallin also exhibit properties dominated by those of the mutant protein in structural aspects, oligomeric size, urea-induced unfolding and more importantly in the chaperone-like activity, which may further explain presenile cataract formation in affected individuals.

However, environmental factors, life style and susceptibility of the mixed oligomers (properties of which are dominated by the mutant subunits) to age-related modifications including oxidation, deamidation, glycation and proteolysis could contribute to the early onset of cataract in the mutation-affected individuals.

**METAL IONS:  
PRESENILE  
CATARACTOGENESIS**

**4**

#### 4.1 INTRODUCTION:

Cataract development is a complex process involving multiple factors. Age is one of the major risk factor associated with cataract. The lens core contains proteins formed *in utero* and in the absence of any protein turnover, these long-lived proteins become vulnerable to post-translational modifications. All the three crystallins,  $\alpha$ ,  $\beta$  and  $\gamma$ , are known to undergo such modifications. A majority of these post-translational modifications in  $\alpha$ -crystallins cause conformational changes (unfolding), resulting in their decreased molecular chaperone-like activity and/or formation of their high molecular weight aggregates that can scatter light (Table 4.1). Most of these modifications are also seen in cataractous lenses, some of which may make  $\alpha$ -crystallins susceptible to cleavage and further modifications. Young, aged, and senile cataract lenses contain crystallin fragments (<3.5 kDa), accumulation of which increases with age (Santoshkumar *et al.*, 2008). Though, these post-translational modifications are considered to be the main reason for senile cataractogenesis, most of the modifications in these proteins appear to have occurred at a very early age. Deamidation, modification of the C-terminal, cleavage of C-terminal (between Serine 172 and 173) and phosphorylation of human  $\alpha$ A-crystallin all occur over the first 20-25 years, followed by no significant increase (Dilley and Harding, 1975; Takemoto, 1995b; Takemoto, 1996a; Takemoto, 1998; Lampi *et al.*, 1998).

Our earlier studies (Singh *et al.*, 2006; Singh *et al.*, 2007b) have shown that (i) expression of G98R $\alpha$ A-crystallin (but not  $\alpha$ A-crystallin) in *E. coli* leads to inclusion bodies formation, suggesting that the G98R mutation in  $\alpha$ A-crystallin leads to folding defects, resulting in aggregation in the crowded milieu of cells, (ii) G98R $\alpha$ A-crystallin exhibits structural differences and loss of its chaperone-like activity towards DTT-induced aggregation of insulin, (iii) the mutation leads to destabilization of the protein towards heat- and urea-induced unfolding, increased susceptibility to proteolysis with transient population of aggregation-prone proteolytic fragments, (iv) co-expression of the wild type and the mutant protein in *E. coli* rescues the mutant protein from aggregation and inclusion body formation, (v) G98R $\alpha$ A-crystallin, like wild type protein, exchanges subunits, and forms mixed oligomers with the wild type subunits leading to decreased propensity to aggregate. Thus, though the mutation results in drastic folding defects and aggregation, mixed oligomer formation with wild type subunits alleviates the folding defect and prevents aggregation of the mutant protein. This phenomenon may underlie the molecular basis for the absence of congenital cataract. However, the molecular basis for the early onset (presenile) of cataract



**Table 4.1:** Post-translational modifications in  $\alpha$ -crystallins from human lens and their possible effects

<i>In vivo</i> Modifications	Possible Effects
Truncation of N-term region in $\alpha A$ and $\alpha B$ (Lund <i>et al.</i> , 1996; Kamei <i>et al.</i> , 1997; Santoshkumar <i>et al.</i> , 2008).	Truncated peptides bound to $\alpha$ -crystallins decreased their molecular chaperone properties and few peptides enhanced aggregation (Santoshkumar <i>et al.</i> , 2008).
Truncation of C-term region of $\alpha A$ at Asp151, Thr168, Ser172 and $\alpha B$ at Lys174 (Takemoto, 1995a; Lund <i>et al.</i> , 1996; Takemoto, 1998; Ma <i>et al.</i> , 1998).	Decrease in molecular chaperone properties (Takemoto <i>et al.</i> , 1993; Andley <i>et al.</i> , 1996) and also possible aggregation (Siezen <i>et al.</i> , 1979).
Racemization of Asp58 and Asp151 of $\alpha A$ (Fujii <i>et al.</i> , 1999; Fujii <i>et al.</i> , 2003) and Asp36 and Asp62 in $\alpha B$ (Fujii <i>et al.</i> , 1994).	Decrease in chaperone activity (Fujii <i>et al.</i> , 2001).
Phosphorylation of various Ser in both $\alpha A$ and $\alpha B$ (Miesbauer <i>et al.</i> , 1994; Takemoto, 1996a; Ma <i>et al.</i> , 1998; Hanson <i>et al.</i> , 2000).	Increase in molecular chaperone properties (van Boekel <i>et al.</i> , 1996; Ecroyd <i>et al.</i> , 2007; Ahmad <i>et al.</i> , 2008).
Deamidation of various Gln and Asn of both $\alpha A$ and $\alpha B$ (Miesbauer <i>et al.</i> , 1994; Lund <i>et al.</i> , 1996; Lampi <i>et al.</i> , 1998; Ma <i>et al.</i> , 1998; Takemoto and Boyle, 1998; Hanson <i>et al.</i> , 2000; Srivastava and Srivastava, 2003).	Reduced chaperone activity and increased aggregation size of $\alpha A$ (Gupta and Srivastava, 2004a) and $\alpha B$ (Gupta and Srivastava, 2004b).
Glycation i.e. non-enzymatic reaction of sugar with lysines in $\alpha A$ and $\alpha B$ leads to formation of AGEs, Advanced Glycation End products (Araki <i>et al.</i> , 1992; Swamy <i>et al.</i> , 1992; Abraham <i>et al.</i> , 1994; Argirov <i>et al.</i> , 2004).	Formation of AGEs results in decrease of molecular chaperone properties (Cherian and Abraham, 1995; van Boekel <i>et al.</i> , 1996; Derham and Harding, 2002). Single AGE modification OP-lysine on $\alpha B$ impaired chaperone activity (Bhattacharyya <i>et al.</i> , 2007).
Carbamylation i.e. non-enzymatic reaction of isocyanate with mostly lysine (Lapko <i>et al.</i> , 2001).	Resulted in decrease in aggregate size and no change in chaperone activity (van Boekel <i>et al.</i> , 1996) but more drastic carbamylation resulted in decrease of chaperone activity (Plater <i>et al.</i> , 1997). It causes gross conformational change and increased aggregation (Beswick and Harding, 1987).
Mixed disulfide formation (Garner and Spector, 1980; Lou and Dickerson, 1992).	Decrease in molecular chaperone properties (Cherian <i>et al.</i> , 1997; Cherian and Abraham, 1995).
Acetylation (Lin <i>et al.</i> , 1998; Lapko <i>et al.</i> , 2001).	Unknown
Oxidation of Met in $\alpha A$ (Lund <i>et al.</i> , 1996; Hanson <i>et al.</i> , 2000).	Decrease in molecular chaperone properties (Cherian and Abraham, 1995).
Oxidation of Cys131 and 142 of $\alpha A$ to form an intramolecular disulfide bond (Miesbauer <i>et al.</i> , 1994; Lund <i>et al.</i> , 1996; Takemoto, 1996b; Takemoto, 1996c; Hanson <i>et al.</i> , 2000).	Decrease in molecular chaperone properties (Cherian and Abraham, 1995; van Boekel <i>et al.</i> , 1996; Cherian-Shaw <i>et al.</i> , 1999).

formation and the dominant effects of the mutation are not completely understood. Environmental factors and/or post translational modifications might have a role in the early onset of cataract. Since the structure and chaperone activity of the mixed oligomers were dominated by those of the mutant subunits (Singh *et al.*, 2007b), it is possible that the system is vulnerable to age-related modifications of the lens proteins and packing alterations, or other environmental risk factors that could augment the deleterious effects of the mutation and be involved in presenile cataract formation in the mutation-affected individuals.

Environmental stress, whether it is increased temperature, alteration of cytoplasmic pH or deposition of ions, would presumably trigger the increased expression of protective species. Treatment of lens epithelial cells with  $\text{Cu}^{2+}$  leads to selective up-regulation of the small heat shock proteins (sHsps),  $\alpha$ A- and  $\alpha$ B-crystallin (Hawse *et al.*, 2003). Further, mild environmental changes (e.g. the addition of  $\text{Mg}^{2+}$  and  $\text{Ca}^{2+}$  or EDTA, as well as variations of buffer pH) influence the heat stability and chaperone-like activity of native  $\alpha$ -crystallin (Koretz *et al.*, 1998). Thus, it is possible that this mutation manifests its phenotype or severity under the influence of certain environmental or risk factors.

Among different environmental risk factors interfering with structural organization of proteins, divalent metal ions play an important role. Age-dependent accumulation of heavy metal ions such as  $\text{Cu}^{2+}$ ,  $\text{Cd}^{2+}$ ,  $\text{Zn}^{2+}$  and  $\text{Ca}^{2+}$  is believed to be one of the risk factors for cataractogenesis as elevated levels of these metal ions are found in cataractous lenses (Stanojević-Paović *et al.*, 1987; Rácz and Erdöhelyi, 1988; Srivastava *et al.*, 1992; Rasi *et al.*, 1992; Cekic, 1998). These metal ions represent a risk in terms of both structural destabilization and functional failure.  $\text{Cu}^{2+}$  and  $\text{Cd}^{2+}$  (though less potent) are redox-active metal ions that are important components of oxidative stress (Gaggelli *et al.*, 2006; Barnham *et al.*, 2004; Hawse *et al.*, 2006). Oxidation contributes to many post-translational modifications associated with aging and is the hallmark of senile cataract (Truscott, 2005). Lens proteins have increased susceptibility to oxidation because of the high level of oxidants present in and around the lens (Spector and Garner, 1981; Giblin *et al.*, 1984). Though  $\text{Cu}^{2+}$  is a co-factor of several critical enzymes, its ability, shared with other transition metal ions, to catalyze production of reactive oxygen species (ROS) such as peroxy radical ( $\text{HO}_2^{\bullet}$ ), superoxide anion radical ( $\text{O}_2^{\bullet-}$ ), hydrogen peroxide ( $\text{H}_2\text{O}_2$ ) and finally hydroxyl radical ( $\text{OH}^{\bullet}$ ) in the presence of ascorbate and oxygen through Fenton-type reaction (Khan and Martell, 1967; Gaggelli *et al.*, 2006), can lead to the oxidation of amino acid side chains,

fragmentation of the protein and formation of protein-protein cross-links (Stadtman and Oliver, 1991). Incubation of calf lens  $\alpha$ -crystallin with  $H_2O_2$  and  $FeCl_3$  resulted in 80% loss of its chaperone activity (Cherian and Abraham, 1995). Oxidation results in disintegration of the oligomeric structure and compromised chaperone-like activity of  $\alpha A$ - and  $\alpha B$ -crystallin (Rajan *et al.*, 2006).

Considering the fact that these heavy metal ions are potential environmental risk factors, we set out to investigate if these metal ions can modulate the structure and function of mutant G98R $\alpha A$ -crystallin, and to see if these risk factors along with the mutation cause presenile cataract in the affected individuals.

## 4.2 EXPERIMENTAL PROCEDURES:

### 4.2.1 Materials:

Coumarin-3-carboxylic acid (3-CCA),  $CdCl_2$ , sodium salt of fluorescein and N-acetyl tryptophanamide (NATA) were from Sigma (St. Louis, USA). Sodium salt of 2,6 dichlorophenolindophenol (DCI) and ethylenediamine tetraacetic acid (EDTA) were obtained from SRL (Mumbai, India). Analytical reagent grade  $CuCl_2$  was supplied by Qualigens (Mumbai, India).  $CaCl_2$  and  $ZnCl_2$  standard solutions were purchased from Fluka (Switzerland). All other reagents used in this study were of analytical grade.

### 4.2.2 Purification of $\alpha A$ -crystallins and exchange of buffer:

Both  $\alpha A$ - and G98R $\alpha A$ -crystallin were purified as mentioned earlier in Chapter 2. The two proteins were passed through a desalting PD10 column to remove EDTA and to exchange buffer with either buffer A (20 mM phosphate, pH 7.4, containing 100 mM NaCl) or buffer B (20 mM HEPES-NaOH, pH 7.4, containing 100 mM NaCl).

### 4.2.3 Metal-binding studies:

Use of glycine in  $Cu^{2+}$ -binding studies was proposed to reveal tight-binding of the ligand (Jackson *et al.*, 2001; Thompsett *et al.*, 2005); it avoids less- or non-specific interaction of  $Cu^{2+}$  and it also avoids the formation of copper hydroxide. Therefore, we have used the stock solution of  $Cu^{2+}$  in the presence of glycine [ $Cu(gly)_2$ ] formed by mixing  $Cu^{2+}$  and glycine in 1:2 (M/M) ratio for all our experiments. For avoiding non-specificity and for sake of comparison, we have used other metal ions also in complex with glycine.

#### 4.2.4 Fluorescence spectroscopic analysis:

Fluorescence emission spectra were recorded at room temperature from 310-400 nm (5 nm slit width) with the excitation wavelength set at 295 nm (5 nm slit width) using a Hitachi F4500 Fluorescence Spectrophotometer.  $\alpha$ A- and G98R $\alpha$ A-crystallin (5  $\mu$ M subunits i.e. 0.1 mg/ml in buffer A) were titrated with increasing concentrations of  $\text{Cu}^{2+}$ . Samples were equilibrated for two minutes by magnetically stirring after each addition of  $\text{Cu}^{2+}$ . Control experiments were performed using NATA (5  $\mu$ M), thyroglobulin (0.1 mg/ml) and  $\alpha$ -synuclein (0.1 mg/ml; excitation 275 nm; emission 285-350 nm). The  $\text{Cu}^{2+}$  concentrations in spectroscopic measurements were in the range of 0-50  $\mu$ M. Extent of fluorescence quenching was calculated using the formula  $(F_0-F)/F_0$ , where  $F_0$  and  $F$  are fluorescence intensities at 337 nm (in the case of  $\alpha$ -synuclein, 300 nm) in the absence and in the presence of specified concentrations of  $\text{Cu}^{2+}$  respectively. Data were fitted by non-linear regression in GraphPad Prism 4.0 software using the One-site binding equation  $Y=B_{\max} * X / (Kd+X)$  where  $B_{\max}$  is the maximum extent of quenching and  $Kd$  is the dissociation constant.

#### 4.2.5 Isothermal titration calorimetry:

Isothermal titration calorimetry (ITC) was performed using a VP-ITC instrument (Microcal Inc., Northampton, USA) to determine the enthalpy changes of  $\alpha$ A- and G98R $\alpha$ A-crystallin on binding to  $\text{Cu}^{2+}$ . In all the titration experiments, 2  $\mu$ l aliquots from a stock of 1 mM  $\text{Cu}^{2+}$  in buffer B were injected (total 60 injections, each with a spacing of 240 seconds) into the cell containing 0.6 mg/ml ( $\approx$ 30  $\mu$ M)  $\alpha$ A-crystallin or 0.4 mg/ml ( $\approx$ 20  $\mu$ M) G98R $\alpha$ A-crystallin in buffer B at 30°C. In a control experiment, the corresponding copper solution was injected into buffer B alone in the sample cell. After subtracting the buffer blank from each experimental titration, the integrated heat of each injection was used for fitting to binding models using the program Microcal Origin 7.0. The overall dissociation constant,  $Kd_{\text{app}}$ , from ITC results was calculated from the association constants using the formula,  $Kd_{\text{app}} = 1/(K1 * K2 * k3 * \dots * Kn)^{1/n}$ .

#### 4.2.6 Effect of $\alpha$ A- and G98R $\alpha$ A-crystallin on the ascorbate-mediated $\text{Cu}^{2+}$ -catalyzed generation of ROS:

Ascorbate-mediated copper-induced  $\text{OH}^{\bullet}$  (hydroxyl radical) generation was followed using coumarin-3-carboxylic acid (3-CCA) as a probe (Manevich *et al.*, 1997). Upon reaction

with OH<sup>-</sup>, non-fluorescent 3-CCA is converted to its fluorescent derivative 7-hydroxycoumarin-3-carboxylic acid (7-OH-CCA), whose fluorescence intensity was monitored at 450 nm with the excitation at 395 nm, using a Spectramax Gemini XS microplate spectrofluorometer (Molecular Devices, LA, USA). Increase in fluorescence upon the addition of Cu<sup>2+</sup> (1 μM) to buffer A containing ascorbate (300 μM) and 3-CCA (100 μM) in the absence or in the presence of indicated concentrations of various proteins was measured in a 96 well plate format.

ROS generation was also measured by the monitoring fluorescence decay of a dye, fluorescein, upon the addition of an aliquot of Cu<sup>2+</sup> (10 μM) to a cuvette containing ascorbate (300 μM) and fluorescein (0.2 μM) in buffer A in the presence of buffer or indicated concentrations of various proteins. Fluorescence intensity decay of fluorescein (Ou *et al.*, 2002) at 515 nm was monitored at 25°C using a Hitachi F4500 Fluorescence Spectrophotometer with the excitation set at 493 nm. The excitation and emission band passes were set at 2.5 nm each. Initial fluorescence intensities (immediately after the addition of Cu<sup>2+</sup> solution) were normalized. The % inhibition of ROS generation by the proteins was calculated using the formula,  $[(F-F_0)/(1-F_0)] \times 100$  where F<sub>0</sub> and F are the relative fluorescence intensities at 14 min of the reaction in the absence and in the presence of proteins respectively.

#### 4.2.7 Estimation of ascorbate consumption:

Copper-catalyzed oxidation of ascorbate to dihydroascorbate results in consumption of ascorbate, which was followed by measuring time-dependent change in OD<sub>610 nm</sub> of a redox dye, 2,6 dichlorophenol indophenol (DCI), in buffer A on a Hitachi-200-20 Spectrophotometer. Ascorbate (300 μM) was incubated with 5 μM Cu<sup>2+</sup> in the absence or in the presence of protein samples (25 μg/ml) for 15 min at 25°C. An aliquot (50 μl) of the samples was withdrawn at different time points and the residual ascorbate was estimated using DCI: typically 50 μl of this solution was equilibrated for two minutes with 450 μl of DCI dye (60 μM) in buffer A containing 0.4 mM EDTA to complete the reaction between the residual ascorbate and DCI, before measuring the absorbance of the sample. Percentage of ascorbate remaining was calculated using the formula  $[(A_0-A_s)/(A_0-A)] \times 100$  where A<sub>0</sub> is the absorbance of DCI solution alone, A<sub>s</sub> is absorbance of sample after 15 min of incubation with Cu<sup>2+</sup> in the absence or in the presence of different proteins and A is the residual absorbance after ascorbate-DCI reaction.

#### 4.2.8 Metal ions-induced self-aggregation of $\alpha$ -crystallins and its reversibility:

Metal ion-induced aggregation of 0.1 mg/ml of  $\alpha$ A-crystallin or G98R $\alpha$ A-crystallin or their mixed oligomer ( $\approx 5 \mu\text{M}$ ) in buffer B at 37°C was monitored by light scattering as a function of increasing concentrations of different metal ions. Light scattering was measured using Hitachi F-4000 Fluorescence Spectrophotometer with the excitation and emission wavelengths set at 465 nm. Each sample was titrated with increasing concentrations of indicated metal ions; after each addition the sample was incubated for 10 min with stirring, before measuring the light scattering. A similar experiment was also performed using 0.4 mg/ml of  $\alpha$ A-crystallin or G98R $\alpha$ A-crystallin in the presence of varying concentrations of  $\text{Cu}^{2+}$ . In another experiment, 0.1 mg/ml of G98R $\alpha$ A-crystallin,  $\alpha$ A-crystallin or their mixed oligomer was incubated for 30 min at 37°C with 30, 90 and 90  $\mu\text{M}$   $\text{Cu}^{2+}$  respectively. Subsequently, EDTA at a final concentration of 200  $\mu\text{M}$  was added and decrease in light scattering at 465 nm was monitored for 20 min. Excitation and emission band widths were set at 3 nm.

#### 4.2.9 Chaperone assay:

The chaperone-like activity of both the proteins was probed by their ability to prevent the aggregation of insulin and citrate synthase (CS) as described in previous chapters. Insulin aggregation assays were performed in the absence or in the presence of 0.1 mg/ml wild type or mutant protein ( $\approx 5 \mu\text{M}$ ) with or without 15  $\mu\text{M}$   $\text{Cu}^{2+}$ . Similarly, CS was aggregated with or without indicated concentrations of different metal ions, in the absence or in the presence of 20  $\mu\text{g/ml}$  ( $\approx 1 \mu\text{M}$ )  $\alpha$ A-, G98R $\alpha$ A-crystallin or their mixed-oligomer. The chaperone to substrate ratio (w/w) was 0.5:1 in the case of insulin and  $\sim 1:1$  in the case of CS aggregation.

#### 4.2.10 Circular dichroism:

Near- and far-UV circular dichroism (CD) spectra of 50  $\mu\text{M}$  protein samples (1.0 mg/ml) were recorded in the absence or in the presence of 150  $\mu\text{M}$   $\text{Cu}^{2+}$  (molar ratio of protein to  $\text{Cu}^{2+}$  was maintained at 1:3) in buffer B at room temperature using a JASCO J-815 Spectropolarimeter.

#### 4.2.11 Dynamic light scattering:

The hydrodynamic radii ( $R_h$ ) of both the proteins (25  $\mu\text{M}$ ) were determined by dynamic light scattering measurements in the absence or in the presence of 75  $\mu\text{M}$   $\text{Cu}^{2+}$  (molar ratio of protein to  $\text{Cu}^{2+}$  was maintained at 1:3) using a Photocor Dynamic Light Scattering Instrument from Photocor Instruments Inc. (MD, USA). The data were fitted and analyzed using Dynals v2.0 software provided with the instrument.

#### 4.2.12 Effect of $\text{Cu}^{2+}$ on the thermal stability of $\alpha\text{A}$ - and G98R $\alpha\text{A}$ -crystallin:

The thermal aggregation of 0.2 mg/ml ( $\equiv$  10  $\mu\text{M}$ ) of the wild type and mutant protein, in buffer B, in the presence or in the absence of 30  $\mu\text{M}$   $\text{Cu}^{2+}$ , was studied from 25°C to 85°C with 1°C increments by measuring the light scattering at 465 nm on a Fluorolog-3 fluorescence spectrophotometer (Jobin Yvon, USA). Protein samples were equilibrated for 2 min at each temperature.

### 4.3 RESULTS AND DISCUSSION:

#### 4.3.1 Binding of $\text{Cu}^{2+}$ to $\alpha\text{A}$ - and G98R $\alpha\text{A}$ -crystallin:

We have investigated  $\text{Cu}^{2+}$ -binding to  $\alpha\text{A}$ -crystallins by fluorescence quenching as well as isothermal titration calorimetry. As reported in earlier  $\text{Cu}^{2+}$ -binding studies which have used fluorescence quenching (Jackson *et al.*, 2001) and isothermal titration calorimetry (Thompsett *et al.*, 2005), we have used  $\text{Cu}^{2+}$  along with glycine to avoid less- or non-specific interaction of  $\text{Cu}^{2+}$  and the formation of copper hydroxide.

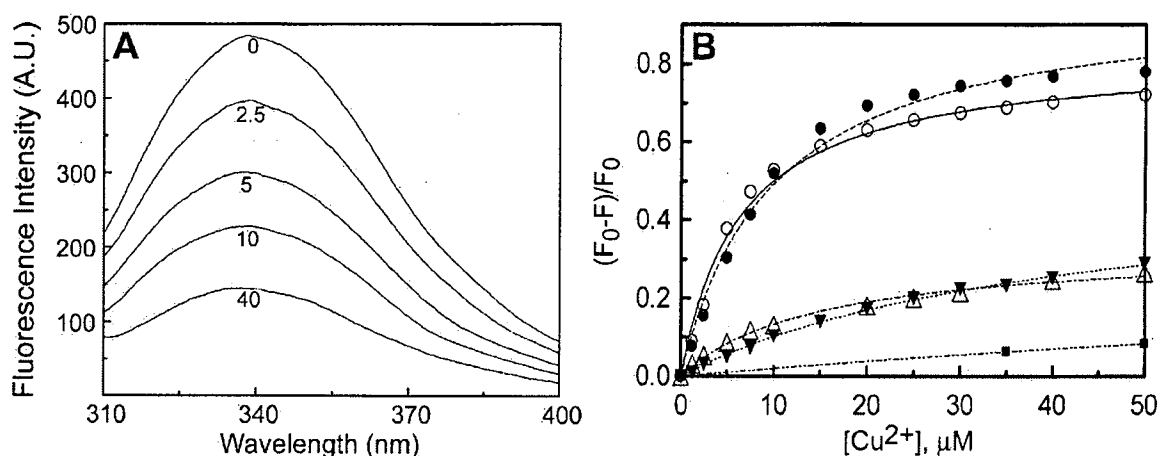
##### 4.3.1.1 Studies using fluorescence spectroscopy:

Titration of  $\alpha\text{A}$ -crystallin (in buffer A) with increasing concentrations of  $\text{Cu}^{2+}$  leads to quenching of its tryptophan fluorescence (Figure 1 A). We have also included controls to show the specific nature of fluorescence quenching of  $\alpha\text{A}$ -crystallin by the low concentration of  $\text{Cu}^{2+}$ . Neither thyroglobulin, a protein with molecular mass (669 kDa) comparable to that of  $\alpha\text{A}$ -crystallin, nor N-acetyl tryptophanamide (NATA) exhibits significant fluorescence quenching in the same concentration range of  $\text{Cu}^{2+}$  (Figure 1 B).  $\alpha$ -Synuclein, a known  $\text{Cu}^{2+}$ -binding protein (Rasia *et al.*, 2005), does not exhibit fluorescence quenching to a similar extent. We have earlier shown that addition of diamagnetic  $\text{Zn}^{2+}$  or  $\text{Zn}^{2+}$ -mimetic,



paramagnetic  $\text{Co}^{3+}$  does not lead to significant quenching of tryptophan fluorescence of the  $\alpha$ -crystallins. Further, lifetime measurements showed the predominant involvement of the static component in the observed tryptophan fluorescence quenching by  $\text{Cu}^{2+}$  (Ahmad *et al.*, 2008b). It is, therefore, evident that the observed fluorescence quenching of  $\alpha$ A-crystallin is due to specific  $\text{Cu}^{2+}$ -binding proximal to the tryptophan residues and not due to general collisional quenching of fluorescence by the paramagnetic  $\text{Cu}^{2+}$ .

In order to find out whether the observed conformational alteration upon G98R mutation could affect its  $\text{Cu}^{2+}$ -binding property, we have compared the extent of fluorescence quenching of  $\alpha$ A-crystallin and G98R $\alpha$ A-crystallin as a function of the concentration of  $\text{Cu}^{2+}$  (Figure 1 B). Both the proteins exhibit similar  $\text{Cu}^{2+}$ -binding properties. Analysis of these binding curves obtained from the fluorescence quenching data (described in experimental procedures), yielded apparent dissociation constants,  $K_{d,app}$ , of  $6.4 \times 10^{-6}$  M and  $9.8 \times 10^{-6}$  for  $\alpha$ A- and G98R $\alpha$ A-crystallin respectively.

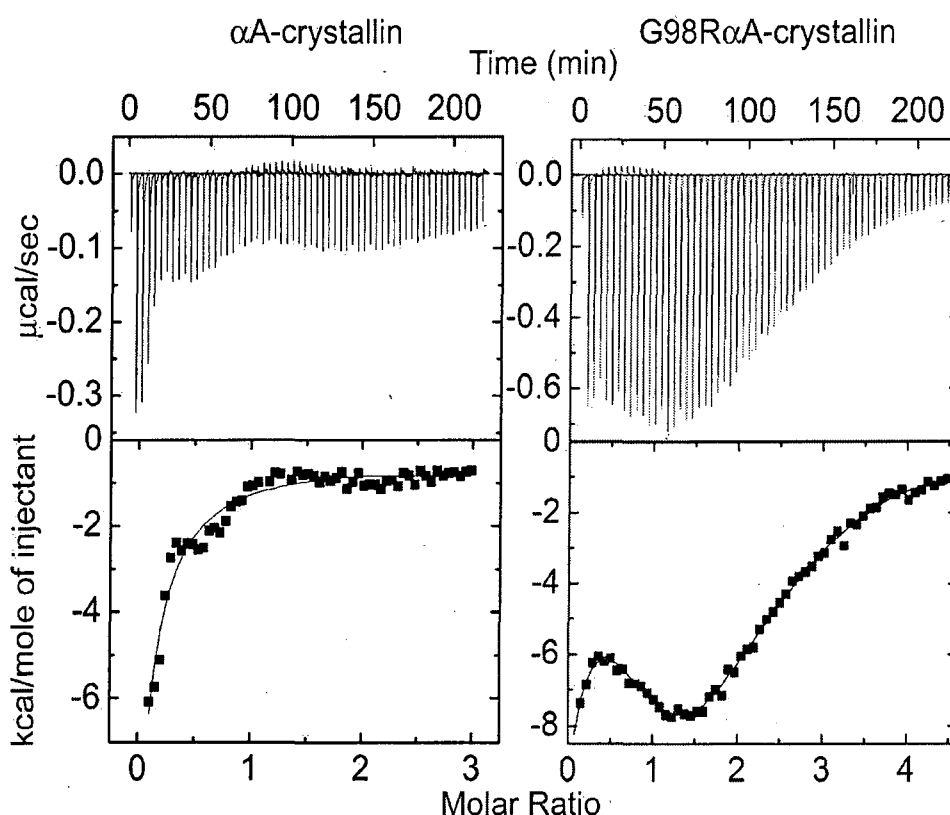


**Figure 1: Quenching of intrinsic fluorescence upon binding of  $\text{Cu}^{2+}$ .** (A) Intrinsic tryptophan fluorescence spectra of 0.1 mg/ml  $\alpha$ A-crystallin in buffer A at indicated concentrations (in  $\mu\text{M}$ ) of  $\text{Cu}^{2+}$ . (B) Extent of fluorescence quenching  $[(F_0-F)/F_0]$ , where  $F_0$  and  $F$  are the fluorescence intensities at 337 nm (300 nm in the case of  $\alpha$ -synuclein) in the absence and in the presence of  $\text{Cu}^{2+}$  respectively] of 0.1 mg/ml ( $\equiv 5 \mu\text{M}$  of subunits)  $\alpha$ A- ( $\circ$ ) and G98R $\alpha$ A-crystallin ( $\bullet$ ) with increasing concentration of  $\text{Cu}^{2+}$  at 25°C. 5  $\mu\text{M}$  NATA ( $\blacksquare$ ), 0.1 mg/ml of thyroglobulin ( $\triangle$ ) and  $\alpha$ -synuclein ( $\blacktriangledown$ ) are used as controls.

#### 4.3.1.2 Studies using isothermal titration calorimetry:

We have also studied  $\text{Cu}^{2+}$ -binding to  $\alpha$ A-crystallins by isothermal titration calorimetry (ITC). When  $\text{Cu}^{2+}$  (in buffer B with glycine) was injected into the reaction cell filled with buffer B alone, a relatively very small and constant exothermic heat change was

observed (data not shown). Figure 2 shows that a similar titration experiment with both the proteins resulted in large net exothermic heat changes exhibiting characteristic binding isotherms. The observed changes represent net enthalpic and entropic changes including contributions from  $\text{Cu}^{2+}$ -binding as well as the binding-induced secondary, tertiary and quaternary structural changes in  $\alpha\text{A}$ -crystallins (described later). The ITC profiles of  $\alpha\text{A}$ - and G98R $\alpha\text{A}$ -crystallin are significantly different from each other (Figure 2). The profile of enthalpic changes versus molar ratio of  $\text{Cu}^{2+}$  could be best fitted with the sequential mode of binding with three sets of binding sites for  $\alpha\text{A}$ -crystallin and five sets of binding sites for G98R $\alpha\text{A}$ -crystallin (parameters are given in the legend to Figure 2).



**Figure 2: ITC measurements of  $\text{Cu}^{2+}$ -binding to  $\alpha\text{A}$ - and G98R $\alpha\text{A}$ -crystallin.** Upper panel: isotherms of enthalpic changes in  $\alpha\text{A}$ - and G98R $\alpha\text{A}$ -crystallin upon  $\text{Cu}^{2+}$  binding. Lower panel: fitted curve indicating molar heat values as a function of the  $\text{Cu}^{2+}$  to protein molar ratio. Measurements were made at  $30^\circ\text{C}$ .  $\alpha\text{A}$ -crystallin: 3 sequential binding sites,  $K_1 = 4.25 (\pm 1.4) \times 10^4$ ;  $\Delta H_1 = -1.55 (\pm 0.31) \times 10^4$ ;  $\Delta S_1 = -30$ ;  $K_2 = 1.1 (\pm 0.48) \times 10^5$ ;  $\Delta H_2 = 2.04 (\pm 0.4) \times 10^4$ ;  $\Delta S_2 = 90.4$ ;  $K_3 = 1.25 (\pm 0.55) \times 10^5$ ;  $\Delta H_3 = -1.24 (\pm 0.26) \times 10^4$ ;  $\Delta S_3 = -17.6$ . G98R $\alpha\text{A}$ -crystallin: 5 sequential binding sites,  $K_1 = 4.98 (\pm 0.3) \times 10^5$ ;  $\Delta H_1 = -9740 \pm 326$ ;  $\Delta S_1 = -6.07$ ;  $K_2 = 3.22 (\pm 0.2) \times 10^5$ ;  $\Delta H_2 = 8853 (\pm 1480)$ ;  $\Delta S_2 = 54.4$ ;  $K_3 = 9.23 (\pm 0.62) \times 10^4$ ;  $\Delta H_3 = -1.0 (\pm 0.06) \times 10^5$ ;  $\Delta S_3 = -308$ ;  $K_4 = 7.58 (\pm 0.6) \times 10^4$ ;  $\Delta H_4 = 2.012 (\pm 0.13) \times 10^5$ ;  $\Delta S_4 = 686$ ;  $K_5 = 4.0 (\pm 0.3) \times 10^5$ ;  $\Delta H_5 = -1.337 (\pm 0.09) \times 10^5$ ;  $\Delta S_5 = -415$ .

The apparent differences in the number of sequential set of sites between  $\alpha A$ -crystallin and G98R $\alpha A$ -crystallin could be due to the differences in the Cu<sup>2+</sup>-induced structural changes between the wild type and the mutant protein. Thus, the observed sets of binding sites may represent only the apparent differences in the binding affinity. However, we observed that the overall dissociation constants,  $K_{d,app}$ , calculated from the association constants derived from ITC data for both  $\alpha A$ - and G98R $\alpha A$ -crystallin are comparable to those obtained by fluorescence quenching (variation is between 2-3 fold; Table 4.2), indicating that the binding constants obtained by these two methods are consistent. Since the observed  $K_{d,app}$  is the net result of competition between Cu<sup>2+</sup>-protein interaction and Cu<sup>2+</sup>-glycine interactions, the real dissociation constant,  $K_{d,real}$ , can be estimated from the above determined  $K_{d,app}$  using a correction involving the first dissociation constant for Cu(gly)<sub>2</sub> (Thompsett *et al.*, 2005). The values of  $K_{d,real}$  thus obtained for  $\alpha A$ -crystallins reveal close to picomolar affinity and are in good agreement with those obtained from fluorescence quenching studies (Table 4.2).

**Table 4.2:** Comparison of binding constants of Cu<sup>2+</sup>- $\alpha A$ -crystallins interactions, determined by fluorescence spectroscopy and isothermal titration calorimetry

Protein	$K_{d,app}$		$K_{d,real}$	
	Fluorescence	ITC	Fluorescence	ITC
$\alpha A$ -Crystallin	$6.4 \times 10^{-6}$	$12.0 \times 10^{-6}$	$16.6 \times 10^{-12}$	$31.2 \times 10^{-12}$
G98R $\alpha A$ -Crystallin	$9.8 \times 10^{-6}$	$4.7 \times 10^{-6}$	$25.5 \times 10^{-12}$	$12.2 \times 10^{-12}$

$K_{d,real}$  was estimated as product of  $K_{d,app}$  and the first dissociation constant ( $2.6 \times 10^{-6}$  M) of Cu(Gly)<sub>2</sub>.

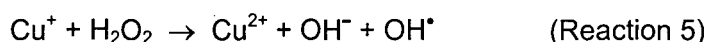
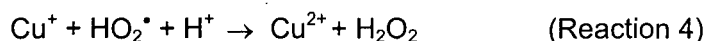
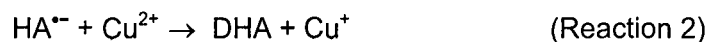
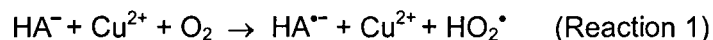
#### 4.3.2 Redox-silencing of Cu<sup>2+</sup> by $\alpha A$ - and G98R $\alpha A$ -crystallin:

Oxidative damage is an important cause of post-translational modifications in age-related cataracts (Garner and Spector, 1980; Srivastava *et al.*, 1980; Takemoto, 1996c; Harrington *et al.*, 2004; Truscott, 2005), and formation of metal ion-catalysed OH<sup>•</sup> in general, has been proposed to contribute to the modifications observed in cataract (Garland, 1990). Identification of hydroxylated amino acids in age-related cataractous lens proteins provides molecular evidence for implicating OH<sup>•</sup> as a cataractogenic species (Fu *et al.*, 1998). Moreover, human cataractous lens homogenates have the capacity to generate higher levels of OH<sup>•</sup> as compared to non-cataractous lenses (Garner *et al.*, 2000a). Since the lens homogenate blocks the Cu<sup>2+</sup>-mediated aqueous phase redox reactions (Ortwerth and James, 1999; Garner *et al.*, 2000b) and  $\alpha A$ -crystallin shows very high Cu<sup>2+</sup>-binding

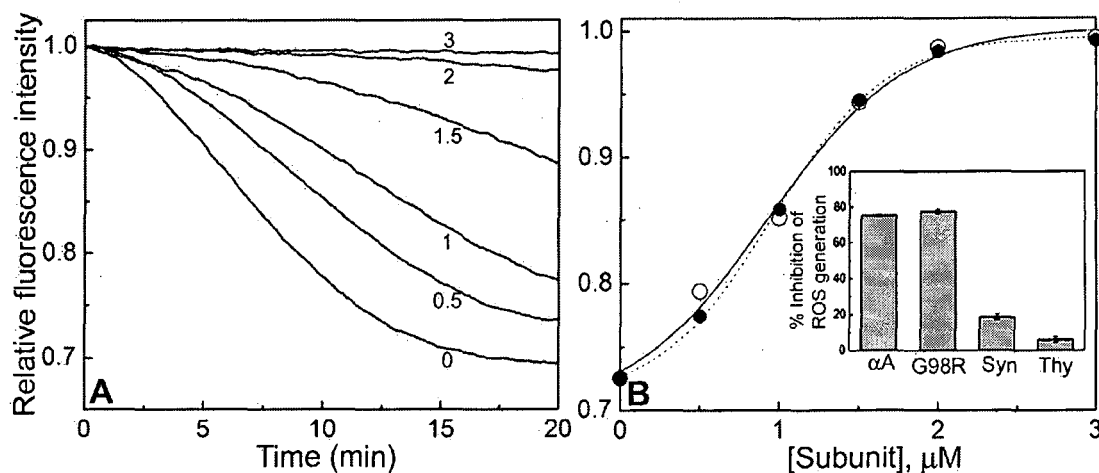
affinity, we tested whether  $\text{Cu}^{2+}$ -binding to  $\alpha\text{A}$ -crystallin has any effect on the redox activity of  $\text{Cu}^{2+}$  and if the G98R mutation in  $\alpha\text{A}$ -crystallin can affect  $\text{Cu}^{2+}$ -catalysed, ascorbate-mediated generation of ROS.

#### 4.3.2.1 Inhibition of ROS generation by $\alpha\text{A}$ -crystallins using fluorescein probe:

Generation of ROS through redox cycling of  $\text{Cu}^{2+}$  requires its reduction, which can be accomplished by biological components such as ascorbate, glutathione, dopamine and cholesterol.  $\text{Cu}^{2+}$ -catalyzes the oxidation of ascorbate ( $\text{HA}^-$ ) to dihydroascorbate (DHA) through the formation of  $\text{Cu}^{2+}$ -ascorbate complex, which binds  $\text{O}_2$ . In this complex  $\text{Cu}^{2+}$  mediates the electron transfer from ascorbate to  $\text{O}_2$  in a series of reactions that lead to concomitant production of ROS species. These reactions can be summarized as follows (Manevich *et al.*, 1997).



Generation of ROS can be monitored using the fluorescent dye, fluorescein, which becomes less- or non-fluorescent upon oxidation by ROS (Ou *et al.*, 2002). Generation of ROS as a function of time in the presence of ascorbate and  $\text{Cu}^{2+}$  is seen as decrease in the fluorescence intensity of fluorescein (Figure 3 A).  $\alpha\text{A}$ -crystallin as well as G98R $\alpha\text{A}$ -crystallin inhibits such decrease in the fluorescence in a concentration-dependent manner (Figure 3 A and B). The observed inhibitory effect is not due to non-specific effects of proteins, as thyroglobulin does not exhibit such inhibitory effect. Moreover,  $\alpha$ -synuclein, a protein known to bind  $\text{Cu}^{2+}$ , is not as effective as the  $\alpha\text{A}$ -crystallins and did not inhibit the decrease in fluorescence intensity of fluorescein as effectively as  $\alpha\text{A}$ - or G98R $\alpha\text{A}$ -crystallin (Figure 3 B, inset).

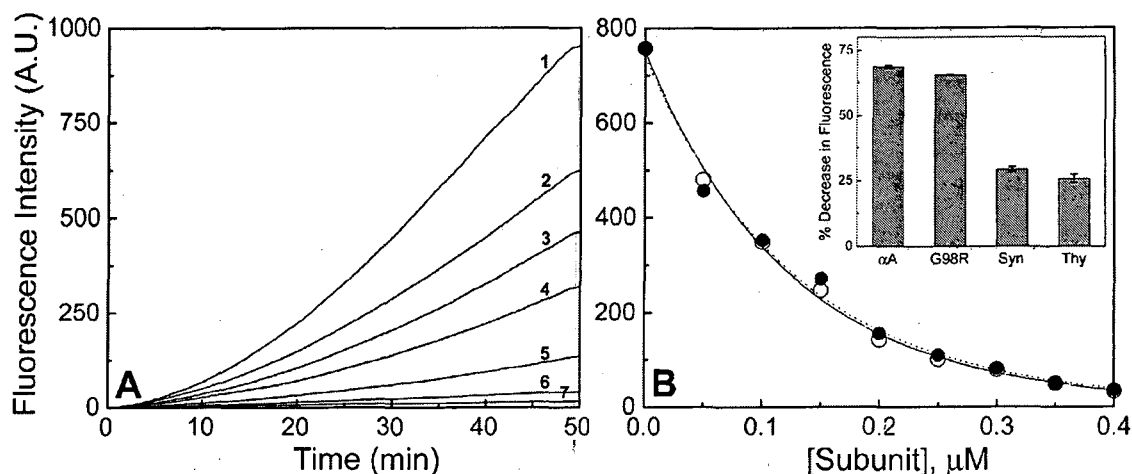


**Figure 3: Redox-silencing of  $\text{Cu}^{2+}$  by  $\alpha$ A- and G98R $\alpha$ A-crystallin.** (A) Fluorescence decay curve of fluorescein upon incubation with 300  $\mu$ M ascorbate and 10  $\mu$ M  $\text{Cu}^{2+}$  in the absence and in the presence of indicated concentrations ( $\mu$ M) of  $\alpha$ A-crystallin. (B) Relative intensity of fluorescein as a function of concentration of  $\alpha$ A- ( $\circ$ ) and G98R $\alpha$ A-crystallin ( $\bullet$ ); Inset shows the % inhibition of ROS generation in the presence of 30  $\mu$ g/ml  $\alpha$ -crystallins ( $\cong$  1.5  $\mu$ M of subunits),  $\alpha$ -synuclein (Syn) ( $\cong$  2.08  $\mu$ M) and thyroglobulin (Thy). Error bars for four experiments are shown.

#### 4.3.2.2 Studies on inhibition of $\text{OH}^\bullet$ generation by $\alpha$ A- and G98R $\alpha$ A-crystallin using another fluorescent probe, 3-CCA:

We have also investigated the generation of the  $\text{OH}^\bullet$ , using another probe, coumarin-3-carboxylic acid (3-CCA). The compound becomes hydroxylated by the radical yielding the fluorescent derivative, 7-hydroxy-3-coumarin carboxylic acid. Because of the non-fluorescent nature of 3-CCA and its high hydroxylation rate constant, the fluorescent detection of 7-OH-CCA enables real-time measurements of the kinetics of  $\text{OH}^\bullet$  generation (Manevich *et al.*, 1997).

Upon incubation of  $\text{Cu}^{2+}$  with ascorbate in the absence of  $\alpha$ A-crystallin, the fluorescence of the solution increases almost linearly with time, indicating the production of  $\text{OH}^\bullet$  (Figure 4 A, curve 1). However, the same experiment performed with increasing concentration of  $\alpha$ A- and G98R $\alpha$ A-crystallin showed that both the proteins inhibited the increase in fluorescence intensity very effectively (Figure 4 A and B). On the other hand, neither thyroglobulin nor  $\alpha$ -synuclein was so effective (Figure 4 B inset). Moreover, Figure 4 B clearly shows that  $\alpha$ A- and G98R $\alpha$ A-crystallin do not differ significantly in their ability to inhibit the increase in the fluorescence.



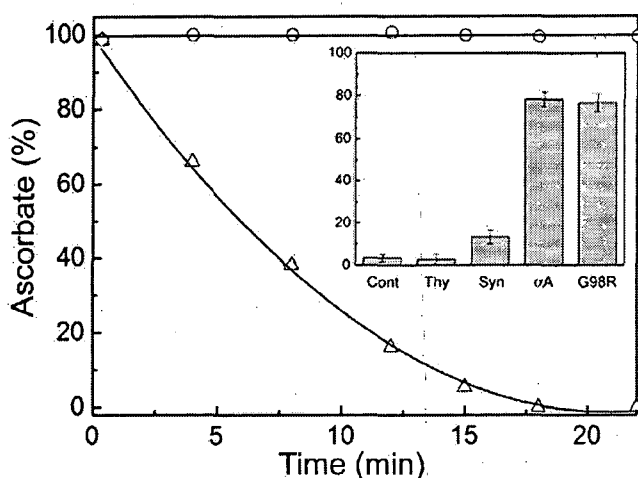
**Figure 4: Inhibition of OH<sup>•</sup> by αA- and G98RαA-Crystallin.** (A) Cu<sup>2+</sup>-ascorbate-mediated OH<sup>•</sup> generation was monitored by fluorescence detection of 7-OH-CCA, formed by the reaction of 3-CCA with OH<sup>•</sup>, in the absence (curve 1) and in the presence of 0.05, 0.1, 0.15, 0.25 and 0.4 μM αA-crystallin (curves 2-6). Curve 7 shows fluorescence in absence of protein and Cu<sup>2+</sup>. (B) Decrease in fluorescence intensity after 2500 sec as a function of concentration of αA- (○) and G98RαA-crystallin (●). Inset shows the % decrease in fluorescence in the presence of 3 μg/ml αA- or G98RαA-crystallin, α-synuclein (Syn) and thyroglobulin (Thy). Error bar for four experiments are also shown.

#### 4.3.2.3 αA- and G98RαA-crystallin prevents Cu<sup>2+</sup>-induced oxidation of ascorbate:

The observed inhibition of the decrease in fluorescence of fluorescein (Figure 3 B) and inhibition of the increase in fluorescence of 3-CCA (Figure 4 B) in the presence of αA-crystallins could be due to (i) prevention of generation of ROS/OH<sup>•</sup> by Cu<sup>2+</sup>/ascorbate system or (ii) scavenging of the generated ROS/OH<sup>•</sup>. Since generation of ROS requires oxidation of ascorbate to dehydroascorbate, we studied Cu<sup>2+</sup>-induced oxidation of ascorbate in the absence and in the presence of αA- and G98RαA-crystallin by measuring residual ascorbate as a function of time using a redox dye (2,6 dichlorophenol indophenol).

Figure 5 shows that αA- and G98RαA-crystallin actually inhibit the oxidation of ascorbate quite effectively. On the other hand, α-synuclein and thyroglobulin are far less effective in preventing oxidation of ascorbate and ROS generation compared to α-crystallins. This result clearly shows that both αA- and G98RαA-crystallin prevent the oxidation of ascorbate and hence prevent the generation of ROS (redox-silencing property).

Equimolar concentration of EDTA does not significantly prevent Cu<sup>2+</sup>-induced oxidation of ascorbate (data not shown). It appears that chelation of Cu<sup>2+</sup> alone is not sufficient for a potent redox-silencing property. Sequestration of Cu<sup>2+</sup> to restrict its



**Figure 5:  $\alpha$ A-crystallin prevents  $\text{Cu}^{2+}$ -induced oxidation of ascorbate.** Ascorbate ( $300 \mu\text{M}$ ) was treated with  $5 \mu\text{M}$   $\text{Cu}^{2+}$  in the absence ( $\Delta$ ) and in the presence ( $\circ$ ) of  $\alpha$ A-crystallin and the residual ascorbate at different time points was estimated using DCI. Inset shows the % residual ascorbate, 15 min after treating ascorbate ( $300 \mu\text{M}$ ) with  $\text{Cu}^{2+}$  ( $5 \mu\text{M}$ ) in the absence (Cont) and in the presence of  $25 \mu\text{g/ml}$  of  $\alpha$ A-, G98R $\alpha$ A-crystallin,  $\alpha$ -synuclein (Syn) and thyroglobulin (Thy). Error bars for four independent experiments are shown.

accessibility to ascorbate determined by structural features and complex stability, may contribute to the observed redox-silencing property of  $\alpha$ A-crystallins.

Recently, we have shown that not only  $\alpha$ A-crystallin but also  $\alpha$ B-crystallin and its phosphorylation mimic, 3D $\alpha$ B-crystallin, bind  $\text{Cu}^{2+}$  selectively and silence its oxidative nature, inhibiting the generation of ROS and thereby conferring cyto-protection (Ahmad *et al.*, 2008b). This is the first demonstration of the redox-silencing of  $\text{Cu}^{2+}$  by any heat shock protein. Considering the earlier report that  $\text{Cu}^{2+}$  increases the expression of  $\alpha$ A- and  $\alpha$ B-crystallin in lens epithelial cells (Hawse *et al.*, 2003) as well as our present results of  $\alpha$ A-crystallin binding  $\text{Cu}^{2+}$  and preventing generation of ROS, it appears that the function of  $\alpha$ A-crystallin in the eye lens, besides its chaperone-like activity, includes preventing or moderating  $\text{Cu}^{2+}$ -induced oxidative stress. The G98R mutation seems to have no detrimental effect on such redox-silencing property of  $\alpha$ A-crystallin as both wild type  $\alpha$ A-crystallin and mutant G98R $\alpha$ A-crystallin exhibit comparable ability in preventing generation of ROS. However, it is possible that post-translational modifications in G98R $\alpha$ A-crystallin with age can alter the redox availability of previously chelated  $\text{Cu}^{2+}$ .

#### 4.3.3 $\text{Cu}^{2+}$ -induced self-aggregation of $\alpha$ A- and G98R $\alpha$ A-crystallin and their mixed oligomer:

When we performed the  $\text{Cu}^{2+}$ -binding experiment, we observed that the G98R $\alpha$ A-crystallin sample ( $0.1 \text{ mg/ml}$ ; buffer A) becomes turbid above the concentration range of  $\text{Cu}^{2+}$  showed in Figure 1 B (i.e.  $>50 \mu\text{M}$ ). On the other hand, the  $\alpha$ A-crystallin sample does not exhibit significant aggregation in this concentration range (but starts aggregating above



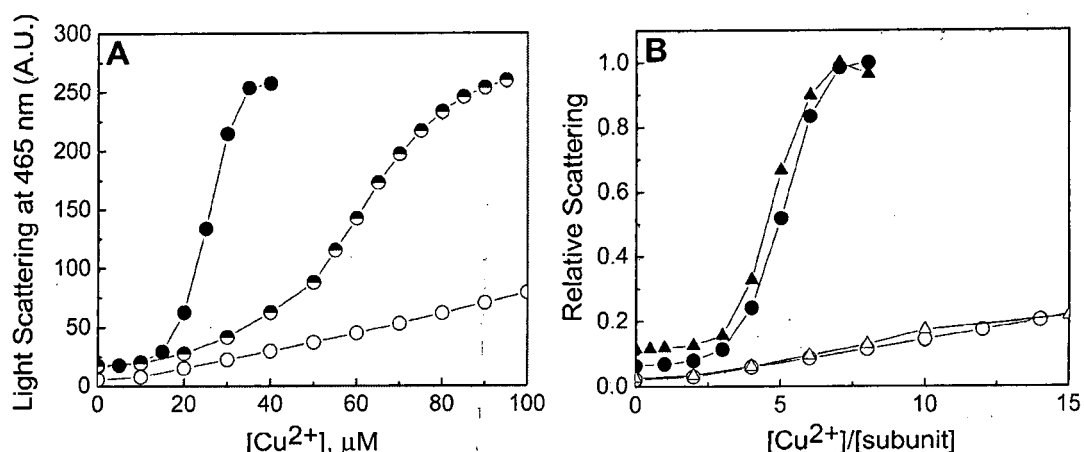
200  $\mu\text{M}$   $\text{Cu}^{2+}$ ). The effect of  $\text{Cu}^{2+}$ -induced self-aggregation of G98R $\alpha$ A-crystallin was found to be more pronounced in buffer B. In order to investigate the relative self-aggregation propensities of wild type  $\alpha$ A-crystallin, the mutant protein and their mixed oligomer and its reversibility, we have used HEPES buffer system in further experiments. The study of self-aggregation and its reversibility is relevant and important for the understanding of the cataract formation in the mutation-affected individuals.

#### **4.3.3.1 G98R $\alpha$ A-crystallin exhibits increased propensity to $\text{Cu}^{2+}$ -induced self-aggregation:**

Figure 6 shows the relative differences in the self-aggregation of  $\alpha$ A- and G98R $\alpha$ A-crystallin as a function of  $\text{Cu}^{2+}$  concentration in buffer B as monitored by light scattering at 37°C. The light scattering of the sample of  $\alpha$ A-crystallin (0.1 mg/ml  $\equiv$  5  $\mu\text{M}$  subunits) increases very gradually as a function of  $\text{Cu}^{2+}$  concentration (Figure 6 A). On the contrary, the light scattering of the sample of G98R $\alpha$ A-crystallin steeply increases above 18  $\mu\text{M}$   $\text{Cu}^{2+}$ . It is, therefore, evident that G98R $\alpha$ A-crystallin exhibits increased propensity for self-aggregation upon binding to  $\text{Cu}^{2+}$ .

As mentioned earlier, we also found that tendency of G98R $\alpha$ A-crystallin to self-aggregate is higher in HEPES buffer compared to the phosphate buffer. Lowering the temperature of the assay to 25°C did not affect the self-aggregation of either of the proteins and their light scattering profiles overlapped with those at 37°C (data not shown).

It is important to note that the light scattering profile of G98R $\alpha$ A-crystallin (Figure 6 A) is sigmoid in nature: at  $\text{Cu}^{2+}$  concentration below  $\sim 18$   $\mu\text{M}$ , the changes in the light scattering are relatively negligible, while above this concentration light scattering increases sharply and saturates at around 40  $\mu\text{M}$ . In order to understand whether the ratio of  $\text{Cu}^{2+}$  to G98R $\alpha$ A-crystallin is important for its self-aggregation propensity, we have performed similar experiment with four times higher concentration (0.4 mg/ml  $\equiv$  20  $\mu\text{M}$  subunits) of G98R $\alpha$ A-crystallin. Figure 6 B shows that the light scattering profiles, as a function of  $[\text{Cu}^{2+}]/[\text{subunit}]$ , of  $\alpha$ A-crystallin or G98R $\alpha$ A-crystallin at two different protein concentrations almost overlap, indicating that the ratio of  $\text{Cu}^{2+}$  to protein (3:1) is critical for the self-aggregation of G98R $\alpha$ A-crystallin.



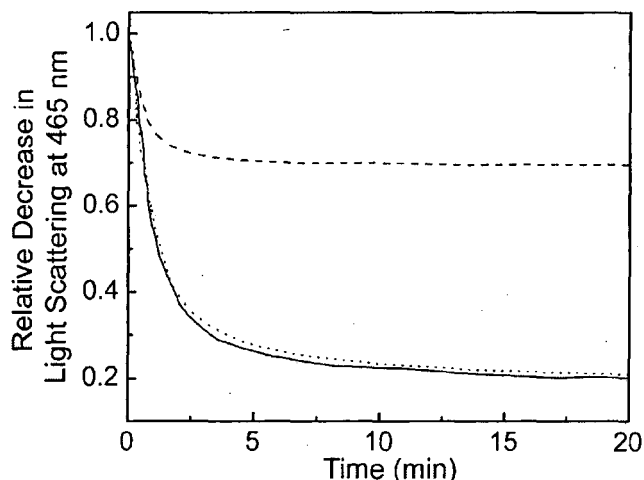
**Figure 6: Cu<sup>2+</sup>-induced aggregation of αA, G98RαA-crystallin and their mixed oligomer.** (A) Aggregation of 0.1 mg/ml (≅ 5 μM) of αA (○), G98RαA (●) and their mixed oligomer (◐) as a function of increasing Cu<sup>2+</sup> equivalents at 37°C in buffer B was monitored by light scattering at 465 nm. (B) Relative scattering of either 0.1 mg/ml (≅ 5 μM) of αA (○) and G98RαA (●) or 0.4 mg/ml (≅ 20 μM) of αA (Δ) and G98RαA (▲) in buffer B in the presence of increasing concentrations of Cu<sup>2+</sup> is plotted against increasing Cu<sup>2+</sup> to subunit (M/M) ratios.

#### 4.3.3.2 Effect of mixed-oligomer formation on the self-aggregation:

Our earlier study showed that αA-crystallin and G98RαA-crystallin undergo subunit exchange to form mixed oligomers, which differ in structural stability and chaperone ability from their respective homo-oligomers (Singh *et al.*, 2007b). We studied the effect of mixed-oligomer formation on the self-aggregation propensity upon Cu<sup>2+</sup>-binding by treating the mixed oligomers (at 1:1 ratio of αA- and G98RαA-crystallin) with increasing concentrations of Cu<sup>2+</sup> (Figure 6 A). The results indicate that (i) mixed oligomer formation leads to significant decrease in the Cu<sup>2+</sup>-induced self-aggregation propensity of G98RαA-crystallin as the light scattering of the mixed oligomer is significantly less at 40 μM Cu<sup>2+</sup> under the condition where G98RαA-crystallin exhibits pronounced light scattering and (ii) at higher concentrations of Cu<sup>2+</sup> (above 40 μM) the mixed oligomer exhibits substantial self-aggregation leading to large increase in light scattering. In other words, mixed oligomer formation leads to a shift in the critical concentration of Cu<sup>2+</sup> from 18 μM (G98RαA-crystallin alone) to about 40 μM, above which the self-aggregation is more pronounced. Nevertheless, it is evident from the results that the mixed oligomers exhibit much higher self-aggregation propensity upon binding Cu<sup>2+</sup> compared to αA-crystallin.

### 4.3.3.3 Reversibility of the $\text{Cu}^{2+}$ -binding and induced aggregation of $\alpha\text{A}$ -, G98R $\alpha\text{A}$ -crystallin and their mixed oligomers:

We have investigated whether the observed  $\text{Cu}^{2+}$ -induced changes are reversible and if wild type  $\alpha\text{A}$ -crystallin, the mutant protein and their mixed oligomers differ in the reversibility of aggregation. Though,  $\alpha\text{A}$ -crystallin exhibits relatively much less propensity for  $\text{Cu}^{2+}$ -induced self-aggregation, treating the sample with high concentrations of  $\text{Cu}^{2+}$  (e.g., 90  $\mu\text{M}$ ) leads to some increase in light scattering (Figure 6 A). We tested the reversibility of such increase in light scattering by treating the sample with 0.2 mM EDTA (Figure 7). Light scattering decreased significantly (>80%), indicating that  $\text{Cu}^{2+}$ -induced self-aggregation of  $\alpha\text{A}$ -crystallin (though relatively much less) is reversible to a large extent. On the other hand, the pronounced aggregation exhibited by G98R $\alpha\text{A}$ -crystallin (even at 30  $\mu\text{M}$   $\text{Cu}^{2+}$ ) is only partially reversible (about 30%) upon treating with the metal ion chelator, EDTA (Figure 7). Mixed oligomers exhibit pronounced self-aggregation upon treating with 90  $\mu\text{M}$   $\text{Cu}^{2+}$  (Figure 6 A). Interestingly, unlike the mutant protein, such  $\text{Cu}^{2+}$ -induced aggregation of the mixed oligomers is found to be reversible (Figure 7) to a large extent (comparable to that of the wild type protein).



**Figure 7: Reversibility of  $\text{Cu}^{2+}$ -induced aggregation of  $\alpha\text{A}$ -, G98R $\alpha\text{A}$ -crystallin and their mixed oligomer.** A solution containing 0.1 mg/ml ( $\approx 5 \mu\text{M}$ ) of  $\alpha\text{A}$  or G98R $\alpha\text{A}$  or their mixed oligomer in buffer B was incubated for 30 min at 37°C with 90, 30 and 90  $\mu\text{M}$  of  $\text{Cu}^{2+}$  respectively.  $\text{Cu}^{2+}$ -induced aggregation was monitored by relative decrease in light scattering of this solution after addition of EDTA (200  $\mu\text{M}$ ).  $\alpha\text{A}$ -crystallin (solid line), G98R $\alpha\text{A}$ -crystallin (dashed line) and their mixed oligomer (dotted line).

We then investigated whether  $\text{Cu}^{2+}$ -induced change in tryptophan fluorescence of these proteins exhibits reversibility. When we treated the  $\text{Cu}^{2+}$ -bound  $\alpha\text{A}$ -, G98R $\alpha\text{A}$ -crystallin and their mixed oligomers with 0.2 mM EDTA, about 89%, 73% and 73% respectively of the observed fluorescence quenching was recovered (data not shown).

Thus, our self-aggregation studies show that G98R $\alpha\text{A}$ -crystallin has markedly increased aggregation propensity upon  $\text{Cu}^{2+}$ -binding and the protein-bound  $\text{Cu}^{2+}$  could be

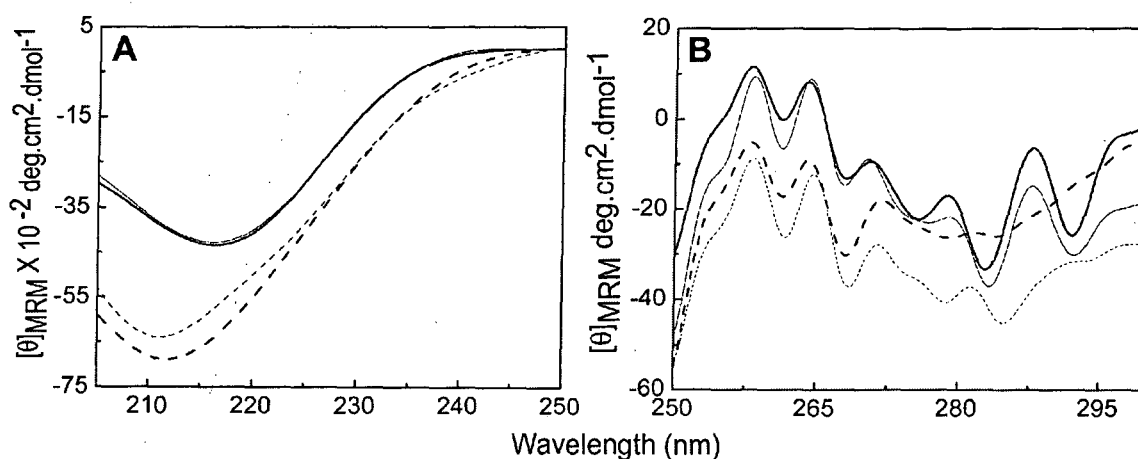
dislodged by the metal ion chelators (albeit require more than stoichiometric concentrations) to a great extent. Increased tendency to self-aggregate can be detrimental to the transparency of the eye lens.

#### 4.3.4 Cu<sup>2+</sup>-induced conformational changes in $\alpha$ A- and G98R $\alpha$ A-crystallin:

As mentioned earlier, G98R $\alpha$ A-crystallin undergoes pronounced self-aggregation above a 3:1 (M/M) ratio of Cu<sup>2+</sup> to the protein. At this critical ratio, Cu<sup>2+</sup>-binding is close to saturation as monitored by fluorescence quenching (inferred from Figure 1 B). In order to investigate conformational changes of  $\alpha$ A- and G98R $\alpha$ A-crystallin, if any, upon binding to Cu<sup>2+</sup>, we performed circular dichroism and dynamic light scattering experiments, at this critical ratio of 3:1 of Cu<sup>2+</sup> to protein.

##### 4.3.4.1 Cu<sup>2+</sup>-induced secondary and tertiary structural changes:

The far-UV CD spectrum of  $\alpha$ A-crystallin does not significantly change upon binding to Cu<sup>2+</sup> and almost overlaps with that of the Cu<sup>2+</sup>-free form of  $\alpha$ A-crystallin, whereas the far-UV CD spectrum of Cu<sup>2+</sup>-bound G98R $\alpha$ A-crystallin exhibits slightly decreased ellipticity compared to that of the Cu<sup>2+</sup>-free protein (Figure 8 A). It indicates that at a 3:1 ratio of Cu<sup>2+</sup> to protein, Cu<sup>2+</sup> can induce secondary structural alterations in G98R $\alpha$ A-crystallin but not in  $\alpha$ A-crystallin. Interestingly, the far-UV CD spectrum of  $\alpha$ A-crystallin shows significant shift in the ellipticity minimum from 218 nm (Cu<sup>2+</sup>-free form) to 212 nm upon Cu<sup>2+</sup>-binding at a much



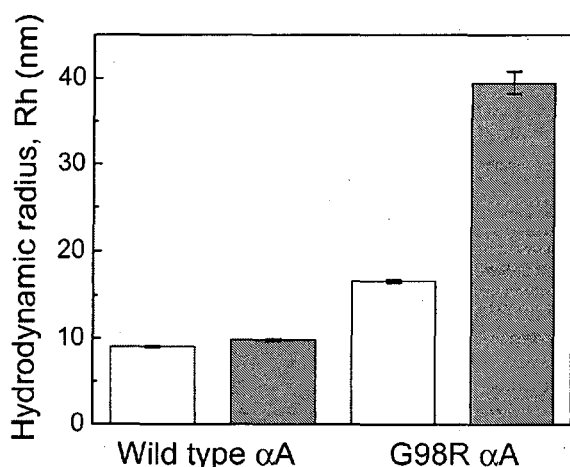
**Figure 8: Cu<sup>2+</sup>-induced structural changes of  $\alpha$ A- and G98R $\alpha$ A-crystallin.** Comparison of far-UV (A) and near-UV (B) CD spectra of 1 mg/ml ( $\approx$  50  $\mu$ M) of  $\alpha$ A- (solid line) and G98R $\alpha$ A-crystallin (dashed line) in the absence (thick) and in the presence (thin) of 150  $\mu$ M Cu<sup>2+</sup> in buffer B.  $[\theta]_{\text{MRRM}}$ , mean residue mass ellipticity.

higher  $\text{Cu}^{2+}$  to protein ratio (10:1), indicating some degree of unfolding (Ahmad *et al.*, 2008b).

Figure 8 B shows the near-UV CD spectra of the wild type and the mutant  $\alpha\text{A}$ -crystallin in the presence and the absence of  $\text{Cu}^{2+}$ . There are subtle differences in the 270-295 nm region (where tryptophan/tyrosine residues contribute to the chirality) of the near-UV CD spectra of the  $\text{Cu}^{2+}$ -bound and free forms of  $\alpha\text{A}$ -crystallin. On the other hand, the near-UV CD spectrum of the  $\text{Cu}^{2+}$ -bound G98R $\alpha\text{A}$ -crystallin differs significantly from that of the protein in the absence of  $\text{Cu}^{2+}$  and shows a dramatic decrease in the chirality between 270-300 nm. Thus, these results indicate that G98R $\alpha\text{A}$ -crystallin is more susceptible to  $\text{Cu}^{2+}$ -induced tertiary structural changes compared to  $\alpha\text{A}$ -crystallin.

#### 4.3.4.2 $\text{Cu}^{2+}$ -induced quaternary structural changes:

We have studied the quaternary structure using DLS (Figure 9). Wild type  $\alpha\text{A}$ -crystallin exhibits mean hydrodynamic radius,  $R_h$ , of approximately 9 nm which increases to 9.8 nm when treated with  $\text{Cu}^{2+}$ . Compared to the wild type protein, G98R $\alpha\text{A}$ -crystallin exhibits a significantly higher  $R_h$  (16.5 nm), which further increases dramatically to approximately 40 nm upon treating with  $\text{Cu}^{2+}$ .



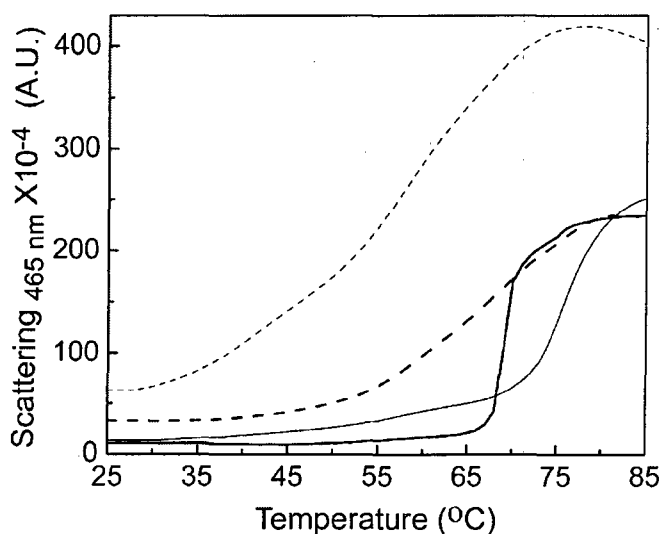
**Figure 9:  $\text{Cu}^{2+}$ -induced quaternary structural changes of  $\alpha\text{A}$ - and G98R $\alpha\text{A}$ -crystallin.** Changes in the mean hydrodynamic radii ( $R_h$ ) of 0.5 mg/ml ( $\equiv 25 \mu\text{M}$ )  $\alpha\text{A}$ - and G98R $\alpha\text{A}$ -crystallin in the absence (open bars) and in the presence of  $75 \mu\text{M}$  of  $\text{Cu}^{2+}$  (filled bars) were determined by dynamic light scattering; pronounced increase in hydrodynamic radius is observed in the case of G98R $\alpha\text{A}$ -crystallin. Error bars for ten experimental data are shown.

Thus, circular dichroism and DLS studies show that the structural changes (particularly in tertiary and quaternary structure) induced by  $\text{Cu}^{2+}$  are more pronounced in the case of G98R $\alpha\text{A}$ -crystallin compared to those in  $\alpha\text{A}$ -crystallin. Formation of such larger aggregates of G98R $\alpha\text{A}$ -crystallin in the presence of  $\text{Cu}^{2+}$  could lead to the clouding of the eye lens.

### 4.3.5 Effect of $\text{Cu}^{2+}$ -binding on thermostability of $\alpha\text{A}$ - and G98R $\alpha\text{A}$ -crystallin:

Having found that  $\text{Cu}^{2+}$ -binding leads to significant changes in the structure of G98R $\alpha\text{A}$ -crystallin, we have investigated whether  $\text{Cu}^{2+}$ -bound and free forms of  $\alpha\text{A}$ - and G98R $\alpha\text{A}$ -crystallin exhibit any differences in their stability. As mentioned earlier, addition of  $\text{Cu}^{2+}$  leads to the fluorescence quenching of both  $\alpha\text{A}$ - and G98R $\alpha\text{A}$ -crystallin. Thus, we have studied the thermostability by monitoring the aggregation of  $\alpha\text{A}$ -crystallins as a function of temperature using light scattering.

Figure 10 shows that  $\alpha\text{A}$ -crystallin exhibits a sharp (cooperative) transition in light scattering around  $67^\circ\text{C}$ . In the presence of  $\text{Cu}^{2+}$  (at the molar ratio of  $\text{Cu}^{2+}$  to protein of 3:1), the light scattering profile of  $\alpha\text{A}$ -crystallin exhibits a gradual increase till about  $68^\circ\text{C}$  and exhibits a sharp transition with an inflection point around  $74^\circ\text{C}$ , indicating that  $\text{Cu}^{2+}$ -binding stabilizes  $\alpha\text{A}$ -crystallin against heat-induced self-aggregation. As mentioned earlier, the light scattering profile of G98R $\alpha\text{A}$ -crystallin increases above  $45^\circ\text{C}$  in a less-cooperative manner (Figure 10). Interestingly, the light scattering profile of the  $\text{Cu}^{2+}$ -bound G98R $\alpha\text{A}$ -crystallin that shows high light scattering to start with possibly due to increase in hydrodynamic radius, exhibits a transition at a much lower temperature ( $35^\circ\text{C}$ ) than the  $\text{Cu}^{2+}$ -free form of G98R $\alpha\text{A}$ -crystallin ( $45^\circ\text{C}$ ).



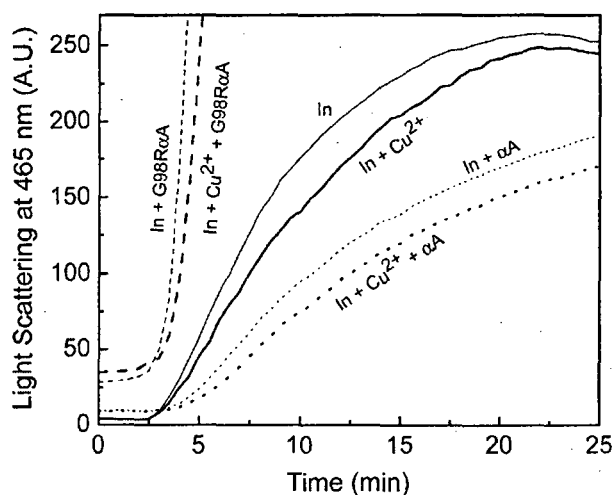
**Figure 10: Thermal stability of wild type and G98R $\alpha\text{A}$ -crystallin.**

Aggregation of  $0.2 \text{ mg/ml}$  ( $\approx 10 \mu\text{M}$ ) of wild type  $\alpha\text{A}$ -crystallin (thick solid line) and the mutant  $\alpha\text{A}$ -crystallin (thick dashed line) in buffer B was monitored by light scattering at  $465 \text{ nm}$  as a function of temperature. Wild type  $\alpha\text{A}$ -crystallin in the presence of  $30 \mu\text{M}$   $\text{Cu}^{2+}$  showed increased stability (thin line) as compared to G98R  $\alpha\text{A}$ -crystallin (thin dashed line).

Thus, our results show that  $\text{Cu}^{2+}$ -binding has a distinct effect on the thermal stability of  $\alpha\text{A}$ - and G98R $\alpha\text{A}$ -crystallin.  $\text{Cu}^{2+}$ -binding stabilizes  $\alpha\text{A}$ -crystallin whereas it further destabilizes G98R $\alpha\text{A}$ -crystallin against heat-induced aggregation.

#### 4.3.6 Effect of $\text{Cu}^{2+}$ on the chaperone-like activity of wild type $\alpha\text{A}$ -crystallin and the mutant G98R $\alpha\text{A}$ -crystallin:

Ganadu *et al.* (2004) have reported that  $\text{Cu}^{2+}$  (at a concentration of 0.1 and 1 mM) enhanced the chaperone-like activity of  $\alpha\text{B}$ -crystallin towards DTT-induced aggregation of insulin. A similar observation was made for  $\alpha\text{A}$ -crystallin (Biswas and Das, 2008). We have investigated the effect of  $\text{Cu}^{2+}$  (at 3:1  $\text{Cu}^{2+}$  to protein ratio) on the chaperone-like activity of  $\alpha\text{A}$ - and G98R $\alpha\text{A}$ -crystallin towards the DTT-induced aggregation of insulin (Figure 11). However, we found that  $\text{Cu}^{2+}$  at this particular concentration ( $15\mu\text{M}$ ) does not significantly increase the chaperone-like activity of  $\alpha\text{A}$ -crystallin. Figure 11 also shows that the light scattering profile in the case of G98R $\alpha\text{A}$ -crystallin does not change significantly in the presence of  $\text{Cu}^{2+}$  indicating that the lack of chaperone-like activity of the mutant protein towards the aggregation of insulin is not significantly changed on its binding to  $\text{Cu}^{2+}$ .



**Figure 11: Chaperone-like activity of  $\alpha\text{A}$ -crystallin and its mutant with and without  $\text{Cu}^{2+}$  using insulin as substrate.** Difference in the chaperone-like activity of the mutant protein with respect to the wild type protein towards DTT-induced aggregation of insulin (0.2 mg/ml) at  $37^\circ\text{C}$  was assayed in the absence and in the presence of  $\text{Cu}^{2+}$ . Aggregation of insulin in the absence (In) or in the presence of 0.1 mg/ml wild type (In+ $\alpha\text{A}$ ) or the mutant (In+G98R $\alpha\text{A}$ )  $\alpha\text{A}$ -crystallin. A similar experiment was performed in the presence of  $15\mu\text{M}$   $\text{Cu}^{2+}$ .

We have also investigated the effect of  $\text{Cu}^{2+}$ -binding on the chaperone activity of both wild type and the mutant protein using heat-induced aggregation (at  $43^\circ\text{C}$ ) of another target protein citrate synthase (CS). The concentration of  $\alpha\text{A}$ -crystallin ( $1\mu\text{M}$ ) was selected such that it prevents the aggregation of CS only partially and hence changes in chaperone activity upon  $\text{Cu}^{2+}$ -binding can be evaluated. G98R $\alpha\text{A}$ -crystallin prevents the aggregation of CS better than  $\alpha\text{A}$ -crystallin at the same concentration (Figure 12 A): the percentage protection is approximately 82% and 18% for G98R $\alpha\text{A}$ - and  $\alpha\text{A}$ -crystallin respectively.

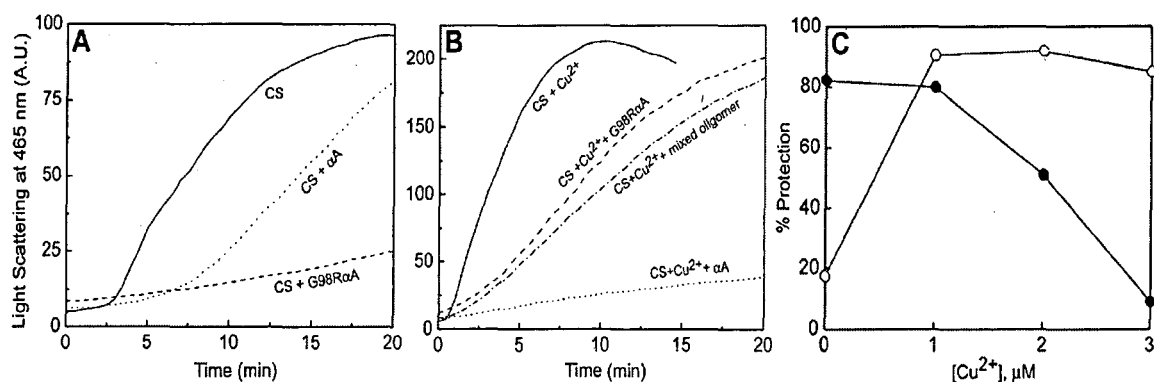
Addition of  $\text{Cu}^{2+}$  promotes the aggregation of CS (compare Figure 12 A and B). The mechanism of action of  $\alpha$ -crystallin would have two components: (i) preferential binding of



$\text{Cu}^{2+}$  which prevents its adverse effect on CS, and (ii) the effect of  $\text{Cu}^{2+}$ -binding on the intrinsic chaperone ability of  $\alpha\text{A}$ -crystallins. If the first mechanism alone is responsible, one would expect light scattering profiles in the presence of the  $\alpha\text{A}$ -crystallins with or without  $\text{Cu}^{2+}$  to overlap. The light scattering profiles of  $\alpha\text{A}$ - and G98R $\alpha\text{A}$ -crystallin with and without  $\text{Cu}^{2+}$  do not overlap (compare Figure 12 A and B). Interestingly, the light scattering profile of  $\alpha\text{A}$ -crystallin in the presence of  $\text{Cu}^{2+}$  is much lower compared to those in the absence of  $\text{Cu}^{2+}$  (Figure 12 A and B). The percentage protection increases from 18% in the absence of  $\text{Cu}^{2+}$  to ~90% in the presence of  $\text{Cu}^{2+}$  (Figure 12 C). This result clearly shows that  $\text{Cu}^{2+}$ -binding significantly increases the intrinsic chaperone ability of  $\alpha\text{A}$ -crystallin.

On the other hand, comparison of light scattering profiles of G98R $\alpha\text{A}$ -crystallin in the absence (Figure 12 A) and in the presence (Figure 12 B) of  $\text{Cu}^{2+}$  (at 3:1 ratio where self-aggregation of G98R $\alpha\text{A}$ -crystallin is not significant; Figure 6) clearly shows that  $\text{Cu}^{2+}$ -binding drastically decreases the chaperone ability of G98R $\alpha\text{A}$ -crystallin. The percentage protection decreases from ~82% in the absence of  $\text{Cu}^{2+}$  to below 10% at 3  $\mu\text{M}$   $\text{Cu}^{2+}$  (Figure 12 C). Despite the greatly enhanced chaperone activity of  $\alpha\text{A}$ -crystallin in the presence of  $\text{Cu}^{2+}$ , mixed oligomers having equimolar concentration of  $\alpha\text{A}$ - and G98R $\alpha\text{A}$ -crystallin show significantly decreased protection upon  $\text{Cu}^{2+}$ -binding (Figure 12 B), possibly due to the alteration of structure upon formation of mixed oligomers.

Thus, our results show that  $\text{Cu}^{2+}$ -binding has profound and opposite influence on the chaperone-like activity of  $\alpha\text{A}$ - and G98R $\alpha\text{A}$ -crystallin towards aggregation of CS at 43°C.



**Figure 12: Effect of  $\text{Cu}^{2+}$  on the chaperone-like activity of  $\alpha\text{A}$ -crystallins using CS as target protein.** (A) Aggregation of 25  $\mu\text{g}/\text{ml}$  CS at was monitored by light scattering at 465 nm in the absence (solid line) and in the presence of 20  $\mu\text{g}/\text{ml}$  ( $\approx 1 \mu\text{M}$ ) of either wild type (dotted line) or mutant protein (dashed line). (B) Aggregation of CS in the presence of 3  $\mu\text{M}$   $\text{Cu}^{2+}$ : CS alone (solid line), in the presence of wild type  $\alpha\text{A}$  (dotted line), G98R $\alpha\text{A}$  (dashed line) and their mixed oligomer (dash dot dash line). (C) % protection of CS aggregation in presence of 1  $\mu\text{M}$   $\alpha\text{A}$ -crystallin ( $\circ$ ) and G98R $\alpha\text{A}$ -crystallin ( $\bullet$ ) as a function of  $\text{Cu}^{2+}$  concentration.

$\text{Cu}^{2+}$ -binding significantly increases the intrinsic chaperone ability of  $\alpha\text{A}$ -crystallin, whereas it decreases that of G98R $\alpha\text{A}$ -crystallin. Earlier, we have also shown that hetero-oligomers of  $\alpha\text{A}$ - and  $\alpha\text{B}$ -crystallin (at 3:1 ratio as present in the eye lens) but not  $\alpha\text{B}$ -crystallin, exhibit increased chaperone-like activity in the presence of  $\text{Cu}^{2+}$  towards CS aggregation (Ahmad *et al.*, 2008b). In the presence of  $\text{Cu}^{2+}$ , G98R $\alpha\text{A}$ -crystallin not only shows higher extent of aggregation but also dominates the properties of mixed oligomers and alleviates the enhancement in chaperone-like activity of  $\alpha\text{A}$ -crystallin. Therefore, increased accumulation of  $\text{Cu}^{2+}$  in lens with age can lead to increased self-aggregation and decrease in chaperone-like activity of G98R $\alpha\text{A}$ -crystallin and its mixed oligomer with wild type  $\alpha\text{A}$ -crystallin, which in turn can compromise the transparency of the eye lens.

#### 4.3.7 Effect of $\text{Zn}^{2+}$ , $\text{Cd}^{2+}$ and $\text{Ca}^{2+}$ on self-aggregation and chaperone-like activity of $\alpha\text{A}$ - and G98R $\alpha\text{A}$ -crystallin:

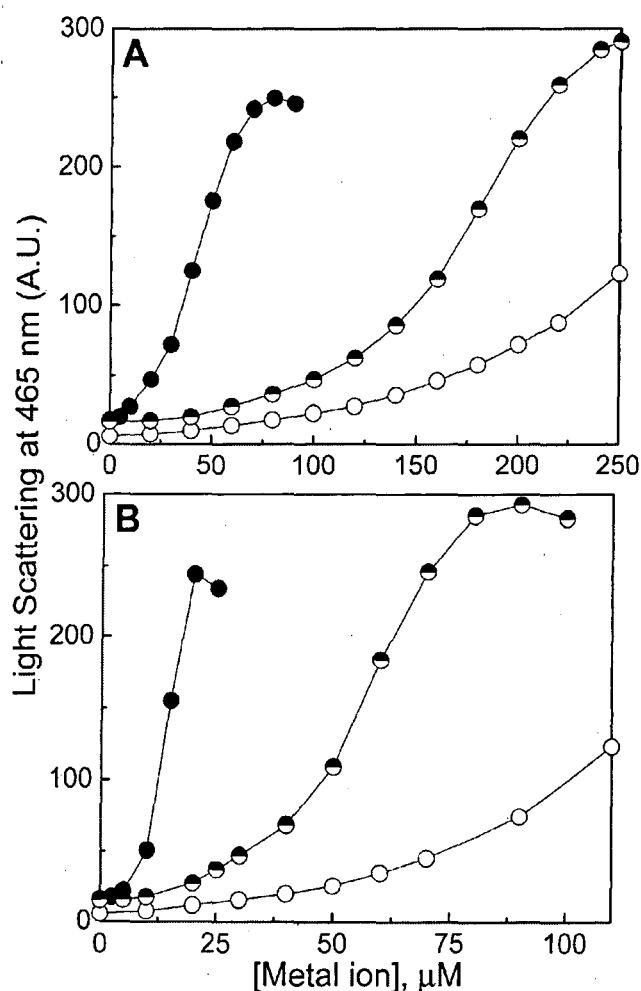
Besides  $\text{Cu}^{2+}$ , elevated levels of  $\text{Zn}^{2+}$ ,  $\text{Cd}^{2+}$  and  $\text{Ca}^{2+}$  have been reported in cataractous lenses (Stanojević-Paović *et al.*, 1987; Rácz and Erdöhelyi, 1988; Srivastava *et al.*, 1992; Rasi *et al.*, 1992; Cekic, 1998). Cigarette smoking has been shown to significantly increase accumulation of lenticular  $\text{Cd}^{2+}$  as well as  $\text{Cu}^{2+}$  (Cekic, 1998). Deposition of these ions can be a potential threat to the structure and function of  $\alpha$ -crystallin and can result in loss of optical properties of eye lens. We have studied the effect of these metal ions on the self-aggregation propensity and chaperone-like activity of the wild type and mutant  $\alpha\text{A}$ -crystallin.

Figure 13 A shows the effect of  $\text{Cd}^{2+}$  on self-aggregation of  $\alpha\text{A}$ -crystallins.  $\alpha\text{A}$ -crystallin shows gradual increase in light scattering with increasing concentration of  $\text{Cd}^{2+}$  and shows significant aggregation only at very high concentrations of  $\text{Cd}^{2+}$  (above 150  $\mu\text{M}$ ). On the other hand, G98R $\alpha\text{A}$ -crystallin starts aggregating at very low concentration of  $\text{Cd}^{2+}$  (above 10  $\mu\text{M}$ ;  $\text{Cd}^{2+}$  to protein molar ratio above 2:1), indicating that the mutant protein is highly prone to  $\text{Cd}^{2+}$ -induced aggregation. In the case of the mixed oligomer, though the light scattering, and hence the self-aggregation, is relatively low at lower concentration of  $\text{Cd}^{2+}$  compared to G98R $\alpha\text{A}$ -crystallin, it eventually aggregates to a similar extent as observed in the case of the mutant protein alone (Figure 13 A).  $\text{Zn}^{2+}$  also has a similar effect on the self-aggregation properties of  $\alpha\text{A}$ -, G98R $\alpha\text{A}$ -crystallin and their mixed oligomer (Figure 13 B): G98R $\alpha\text{A}$ -crystallin and the mixed oligomers exhibit more propensity to  $\text{Zn}^{2+}$ -induced aggregation than the wild type protein. We have found that light scattering of the

samples of  $\alpha$ A- or G98R $\alpha$ A-crystallin or their mixed oligomers do not show significant increase upon treating with  $\text{Ca}^{2+}$  even at concentration as high as 5 mM (data not shown).

In order to investigate the effect of  $\text{Cd}^{2+}$  and  $\text{Zn}^{2+}$  on the chaperone-like activity of these proteins, we have selected the metal ion to protein ratio of 2:1 (M/M) where they do not exhibit significant aggregation (Figure 13). In the absence of metal ions, at the selected target protein to chaperone ratio,  $\alpha$ A-crystallin prevents the aggregation of CS to the extent of about 18% (calculated from light scattering shown in Figure 12 A). In the presence of  $\text{Cd}^{2+}$  or  $\text{Zn}^{2+}$  (Figure 14 A and B),  $\alpha$ A-crystallin prevents the CS aggregation more efficiently. The percentage protection (calculated from the light scattering data shown in Figure 14) is increased from 18% in the absence of metal ions to 88% and 69% in the presence of  $\text{Cd}^{2+}$  or  $\text{Zn}^{2+}$  respectively.

Figure 14 shows that the effect of  $\text{Cd}^{2+}$  and  $\text{Zn}^{2+}$  on the chaperone-like activity of G98R $\alpha$ A-crystallin is opposite to that observed for the wild type protein. These metal ions decrease the chaperone-like activity of G98R $\alpha$ A-crystallin towards the aggregation of CS. The percentage protection decreases from 82% in the absence of the metal ions (calculated from the light scattering data shown in Figure 12 A) to 53% and 27% in the presence of  $\text{Cd}^{2+}$  and  $\text{Zn}^{2+}$  respectively. We have also found that  $\text{Ca}^{2+}$  [even at the metal ion to protein ratio of 500:1 (M/M)] does not have significant



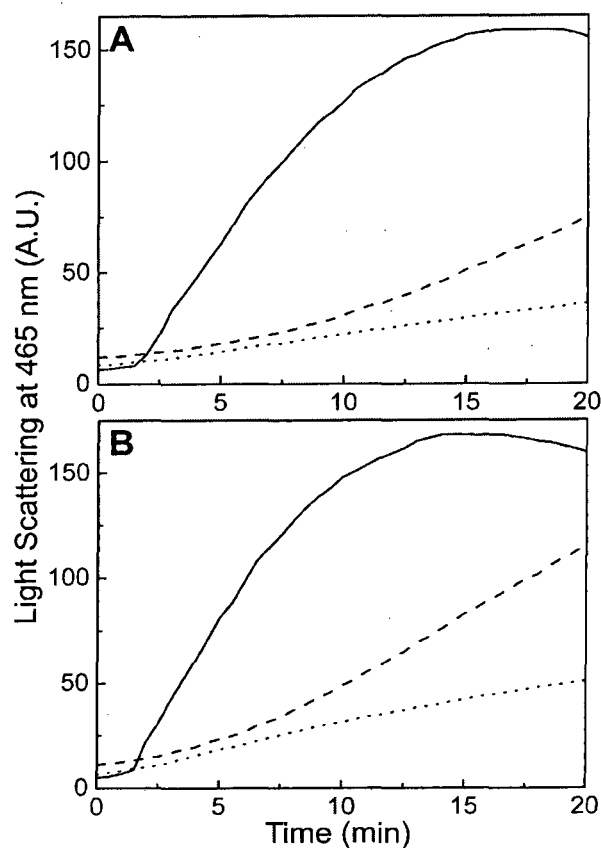
**Figure 13:** Effect of  $\text{Cd}^{2+}$  and  $\text{Zn}^{2+}$  on the aggregation of  $\alpha$ A-, G98R $\alpha$ A-crystallin and their mixed oligomer. Aggregation of wild type  $\alpha$ A-crystallin ( $\circ$ ), mutant  $\alpha$ A-crystallin ( $\bullet$ ) and their mixed oligomer ( $\ominus$ ) in buffer B, at 37°C, was monitored by light scattering at 465 nm with increasing concentrations of  $\text{Cd}^{2+}$  (A) and  $\text{Zn}^{2+}$  (B).

influence on the chaperone-like activity of both the wild type and mutant protein towards the aggregation of CS (data not shown).

In an earlier study, Ganadu *et al.* (2004) showed that  $Zn^{2+}$  significantly increases whereas  $Ca^{2+}$  decreases the chaperone-like activity of  $\alpha B$ -crystallin using insulin as target protein. Similarly, Biswas and Das (2008) reported that chaperone-like activity of  $\alpha A$ - and  $\alpha B$ -crystallin towards  $\beta$ -mercaptoethanol-induced aggregation of insulin is increased as a function of  $Zn^{2+}$  concentration; however,  $Cd^{2+}$  and  $Ca^{2+}$  (at a concentration of 1 mM) slightly decreased their activity. Our present study demonstrates that heavy metal ions such as  $Cu^{2+}$ ,  $Cd^{2+}$  and  $Zn^{2+}$  decrease the chaperone-like activity of G98R $\alpha A$ -crystallin, while they increase the chaperone-like activity of  $\alpha A$ -crystallin towards the aggregation of CS.

#### 4.4 CONCLUSIONS:

Our investigations on the role of heavy metal ions such as  $Cu^{2+}$ ,  $Cd^{2+}$ ,  $Zn^{2+}$  and  $Ca^{2+}$  as potential risk factors in presenile cataractogenesis show that G98R $\alpha A$ -crystallin exhibits affinity for  $Cu^{2+}$  close to picomolar, like wild type  $\alpha A$ -crystallin. Like  $\alpha A$ -crystallin, G98R $\alpha A$ -crystallin exhibits redox-silencing of  $Cu^{2+}$  and inhibits ROS generation. Thus, mutation-induced conformational change does not significantly affect the  $Cu^{2+}$ -binding and redox-silencing properties of  $\alpha A$ -crystallin. However, G98R $\alpha A$ -crystallin differs substantially from the wild type protein in its  $Cu^{2+}$ -induced structural changes, chaperone activity and



**Figure 14: Differences in the chaperone activity of  $\alpha A$ - and G98R $\alpha A$ -crystallin towards heat-induced CS aggregation in the presence of  $Cd^{2+}$  and  $Zn^{2+}$ .** Effect of 2  $\mu M$   $Cd^{2+}$  (A) and  $Zn^{2+}$  (B) on the thermal aggregation of 25  $\mu g/ml$  CS was investigated in the absence (solid line) and in the presence of 20  $\mu g/ml$  ( $\equiv$  1  $\mu M$ ) of either wild type (dotted line) or mutant protein (dashed line). Aggregation was monitored by light scattering at 465 nm.

propensity to self-aggregate. At the critical ratio 3:1(M/M) of  $\text{Cu}^{2+}$  to G98R $\alpha$ A-crystallin (which is close to saturation of  $\text{Cu}^{2+}$ -binding),  $\text{Cu}^{2+}$ -binding causes altered tertiary and quaternary structure (significant increase in the hydrodynamic radius) and adverse effect on its chaperone activity. On the other hand,  $\text{Cu}^{2+}$ -binding enhances the chaperone ability of  $\alpha$ A-crystallin. Above this critical ratio,  $\text{Cu}^{2+}$  promotes self-aggregation of G98R $\alpha$ A-crystallin. Similarly,  $\text{Zn}^{2+}$  and  $\text{Cd}^{2+}$ , but not  $\text{Ca}^{2+}$ , promote self-aggregation of G98R $\alpha$ A-crystallin and have adverse effect on its chaperone-like activity.

Thus, heavy metal ions such as  $\text{Cu}^{2+}$ ,  $\text{Cd}^{2+}$  and  $\text{Zn}^{2+}$  augment the G98R mutational effects in  $\alpha$ A-crystallin such as alteration of structure and aggregation, which are important in the phenotypic manifestation of clouding of the eye lens. Besides environmental factors, life style can also contribute to risk factors. For example, cigarette smoking has been proposed to be a risk factor for cataractogenesis. Smoking is shown to significantly increase accumulation of lenticular  $\text{Cd}^{2+}$  as well as  $\text{Cu}^{2+}$  (Cekic, 1998). Increased susceptibility of the mutant G98R $\alpha$ A-crystallin and its mixed oligomers with wild type  $\alpha$ A-crystallin towards these environmental factors may underlie molecular basis of presenile cataract formation. It may be noted that although  $\text{Ca}^{2+}$  does not induce self-aggregation or change in chaperone-like activity of G98R $\alpha$ A-crystallin, it may play a part in cataract formation by virtue of its activation of calpains (Baruch *et al.*, 2001).

It is interesting to note that (i)  $\alpha$ A-crystallin is predominantly present in the cortical region of the lens (Grey and Schey, 2008), (ii) a gradient of  $\text{Cu}^{2+}$  exists in the lens with the highest concentration being in the cortical region (Srivastava *et al.*, 1992) and (iii) the G98R mutation leads to the ring-like opacity at the age of 16 years before it is blown into the total cataract (Santhiya *et al.*, 2006). It is tempting to speculate that these three independently observed events may have some link. In addition, age-related post-translational modifications, which appear to occur over the first 20-25 years of age (Dilley and Harding, 1975; Takemoto, 1995b; Takemoto, 1996a; Takemoto, 1998; Lampi *et al.*, 1998), could augment the mutational effects as in the case of metal ions observed in the present study.

Thus, our study suggests that changes in environment or life style may have significant impact on the onset and disease progression of these genetically predisposed cataract patients through alteration of protein structure and its properties. In addition, our study provides an example of how environmental factors can augment phenotype(s) in certain genetically predisposed conditions and can influence the manifestation of mutant phenotype(s).

A  
DISEASE-CAUSING  
MUTATION IN  
CLASS I sHSP,  
HSP22

5

## 5.1 INTRODUCTION:

Mammalian sHsps are classified into two classes based on their tissue expression, stress inducibility and *in vivo* oligomerization characteristics. Hsp27,  $\alpha$ B-crystallin, Hsp20 and Hsp22 are classified into class I and show expression in a wide variety of tissues. MKBP, HspB3,  $\alpha$ A-crystallin, cvHsp, HspB9 and ODF1 are categorized into class II and their expression is primarily restricted to ocular (Ile) or myogenic (IIm) or testicular (IIt) tissues. Chapters 2-4 describe our investigations with  $\alpha$ A-crystallin, a class II sHsp. Class I members are predominantly heat-inducible and therefore, play a major role in cell survival under stress conditions. This chapter describes our investigations with HspB8, a recently discovered class I sHsp.

Parallel studies from different laboratories in different contexts led to the identification of HspB8 by different names such as H11 kinase, E2IG1, Hsp20-like protein and Hsp22. HspB8 - before being identified as a sHsp - was described as a  $Mn^{2+}$ -dependent serine-threonine protein kinase (H11) from melanoma cells, which is similar to the protein kinase domain of the large subunit of herpes simplex virus type 2 ribonucleotide reductase, ICP10 (Smith *et al.*, 2000). In another study, H11 was identified as a novel protein in basal keratinocytes that associates with plasma membrane and appears to be required for the keratinocyte growth in culture (Aurelian *et al.*, 2001). Furthermore, upon treatment of MCF-7 (breast cancer cell line) with  $17\beta$ -estradiol (E2), a novel estradiol-inducible gene 1 (E2IG1) was identified (Charpentier *et al.*, 2000). E2IG1 expression was seen only in estrogen receptor (ER) positive MCF-7 cells. Bany and Schultz (2001) made similar observations using artificially induced decidualization (stimulating with progesterone after ovariectomy) in mouse. They found that the expression of an Hsp20-like protein increased during the decidualization process in the uterine tissues, endometrium and myometrium. The sequences of E2IG1 and Hsp20-like protein were later found to be identical to that of HspB8. In a yeast two-hybrid screen, using a phosphorylation-mimicking 3D mutant of Hsp27 as bait and human heart cDNA library as prey, a novel protein was identified as an interacting partner of Hsp27 (Benndorf *et al.*, 2001). The newly identified protein was classified as a sHsp as it shared sequence similarity with other mammalian sHsps in the  $\alpha$ -crystallin domain and was named as Hsp22, as its estimated molecular weight is ~21.6 kDa. Thus, Hsp22 was identified in different contexts and named differently. For the sake of clarity, the protein has been referred to as Hsp22 throughout this chapter.



Human Hsp22 gene was mapped to chromosome 12 using fluorescent *in situ* hybridization technique (Yu *et al.*, 2001). Studies from our laboratory identified a putative HSF1 binding site upstream of its translation start site. Subsequent studies from our and other laboratories has shown that Hsp22 exhibits heat-induced increased expression in cell-type dependent manner (Gober *et al.*, 2003; Chowdary *et al.*, 2004), thus making it third such member of the mammalian sHsp family. Hsp22 is expressed abundantly in human heart, brain, placenta, bladder, skeletal and smooth muscles, and moderately expressed in cervix, prostate, lung, kidney, rectum and colon (Benndorf *et al.*, 2001; Gober *et al.*, 2003). High expression of Hsp22 was also reported in the spinal cord, especially in motor and sensory neurons (Irobi *et al.*, 2004). Using immunoblotting of different pig tissues, Hsp22 was shown to be widely expressed with highest amount detected in stomach, heart, cerebellum, cortex and muscles (Verschuure *et al.*, 2003). Recently, high expression of Hsp22 was reported in rheumatoid arthritis synovial tissue, where Toll-like receptors (TLRs) are also abundantly expressed. It was shown that like  $\alpha$ -crystallin, Hsp22 can also act as an endogenous TLR ligand and lead to the TLR4-dependent dendritic cell activation, thereby, playing a role during the inflammatory process in rheumatoid arthritis (Roelofs *et al.*, 2006).

Smith *et al.* (2000) identified Hsp22 as a homologue of a viral kinase; it was shown to possess certain conserved catalytic motifs characteristic of protein kinases, mutation of which ablated its kinase activity. Moreover, Hsp22 was also shown to have autokinase activity (Smith *et al.*, 2000; Chowdary *et al.*, 2004; Kim *et al.*, 2004) and W51C mutation in the protein increased this activity (Gober *et al.*, 2003). Immunoprecipitated Hsp22 from hearts of transgenic mice was able to phosphorylate an exogenous protein substrate, myelin basic protein (Depre *et al.*, 2002) but purified protein failed to phosphorylate  $\alpha$ -casein or histone H1S (Kim *et al.*, 2004). In another study using rat cardiomyocytes, Hase *et al.* (2005) have shown that Hsp22 is a dual function kinase – it induces hypertrophy at low doses through a kinase-independent activation of Akt, whereas it is proapoptotic at higher doses through protein kinase-dependent mechanisms (inhibition of casein kinase 2). However, the kinase activity of Hsp22, its sequence identity with other kinases and associated functions have been debated (Kim *et al.*, 2004; Gober *et al.*, 2004; Shemetov *et al.*, 2008a).

Through its  $\alpha$ -crystallin domain, Hsp22 was shown to bind Sam68. Sam68 is a RNA-binding protein that associates with c-Src kinase during mitosis, and is absolutely required for HIV-1 production. Overexpression of Hsp22 significantly inhibits Sam68-mediated rev

response element (RRE) as well as constitutive transport element (CTE)-dependent gene expression and thus, can play a role in the post-transcriptional regulation of gene expression (Badri *et al.*, 2006). *In vitro* kinase assays showed that Hsp22 is phosphorylated by protein kinase C (at S14 and T63), p44 MAPK (Erk1) (at S27 and T87) and casein kinase 2, but not by MAPKAPK-2 (Benndorf *et al.*, 2001). Recently, it has been shown that the phosphorylation of Hsp22 (S57) by cAMP-dependent protein kinase *in vitro* affects its structure and decreases chaperone-like activity (Shemetov *et al.*, 2008b).

Hsp22 expression is increased significantly in ischemic myocardium (Depre *et al.*, 2004). Its overexpression induces hypertrophy and exerts a cardioprotective effect through activation of the Akt pathway, a major signaling pathway of cell growth and survival (Depre *et al.*, 2002; Depre *et al.*, 2006). Since cardiac hypertrophy generally results from an adaptation in the rates of protein synthesis and degradation, Hsp22-mediated cardiac hypertrophy partly results from an increased expression, activity, and a subcellular redistribution of the proteasome. Inhibition of the proteasome reverses Hsp22-induced cardiac hypertrophy and also blocks the stimulation of protein synthesis (Hedhli *et al.*, 2008). The protective effect of Hsp22 in heart can also be partly accounted for by its binding and activation of phosphoglucomutase, which leads to the stimulation of synthesis of glycogen, an essential fuel for the stressed heart in conditions of overload and ischemia (Wang *et al.*, 2004). Therefore, Hsp22 represents an integrative sensor in the cardiac adaptation to stress by coordinating cell growth, survival, protein turnover and metabolism.

Members of sHsp family are believed to have anti-apoptotic activity. However, Hsp22 can trigger or block apoptosis in a cell type- (Perkins *et al.*, 2002) or expression-dependent manner (Gober *et al.*, 2003). Along with certain other genes, Hsp22 expression increased in invasive lesions, which induced anchorage independence, increased cell proliferation and protection of breast cancer cells from apoptosis (Yang *et al.*, 2006). Hsp22 is overexpressed in estrogen receptor (ER)-positive breast cancer cells (Charpentier *et al.*, 2000) where cyclin D1 is also overexpressed. Cyclin D1 can regulate Hsp22 levels in a ligand-independent and steroid coactivator-dependent manner (Yang *et al.*, 2006). Recently, Hsp22 was identified as CDK-independent cyclin D1 target, which can mediate cyclin D1's enhancement of radiation sensitivity in breast tumor cells – overexpressed Hsp22 markedly increased radiation sensitivity, whereas its loss blocked the enhancement (Trent *et al.*, 2007). In certain tumor tissues and cell lines (melanoma, sarcoma, colon and prostate cancer) levels of Hsp22 were reduced. Treatment of these cell lines by demethylating agents or transient

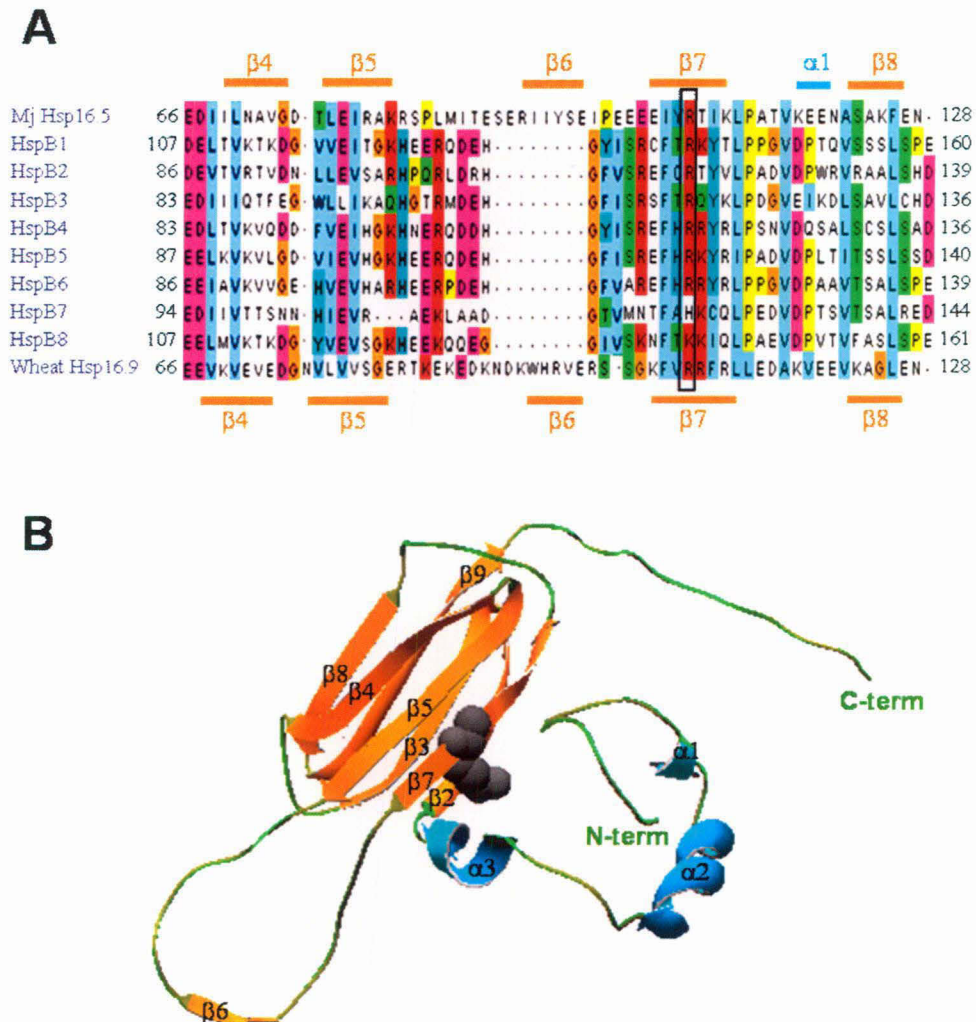
transfection with Hsp22 resulted in caspase- and p38MAPK-dependent apoptosis (Gober *et al.*, 2003). However, heat-shock induced Hsp22 overexpression did not trigger apoptosis in HEK293 cells indicating cell type-specific apoptotic activity. Further, W51C mutation in Hsp22 blocked Hsp22-induced apoptosis in co-transfected cells through activation of ERK survival pathway (Gober *et al.*, 2003). Thus, the effect of Hsp22 on apoptosis is very complex.

Despite several reports of sHsp expression in brain tissues, its role in neuronal cells is still enigmatic. Hsp22 is known to be associated with classic senile plaques in Alzheimer's (Benn *et al.*, 2002). Recently, Hsp22 was also detected in cerebral amyloid angiopathy, a major pathogenic lesion in hereditary cerebral hemorrhage with amyloidosis of the Dutch type (HCHWA-D); it completely prevented the cerebrovascular cell-death induced by A $\beta$ <sub>1-40</sub> peptide of the Dutch type (Wilhelmus *et al.*, 2006). Further, Hsp22 showed a higher binding affinity for A $\beta$ <sub>1-40</sub> peptide of the Dutch type compared to wild type A $\beta$ <sub>1-42</sub> and was more effective in reducing  $\beta$ -sheet formation by A $\beta$ <sub>1-40</sub> peptide of the Dutch type than by A $\beta$ <sub>1-42</sub> (Wilhelmus *et al.*, 2006). In a microarray study, Hsp22 was shown to be induced in primary cortical neuronal cells specifically upon proteasome inhibition by lactacystin. Overexpression of Hsp22 protected against proteasome inhibitor-mediated loss of cell viability by up to 25%, indicating its potentially neuroprotective role (Yew *et al.*, 2005).

However, Hsp22 was directly implicated in neurodegenerative diseases with the identification of the K141N and K141E point mutations in the putative  $\beta$ 7 strand of Hsp22. K141N mutation (in a Belgian and a Czech family) or K141E (in a Bulgarian and an English family) correlate with the development of distal hereditary motor neuropathy (dHMN) type II (Irobi *et al.*, 2004). In subsequent genetic analysis studies in Chinese families, K141N mutation of Hsp22 was also found to be associated with Charcot-Marie-Tooth (CMT) disease type 2L (Tang *et al.*, 2005b). Similarly, several mutations in Hsp27, including that of R140 (which is homologous to the K141 residue in Hsp22), resulting in these disease conditions have been identified (Table 1.4). Moreover, mutation of corresponding residue in  $\alpha$ A-crystallin (R116C/H) causes congenital cataract and that in  $\alpha$ B-crystallin (R120G) causes congenital cataract and desmin related myopathy (Table 1.4). Ectopic expression of mutant Hsp22 in Cos cells, human embryonic kidney cells (HEK293T) and human neuronal cells (SHSY5Y) promoted the formation of cytoplasmic or perinuclear aggregates, similar to DRM-associated R120G $\alpha$ B-crystallin aggregates. Subsequent colocalization and coimmunoprecipitation experiments suggested that Hsp27 is bound more tightly by the

Hsp22 mutants compared to the wild type and trapped in the intracellular aggregates along with the mutant proteins. Further, the viability of N2a mouse neuroblast cells overexpressing the mutant proteins was found to be significantly reduced (Irobi *et al.*, 2004).

Although the susceptible positively charged residue in  $\beta 7$  strand is highly conserved across all mammalian sHsps (Figure 5.1) and is essential for the structural and functional



**Figure 5.1: Structural alignment and mutational site of Hsp22.** (A) Sequence alignment of human Hsp22 with other human sHsps, *M. jannaschii* Hsp 16.5 and *T. aestivum* (wheat) Hsp 16.9 was done using web-based software ClustalW (<http://www.ebi.ac.uk/Tools/clustalw2/index.html>). A part of the region around  $\beta 5$  and  $\beta 7$  strands is shown. Secondary structural elements,  $\beta$ -strand (orange) and  $\alpha$ -helix (cyan), detected in crystal structure of *M. jannaschii* Hsp 16.5 and *T. aestivum* Hsp 16.9 are also shown on the top and the bottom of the alignment adjacent to their corresponding sequences. The black rectangular box shows the highly conserved positively charged residue (lysine or arginine), whose mutation leads to pathology in Hsp22,  $\alpha A$ - and  $\alpha B$ -crystallin. (B) Ribbon diagram of wheat Hsp 16.9 monomer (Protein Databank Accession code 1GME) showing the R108 (equivalent to mutational site K141) in grey.

integrity of  $\alpha$ A-crystallin (Bera *et al.*, 2002),  $\alpha$ B-crystallin (Simon *et al.*, 2007a) and Hsp27 (Chávez Zobel *et al.*, 2005), the effect of these mutations on the structure-function relationship of Hsp22 is not understood. The underlying pathological mechanisms in these disorders are not clear: whether it is misfolding and aggregation of the mutant Hsp22, or its defective cytoprotective and chaperone-like activity leading to misfolding and aggregation of other proteins, or a dysfunction in cell death pathways, or a combination of these effects. Thus, we set out to address the following questions: Can mutated Hsp22 function as a chaperone? What are its structural features? How does it cause pathology? We mutated, cloned, overexpressed and purified Hsp22 mutants to homogeneity in order to compare their properties with those of wild type Hsp22. We studied their secondary and tertiary structure by circular dichroism and fluorescence spectroscopy. We performed gel-filtration chromatography and glycerol density gradient centrifugation of Hsp22 and its mutants to analyze their quaternary structure. We also investigated their chaperone-like activity *in vitro*. The results of these studies are discussed in this chapter.

## 5.2 EXPERIMENTAL PROCEDURES:

### 5.2.1 Materials:

D-Sorbitol was purchased from Sigma (St. Louis, USA). Phenyl Sepharose 6 Fast flow (high sub) matrix, Blue Sepharose CL-6B, Superose-12 HR 10/30 pre-packed gel-filtration column and protein calibration kits were purchased from Amersham Biosciences (Uppsala, Sweden). Ethylene glycol was obtained from Qualigens (Mumbai, India). Rosetta (DE3) competent cells were from Stratagene (CA, USA). Other materials used in this chapter are already described in the previous chapters.

### 5.2.2 Creating the K141N and K141E mutants of Hsp22:

Recombinant human Hsp22 gene cloned in pET-21a(+) was used as a template to generate the mutants (K141NHsp22 and K141EHsp22) using the overlap extension polymerase chain reaction (PCR) method as described in Chapter 2. Briefly, to create the mutant K141NHsp22, two independent PCRs were performed using T7 promoter primer (T7PP) and the mutagenic primer 5'-GCT GGA TTT TGT TTG TGA AGT TC-3' as one primer pair and 5'-GAA CTT CAC AAA CAA AAT CCA GC-3' and T7 terminator primer (T7TP) as the second primer pair. For the other mutant, K141EHsp22, two independent

PCRs were performed using mutagenic primers 5'-GCT GGA TTT TCT CTG TGA AGT TC-3' and 5'-GAA CTT CAC AGA GAA AAT CCA GC-3' with T7PP and T7TP respectively. The resulting partially overlapping fragments were used in a fusion reaction of 10 cycles for allowing extension of the 3'-overlapping ends and further amplified by the T7PP and T7TP added to the same reaction, continued for a further 30 cycles. The amplified fragment was digested and then ligated in the *Xba*I and *Hind*III sites of the pET-21a(+) expression vector. The sequence of this construct was verified by T7 promoter and terminator primers using 3700 ABI automated DNA sequencer. The clones were maintained in DH5 $\alpha$  strain of *E. coli*.

### 5.2.3 Expression and purification of the wild type, K141N and K141E Hsp22:

The human recombinant wild type and the mutant Hsp22 proteins were expressed in Rosetta (DE3) strain of *E. coli* by transforming them with pET-21a(+) expression vectors containing the corresponding coding sequences. The transformed cells were cultured in Luria Bertani medium at 37°C in an incubator shaker and expression was induced with 1 mM IPTG. After harvesting the bacterial cells, these cell pellets were suspended in 100 mM Tris-HCl buffer, pH 8.0, containing 100 mM NaCl, 2 mM EDTA and 0.2% D-sorbitol (TNES buffer). Protease inhibitors PMSF (1 mM), leupeptin (50  $\mu$ M) and pepstatin (1  $\mu$ M) were also added before lysing the cells by sonication. All the three overexpressed proteins partitioned in the soluble fraction of cell lysate following sonication and subsequent centrifugation.

The soluble fraction of cell lysate containing wild type or mutant Hsp22 protein was loaded directly onto a Phenyl Sepharose hydrophobic interaction matrix. Protein was bound to the matrix and 1.5 ml fractions were collected following the elution with step gradients of TNES buffer containing 25% and 40% ethylene glycol. Fractions containing Hsp22 protein with relatively less contaminants were pooled and then precipitated with 5 mM ZnSO<sub>4</sub>. This protein pellet was resolubilized completely in TNES buffer and further purified on a Q-Sepharose ion-exchange column. Ethylene glycol (10%) was also added to the solution before loading onto Q-Sepharose column to avoid on-column aggregation. The ion-exchange column was washed with 100 mM Tris-HCl buffer, pH 8.0, containing 2 mM EDTA, 0.2% D-sorbitol, 10% ethylene glycol and 70 mM NaCl. Wild type Hsp22 was eluted with a step gradient of buffer containing 100 mM NaCl, whereas both K141EHsp22 and K141NHsp22 were eluted in buffer containing 150 mM NaCl. The purified proteins were dialyzed against TNES buffer (to exchange ethylene glycol) and concentrated using a PM 10 MWCO membrane in an Amicon stirred cell ultra-filtration unit. The purity of the wild type

and mutant proteins was checked by SDS-PAGE. The concentrations of the wild type and mutant protein samples were determined spectrophotometrically using an extinction coefficient ( $\epsilon_{280\text{nm}}$ ) of 1.22 for a 1 mg/ml of protein, calculated by a sequence-based method described by Pace *et al.* (1995). The protein samples were stored at 4°C as freezing the samples at -30°C leads to their aggregation upon thawing.

#### 5.2.4 Circular dichroism spectroscopy:

Circular dichroism (CD) spectra were recorded using a JASCO J-715 Spectropolarimeter at 25°C. Spectra were recorded using 1.5 mg/ml of protein in TNES buffer in a 1 cm path length cuvette for the near-UV region and 0.1 cm path length cuvette for the far-UV region. Appropriate buffer spectra were subtracted from the sample spectra. All reported spectra are the average of 4 accumulations, smoothed and expressed as mean residue mass ellipticity,  $[\theta]_{\text{MRM}}$ , in units of  $\text{deg cm}^2 \text{dmol}^{-1}$ .  $[\theta]_{\text{MRM}}$  values were calculated using the formula  $[\theta]_{\text{MRM}} = ([\theta] \text{ in degrees} \times 115 \times 100) / (\text{concentration in mg/ml} \times \text{path length in cm})$ .

#### 5.2.5 Fluorescence studies:

All fluorescence measurements were carried out using a Hitachi F-4500 Fluorescence Spectrophotometer with excitation and emission band passes set at 5 nm each. Intrinsic tryptophan fluorescence spectra of the wild type and mutant Hsp22 (0.2 mg/ml in TNES buffer) were recorded by exciting the sample at 295 nm. Hydrophobic probe, bis-ANS, was used at a final concentration of 10  $\mu\text{M}$  to probe the surface hydrophobicity. The wild type and the mutant Hsp22 (0.2 mg/ml) were incubated with bis-ANS at 25°C for 30 min. Excitation wavelength was set at 390 nm and emission spectra were recorded from 400 to 600 nm. All the spectra were recorded in the corrected spectrum mode.

#### 5.2.6 FPLC gel permeation chromatography:

Quaternary structure of wild type and mutant Hsp22 was investigated by gel-filtration chromatography on a Superose-12 HR 10/30 pre-packed FPLC column (dimensions 1  $\times$  30 cm). A 1.5 mg/ml solution of wild type or mutant Hsp22 in TNES buffer was filtered with 0.22  $\mu$  syringe filter and 200  $\mu\text{l}$  of this sample was injected onto the column pre-equilibrated with the same buffer. The proteins were eluted at a flow rate of 0.4 ml/min. Molecular weight



standards comprising carbonic anhydrase (28.7 kDa),  $\beta$ -lactoglobulin (36 kDa), ovalbumin (45 kDa), bovine serum albumin (67 kDa) and aldolase (158 kDa) were used for calibration.

### 5.2.7 Glycerol density gradient centrifugation:

Density gradient centrifugation was performed essentially as described by Lambert *et al.* (1999). Wild type and mutant Hsp22 (0.6 mg/ml) were loaded on top of an 11 ml linear gradient of glycerol (5 to 25% v/v) in TNES buffer. Samples were centrifuged in a Beckman SW41 rotor for 18 h at 30000 rpm and 4°C. Fractions (~0.3 ml) were withdrawn from the top of each tube using a Haake-Buchler Auto Densi-Flow IIC gradient former/remover. Absorbance of the fractions at 280 nm was measured using a Shimadzu UV-1601 Spectrophotometer. To estimate the molecular weight of the protein, carbonic anhydrase,  $\beta$ -lactoglobulin, ovalbumin and bovine serum albumin were used as molecular weight standards.

### 5.2.8 Isolation and purification of native zeta-crystallin from guinea pig lens:

Native  $\zeta$ -crystallin from guinea pig lens was isolated and purified as described earlier (Rao *et al.*, 1992). Briefly, four lenses were homogenized in 10 mM Tris buffer, pH 7.4, containing 0.5 mM EDTA and centrifuged at 5000 X g for 15 min. The supernatant was passed through a Blue Sepharose CL-6B column.  $\zeta$ -Crystallin binds to this column by virtue of its nucleotide binding sites. The column was washed with the homogenizing buffer containing 0.1 M NaCl and the bound protein was eluted using buffer containing 1 M NaCl. Protein was desalted by dialysis. The protein, thus, obtained was found to be more than 98% pure.

### 5.2.9 Assay for chaperone-like activity:

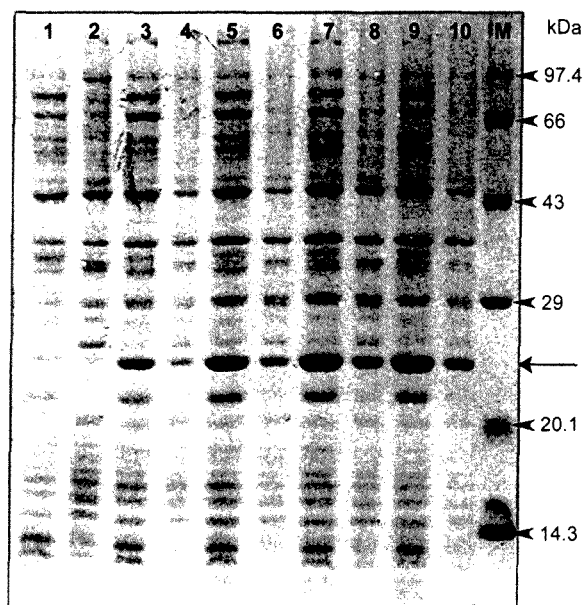
The chaperone-like activity of the wild type or mutant proteins was assayed by their ability to prevent the heat-induced aggregation of  $\zeta$ -crystallin or that of citrate synthase (CS).  $\zeta$ -Crystallin (0.1 mg/ml) in 50 mM Tris-HCl, pH 7.4, containing 0.1 mM DTT, 100 mM NaCl was incubated in the absence or the presence of wild type or K141NHsp22 or K141EHsp22 at 48°C. In another experiment, CS (25  $\mu$ g/ml) in 40 mM HEPES-KOH buffer, pH 7.4, was aggregated at 43°C in the absence or the presence of individual proteins. The extent of CS or  $\zeta$ -crystallin aggregation was measured as a function of time by monitoring the scattering at

465 nm in a Hitachi F-4000 Fluorescence Spectrofluorometer. Excitation and emission band passes were set at 3 nm each.

### 5.3 RESULTS AND DISCUSSION:

#### 5.3.1 Cloning, expression and purification of mutant Hsp22:

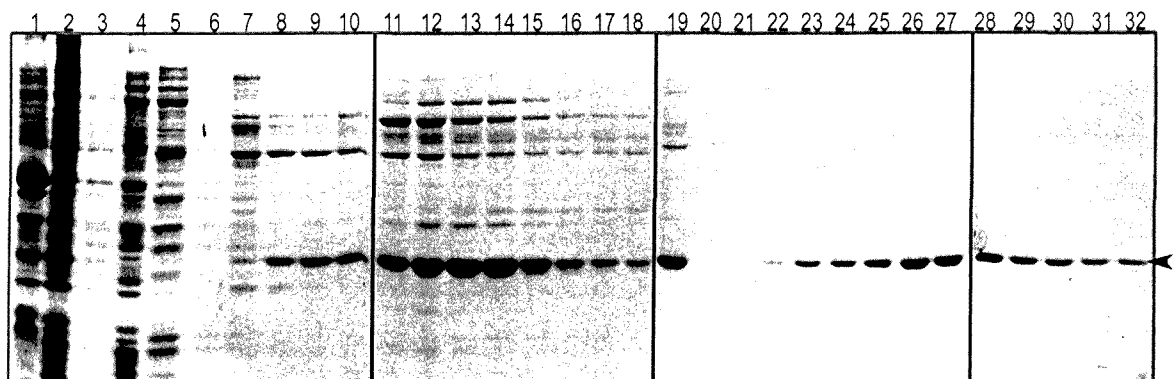
With an objective to study the effect of K141N/E mutation in human Hsp22 and understand its structure-function relationship, we generated the K141N/E mutants of Hsp22 using the site-directed mutagenesis approach. The wild type as well as mutant Hsp22 coding sequences were cloned into pET-21a(+) prokaryotic expression vector. Hsp22, K141NHsp22 and K141EHsp22 proteins were overexpressed in *E. coli* Rosetta (DE3). Upon induction profiling, maximum expression of Hsp22 was seen around 4 h in the soluble fraction of the cell lysate (Figure 5.2). Similar results were obtained for K141NHsp22 and K141EHsp22. Thus, unlike G98R $\alpha$ A-crystallin, both K141NHsp22 and K141EHsp22 mutant proteins do not show formation of inclusion bodies and are expressed predominantly in soluble fraction of *E. coli*. It should be noted that Hsp22 shows an aberrant mobility on SDS-PAGE and migrates as a band with apparent molecular mass of about 25 kDa, but not as a 22 kDa protein (Benndorf *et al.*, 2001; Chowdary *et al.*, 2004).



**Figure 5.2: Induction profile of *E. coli* cells overexpressing human Hsp22.** Lanes 1, 3, 5, 7 & 9 represent soluble fraction of cells grown at 37°C expressing Hsp22 for 0, 1, 2, 3 and 4 h post-induction by 1 mM IPTG respectively. Lanes 2, 4, 6, 8 & 10 represent their corresponding insoluble fractions. Lane M: medium range molecular-weight protein standards (Bangalore Genei) with molecular masses in kDa shown next to the bands. Slender arrow indicates the position of Hsp22 band. Protein loaded in each well was normalized to the OD of the culture at the corresponding time. The mutant proteins, K141NHsp22 and K141EHsp22, showed similar induction profile. Note the abnormal mobility (~25 kDa) of Hsp22 protein on SDS-PAGE.

We have purified human Hsp22 by subjecting the lysate to hydrophobic interaction chromatography on Phenyl Sepharose matrix (Figure 5.3). Hsp22 eluted with 40% ethylene glycol was precipitated with  $ZnSO_4$ . Earlier, in our laboratory, Chowdary *et al.* (2004) have shown that Hsp22 salted out with ammonium sulfate was sparingly soluble in TNES buffer compared with Hsp22 precipitated with  $ZnSO_4$ . Addition of 0.2% D-sorbitol, a co-solute, to the buffer improved the solubility of the protein. Further purification of resolubilized Hsp22 pellet was carried out by ion exchange chromatography on Q-Sepharose matrix (Figure 5.3) as described in the experimental procedures. K141NHsp22 and K141EHsp22 were purified in a similar way except that the final elution on Q-Sepharose was done with buffer containing 150 mM NaCl.

The proteins thus obtained were found to be homogeneous as determined by SDS-PAGE. Hsp22 is known to auto-degrade upon storage even at 4°C due to the spontaneous non-enzymatic cleavage of labile peptide bonds present in its sequence (Chowdary *et al.*, 2004). Hsp22 undergoes more auto-degradation in lower pH buffer and was shown to be relatively more stable at pH 8.0 (Chowdary *et al.*, 2004). The mutant proteins, K141NHsp22 and K141EHsp22, also showed similar behavior. Therefore, protein was purified using TNES buffer, pH 8.0, and stored in the same buffer for not longer than 3 days.



**Figure 5.3: Purification of Hsp22.** Lane 1 and 2: insoluble and soluble fraction after lysing the *E. coli* cells overexpressing Hsp22 respectively. Lane 3 and 4: flow-through after loading and reloading lysate supernatant on Phenyl Sepharose column respectively. Lanes 5 and 6: washing with 30 ml TNES to remove all unbound proteins. Lane 7: washing with 20 ml TNES containing 25% ethylene glycol. Lanes 8-18: 1.5 ml fractions collected upon elution with 20 ml TNES containing 40% ethylene glycol. Comparatively pure fractions were pooled and precipitated with 5 mM  $ZnSO_4$ . Lane 19: resolubilized Hsp22 precipitate, which was loaded onto a Q-Sepharose column. Lane 20 and 21: flow-through obtained from Q-Sepharose column. Lane 22: washing with 20 ml TNES buffer containing 70 mM NaCl. Lane 23-32: various fractions indicating elution using TNES buffer containing 100 mM NaCl. Arrow head indicates the position of the Hsp22 on SDS-PAGE. Both K141NHsp22 and K141EHsp22 were purified in a similar way except that final elution on Q-Sepharose column was done using buffer containing 150 mM NaCl.

### 5.3.2 Study of conformational change in K141NHsp22 and K141EHsp22:

In order to understand if mutant Hsp22 proteins adopt a different conformation than wild type Hsp22, we analyzed its secondary, tertiary and quaternary structure using circular dichroism, fluorescence, gel-filtration and glycerol density gradient centrifugation techniques.

#### 5.3.2.1 Secondary and tertiary structure analyses using circular dichroism:

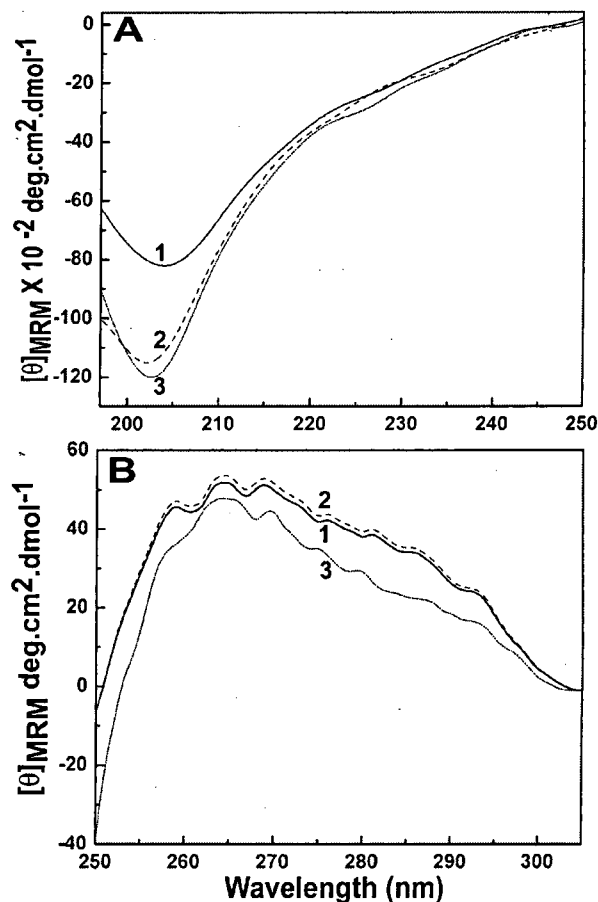
Hsp22 contains the conserved  $\alpha$ -crystallin domain in its C-terminal region. As discussed in Chapter 1,  $\alpha$ -crystallin domain exhibits a  $\beta$ -sandwich fold. However, predictions of the secondary structural propensities using various prediction algorithms indicated that Hsp22 contains predominantly unordered structures – random coil content predicted by different algorithms ranged between 73 and 80% (Chowdary *et al.*, 2004). Interestingly, the far-UV CD spectrum of Hsp22 does not exhibit the typical  $\beta$ -sheet structure observed in other sHsps such as  $\alpha$ A-crystallin (Chowdary *et al.*, 2004; Kim *et al.*, 2004). In agreement with the predictions, estimation of secondary structure based on analysis of CD spectra showed that about 35% of Hsp22 is  $\beta$ -sheet, 5% is  $\alpha$ -helices and 60% is unordered structure (Kim *et al.*, 2006). Although Hsp22 seems to belong to the group of intrinsically disordered proteins (Uversky *et al.*, 2005), it is not completely unfolded and possesses predominantly randomly coiled structure with some  $\beta$ -sheet (Chowdary *et al.*, 2004; Kim *et al.*, 2004; Hu *et al.*, 2007).

As shown in Figure 5.4 A, the far-UV CD spectrum of human Hsp22 is suggestive of a predominantly randomly coiled structure, in agreement with the previous studies. The figure also shows the far-UV CD spectrum of K141NHsp22 and K141EHsp22, which almost overlap with each other with subtle variations. The K141N/E mutation results in increase in the negative ellipticity and a shift of the maximum towards lower wavelength to ~203 nm. Thus, the far-UV CD spectra of mutant Hsp22 proteins indicate increase in unordered structure. As similar behavior was also seen for G98R $\alpha$ A-crystallin, it is possible that the mutation bearing region in the sequence, which has strand propensity in the wild type Hsp22 ( $\beta$ 7-strand), is perturbed in the mutant proteins.

In a parallel study on K141EHsp22, Kim *et al.* (2006) obtained similar results. They also observed that the K141E mutation resulted in increase of the apparent rate constant of trypsinolysis. Thus, our studies taken together with that of Kim *et al.* (2004) indicate that the

mutation K141N and K141E in  $\beta 7$  strand of Hsp22 leads to partial unfolding and destabilization of Hsp22 secondary structure.

Tertiary structure of Hsp22 and its mutants was studied by near-UV CD spectroscopy (Figure 5.4 B). The near-UV CD spectrum of Hsp22 shows that the aromatic amino acids are in a chiral environment, indicating a tertiary structure at least in some regions of the polypeptide. The fine structure in the near-UV CD spectrum of Hsp22 is retained in the case of both K141NHsp22 and K141EHsp22. However, K141NHsp22 shows decreased ellipticity compared to the wild type, whereas K141EHsp22 near-UV CD spectrum almost overlaps with that of the wild type protein. This result indicates that the K141N mutation leads to tertiary structural alterations resulting in decreased chirality at the aromatic residues, whereas K141E mutation does not markedly affect the tertiary structural packing.



**Figure 5.4: Circular dichroism (CD) spectra of wild type and mutant Hsp22.** Far-UV (A) and Near-UV CD spectra (B) of the wild type (curve 1), K141EHsp22 (curve 2) and K141NHsp22 (curve 3).  $[\theta]_{MRM}$ , mean residue mass ellipticity.

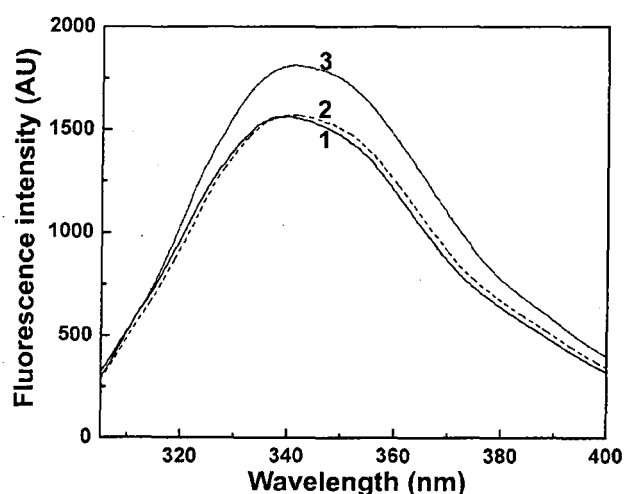
### 5.3.2.2 Fluorescence studies to analyze structure and surface hydrophobicity:

Intrinsic fluorescence data can reflect gross positioning of tryptophan residues in a protein, which in turn gives information on tertiary and/or quaternary structure of a protein (Kronman and Holmes, 1971; Burstein *et al.*, 1973). Hsp22 has four tryptophans in its sequence – three are located in the N-terminal domain (W48, W51 and W60) and fourth is located at the beginning of the  $\alpha$ -crystallin domain (W96). To understand the changes in the micro-environment around these tryptophan residues upon K141N/E mutation, we recorded

intrinsic fluorescence spectra of Hsp22, K141NHsp22 and K141EHsp22 (Figure 5.5). Hsp22 spectrum exhibits an emission maximum at 340 nm, indicating that the tryptophans are in a relatively polar environment. By fluorescence quenching experiments using potassium iodide (KI) and fitting the intrinsic fluorescence spectra into various spectral components, it was shown that around 60% of the tryptophan residues in Hsp22 were highly accessible and/or located on the protein surface (Kim *et al.*, 2006).

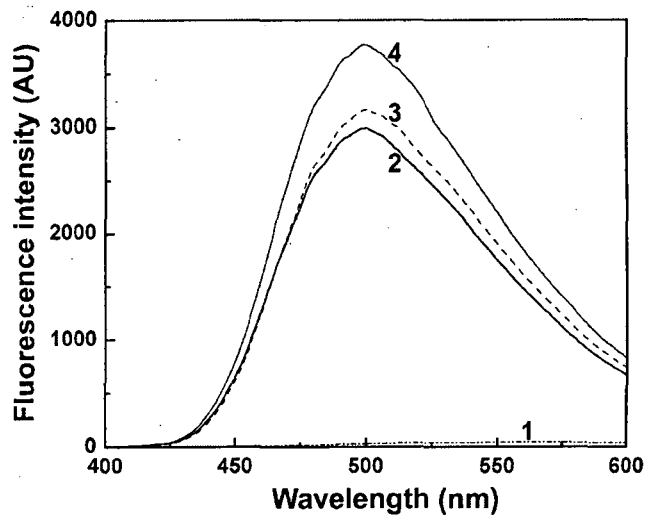
The fluorescence spectrum of K141NHsp22 exhibits significantly higher fluorescence intensity indicating a change in the local microenvironment of the tryptophans. On the other hand, K141EHsp22 showed a fluorescence spectrum similar to that of Hsp22. However, the emission maximum (340 nm) is not significantly altered upon mutation. Consistent with the results obtained by near-UV CD, K141E mutation does not lead to significant changes in the tertiary structural packing of the protein, whereas the mutant K141NHsp22 appears to have adopted a different tertiary structure from that of the wild type protein. In line with our results, percentage accessibility of the tryptophan residues was not found to be changed upon K141E mutation in Hsp22 (Kim *et al.*, 2006).

In addition to various factors, hydrophobic interactions play an important role in the binding of the non-native target proteins to the chaperone. Therefore, we have compared the accessible hydrophobic surfaces of the wild type and mutant Hsp22 proteins using bis-ANS, a hydrophobic probe whose fluorescence intensity increases several fold upon binding to hydrophobic surfaces of a protein. The fluorescence spectra of bis-ANS bound to Hsp22, K141NHsp22 and K141EHsp22 at room temperature (25°C) are shown in Figure 5.6. A several fold increase in the fluorescence intensity of bis-ANS, accompanied by a blue shift in emission maximum to 495 nm, could be seen when Hsp22 was bound to it. The fluorescence intensity was



**Figure 5.5: Intrinsic tryptophan fluorescence of the wild type and the mutant Hsp22.** Intrinsic tryptophan fluorescence spectra of the 0.2 mg/ml wild type Hsp22 (curve 1), K141EHsp22 (curve 2) and K141NHsp22 (curve 3) in TNES buffer.

higher in the presence of K141NHsp22 than in the presence of the wild type protein or K141EHsp22, suggesting an increase in the accessible hydrophobic surface of the protein. On the other hand, emission spectra of bis-ANS bound to Hsp22 and K141EHsp22 differ very slightly from each other, indicating no significant difference in surface hydrophobicity. Titration of K141EHsp22 and Hsp22 with bis-ANS yielded almost overlapping curves, which were markedly different from that obtained for Hsp27 (Kim *et al.*, 2006).



**Figure 5.6: Fluorescence spectrum of bis-ANS bound to the wild type and mutant Hsp22.** Fluorescence spectra of bis-ANS (10  $\mu$ M) in buffer alone (curve 1) and in the presence of 0.2 mg/ml wild type (curve 2), K141EHsp22 (curve 3) and K141NHsp22 (curve 4).

Thus, K141E mutation does not strongly affect the hydrophobic properties of Hsp22. However, there is a conformational change resulting in the exposure of normally buried hydrophobic residues in the case of K141NHsp22. These differences in surface hydrophobicity can also be due to the mutation-induced changes in the quaternary structure.

### 5.3.2.3 Quaternary structural studies:

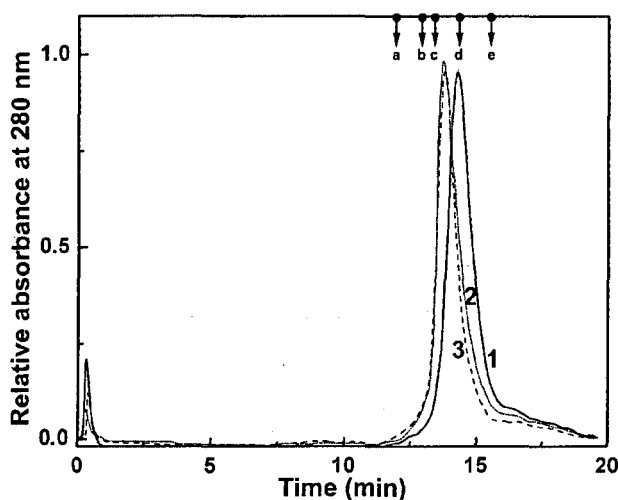
Most sHsps generally assemble into large multimeric complexes. For instance,  $\alpha$ -crystallin exists as a polydisperse oligomer with an apparent molecular mass of  $\sim$ 650 kDa in the native state. However, quaternary structure of Hsp22 is debatable. Unlike other sHsps, using size-exclusion chromatography and glycerol density gradient centrifugation, Hsp22 was shown to be monomeric *in vitro* (Chowdary *et al.*, 2004). Much of the *in vivo* data suggest that Hsp22 predominantly exists in the form of monomers, dimers or even tetramers (Benndorf *et al.*, 2001; Chavez Zobel *et al.*, 2003). Coimmunoprecipitation experiments showed that FLAG- and Myc-tagged Hsp22 interacted with each other (Sun *et al.*, 2004). Further, Hsp22, although at a higher concentration, was shown to form dimers and higher oligomers after crosslinking (Kim *et al.*, 2004; Kim *et al.*, 2006). Though the sequence of



Hsp22 contains three cysteine residues, these residues are not involved in formation of intra- or inter-molecular disulphide bonds (Chowdary *et al.*, 2004). We have investigated the effect of K141N/E mutation on oligomeric structure of Hsp22 by gel-filtration chromatography and glycerol density gradient centrifugation.

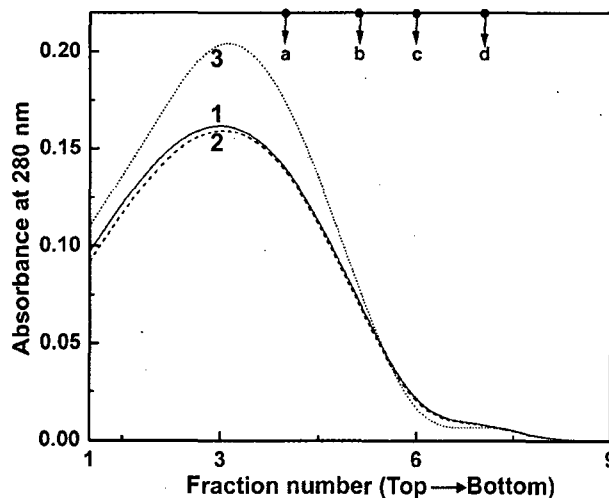
The elution pattern of Hsp22, K141NHsp22 and K141EHsp22 along with the positions of the elution volumes of molecular-mass standards is shown in Figure 5.7. Hsp22 eluted at an elution volume corresponding to a molecular mass of 36 kDa in close agreement with the other studies (Chowdary *et al.*, 2004; Kim *et al.*, 2004; Kim *et al.*, 2006). Kim *et al.* (2006) showed that Hsp22, on a native gradient-PAGE in presence of Coomassie G250 (blue native electrophoresis), migrated as a single band with an apparent molecular mass of 35-38 kDa. This is higher than the molecular mass expected for the monomer but lower than that of the dimer. Since hydrodynamic radius significantly influences the elution position of a protein on gel-filtration chromatography, it is possible that Hsp22 is less compact due to its predominantly randomly coiled structure and forms extended monomers.

Gel-filtration chromatography shows that the K141NHsp22 and K141EHsp22 elute prior to the wild type Hsp22 indicating that the size of the mutant protein is larger compared to that of the Hsp22. The molecular mass of K141NHsp22 and K141EHsp22 estimated using the elution volumes of the standard proteins was found to be ~40 kDa, still less than that of the dimers. Heating at 70°C for 30 min does not affect the elution profile of Hsp22 or K141EHsp22 indicating that they have high thermal stability like other intrinsically disordered proteins (Kim *et al.*, 2006). Since the K141N/E mutations cause secondary structural unfolding, it is possible that K141NHsp22 and K141EHsp22 are less compact and globular than Hsp22.



**Figure 5.7:** Elution profile of human Hsp22, K141NHsp22 and K141EHsp22 on a Superose 12 HR10/30 FPLC column. Elution profiles of the wild type (curve 1), K141NHsp22 (curve 2) and K141EHsp22 (curve 3). The elution positions of molecular mass standards are indicated by down arrows. a, aldolase (158 kDa); b, BSA (67 kDa); c, ovalbumin (45 kDa); d,  $\beta$ -lactoglobulin (36 kDa); e, carbonic anhydrase (28.7 kDa).

Glycerol density gradient centrifugation, which relies on sedimentation of proteins through a density gradient of glycerol, is another technique for estimating the molecular mass of proteins. Figure 5.8 shows the glycerol density gradient profile of human Hsp22 and its disease-causing mutants. The molecular mass of Hsp22 estimated by glycerol density gradient centrifugation is 22.4 kDa, which is very close to the molecular mass expected for the monomer (21.6 kDa) and identical to that observed by Chowdary *et al.* (2004). Like wild type Hsp22, both K141NHsp22 and K141EHsp22 migrated as a broad peak with apparent molecular mass of ~22.4 kDa.



**Figure 5.8: Glycerol density gradient centrifugation of Hsp22, K141NHsp22 and K141EHsp22.** Sedimentation of the wild type (curve 1), K141EHsp22 (curve 2) and K141NHsp22 (curve 3) through a 5-25% linear gradient of glycerol. On X-axis is the number of fractions collected from the top of the gradient (fraction size - 0.3 ml). The positions of molecular mass standards are indicated by down arrows. a, carbonic anhydrase (28.7 kDa); b,  $\beta$ -lactoglobulin (36 kDa); c, ovalbumin (45 kDa); d, BSA (67 kDa).

Interestingly, Hsp22 lacks the conserved IXI motif that is found to be important in oligomerization and chaperone-like activity of some plant and bacterial sHsps. Moreover, as seen in the crystal structures of *M. jannaschii* Hsp16.5 and wheat Hsp16.9, IXI motif forms inter-subunit contacts - its isoleucines bind in a hydrophobic groove between the  $\beta$ 4 and  $\beta$ 8 strands of the  $\alpha$ -crystallin domain of neighboring subunits (Kim *et al.*, 1998; van Montfort *et al.*, 2001). Nevertheless, Hsp22 stands out as a unique sHsp as it exists as a monomer even though it has an N-terminal domain and a C-terminal extension comparable in length with the other multimeric members of the sHsp family. Thus, our results indicate that although the K141N mutation, and to a lesser extent K141E mutation, affect the secondary and tertiary structure of Hsp22, they do not significantly influence the oligomeric structure of the protein and all the three proteins exist as a monomer *in vitro*.

Taken together, our structural studies along with the parallel study on K141EHsp22 by Kim *et al.* (2006) suggest that the mode of folding of secondary structural elements, side-chain packing of the aromatic residues, surface hydrophobicity as well as quaternary

structure are altered to a certain extent upon K141N/E mutation in Hsp22. Structural changes induced by the pathological mutations in the  $\beta$ 7 strand of  $\alpha$ A-crystallin (R116C/H) and  $\alpha$ B-crystallin (R120G) are known to have a detrimental effect on their chaperone-like activity (Kumar *et al.*, 1999; Bova *et al.*, 1999; Shroff *et al.*, 2000; Gu *et al.*, 2008). Since the corresponding K141N/E mutations in Hsp22 cause structural changes, we have investigated mutation-induced changes in their chaperone-like activity, if any.

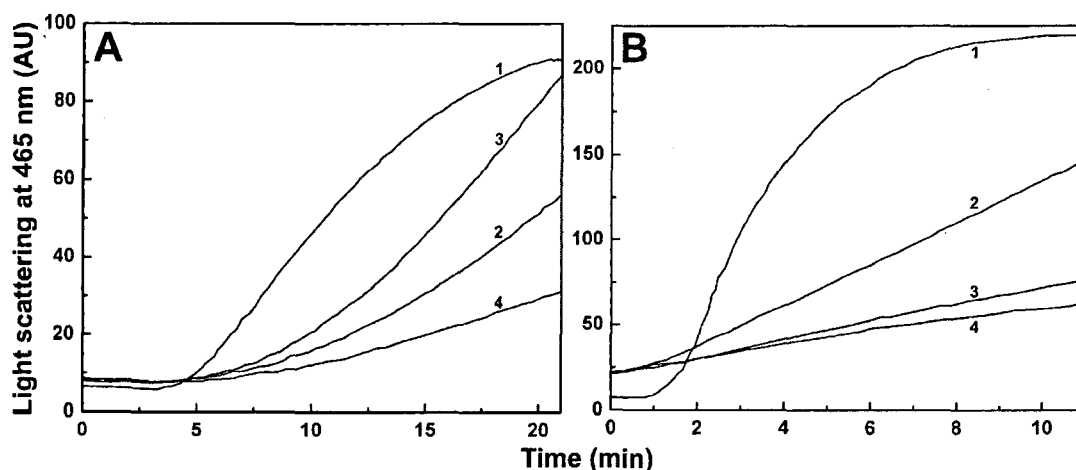
### 5.3.3 Changes in chaperone activity of Hsp22 upon K141N/E mutation:

Like many other sHsps, Hsp22 is known to possess chaperone-like activity *in vitro* and prevents aggregation of partially denatured model proteins (Chowdary *et al.*, 2004; Kim *et al.*, 2004). Hsp22 appears to be the first candidate of the sHsp family that is monomeric *in vitro* and also exhibits chaperone-like activity, since the sHsps known so far that exhibit chaperone-like activity are multimeric in nature (Chowdary *et al.*, 2004). Hsp22 overexpression was shown to inhibit the aggresome formation by R120G $\alpha$ B-crystallin in cells through a direct chaperone-like activity by transiently interacting with the mutant protein (Chávez Zobel *et al.*, 2003). In addition, it has been shown that Hsp22 can accomplish its chaperone function *in vivo*, as it prevents the formation of inclusion bodies by Htt43Q (huntingtin protein containing 43 glutamines) as efficiently as Hsp40 and maintains Htt43Q in a soluble state competent for rapid degradation, whereas other sHsps such as  $\alpha$ B-crystallin and Hsp27 failed to do so (Carra *et al.*, 2005). Recently, it was shown that the formation of stable complex between Hsp22 and Bag3, a protein that may facilitate the disposal of doomed proteins by stimulating macroautophagy, was essential for the Hsp22-induced Htt43Q degradation (Carra *et al.*, 2008). Similar chaperone-like activity was also seen with another polyglutamine protein, AR65Q (androgen receptor protein containing 65 glutamines) (Carra *et al.*, 2005).

We have investigated whether mutation affects the chaperone-like activity of Hsp22 against the heat-induced aggregation of citrate synthase (CS) and  $\zeta$ -crystallin at 43°C and 48°C respectively (Figure 5.9). We have selected chaperone to target protein ratio [4:1 (w/w) in both the cases] such that wild type Hsp22 exhibits nearly 50% protection against aggregation. Figure 5.9 A shows the effect of Hsp22 and its mutants on the aggregation of CS. At the same ratio, where Hsp22 protects the aggregation of CS to nearly 50% (curve 2), K141EHsp22 exhibits very less protection (curve 3). Interestingly, K141NHsp22 prevents the aggregation of CS to a greater extent than the wild type Hsp22 (curve 4).

We tested the chaperone-like activity of Hsp22, K141NHsp22 and K141EHsp22 with another model aggregation system, zeta-crystallin.  $\zeta$ -Crystallin binds NADPH and has quinone-reductase activity (Rao *et al.*, 1992). It was shown earlier that  $\zeta$ -crystallin aggregates at temperatures beyond 40°C (Raman *et al.*, 1995a). As shown in Figure 5.9 B,  $\zeta$ -crystallin aggregates as a function of time upon incubation at 48°C (curve 1). Hsp22 prevents this aggregation to nearly 45% at 4:1 (w/w) ratio (curve 2). Intriguingly, light scattering seen in the presence of K141EHsp22 (curve 3) and K141NHsp22 (curve 4) was considerably less. This shows that mutant proteins can prevent the aggregation of  $\zeta$ -crystallin more effectively than the wild type with K141NHsp22 being the most effective.

Using rhodanese and alcohol dehydrogenase as model substrates, Kim *et al* (2006) showed that K141EHsp22 exhibits markedly decreased chaperone-like activity compared to Hsp22. Moreover, K141EHsp22 was slightly more effective than Hsp22 in retarding the onset of DTT-induced insulin aggregation. Therefore, depending on the nature of protein substrate, K141EHsp22 exhibits an increase or decrease in its chaperone-like activity. Loss of chaperone-like activity against few substrates can at least be partly responsible for the development of the neuromuscular disorders caused by the K141E mutation in Hsp22. K141NHsp22 showed increased chaperone-like activity with CS and  $\zeta$ -crystallin *in vitro*; nevertheless it is possible that it can behave differently *in vivo*. Indeed, K141NHsp22 and



**Figure 5.9: Chaperone-like activity of Hsp22 and its mutants.** (A) Thermally induced aggregation of citrate synthase (20  $\mu$ g/ml) alone (curve 1) and in the presence of wild type Hsp22 (curve 2), K141EHsp22 (curve 3) and K141NHsp22 (curve 4). (B) Heat-induced aggregation profile of  $\zeta$ -crystallin (0.1 mg/ml) alone (curve 1) and in the presence of wild type Hsp22 (curve 2), K141EHsp22 (curve 3) and K141NHsp22 (curve 4). Ratio of chaperone to substrate (w/w) was selected as 4:1 such that aggregation is nearly 50% protected by wild type protein.

K141EHsp22 were 2-3 fold less effective than wild type Hsp22 in preventing Htt43Q aggregation *in vivo*. The mutations also resulted in a reduction in the cytoprotective ability of Hsp22 as determined from the increase in the Htt43Q-containing cell debris collected from the cells expressing the mutants when compared with the wild type Hsp22 (Carra *et al.*, 2005).

sHsp-target protein interactions depend on the molecular mass of the target protein, complementarities of the interacting surfaces, hydrophobicity and complex stability (Rajaraman *et al.*, 2001). The cataract-causing R116C $\alpha$ A- and R49C $\alpha$ A-crystallin exhibit enhanced substrate-binding to the non-native T4 lysozyme. Such enhanced binding due to the increase in stability of the complex of mutant  $\alpha$ A-crystallin and non-native T4 lysozyme is predicted to promote the unfolding of substrates (Koteiche and Mchaourab, 2006). The mechanism of action may also vary significantly depending on the properties of sHsp and substrates. For instance  $\alpha$ A- or  $\alpha$ B-crystallin make reversible, transient interactions with early unfolding intermediates of citrate synthase such that the enzyme can be reactivated whereas the binding with late unfolding intermediates is irreversible (Rajaraman *et al.*, 2001). Contrary to this, murine Hsp25 binds irreversibly with thermally denatured citrate synthase and prevents its aggregation, but the enzyme cannot be reactivated (Ehrnsperger *et al.*, 1997). Binding to the aggregation-prone intermediates of substrate proteins and their subsequent release for eventual refolding/reactivation is an important feature of chaperone function. Thus, it is possible that although K141EHsp22 and especially K141NHsp22 exhibit increased chaperone activity, studied by virtue of decrease in light scattering, it can be due to its enhanced substrate binding capacity and/or its irreversible binding with substrates. Such binding can lead to the toxic gain of function inside the cells (Irobi *et al.*, 2004; Koteiche and Mchaourab, 2006).

#### 5.4 CONCLUSIONS:

As mentioned earlier structural and functional characterization of the K141NHsp22 and K141EHsp22 will help in elucidating their role in neuromuscular disorders. Our results show that unlike G98R $\alpha$ A-crystallin, both K141NHsp22 and K141EHsp22 are expressed in soluble fraction. However, both mutants form aggregates when expressed in different cell lines with K141NHsp22 being more aggregation-prone (Irobi *et al.*, 2004; Fontaine *et al.*, 2006). Although K141NHsp22 and K141EHsp22 show partial secondary structural unfolding, both the mutant proteins possess a predominantly randomly coiled structure like

wild type Hsp22. K141NHsp22, which is involved in both CMT and dHMN, is more deviating of the two Hsp22 mutants in structural and functional properties. The K141N mutation has more pronounced effect on the structural destabilization of Hsp22 compared to K141E. Although K141NHsp22 showed enhanced chaperone-like activity with a few model substrates and K141EHsp22 showed substrate-dependent changes in chaperone-like activity, it is currently not known how these 'mutated chaperones' act on other proteins involved in motor neuron function.

The interaction of Hsp22 with multiple protein partners and its chaperone-like activity can account for a plethora of different functions ascribed to this protein. Hsp22, like other members of sHsp family, forms hetero-oligomeric complexes with Hsp27, MKBP, HspB3,  $\alpha$ B-crystallin, Hsp20 and cvHsp (Benndorf *et al.*, 2001; Sun *et al.*, 2004; Fontaine *et al.*, 2005). Mutation-induced destabilization resulting in partial unfolding, in turn, can alter the interaction of partially unfolded Hsp22 with other sHsps that are abundant in neurons. Using quantitative FRET, yeast two-hybrid and chemical crosslinking methods, aberrantly increased interactions of K141NHsp22 and K141EHsp22 with themselves, with wild type Hsp22,  $\alpha$ B-crystallin and Hsp27 were demonstrated (Fontaine *et al.*, 2006). Similarly, S135F, a mutation in Hsp27 that causes both dHMN and CMT, also shows increased interaction with Hsp22 (Fontaine *et al.*, 2006). The interaction characteristics of K141NHsp22 were more deviating from Hsp22 than the characteristics of K141EHsp22. Thus, it is possible that the enhanced chaperone-like activity exhibited by K141NHsp22 is due to its increased tendency to interact or bind with the substrate proteins.

Increased interactions involving mutant Hsp22 may be the molecular basis for their toxic gain of function effect and increased tendency to form cytoplasmic protein aggregates. Both the mutations caused aberrant interaction with Hsp27, which is sequestered in the intracellular aggregates formed by Hsp22 mutants (Irobi *et al.*, 2004). Such sequestration could remove a portion of wild type protein from other essential functions within the cell. This could be of particular significance in specific cell types such as sensory or motor neurons, where a basal level of expression may be critical.

In conclusion, our study shows the importance of the conserved lysine in  $\beta$ 7 strand of Hsp22. This lysine appears to play an important role in the structure and properties of Hsp22. K141N/E mutation in the  $\beta$ 5- $\beta$ 7 region of Hsp22 has a deleterious effect on its structural and functional integrity. Prediction of disordered regions using different programs indicates that residues 137-141 are located on the border of the unordered and ordered

regions of Hsp22 (Kasakov *et al.*, 2007). Very often, such parts of the molecules are involved in inter- or intra-molecular interactions and play an important role in recognition and cell signaling (Uversky *et al.*, 2005). The importance of  $\beta$ 5- $\beta$ 7 region is further highlighted by the fact that mutation of a nearby conserved lysine 137 to glutamic acid (K137E) and the double mutation of lysine 137 and 141 to glutamic acid (K137,141E) lead to an increase in unordered structure in Hsp22 and increased susceptibility to trypsinolysis. Both mutations show decreased chaperone-like activity compared to wild type Hsp22 with K137EHsp22 being less effective (Kasakov *et al.*, 2007).

Differences in the structure and interactions of Hsp22 upon K141N/E may be important in progression of the disease particularly during aging when the total levels of Hsp and the general heat shock response to stress may be reduced (Soti and Csermely, 2003; Morrow and Tanguay, 2003). Hence, neurons from aged human expressing mutated Hsp22 may not successfully control mutated or damaged protein accumulation. The different regions such as anterior horn cells or peripheral nerves, in which the aggregates can accumulate may be associated with different phenotypes (CMT or dHMN), caused by the same amino acid change (K141N). However, whether the aggregates of Hsp22 and Hsp27 observed in experiments with different cell lines also occur during the degeneration of neurons in individuals with dHMN or CMT is an open question. Nevertheless, future *in vivo* studies on K141NHsp22 and K141EHsp22 by the generation of animal models or other means should shed light on understanding the relation between the changes in structure, chaperone-like activity and consequent pathology.



CONCLUDING  
REMARKS

6

In this thesis, we have addressed the structural and functional role of disease-causing point mutations in two sHsps which highlight the importance of  $\beta 5$ - $\beta 7$  region of sHsps. This region harbours nearly 80% of the disease-causing mutations present in ' $\alpha$ -crystallin domain'. We have selected Hsp22, a class I sHsp, having K141N/E mutation in  $\beta 7$  strand that causes hereditary peripheral neuropathies and  $\alpha A$ -crystallin, a class II sHsp, having G98R mutation that causes presenile cataract.

G98R mutation in  $\beta 5$  strand of  $\alpha A$ -crystallin results in formation of inclusion bodies in *E.coli* indicating that the mutant protein has inherent folding defects. The mutant protein, refolded from inclusion bodies, shows altered secondary and tertiary structure, and forms large oligomers. Despite showing increased bis-ANS (hydrophobic surface probe) binding compared to wild type  $\alpha A$ -crystallin, G98R $\alpha A$ -crystallin has compromised chaperone activity. The mutant protein is structurally more unstable and unfolds at a lower concentration of urea as compared to the wild type protein. The mutant protein is more susceptible to proteolysis and transiently populates fragments that are prone to aggregation. Unlike the wild type protein, it is also susceptible to heat-induced aggregation.

Thus, the G98R mutation causing folding defects as well as drastic differences in the structure and stability of the mutant protein would be expected to result in congenital cataract formation. However, the cataract formation ascribed to this mutation is presenile in nature with onset at the age of 16 years. Formation of mixed oligomer between the wild type and mutant subunits might be crucial in the context of such dominant negative character. FRET studies show that the mutant protein can exchange its subunits with wild type  $\alpha A$ -crystallin and also with itself. Our study shows that the mixed oligomers of the wild type and G98R $\alpha A$ -crystallin exhibit properties dominated by those of the mutant protein in structural aspects, oligomeric size, chaperone-like activity and urea-induced unfolding. However, mixed oligomer formation leads to a decreased propensity to aggregate (as a function of temperature or upon proteolysis) as compared to the homo-oligomers of the mutant protein. Co-expression studies show that wild type  $\alpha A$ -crystallin can rescue the mutant from partitioning into inclusion. Such mixed oligomer formation seems to be a balancing factor, which prevents congenital cataract.

It is possible that the balancing factors are vulnerable to age-related modifications of the lens proteins or other environmental risk factors, and is probably overcome by other factor(s) in due course of time, triggering cataract formation. We have tested one such environmental risk factor represented by heavy metal ions such as  $\text{Cu}^{2+}$ ,  $\text{Cd}^{2+}$ ,  $\text{Zn}^{2+}$  and

$\text{Ca}^{2+}$ . Using ITC and fluorescence spectroscopy, we have shown that wild type protein binds  $\text{Cu}^{2+}$  selectively with picomolar affinity, exhibits redox-silencing and inhibits ROS generation. Mutation-induced conformational changes do not significantly affect the  $\text{Cu}^{2+}$ -binding and redox-silencing properties of  $\alpha\text{A}$ -crystallin. However, binding of  $\text{Cu}^{2+}$  and other ions such as  $\text{Cd}^{2+}$  and  $\text{Zn}^{2+}$  promotes the self aggregation of mutant protein. The extent of aggregation is less pronounced in the case of the mixed oligomer. Heavy metal ions such as  $\text{Cu}^{2+}$ ,  $\text{Cd}^{2+}$  and  $\text{Zn}^{2+}$  have adverse effect on the chaperone-like activity of the mutant G98R $\alpha\text{A}$ -crystallin, whereas they increase the chaperone-like activity of wild type  $\alpha\text{A}$ -crystallin. Thus, our study shows various factors that may underlie the molecular basis for the presenile onset and the absence of congenital cataract in mutation-affected individuals.

As stated earlier, a large number of mutations in  $\beta 5$  and  $\beta 7$  strands of sHsps are associated with pathology. We have investigated structural and functional changes due to K141N/E mutation in  $\beta 7$  strand of Hsp22, which are known to be associated with neuromuscular disorders. Unlike G98R $\alpha\text{A}$ -crystallin, both K141NHsp22 and K141EHsp22 are expressed in the soluble fraction. Although K141NHsp22 and K141EHsp22 showed partial secondary structural unfolding, both the mutant proteins possess a predominantly randomly coiled structure like wild type Hsp22. K141NHsp22, which is involved in both CMT and dHMN, has more pronounced effect on the structural destabilization compared to K141EHsp22. Interestingly, K141NHsp22 shows enhanced chaperone-like activity with a few model substrates and K141EHsp22 shows substrate-dependent changes in chaperone-like activity. Most sHsps interact with each other and these interactions appear to be important for regulation of sHsp function *in vivo* and *in vitro*. A few *in vivo* studies have shed light on some of the faulty interactions of these mutants. More detailed studies on the interaction of Hsp22 with other sHsps or components of neuronal system and signal transduction cascade should unravel the basis of the neuropathy.

The  $\beta 5$ - $\beta 7$  region is comparatively shorter in metazoan sHsps and is sensitive to mutations. Our studies, *inter alia*, highlight the importance of this region and provide an insight into molecular basis for the pathologies caused by these mutations.

Progress in recent years in the identification of pathological mutations in various sHsp family members has not only provided a challenge but also offered an opportunity to fill the gaps in our current understanding of the functioning of these sHsps. Recently, a couple of synonymous mutations and a promoter polymorphism in sHsps have been implicated in neuropathology. Synonymous mutations c.582C>T (T194T) in Hsp22 (Zhang

*et al.*, 2005) and c.379C>A (R127R) in Hsp27 (Houlden *et al.*, 2008) have been correlated with the development of CMT and dHMN respectively. In another study, a conserved nucleotide change (c. -217 T>C) in the Heat Shock Element (HSE) of the Hsp27 promoter was identified in an amyotrophic lateral sclerosis (ALS) patient, which impairs its stress response (Dierick *et al.*, 2007). Although such mutations or polymorphisms do not produce altered coding sequences, they are known to alter protein levels and conformation (Chamary *et al.*, 2006; Parmley and Hurst, 2007). Mutations discovered thus far appear to be just the tip of the iceberg and the discovery of newer mutations is likely to implicate an increasing number of sHsps in several cellular functions and pathologies.

In general, the structural and functional aspects of most sHsps have not been completely understood so far. Detailed insight into the structural and functional role of individual sHsps as well as their interactions with other sHsps would help in designing strategies to mitigate the pathological complications.

# BIBLIOGRAPHY

- Abraham EC, Cherian M, Smith JB. (1994) *Biochem Biophys Res Commun* **201**:1451-1456.
- Ackerley S, James PA, Kalli A, French S, Davies KE, Talbot K. (2006) *Hum Mol Genet* **15**:347-354.
- Ahmad MF, Raman B, Ramakrishna T, Rao CM. (2008a) *J Mol Biol* **375**:1040-1051.
- Ahmad MF, Singh D, Taiyab A, Ramakrishna T, Raman B, Rao CM. (2008b) *J Mol Biol* **382**:812-824.
- Andley UP, Mathur S, Griest TA, Petrash JM. (1996) *J Biol Chem* **271**:31973-31980.
- Andley UP, Patel HC, Xi JH. (2002) *J Biol Chem* **277**:10178-10186.
- Andley UP, Song Z, Wawrousek EF, Brady JP, Bassnett S, Fleming TP. (2001) *FASEB J* **15**:221-229.
- Andley UP. (2007) *Prog Retin Eye Res* **26**:78-98.
- Anfinsen CB. (1973) *Science* **181**:223-230.
- Aquilina JA, Benesch JL, Ding LL, Yaron O, Horwitz J, Robinson CV. (2005) *J Biol Chem* **280**:14485-14491.
- Araki N, Ueno N, Chakrabarti B, Morino Y, Horiuchi S. (1992) *J Biol Chem* **267**:10211-10214.
- Argirov OK, Lin B, Ortwerth BJ. (2004) *J Biol Chem* **279**:6487-6495.
- Arrigo AP, Paul C, Ducasse C, Manero F, Kretz-Remy C, Virost S, Javouhey E, Mounier N, Diaz-Latoud C. (2002) *Prog Mol Subcell Biol* **28**:185-204.
- Augusteyn RC. (1998) *Int J Biol Macromol* **22**:253-262.
- Aurelian L, Smith CC, Winchurch R, Kulka M, Gyotoku T, Zaccaro L, Chrest FJ, Burnett JW. (2001) *J Invest Dermatol* **116**:286-295.
- Badri KR, Modem S, Gerard HC, Khan I, Bagchi M, Hudson AP, Reddy TR. (2006) *J Cell Biochem* **99**:1353-1362.
- Bai F, Xi JH, Wawrousek EF, Fleming TP, Andley UP. (2003) *J Biol Chem* **278**:36876-36886.
- Bany BM, Schultz GA. (2001) *Biol Reprod* **64**:284-292.
- Barbato R, Menabò R, Dainese P, Carafoli E, Schiaffino S, Di Lisa F. (1996) *Circ Res* **78**:821-828.
- Barnham KJ, Masters CL, Bush AI. (2004) *Nat Rev Drug Discov* **3**:205-214.
- Baruch A, Greenbaum D, Levy ET, Nielsen PA, Gilula NB, Kumar NM, Bogoy M. (2001) *J Biol Chem* **276**:28999-29006.
- Beby F, Commeaux C, Bozon M, Denis P, Edery P, Morlé L. (2007) *Arch Ophthalmol* **125**:213-216.
- Beechem JM, Brand L. (1985) *Ann Rev Biochem* **54**:43-71.
- Benn SC, Perrelet D, Kato AC, Scholz J, Decosterd I, Mannion RJ, Bakowska JC, Woolf CJ. (2002) *Neuron* **36**:45-56.
- Bennardini F, Wrzosek A, Chiesi M. (1992) *Circ Res* **71**:288-294.
- Benndorf R, Sun X, Gilmont RR, Biederman KJ, Molloy MP, Goodmurphy CW, Cheng H, Andrews PC, Welsh MJ. (2001) *J Biol Chem* **276**:26753-26761.
- Bera S, Abraham EC. (2002) *Biochemistry* **41**:297-305.
- Bera S, Thampi P, Cho WJ, Abraham EC. (2002) *Biochemistry* **41**:12421-12426.
- Berengian AR, Bova MP, Mchaourab HS. (1997) *Biochemistry* **36**:9951-9957.

- Berengian AR, Parfenova M, Mchaourab HS. (1999) *J Biol Chem* **274**:6305-6314.
- Berry V, Francis P, Reddy MA, Collyer D, Vithana E, MacKay I, Dawson G, Carey AH, Moore A, Bhattacharya SS, Quinlan RA. (2001) *Am J Hum Genet* **69**:1141-1145.
- Beswick HT, Harding JJ. (1987) *Exp Eye Res* **45**:569-578.
- Bhattacharyya J, Shipova EV, Santhoshkumar P, Sharma KK, Ortwerth BJ. (2007) *Biochemistry* **46**:14682-14692.
- Biswas A, Das KP. (2004) *J Biol Chem* **279**:42648-42657.
- Biswas A, Das KP. (2007) *Biopolymers* **85**:189-197.
- Biswas A, Das KP. (2008) *Biochemistry* **47**:804-816.
- Biswas S, Harris F, Dennison S, Singh J, Phoenix DA. (2004) *Trends Mol Med* **10**:78-84.
- Bluhm WF, Martin JL, Mestrlil R, Dillmann WH. (1998) *Am J Physiol* **275**:H2243-H2249.
- Boelens WC, Croes Y, de Ruwe M, de Reu L, de Jong WW. (1998) *J Biol Chem* **273**:28085-28090.
- Bova MP, Ding LL, Horwitz J, Fung BK. (1997) *J Biol Chem* **272**:29511-29517.
- Bova MP, Mchaourab HS, Han Y, Fung BK. (2000) *J Biol Chem* **275**:1035-1042.
- Bova MP, Yaron O, Huang Q, Ding L, Haley DA, Stewart PL, Horwitz J. (1999) *Proc Natl Acad Sci USA* **96**:6137-6142.
- Boyle DL, Takemoto L, Brady JP, Wawrousek EF. (2003) *BMC Ophthalmol* **3**:3.
- Boyle DL, Takemoto L. (1994) *Exp Eye Res* **58**:9-15.
- Boyle DL, Takemoto L. (1996) *Curr Eye Res* **15**:577-582.
- Brady JP, Garland D, Duglas-Tabor Y, Robison WG Jr, Groome A, Wawrousek EF. (1997) *Proc Natl Acad Sci USA* **94**:884-889.
- Brady JP, Garland DL, Green DE, Tamm ER, Giblin FJ, Wawrousek EF. (2001) *Invest Ophthalmol Vis Sci* **42**:2924-2934.
- Brown Z, Ponce A, Lampi K, Hancock L, Takemoto L. (2007) *Curr Eye Res* **32**:1051-1054.
- Bruet JM, Ducasse C, Bonniaud P, Ravagnan L, Susin SA, Diaz-Latoud C, Gurbuxani S, Arrigo AP, Kroemer G, Solary E, Garrido C. (2000) *Nat Cell Biol* **2**:645-652.
- Bukach OV, Seit-Nebi AS, Marston SB, Gusev NB. (2004) *Eur J Biochem* **271**:291-302.
- Bukau B, Deuerling E, Pfund C, Craig EA. (2000) *Cell* **101**:119-122.
- Bullard B, Ferguson C, Minajeva A, Leake MC, Gautel M, Labeit D, Ding L, Labeit S, Horwitz J, Leonard KR, Linke WA. (2004) *J Biol Chem* **279**:7917-7924.
- Burstein EA, Vedenkina NS, Ivkova MN. (1973) *Photochem Photobiol* **18**:263-279.
- Candido EP. (2002) *Prog Mol Subcell Biol* **28**:61-78.
- Carra S, Seguin SJ, Lambert H, Landry J. (2008) *J Biol Chem* **283**:1437-1444.
- Carra S, Sivilotti M, Chavez Zobel AT, Lambert H, Landry J. (2005) *Hum Mol Genet* **14**:1659-1669.
- Carver JA, Aquilina JA, Truscott RJ. (1993) *Biochim Biophys Acta* **1164**:22-28.
- Carver JA, Lindner RA. (1998) *Int J Biol Macromol* **22**:197-209.



- Cekic O. (1998) *Br J Ophthalmol* **82**:186-188.
- Chamary JV, Parmley JL, Hurst LD. (2006) *Nat Rev Genet* **7**:98-108.
- Charpentier AH, Bednarek AK, Daniel RL, Hawkins KA, Laffin KJ, Gaddis S, MacLeod MC, Aldaz CM. (2000) *Cancer Res* **60**:5977-5983.
- Chávez Zobel AT, Lambert H, Thériault JR, Landry J. (2005) *Cell Stress Chaperones* **10**:157-166.
- Chávez Zobel AT, Loranger A, Marceau N, Thériault JR, Lambert H, Landry J. (2003) *Hum Mol Genet* **12**:1609-1620.
- Chen Q, Liu JB, Horak KM, Zheng H, Kumarapeli AR, Li J, Li F, Gerdes AM, Wawrousek EF, Wang X. (2005) *Circ Res* **97**:1018-1026.
- Cherian M, Abraham EC. (1995) *Biochem Biophys Res Commun* **208**:675-679.
- Cherian M, Smith JB, Jiang XY, Abraham EC. (1997) *J Biol Chem* **272**:29099-29103.
- Chowdary TK, Raman B, Ramakrishna T, Rao CM. (2004) *Biochem J* **381**:379-387.
- Chung KW, Kim SB, Cho SY, Hwang SJ, Park SW, Kang SH, Kim J, Yoo JH, Choi BO. (2008) *Exp Mol Med* **40**:304-312.
- Cobb BA, Petrash JM. (2000) *Biochemistry* **39**:15791-15798.
- Cobb BA, Petrash JM. (2002) *Biochemistry* **41**:483-490.
- Craig EA. (1993) *Science* **260**:1902-1903.
- Dabir DV, Trojanowski JQ, Richter-Landsberg C, Lee VM, Forman MS. (2004) *Am J Pathol* **164**:155-166.
- Das BK, Liang JJ, Chakrabarti B. (1997) *Curr Eye Res* **16**:303-309.
- Das BK, Liang JJ. (1997) *Biochem Biophys Res Commun* **236**:370-374.
- Das KP, Petrash JM, Surewicz WK. (1996) *J Biol Chem* **271**:10449-10452.
- Das KP, Surewicz WK. (1995) *FEBS Lett* **369**:321-325.
- Datta SA, Rao CM. (1999) *J Biol Chem* **274**:34773-34778.
- Datta SA, Rao CM. (2000) *J Biol Chem* **275**:41004-41010.
- de Jong WW, Caspers GJ, Leunissel JA. (1998) *Int J Biol Macromol* **22**:151-162.
- de Jong WW, Zweers A, Versteeg M, Nuy-Terwindt EC. (1984) *Eur J Biochem* **141**:131-140.
- Depré C, Hase M, Gaussin V, Zajac A, Wang L, Hittinger L, Ghaleh B, Yu X, Kudej RK, Wagner T, Sadoshima J, Vatner SF. (2002) *Circ Res* **91**:1007-1014.
- Depré C, Kim SJ, John AS, Huang Y, Rimoldi OE, Pepper JR, Dreyfus GD, Gaussin V, Pennell DJ, Vatner DE, Camici PG, Vatner SF. (2004) *Circ Res* **95**:433-440.
- Depré C, Wang L, Sui X, Qiu H, Hong C, Hedhli N, Ginion A, Shah A, Pelat M, Bertrand L, Wagner T, Gaussin V, Vatner SF. (2006) *Circ Res* **98**:280-288.
- Derham BK, Harding JJ. (1999) *Prog Retin Eye Res* **18**:463-509.
- Derham BK, Harding JJ. (2002) *Biochem J* **364**:711-717.

- Derham BK, van Boekel MA, Muchowski PJ, Clark JI, Horwitz J, Hepburne-Scott HW, de Jong WW, Crabbe MJ, Harding JJ. (2001) *Eur J Biochem* **268**:713-721.
- Deuerling E, Bukau B. (2004) *Crit Rev Biochem Mol Biol* **39**:261-277.
- Devi RR, Yao W, Vijayalakshmi P, Sergeev YV, Sundaresan P, Hejtmancik JF. (2008) *Mol Vis* **14**:1157-1170.
- Diaz-Latoud C, Buache E, Javouhey E, Arrigo AP. (2005) *Antioxid Redox Signal* **7**:436-445.
- Dierick I, Irobi J, Janssens S, Theuns J, Lemmens R, Jacobs A, Corsmit E, Hersmus N, Van Den Bosch L, Robberecht W, De Jonghe P, Van Broeckhoven C, Timmerman V. (2007) *Hum Mutat* **28**:830.
- Dilley KJ, Harding JJ. (1975) *Biochim Biophys Acta* **386**:391-408.
- Dudich IV, Zav'yalov VP, Pfeil W, Gaestel M, Zav'yalova GA, Denesyuk AI, Korpela T. (1995) *Biochim Biophys Acta* **1253**:163-168.
- Ecroyd H, Meehan S, Horwitz J, Aquilina JA, Benesch JL, Robinson CV, Macphee CE, Carver JA. (2007) *Biochem J* **401**:129-141.
- Ehrnsperger M, Gräber S, Gaestel M, Buchner J. (1997) *EMBO J* **16**:221-229.
- Ellis J. (1987) *Nature* **328**:378-379.
- Ellis RJ, Hartl FU. (1999) *Curr Opin Struct Biol* **9**:102-110.
- Evgrafov OV, Mersyanova I, Irobi J, Van Den Bosch L, Dierick I, Leung CL, Schagina O, Verpoorten N, Van Impe K, Fedotov V, Dadali E, Auer-Grumbach M, Windpassinger C, Wagner K, Mitrovic Z, Hilton-Jones D, Talbot K, Martin JJ, Vasserman N, Tverskaya S, Polyakov A, Liem RK, Gettemans J, Robberecht W, De Jonghe P, Timmerman V. (2004) *Nat Genet* **36**:602-606.
- Fagerholm PP, Philipson BT, Lindström B. (1981) *Exp Eye Res* **33**:615-620.
- Fan GC, Chu G, Mitton B, Song Q, Yuan Q, Kranias EG. (2004) *Circ Res* **94**:1474-1482.
- Fardeau M, Godet-Guillain J, Tome FM, Collin H, Gaudeau S, Boffety C, Vernant P. (1978) *Rev Neurol (Paris)* **134**:411-425.
- Feil IK, Malfois M, Hendle J, van Der Zandt H, Svergun DI. (2001) *J Biol Chem* **276**:12024-12029.
- Fontaine JM, Sun X, Benndorf R, Welsh MJ. (2005) *Biochem Biophys Res Commun* **337**:1006-1011.
- Fontaine JM, Sun X, Hoppe AD, Simon S, Vicart P, Welsh MJ, Benndorf R. (2006) *FASEB J* **20**:2168-2170.
- Francis PJ, Berry V, Bhattacharya SS, Moore AT. (2000) *J Med Genet* **37**:481-488.
- Fu L, Liang JJ. (2003) *Invest Ophthalmol Vis Sci* **44**:1155-1159.
- Fu S, Dean R, Southan M, Truscott R. (1998) *J Biol Chem* **273**:28603-28609.
- Fujii N, Awakura M, Takemoto L, Inomata M, Takata T, Fujii N, Saito T. (2003) *Mol Vis* **9**:315-322.
- Fujii N, Hiroki K, Matsumoto S, Masuda K, Inoue M, Tanaka Y, Awakura M, Akaboshi M. (2001) *Photochem Photobiol* **74**:477-482.
- Fujii N, Ishibashi Y, Satoh K, Fujino M, Harada K. (1994) *Biochim Biophys Acta* **120**:157-163.

- Fujii N, Shimmyo Y, Sakai M, Sadakane Y, Nakamura T, Morimoto Y, Kinouchi T, Goto Y, Lampi K. (2007) *Amino Acids* **32**:87-94.
- Fujii N, Takemoto LJ, Momose Y, Matsumoto S, Hiroki K, Akaboshi M. (1999) *Biochem Biophys Res Commun* **265**:746-751.
- Gaggelli E, Kozlowski H, Valensin D, Valensin G. (2006) *Chem Rev* **106**:1995-2044.
- Ganadu ML, Aru M, Mura GM, Coi A, Mlynarz P, Kozlowski H. (2004) *J Inorg Biochem* **98**:1103-1109.
- Ganea E. (2001) *Curr Protein Pept Sci* **2**:205-225.
- Garland D. (1990) *Exp Eye Res* **50**:677-682.
- Garner B, Davies MJ, Truscott RJW. (2000a) *Exp Eye Res* **70**:81-88.
- Garner B, Roberg K, Qian M, Eaton JW, Truscott RJW. (2000b) *Exp Eye Res* **71**:599-607.
- Garner MH, Spector A. (1980) *Proc Natl Acad Sci USA* **77**:1274-1277.
- Ghosh JG, Clark JI. (2005) *Protein Sci* **14**:684-695.
- Ghosh JG, Houck SA, Doneanu CE, Clark JI. (2006) *J Mol Biol* **364**:364-375.
- Giblin FJ, McCready JP, Kodama T, Reddy VN. (1984) *Exp Eye Res* **38**:87-93.
- Glover JR, Lindquist S. (1998) *Cell* **94**:73-82.
- Gober MD, Depre C, Aurelian L. (2004) *Biochem Biophys Res Commun* **321**:267-268.
- Gober MD, Smith CC, Ueda K, Toretzky JA, Aurelian L. (2003) *J Biol Chem* **278**:37600-37609.
- Goenka S, Raman B, Ramakrishna T, Rao CM. (2001) *Biochem J* **359**:547-556.
- Goldfarb LG, Vicart P, Goebel HH, Dalakas MC. (2004) *Brain* **127**:723-734.
- Golenhofen N, Ness W, Koob R, Htun P, Schaper W, Drenckhahn D. (1998) *Am J Physiol* **274**:H1457-H1464.
- Golenhofen N, Perng MD, Quinlan RA, Drenckhahn D. (2004) *Histochem Cell Biol* **122**:415-425.
- Goodsell DS. (1991) *Trends Biochem Sci* **16**:203-206.
- Graw J, Klopp N, Illig T, Preising MN, Lorenz B. (2006) *Graefes Arch Clin Exp Ophthalmol* **244**:912-919.
- Graw J. (2004) *Int J Dev Biol* **48**:1031-1044.
- Grey AC, Schey KL. (2008) *Mol Vis* **14**:171-179.
- Groenen PJ, Merck KB, de Jong WW, Bloemendal H. (1994) *Eur J Biochem* **225**:1-19.
- Gu F, Luo W, Li X, Wang Z, Lu S, Zhang M, Zhao B, Zhu S, Feng S, Yan YB, Huang S, Ma X. (2008) *Hum Mutat* **29**:769.
- Gupta R, Srivastava OP. (2004a) *J Biol Chem* **279**:44258-44269.
- Gupta R, Srivastava OP. (2004b) *Invest Ophthalmol Vis Sci* **45**:206-214.
- Haley DA, Bova MP, Huang QL, Mchaourab HS, Stewart PL. (2000) *J Mol Biol* **298**:261-272.
- Hansen JE, Gafni A. (1993) *J Biol Chem* **268**:21632-21636.
- Hansen L, Yao W, Eiberg H, Kjaer KW, Baggesen K, Hejtmancik JF, Rosenberg T. (2007) *Invest Ophthalmol Vis Sci* **48**:3937-3944.

- Hanson SR, Hasan A, Smith DL, Smith JB. (2000) *Exp Eye Res* **71**:195-207.
- Harding AE, Thomas PK. (1980) *Brain* **103**:259-280.
- Harding JJ. (1997) Lens. In: *Biochemistry of the Eye* 94-135. (Ed: Harding JJ. Chapman and Hall, London).
- Harrington V, McCall S, Huynh S, Srivastava K, Srivastava OP. (2004) *Mol Vis* **10**:476-489.
- Hartl FU, Hayer-Hartl M. (2002) *Science* **295**:1852-1858.
- Hase M, Depre C, Vatner SF, Sadoshima J. (2005) *Biochem J* **388**:475-483.
- Haslbeck M, Buchner J. (2002) *Prog Mol Subcell Biol* **28**:37-59.
- Haslbeck M, Franzmann T, Weinfurter D, Buchner J. (2005) *Nat Struct Mol Biol* **12**:842-846.
- Haslbeck M, Walke S, Stromer T, Ehrnsperger M, White HE, Chen S, Saibil HR, Buchner J. (1999) *EMBO J* **18**:6744-6751.
- Hawkins JW, Van Keuren ML, Piatigorsky J, Law ML, Patterson D, Kao FT. (1987) *Hum Genet* **76**:375-380.
- Hawse JR, Cumming JR, Oppermann B, Sheets NL, Reddy VN, Kantorow M. (2003) *Invest Ophthalmol Vis Sci* **44**:672-679.
- Hawse JR, Padgaonkar VA, Leverenz VR, Pelliccia SE, Kantorow M, Giblin FJ. (2006) *Mol Vis* **12**:342-349.
- Hayes VH, Devlin G, Quinlan RA. (2008) *J Biol Chem* **283**:10500-10512.
- Head MW, Corbin E, Goldman JE. (1993) *Am J Pathol* **143**:1743-1753.
- Hedhli N, Wang L, Wang Q, Rashed E, Tian Y, Sui X, Madura K, Depre C. (2008) *Cardiovasc Res* **77**:497-505.
- Hejtmancik JF. (2008) *Semin Cell Dev Biol* **19**:134-149.
- Hess JF, FitzGerald PG. (1998) *Mol Vis* **4**:29-32.
- Hilz H, Wieggers U, Adamietz P. (1975) *Eur J Biochem* **56**:103-108.
- Ho SN, Hunt HD, Horton RM, Pullen JK, Pease LR. (1989) *Gene* **77**: 51-59.
- Höfheld J, Cyr DM, Patterson C. (2001) *EMBO Rep* **2**:885-890.
- Hollander JM, Martin JL, Belke DD, Scott BT, Swanson E, Krishnamoorthy V, Dillmann WH. (2004) *Circulation* **110**:3544-3552.
- Hook DW, Harding JJ. (1997) *Eur J Biochem* **247**:380-385.
- Horwitz J, Bova MP, Huang QL, Ding LL, Yaron O, Lohman S. (1998) *Int J Biol Macromol* **22**:263-269.
- Horwitz J. (1992) *Proc Natl Acad Sci USA* **89**:10449-10453.
- Horwitz J. (2000) *Semin Cell Dev Biol* **11**:53-60.
- Houlden H, Laura M, Wavrant-De Vrièze F, Blake J, Wood N, Reilly MM. (2008) *Neurology* **71**:1660-1668.
- Hsu CD, Kymes S, Petrash JM. (2006) *Invest Ophthalmol Vis Sci* **47**:2036-2044.

- Hu Z, Chen L, Zhang J, Li T, Tang J, Xu N, Wang X. (2007) *J Neurosci Res* **85**:2071-2079.
- Ikeda Y, Abe A, Ishida C, Takahashi K, Hayasaka K, Yamada M. (2008) *J Neurol Sci* doi:10.1016/j.jns.2008.09.031.
- Inagaki N, Hayashi T, Arimura T, Koga Y, Takahashi M, Shibata H, Teraoka K, Chikamori T, Yamashina A, Kimura A. (2006) *Biochem Biophys Res Commun* **342**:379-386.
- Ingolia TD, Craig EA. (1982) *Proc Natl Acad Sci USA* **79**:2360-2364.
- Irobi J, Van Impe K, Seeman P, Jordanova A, Dierick I, Verpoorten N, Michalik A, De Vriendt E, Jacobs A, Van Gerwen V, Vennekens K, Mazanec R, Tournev I, Hilton-Jones D, Talbot K, Kremensky I, Van Den Bosch L, Robberecht W, Van Vandekerckhove J, Van Broeckhoven C, Gettemans J, De Jonghe P, Timmerman V. (2004) *Nat Genet* **36**:597-601.
- Ito H, Kamei K, Iwamoto I, Inaguma Y, Tsuzuki M, Kishikawa M, Shimada A, Hosokawa M, Kato K. (2003) *Cell Mol Life Sci* **60**:1217-1223.
- Iwaki T, Iwaki A, Tateishi J, Sakaki Y, Goldman JE. (1993) *Am J Pathol* **143**:487-495.
- Iwaki T, Kume-Iwaki A, Goldman JE. (1990) *J Histochem Cytochem* **38**:31-39.
- Jackson GS, Murray I, Hosszu LLP, Gibbs N, Waltho JP, Clarke AR, Collinge J. (2001) *Proc Natl Acad Sci USA* **98**:8531-8535.
- Jaenicke R, Slingsby C. (2001) *Crit Rev Biochem Mol Biol* **36**:435-499.
- Jakob U, Gaestel M, Engel K, Buchner J. (1993) *J Biol Chem* **268**:1517-1520.
- James PA, Rankin J, Talbot K. (2008) *J Neurol Neurosurg Psychiatry* **79**:461-463.
- Jiao W, Li P, Zhang J, Zhang H, Chang Z. (2005) *Biochem Biophys Res Commun* **335**:227-231.
- Kamei A, Iwase H, Masuda K. (1997) *Biochem Biophys Res Commun* **231**:373-378.
- Kamradt MC, Chen F, Sam S, Cryns VL. (2002) *J Biol Chem* **277**:38731-38736.
- Kappé G, Aquilina JA, Wunderink L, Kamps B, Robinson CV, Garate T, Boelens WC, de Jong WW. (2004) *Proteins* **57**:109-117.
- Kappé G, Franck E, Verschuure P, Boelens WC, Leunissen JA, de Jong WW. (2003) *Cell Stress Chaperones* **8**:53-61.
- Kapphahn RJ, Ethen CM, Peters EA, Higgins L, Ferrington DA. (2003) *Biochemistry* **42**:15310-15325.
- Kasakov AS, Bukach OV, Seit-Nebi AS, Marston SB, Gusev NB. (2007) *FEBS J* **274**:5628-5642.
- Kato K, Hasegawa K, Goto S, Inaguma Y. (1994) *J Biol Chem* **269**:11274-11278.
- Kelley MJ, David LL, Iwasaki N, Wright J, Shearer TR. (1993) *J Biol Chem* **268**:18844-18849.
- Kelly KJ, Baird NR, Greene AL. (2001) *Kidney Int* **59**:1798-1802.
- Khan AO, Aldahmesh MA, Meyer B. (2007) *Am J Ophthalmol* **144**:949-952.
- Khan MM, Martell AE. (1967) *J Am Chem Soc* **89**:4176-4185.
- Kijima K, Numakura C, Goto T, Takahashi T, Otagiri T, Umetsu K, Hayasaka K. (2005) *J Hum Genet* **50**:473-476.
- Kim KK, Kim R, Kim SH. (1998) *Nature* **394**:595-599.

- Kim MV, Kasakov AS, Seit-Nebi AS, Marston SB, Gusev NB. (2006) *Arch Biochem Biophys* **454**:32-41.
- Kim MV, Seit-Nebi AS, Marston SB, Gusev NB. (2004) *Biochem Biophys Res Commun* **315**:796-801.
- Kokke BP, Boelens WC, de Jong WW. (2001) *Cell Stress Chaperones* **6**:360-367.
- Koretz JF, Doss EW, LaButti JN. (1998) *Int J Biol Macromol* **22**:283-294.
- Koteiche HA, Berengian AR, Mchaourab HS. (1998) *Biochemistry* **37**:12681-12688.
- Koteiche HA, Mchaourab HS. (1999) *J Mol Biol* **294**:561-577.
- Koteiche HA, Mchaourab HS. (2006) *J Biol Chem* **281**:14273-14279.
- Kronman MJ, Holmes LG. (1971) *Photochem Photobiol* **14**:113-134.
- Kumar LV, Ramakrishna T, Rao CM. (1999) *J Biol Chem* **274**:24137-24141.
- Kumar LV, Rao CM. (2000) *J Biol Chem* **275**:22009-22013.
- Kumar MS, Reddy PY, Sreedhar B, Reddy GB. (2005) *Biochem J* **391**:335-341.
- Kumar TK, Jayaraman G, Lin WY, Yu C. (1996) *Biochim Biophys Acta*, **1294**:103-105.
- Lakowicz J. (1983) *Energy Transfer*. In: *Principles of Fluorescence Spectroscopy* 368-391 (Ed: Lakowicz J. Plenum Press, New York).
- Lambert H, Charette SJ, Bernier AF, Guimond A, Landry J. (1999) *J Biol Chem* **274**:9378-9385.
- Lampi KJ, Ma Z, Hanson SR, Azuma M, Shih M, Shearer TR, Smith DL, Smith JB, David LL. (1998) *Exp Eye Res* **67**:31-43.
- Lapko VN, Smith DL, Smith JB. (2001) *Protein Sci* **10**:1130-1136.
- Laskey RA, Honda BM, Mills AD, Finch JT. (1978) *Nature* **275**:416-420.
- Latchman DS. (2005) *Int J Hyperthermia* **21**:393-402.
- Lee GJ, Roseman AM, Saibil HR, Vierling E. (1997) *EMBO J* **16**:659-671.
- Leroux MR, Melki R, Gordon B, Batelier G, Candido EP. (1997) *J Biol Chem* **272**:24646-24656.
- Li H, Li C, Lu Q, Su T, Ke T, Li DW, Yuan M, Liu J, Ren X, Zhang Z, Zeng S, Wang QK, Liu M. (2008) *Biochim Biophys Acta* **1782**:303-309.
- Liang JJ, Liu BF. (2006) *Protein Sci* **15**:1619-1627.
- Lin PP, Barry RC, Smith DL, Smith JB. (1998) *Protein Sci* **7**:1451-1457.
- Litt M, Kramer P, LaMorticella DM, Murphey W, Lovrien EW, Weleber RG. (1998) *Hum Mol Genet* **7**:471-474.
- Liu C, Welsh MJ. (1999) *Biochem Biophys Res Commun* **255**:256-261.
- Liu M, Ke T, Wang Z, Yang Q, Chang W, Jiang F, Tang Z, Li H, Ren X, Wang X, Wang T, Li Q, Yang J, Liu J, Wang QK. (2006b) *Invest Ophthalmol Vis Sci* **47**:3461-3466.
- Liu XQ, Yang XQ, Xie FH, Song LY, Zhang GQ, Qian SJ. (2007) *Protein Expr Purif* **51**:179-186.
- Liu Y, Zhang X, Luo L, Wu M, Zeng R, Cheng G, Hu B, Liu B, Liang JJ, Shang F. (2006a) *Invest Ophthalmol Vis Sci* **47**:1069-1075.
- Lou MF, Dickerson JE Jr. (1992) *Exp Eye Res* **55**:889-896.

- Lund AL, Smith JB, Smith DL. (1996) *Exp Eye Res* **63**:661-672.
- Ma ZX, Hanson SRA, Lampi KJ, David LL, Smith DL, Smith JB. (1998) *Exp Eye Res* **67**:21-30.
- Macario AJ, Conway de Macario E. (2005) *N Engl J Med* **353**:1489-1501.
- Macario AJ, Grippo TM, de Macario EC. (2005) *Genet Med* **7**:3-12.
- Mackay DS, Andley UP, Shiels A. (2003) *Eur J Hum Genet* **11**:784-793.
- MacRae TH. (2000) *Cell Mol Life Sci* **57**:899-913.
- Maloyan A, Gulick J, Glabe CG, Kayed R, Robbins J. (2007) *Proc Natl Acad Sci USA* **104**:5995-6000.
- Maloyan A, Sanbe A, Osinska H, Westfall M, Robinson D, Imahashi K, Murphy E, Robbins J. (2005) *Circulation* **112**:3451-3461.
- Manevich Y, Held KD, Biaglow JE. (1997) *Radiat Res* **148**:580-591.
- Mao YW, Liu JP, Xiang H, Li DW. (2004) *Cell Death Differ* **11**:512-526.
- Marini I, Moschini R, Del Corso A, Mura U. (2000) *J Biol Chem* **275**:32559-32565.
- Martin JL, Mestrlil R, Hilal-Dandan R, Brunton LL, Dillmann WH. (1997) *Circulation* **96**:4343-4348.
- Merck KB, De Haard-Hoekman WA, Oude Essink BB, Bloemendal H, de Jong WW. (1992) *Biochim Biophys Acta* **1130**:267-276.
- Middelberg, APJ. (2002) *Trends Biotechnol* **20**:437-443.
- Miesbauer LR, Zhou X, Yang Z, Yang Z, Sun Y, Smith DL, Smith JB. (1994) *J Biol Chem* **269**:12494-12502.
- Minton AP. (1997) *Curr Opin Biotechnol* **8**:65-69.
- Mogk A, Mayer MP, Deuerling E. (2002) *Chembiochem* **3**:807-814.
- Mogk A, Tomoyasu T, Goloubinoff P, Rüdiger S, Röder D, Langen H, Bukau B. (1999) *EMBO J* **18**:6934-6949.
- Mornon JP, Halaby D, Malfois M, Durand P, Callebaut I, Tardieu A. (1998) *Int J Biol Macromol* **22**:219-227.
- Morozov V, Wawrousek EF. (2006) *Development* **133**:813-821.
- Morrison LE, Whittaker RJ, Klepper RE, Wawrousek EF, Glembotski CC. (2004) *Am J Physiol Heart Circ Physiol* **286**:H847-H855.
- Morrow G, Tanguay RM. (2003) *Semin Cell Dev Biol* **14**:291-299.
- Morrow JA, Hatters DM, Lu B, Hochtl P, Oberg KA, Rupp B, Weisgraber KH. (2002) *J Biol Chem* **277**:50380-50385.
- Motohashi K, Watanabe Y, Yohda M, Yoshida M. (1999) *Proc Natl Acad Sci USA* **96**:7184-7189.
- Muchowski PJ, Bassuk JA, Lubsen NH, Clark JI. (1997) *J Biol Chem* **272**:2578-2582.
- Muchowski PJ, Clark JI. (1998) *Proc Natl Acad Sci USA* **95**:1004-1009.
- Muchowski PJ, Valdez MM, Clark JI. (1999a) *Invest Ophthalmol Vis Sci* **40**:951-958.
- Muchowski PJ, Wacker JL. (2005) *Nat Rev Neurosci* **6**:11-22.
- Muchowski PJ, Wu GJ, Liang JJ, Adman ET, Clark JI. (1999b) *J Mol Biol* **289**:397-411.

- Murugesan R, Santoshkumar P, Sharma KK. (2007) *Mol Vis* **13**:2301-2309.
- Musci G, Metz GD, Tsunematsu H, Berliner LJ. (1985) *Biochemistry* **24**:2034-2039.
- Narberhaus F. (2002) *Microbiol Mol Biol Rev* **66**:64-93.
- Nath D, Rawat U, Anish R, Rao M. (2002) *Protein Sci* **11**:2727-2734.
- Ngo JT, Klisak I, Dubin RA, Piatigorsky J, Mohandas T, Sparkes RS, Bateman JB. (1989) *Genomics* **5**:665-669.
- Nicholl ID, Quinlan RA. (1994) *EMBO J* **13**:945-953.
- Ortwerth BJ, James HL. (1999) *Biochem Biophys Res Commun* **259**:706-710.
- Ortwerth BJ, Olesen PR. (1992) *Exp Eye Res* **55**:777-783.
- Ou B, Hampsch-Woodill M, Flanagan J, Deemer EK, Prior RL, Huang D. (2002) *J Agric Food Chem* **50**:2772-2777.
- Pace CN, Vajdos F, Fee L, Grimsley G, Gray T. (1995) *Protein Sci* **4**:2411-2423.
- Parnley JL, Hurst LD. (2007) *Bioessays* **29**:515-519.
- Pasta SY, Raman B, Ramakrishna T, Rao CM. (2002) *J Biol Chem* **277**:45821-45828.
- Pasta SY, Raman B, Ramakrishna T, Rao CM. (2003) *J Biol Chem* **278**:51159-51166.
- Pasta SY, Raman B, Ramakrishna T, Rao CM. (2004) *Mol Vis* **10**:655-662.
- Perkins D, Pereira EF, Gober M, Yarowsky PJ, Aurelian L. (2002) *J Virol* **76**:1435-1449.
- Perng MD, Cairns L, van den IP, Prescott A, Hutcheson AM, Quinlan RA. (1999b) *J Cell Sci* **112**:2099-2112.
- Perng MD, Muchowski PJ, van den IJssel P, Wu GJ, Hutcheson AM, Clark JI, Quinlan RA. (1999a) *J Biol Chem* **274**:33235-33243.
- Perng MD, Wen SF, van den IP, Prescott AR, Quinlan RA. (2004) *Mol Biol Cell* **15**:2335-2346.
- Perng MD, Zhang Q, Quinlan RA. (2007) *Exp Cell Res* **313**:2180-2188.
- Pilotto A, Marziliano N, Pasotti M, Grasso M, Costante AM, Arbustini E. (2006) *Biochem Biophys Res Commun* **346**:1115-1117.
- Pipkin W, Johnson JA, Creazzo TL, Burch J, Komalavilas P, Brophy C. (2003) *Circulation* **107**:469-476.
- Plater ML, Goode D, Crabbe MJ. (1997) *Ophthalmic Res* **29**:421-428.
- Pras E, Frydman M, Levy-Nissenbaum E, Bakhan T, Raz J, Assia EI, Goldman B, Pras E. (2000) *Invest Ophthalmol Vis Sci* **41**:3511-3515.
- Prévile X, Salvemini F, Giraud S, Chauffour S, Paul C, Stepien G, Ursini MV, Arrigo AP. (1999) *Exp Cell Res* **247**:61-78.
- Quax-Jeuken Y, Quax W, van Rens G, Khan PM, Bloemendal H. (1985) *Proc Natl Acad Sci USA* **82**:5819-5823.
- Quinlan R. (2002) *Prog Mol Subcell Biol* **28**:219-234.
- Rác P, Erdöhelyi A. (1988) *Ophthalmic Res* **20**:10-13.



- Rajan S, Horn C, Abraham EC. (2006) *Mol Cell Biochem* **288**:125-134.
- Rajaraman K, Raman B, Ramakrishna T, Rao CM. (2001) *FEBS Lett* **497**:118-123.
- Rajaraman K, Raman B, Rao CM. (1996) *J Biol Chem* **271**:27595-27600.
- Rajasekaran NS, Connell P, Christians ES, Yan LJ, Taylor RP, Orosz A, Zhang XQ, Stevenson TJ, Peshock RM, Leopold JA, Barry WH, Loscalzo J, Odelberg SJ, Benjamin IJ. (2007) *Cell* **130**:427-439.
- Raman B, Ramakrishna T, Rao CM. (1995a) *FEBS Lett* **365**:133-136.
- Raman B, Ramakrishna T, Rao CM. (1995b) *J Biol Chem* **270**:19888-19892.
- Raman B, Ramakrishna T, Rao CM. (1997) *FEBS Lett* **416**:369-372.
- Raman B, Rao CM. (1994) *J Biol Chem* **269**:27264-27268.
- Raman B, Rao CM. (1997) *J Biol Chem* **272**:23559-23564.
- Rao CM, Zigler SJ, Raman B. (1993) *Invest Ophthalmol Vis Sci* **34**:988.
- Rao PV, Krishna CM, Zigler JS Jr. (1992) *J Biol Chem* **267**:96-102.
- Rasi V, Costantini S, Moramarco A, Giordano R, Giustolisi R, Balacco Gabrieli C. (1992) *Ann Ophthalmol* **24**:459-464.
- Rasia RM, Bertoncini CW, Marsh D, Hoyer W, Cherny D, Zweckstetter M, Griesinger C, Jovin TM, Fernández CO. (2005) *Proc Natl Acad Sci USA* **102**:4294-4299.
- Rawat U, Rao M. (1998) *J Biol Chem* **273**:9415-9423.
- Ray PS, Martin JL, Swanson EA, Otani H, Dillmann WH, Das DK. (2001) *FASEB J* **15**:393-402.
- Reddy GB, Das KP, Petrash JM, Surewicz WK. (2000) *J Biol Chem* **275**:4565-4570.
- Reddy GB, Kumar PA, Kumar MS. (2006) *IUBMB Life* **58**:632-641.
- Renkawek K, Stege GJ, Bosman GJ. (1999) *Neuroreport* **10**:2273-2276.
- Richter L, Flodman P, Barria von-Bischhoffshausen F, Burch D, Brown S, Nguyen L, Turner J, Spence MA, Bateman JB. (2008) *Am J Med Genet Part-A* **146**:833-842.
- Roelofs MF, Boelens WC, Joosten LA, Abdollahi-Roodsaz S, Geurts J, Wunderink LU, Schreurs BW, van den Berg WB, Radstake TR. (2006) *J Immunol* **176**:7021-7027.
- Saha S, Das KP. (2007) *Protein J* **26**:315-326.
- Sanbe A, Yamauchi J, Miyamoto Y, Fujiwara Y, Murabe M, Tanoue A. (2007) *J Biol Chem* **282**:555-563.
- Sanger F. (1949) *Biochem J* **44**:126-128.
- Santhiya ST, Soker T, Klopp N, Illig T, Prakash MV, Selvaraj B, Gopinath PM, Graw J. (2006) *Mol Vis* **12**:768-773.
- Santhoshkumar P, Udupa P, Murugesan R, Sharma KK. (2008) *J Biol Chem* **283**:8477-8485.
- Sax CM, Piatigorsky J. (1994) *Adv Enzymol Relat Areas Mol Biol* **69**:155-201.
- Schein CH. (1989) *BioTechnology* **7**:1141-1148.
- Selcen D, Engel AG. (2003) *Ann Neurol* **54**:804-810.

- Sharma KK, Kaur H, Kester K. (1997) *Biochem Biophys Res Commun* **239**:217-222.
- Sharma KK, Kumar GS, Murphy AS, Kester K. (1998) *J Biol Chem* **273**:15474-15478.
- Sharma KK, Kumar RS, Kumar GS, Quinn PT. (2000) *J Biol Chem* **275**:3767-3771.
- Shashidharamurthy R, Koteiche HA, Dong J, McHaourab HS. (2005) *J Biol Chem* **280**:5281-5289.
- Shemetov AA, Seit-Nebi AS, Bukach OV, Gusev NB. (2008b) *Biochemistry (Mosc)* **73**:200-208.
- Shemetov AA, Seit-Nebi AS, Gusev NB. (2008a) *J Neurosci Res* **86**:264-269.
- Shi L, Palleros DR, Fink AL. (1994) *Biochemistry* **33**:7536-7546.
- Shinohara H, Inaguma Y, Goto S, Inagaki T, Kato K. (1993) *J Neurol Sci* **2**:203-208.
- Shroff NP, Cherian-Shaw M, Bera S, Abraham EC. (2000) *Biochemistry* **39**:1420-1426.
- Siezen RJ, Bindels JG, Hoenders HJ. (1979) *Exp Eye Res* **28**:551-567.
- Simon S, Fontaine JM, Martin JL, Sun X, Hoppe AD, Welsh MJ, Benndorf R, Vicart P. (2007b) *J Biol Chem* **282**:34276-34287.
- Simon S, Michiel M, Skouri-Panet F, Lechaire JP, Vicart P, Tardieu A. (2007a) *Biochemistry* **46**:9605-9614.
- Singh BN, Rao KS, Ramakrishna T, Rangaraj N, Rao CM. (2007a) *J Mol Biol* **366**:756-767.
- Singh D, Raman B, Ramakrishna T, Rao CM. (2006) *Mol Vis* **12**:1372-1379.
- Singh D, Raman B, Ramakrishna T, Rao CM. (2007b) *J Mol Biol* **373**:1293-1304.
- Skre H. (1974) *Clin Genet* **6**:98-118.
- Slavotinek AM, Biesecker LG. (2001) *Trends Genet* **17**:528-535.
- Smith CC, Yu YX, Kulka M, Aurelian L. (2000) *J Biol Chem* **275**:25690-25699
- Smith JB, Liu Y, Smith DL. (1996) *Exp Eye Res* **63**:125-128.
- Smulders RH, de Jong WW. (1997) *FEBS Lett* **409**:101-104.
- Smulders RHPH, Carver JA, Lindner RA, van Boekel MA, Bloemendal H, de Jong WW. (1996) *J Biol Chem* **271**:29060-29066.
- Smulders RHPH, Merck KB, Aendekerk J, Howritz J, Takemoto L, Slingsby C, Bloemendal H, de Jong WW. (1995) *Eur J Biochem* **232**:834-838.
- Smulders RHPH, van Boekel MAM, de Jong WW. (1998) *Int J Biol Macromol* **22**:187-196.
- Sobott F, Benesch JL, Vierling E, Robinson CV. (2002) *J Biol Chem* **277**:38921-38929.
- Sorensen HP, Mortensen KK. (2005) *Microb Cell Fact* **4**:1.
- Soti C, Csermely P. (2003) *Exp Gerontol* **38**:1037-1040.
- Spector A, Garner WH. (1981) *Exp Eye Res* **33**:673-681.
- Spector A. (1984) *Invest Ophthalmol Vis Sci* **25**:130-146.
- Spolaore B, Bermejo R, Zamboni M, Fontana A. (2001) *Biochemistry* **40**:9460-9468.
- Srinivas V, Raman B, Rao KS, Ramakrishna T, Rao CM. (2003) *Protein Sci* **12**:1262-1270.
- Srivastava OP, Srivastava K. (2003) *Mol Vis* **9**:110-118.
- Srivastava SK, Lal AK, Ansari NH. (1980) *Exp Eye Res* **31**:425-433.

- Srivastava VK, Varshney N, Pandey DC. (1992) *Acta Ophthalmol (Copenhagen)* **70**:839-841.
- Stadtman ER, Oliver CN. (1991) *J Biol Chem* **266**:2005-2008.
- Stamler R, Kappé G, Boelens W, Slingsby C. (2005) *J Mol Biol* **353**:68-79.
- Stanojević-Paović A, Hristić V, Cuperlović M, Jovanović S, Krsmanović J. (1987) *Ophthalmic Res* **19**:230-234.
- Stempfer G, Höll-Neugebauer B, Rudolph R. (1996) *Nature Biotechnol* **14**:329-334.
- Stock AD, Spallone PA, Dennis TR, Netski D, Morris CA, Mervis CB, Hobart HH. (2003) *Am J Med Genet Part-A* **120**:320-325.
- Studer S, Obrist M, Lentze N, Narberhaus F. (2002) *Eur J Biochem* **269**:3578-3586.
- Sugiyama Y, Suzuki A, Kishikawa M, Akutsu R, Hirose T, Waye MM, Tsui SK, Yoshida S, Ohno S. (2000) *J Biol Chem* **275**:1095-1104.
- Sun TX, Akhtar NJ, Liang JJ. (1998) *FEBS Lett* **430**:401-404.
- Sun TX, Akhtar NJ, Liang JJ. (1999) *J Biol Chem* **274**:34067-34071.
- Sun TX, Das BK, Liang JJ. (1997) *J Biol Chem* **272**:6220-6225.
- Sun TX, Liang JJ. (1998) *J Biol Chem* **273**:286-290.
- Sun X, Fontaine JM, Rest JS, Shelden EA, Welsh MJ, Benndorf R. (2004) *J Biol Chem* **279**:2394-2402.
- Surewicz WK, Olesen PR. (1995) *Biochemistry* **34**:9655-9660.
- Suzuki A, Sugiyama Y, Hayashi Y, Nyu-i N, Yoshida M, Nonaka I, Ishiura S, Arahata K, Ohno S. (1998) *J Cell Biol* **140**:1113-1124.
- Swamy MS, Abraham A, Abraham EC. (1992) *Exp Eye Res* **54**:337-345.
- Swamy MS, Abraham EC. (1991) *Curr Eye Res* **10**:213-220.
- Takemoto L, Boyle D. (1998) *Exp Eye Res* **67**:119-120.
- Takemoto L, Emmons T, Horwitz J. (1993) *Biochem J* **294**:435-438.
- Takemoto L. (1996b) *Exp Eye Res* **63**:585-590.
- Takemoto LJ. (1995a) *Curr Eye Res* **14**:837-841.
- Takemoto LJ. (1995b) *Exp Eye Res* **60**:721-724.
- Takemoto LJ. (1996a) *Exp Eye Res* **62**:499-504.
- Takemoto LJ. (1996c) *Biochem Biophys Res Commun* **223**:216-22.
- Takemoto LJ. (1998) *Exp Eye Res* **66**:263-266.
- Tang B, Liu X, Zhao G, Luo W, Xia K, Pan Q, Cai F, Hu Z, Zhang C, Chen B, Zhang F, Shen L, Zhang R, Jiang H. (2005a) *Arch Neurol* **62**:1201-1207.
- Tang BS, Zhao GH, Luo W, Xia K, Cai F, Pan Q, Zhang RX, Zhang FF, Liu XM, Chen B, Zhang C, Shen L, Jiang H, Long ZG, Dai HP. (2005b) *Hum Genet* **116**:222-224.
- Taylor RP, Benjamin IJ. (2005) *J Mol Cell Cardiol* **38**:433-444.

- Thériault JR, Lambert H, Chávez-Zobel AT, Charest G, Lavigne P, Landry J. (2004) *J Biol Chem* **279**:23463-23471.
- Thompson AR, Abdelraheim SR, Daniels M, Brown DR. (2005) *J Biol Chem* **280**:42750-42758.
- Trent S, Yang C, Li C, Lynch M, Schmidt EV. (2007) *Cancer Res* **67**:10774-10781.
- Treweek TM, Rekas A, Lindner RA, Walker MJ, Aquilina JA, Robinson CV, Horwitz J, Perng MD, Quinlan RA, Carver JA. (2005) *FEBS J* **272**:711-724.
- Trivedi VD, Raman B, Ramakrishna T, Rao CM. (1999) *J Biochem Biophys Methods* **40**:49-55.
- Truscott RJ. (2005) *Exp Eye Res* **80**:709-725.
- Uversky VN, Oldfield CJ, Dunker AK. (2005) *J Mol Recognit* **18**:343-384.
- van Boekel MA, Hoogakker SE, Harding JJ, de Jong WW. (1996) *Ophthalmic Res* **28**S1:32-38.
- van de Klundert FAJM, Gysen RHPH, Lindner MLJ, Jaenicke RAR, Carver JA, de Jong WW. (1998) *Eur J Biochem* **258**:1014-1021.
- van den IJssel P, Wheelock R, Prescott A, Russell P, Quinlan RA. (2003) *Exp Cell Res* **287**:249-261.
- van den Oetelaar PJ, Hoenders HJ. (1989) *Biochim Biophys Acta* **995**:91-96.
- van den Oetelaar PJ, van Someren PF, Thomson JA, Siezen RJ, Hoenders HJ. (1990) *Biochemistry* **29**:3488-3493.
- van Montfort RL, Basha E, Friedrich KL, Slingsby C, Vierling E. (2001) *Nat Struct Biol* **8**:1025-1030.
- van Noort JM, van Sechel AC, Bajramovic JJ, el Ouagmiri M, Polman CH, Lassmann H, Ravid R. (1995) *Nature* **375**:798-801.
- van Veen T, van Winsen L, Crusius JB, Kalkers NF, Barkhof F, Peña AS, Polman CH, Uitdehaag BM. (2003) *Neurology* **61**:1245-1249.
- Vanita V, Singh JR, Hejtmancik JF, Nürnberg P, Hennies HC, Singh D, Sperling K. (2006) *Mol Vis* **12**:518-522.
- Veinger L, Diamant S, Buchner J, Goloubinoff P. (1998) *J Biol Chem* **273**:11032-11037.
- Velasco PT, Lukas TJ, Murthy SN, Duglas-Tabor Y, Garland DL, Lorand L. (1997) *Exp Eye Res* **65**:497-505.
- Verschuure P, Tatard C, Boelens WC, Grongnet JF, David JC. (2003) *Eur J Cell Biol* **82**:523-530.
- Vicart P, Caron A, Guicheney P, Li Z, Prevost MC, Faure A, Chateau D, Chapon F, Tome F, Dupret JM, Paulin D, Fardeau M. (1998) *Nat Genet* **20**:92-95.
- Vleminckx V, Van Damme P, Goffin K, Delye H, Van Den BL, Robberecht W. (2002) *J Neuropathol Exp Neurol* **61**:968-974.
- Vos MJ, Hageman J, Carra S, Kampinga HH. (2008) *Biochemistry* **47**:7001-7011.
- Wagstaff MJ, Collaco-Moraes Y, Smith J, de Belleruche JS, Coffin RS, Latchman DS. (1999) *J Biol Chem* **274**:5061-5069.
- Walsh MT, Sen AC, Chakrabarti B. (1991) *J Biol Chem* **266**:20079-20084.
- Wang K, Spector A. (1996) *Eur J Biochem* **242**:56-66.

- Wang K, Spector A. (2000) *Eur J Biochem* **267**:4705-4712.
- Wang L, Zajac A, Hedhli N, Depre C. (2004) *Mol Cell Biochem* **265**:71-78.
- Wang X, Osinska H, Klevitsky R, Gerdes AM, Nieman M, Lorenz J, Hewett T, Robbins J. (2001) *Circ Res* **89**:84-91.
- Wilhelmus MM, Boelens WC, Otte-Höller I, Kamps B, Kusters B, Maat-Schieman ML, de Waal RM, Verbeek MM. (2006) *Acta Neuropathol* **111**:139-149.
- Wistow G. (1985) *FEBS Lett* **181**:1-6.
- Wotton D, Freeman K, Shore D. (1996) *J Biol Chem* **271**:2717-2723.
- Xi JH, Bai F, Andley UP. (2003) *J Cell Sci* **116**:1073-1085.
- Xi JH, Bai F, Gross J, Townsend RR, Memko AS, Andley UP. (2008) *J Biol Chem* **283**:5801-5814.
- Xia C, Liu H, Chang B, Cheng C, Cheung D, Wang M, Huang Q, Horwitz J, Gong X. (2006) *Invest Ophthalmol Vis Sci* **47**:3004-3010.
- Yang C, Salerno JC, Koretz JF. (2005) *Mol Vis* **11**:641-647.
- Yang C, Trent S, Ionescu-Tiba V, Lan L, Shioda T, Sgroi D, Schmidt EV. (2006) *Cancer Res* **66**:11649-11658.
- Yew EH, Cheung NS, Choy MS, Qi RZ, Lee AY, Peng ZF, Melendez AJ, Manikandan J, Koay ES, Chiu LL, Ng WL, Whiteman M, Kandiah J, Halliwell B. (2005) *J Neurochem* **94**:943-956.
- Yoshida K, Aki T, Harada K, Shama KM, Kamoda Y, Suzuki A, Ohno S. (1999) *Cell Struct Funct* **24**:181-185.
- Yu YX., Heller A, Liehr T, Smith CC Aurelian L. (2001) *Int J Oncol* **18**:905-911.
- Zhai J, Lin H, Julien JP, Schlaepfer WW. (2007) *Hum Mol Genet* **16**:3103-3116.
- Zhang FF, Tang BS, Zhao GH, Chen B, Zhang C, Luo W, Liu XM, Xia K, Cai F, Hu ZM, Yan XX, Zhang RX, Guo P. (2005) *Zhonghua Yi Xue Yi Chuan Xue Za Zhi* **22**:361-363.
- Züchner S, Vance JM. (2006) *Nat Clin Pract Neurol* **2**:45-53.